In presenting the dissertation as a partial fulfillment of the requirements for an advanced degree from the Georgia Institute of Technology, I agree that the Library of the Institute shall make it available for inspection and circulation in accordance with its regulations governing materials of this type. I agree that permission to copy from, or to publish from, this dissertation may be granted by the professor under whose direction it was written, or, in his absence, by the Dean of the Graduate Division when such copying or publication is solely for scholarly purposes and does not involve potential financial gain. It is understood that any copying from, or publication of, this dissertation which involves potential financial gain will not be allowed without written permission.

_____

_____

7/25/68

INFLUENCE OF THE BAUSCHINGER EFFECT ON PLASTIC RESONANCE

A THESIS

Presented to

The Faculty of the Division of Graduate

Studies and Research

by

Thou-Han Liu

In Partial Fulfillment

of the Requirements for the Degree

Doctor of Philosophy in the

School of Engineering Science and Mechanics

Georgia Institute of Technology

November, 1970

INFLUENCE OF THE BAUSCHINGER EFFECT

ON PLASTIC RESONANCE

Approved:

Chairman

Date approved by Chairman: 11/30/70

ACKNOWLEDGMENTS

I would like to take this opportunity to express my deepest appreciation to my advisor and friend, Dr. Edward R. Wood, for his interest, encouragement, guidance and advice throughout my graduate program. His research provided the concept and background which were required in initiating this study. Appreciation is also due the other members of my doctoral committee, Dr. W. W. King, Dr. J. M. Osborn, Dr. G. M. Rentzepis, Dr. R. W. Shreeves and Dr. J. T. S. Wang for their interest, guidance and invaluable suggestions.

I am deeply indebted to Dr. Milton E. Raville, Director of the School of Engineering Science and Mechanics, who arranged the financial assistance during the years of my study at Tech. In addition, the author is grateful for the financial support of the National Defense Education Act (NDEA). Sincere gratitude is due Dr. James T. S. Wang for his close guidance and advice during these years.

I would like to dedicate this thesis to my wife, Rita, whose love, patience and understanding have made this work possible. Special appreciation is due my father, Mr. Tso-pung Liu, who encouraged and helped me to come to this country and enter graduate school.

Finally, the author would extend his sincere thanks to Mrs. Jackie Van Hook for her wonderful typing and to the staff of the Rich Electronic Computer Center for their service.

TABLE OF CONTENTS

TABLE OF CONTENTS (Continued)

LIST OF TABLES

LIST OF ILLUSTRATIONS

LIST OF ILLUSTRATIONS (Continued)

LIST OF ILLUSTRATIONS (Continued)

LIST OF ILLUSTRATIONS (Continued)

LIST OF SYMBOLS

A = amplitude of the alternating applied-stress at the free end of the bar

$a(x,t)$ = particle acceleration of the bar

B = applied mean stress at the free end of the bar

C_o = acoustic elastic wave speed

E_o = Young's modulus; $\left(\frac{d\sigma}{d\epsilon}\right)$ in the elastic region of the stress-strain curve

E_1 = plastic modulus; $\left(\frac{d\sigma}{d\epsilon}\right)$ in the plastic region of the stress-strain curve

H = hysteresis energy

K = kinetic energy

k = strain-rate constant

ℓ = length of the bar

$m(x)$ = mass per unit volume of the bar

T = period of the oscillation

$u(x,t)$ = particle displacement of the bar

$v(x,t)$ = particle velocity of the bar

v_o = velocity parameter corresponding to the yield stress

W = external work

ρ = density of the bar

ρ_o = initial density of the bar

$\sigma(x,t)$ = engineering stress

σ_o = initial engineering yield stress

σ_m = mean stress

$\epsilon(x,t)$ = engineering strain

ϵ_o = initial engineering yield strain

ϵ^p = plastic strain

$\dot{\epsilon}^p$ = plastic strain rate

ω = loading frequency

ω_B = beating frequency

ω_N = resonance frequency

ω_n = first fundamental natural frequency of an elastic bar

SUMMARY

This study examines the problem of plastic resonance of longitudinal elastic-visco-plastic stress waves in finite bars. Considered here is a homogeneous fixed-free bar subjected to an axially-applied oscillating stress at its free end. The loading parameters are given by the amplitude of the oscillating stress, mean stress and loading frequency. Under high dynamic load, the material exhibits strain-rate sensitive behavior which is governed by Malvern's theory in both upper and lower yield stress regions. A basic bilinear static stress-strain relation is described by the Prandtl elastic-plastic model. The Bauschinger effect was then included. The plastic hysteresis loop is presented, and the wave reflections and interactions are also taken into consideration. The problem is solved by the method of characteristics. A quasi-numerical integration is applied for solutions on the characteristic plane. The UNIVAC 1108 digital computer and the CALCOMP plotter were employed to calculate and plot numerical results.

Interesting results on the amplification effect due to dynamic response of the bar with and without the Bauschinger Effects are presented. Since the degree of strain-hardening is a parameter of the material, it is possible to show the resonant effect for various degrees of plasticity. Elastic resonance is a limiting case. A check on the numerical results was given based on the theory of conservation of energy. Finally a comparison is made with and without the Bauschinger effect.

CHAPTER I

HISTORICAL DEVELOPMENT

I. Introduction

The investigation of elastic wave propagation in a solid medium has a long and distinguished history. Stokes, Poisson, Rayleigh, and Kelvin were associated with much of the fundamental work in this area. Later, this work was extended by Lamb and Love. By comparison, the study of wave propagation in solid media, which are not perfectly elastic and which exhibit dissipative phenomenon, is a relatively new field. Only during the last three decades have many important theories and experimental advances resulted in this field. For instance, one-dimensional plastic wave propagation did not begin to seriously interest many researchers until the Second World War. The war made it necessary to better understand the dynamic behavior of materials subjected to high stress.

It is noted in most mechanical analysis or design that material behavior will deviate from a purely elastic relation. (Hooke's Law) under high dynamic loads. Generally, a more realistic dynamic constitutive relation is considered in this case. This relation will be nonlinear and dependent on the loading path. The stress-strain curve may exhibit hysteresis loops such that the resulting stress-strain relations are not single-valued. It has also been found that the dynamic relations between stress and strain are generally time dependent. In all, dynamic

plastic response in a solid occurs when the magnitude of applied dynamic load is sufficiently high to produce plastic strain. Consequently, this results in plastic wave propagation.

Among various plastic wave propagation problems, considerable interest and effort have been directed at the problem of elastic-plastic loading and unloading in a one-dimensional semi-infinite domain. More complicated boundary value problems in dynamic plasticity have presented a difficult problem. This is mainly due to the nature of complexity resulting from wave interactions and reflections at the boundaries. Now, because of increased interest in plastic and composite materials, plastic design becomes necessary for certain of today's dynamic problems. For this reason a better definition of material dynamic properties has been sought by experimental investigators. In addition, new high-speed electronic computers make it possible to treat the more complicated problems. In the future, more work on boundary value problems in dynamic plasticity can be expected.

The term "plastic resonance" was first introduced by Kalaski and Wladarczyk [1] in 1967, but no related work has appeared in the literature since then. A primary purpose of this study will be to investigate this resonance phenomenon in a finite, homogeneous, elasto-visco-plastic, fixed-free bar, allowing for strain-rate effect. The Bauschinger effect will be considered in order to explore its effect on plastic resonance. In other words, a comparison will be made for plastic resonance by considering the "Bauschinger effect" and without considering this effect. An oscillating load will be introduced at the free end of the bar, and various frequencies of loading will be studied. As a result,

the bar's frequency response spectrum will be obtained. The influence of strain-hardening of the material (degree of plasticity) on the dynamic response of the bar will be one of the aspects of this investigation. For a limiting value of strain-hardening, the bar will be considered perfectly elastic. In this case, the response under sinusoidal loading can be checked by a normal mode solution for an elastic bar. In addition, based upon the constitutive equations described in this study, it is desired to study the dynamic plastic behavior of a bar under various oscillatory loading conditions. Finally, results of this study will be compared with those of Kalaski and Wladarczyk.

II. Historical Background

The first treatment of the propagation of plastic waves was published in 1930 by Donnell [2], who considered the propagation of a disturbance along a thin semi-infinite wire of a solid which possessed a bilinear stress-strain relation. The material was assumed to be elastic for stresses below the yield stress and had a value of Young's modulus of E_0. For stresses greater than the yield stress σ_o, the stress-strain relations followed another linear curve which had a gradient of $E_1 (E_1 < E_0)$. The material was totally elastic during unloading. He found that due to a constant applied stress σ ($\sigma > \sigma_o$) at one end of the bar, an elastic wave front of magnitude σ_o would propagate along the bar with an elastic velocity $(E_o/\rho_o)^{1/2}$, and behind this, a second wave front with higher stress σ propagated at a lower velocity $(E_1/\rho_o)^{1/2}$.

As already mentioned, after Donnell's work plastic wave propagation received little further attention until the Second World War.

During the war, von Karman [3] in this country, Taylor [4] in Great Britain, and Rakhmatulin [5] in the Soviet Union obtained independently formal solutions for plastic waves with more general stress-strain relations. Their assumptions of the material's stress-strain property were a distinct yield point at σ_o with the stress-strain curve concave toward the strain axis. Further theoretical work was carried out by White and Griffis [6, 7]. In their subsequent paper, they extended Donnell's work to include effects of unloading for determining the residual strain. Later, they explored uniaxial compressive impact on elastic-plastic materials and found that the form of the engineering stress-strain curve in the high stress region differs significantly from that observed in tension because of the increase in cross-sectional area with compression.

Early experimental verification of the theory was carried out by Duwez and Clark [8, 9]. They measured the distribution of permanent strain in a copper wire which had been intensively stretched by a falling weight. They found that the distribution of permanent strain along the wire was reasonably in agreement with the theory. The conclusion drawn from their experiments was that static and dynamic stress-strain curves were almost the same and that strain rate effects, if they existed, were quite small.

In a paper presented in 1950, Von Karman and Duwez [10] brought together results of their wartime theoretical and experimental investigations. There were two main topics brought into attention: (1) the existence of a strain plateau and (2) the influence due to strain rate. While the first topic was left open to discussion (debate) for many

years, the second topic, the question of strain-rate or dynamic stress-strain effects, opened up a new area of research in plasticity, which continues to be the subject of considerable experimental and theoretical study.

Lee [11] applied the Karman-Taylor theory to solution of a typical plastic wave boundary value problem. He considered a finite bar impacting a rigid target. The method he used was based upon numerical integration along characteristics. He was able to determine the unknown elastic-plastic boundaries in the characteristic plane. He also showed that the elastic portion of the loading wave is reflected by the free end of the bar as an unloading wave which travels back along the bar at the elastic velocity and is progressively absorbed as it penetrates the oncoming plastic wave front. A so called critical impact velocity was obtained in order to determine the character of this reflected elastic wave front.

In the early fifties, considerable interest in plastic waves had been placed on obtaining more accurate information about dynamic stress-strain characteristics. At this time a theory on strain-rate effects in plastic wave propagation was proposed by Malvern [12,13]. Malvern's theory predicted that the front of a disturbance would travel with elastic velocity even if the metal was incrementally stressed into the plastic region. This was in agreement with substantially similar results obtained experimentally by Bell [14], and later by Sternglass and Stuart [15] and Alter and Curtis [16]. In 1953, J. D. Campbell [17] carried out a series of tests based upon repeated impact loadings and found a dynamic stress-strain curve fifteen to twenty percent above the corresponding

static curve. In 1961, Hopkins [18] clarified the importance of strain-rate effects on plastic wave analysis, but concluded that the strain-rate independent theory provides reasonably satisfactory results for materials without a well defined yield point and without undue strain-rate sensitivity.

It was Morland [19], who was perhaps the first to consider elastic-plastic unloading in plastic wave propagation. He treats the case of pure one-dimensional strain corresponding to motion in a semi-infinite block due to a normal force applied uniformly over the free surface. Strain-rate effects were neglected in development of the theory. In his study, he was able to discuss the subsequent wave interactions and also the formation and propagation of shock waves. Following this, Osiecki [20] examined the plastic wave problem for a semi-infinite bar. The bar was characterized by a bilinear stress-strain curve where lower yield and the Bauschinger effect were included. A plastic hysteresis loop was introduced into his description of the Prandtl model. A rate-independent solution was developed for plastic waves resulting from a periodic pulse applied at one end of the bar. He concluded that from the computations quoted, the process of the vibration becoming steady state is relatively rapid. This conclusion was confirmed by several experimental investigations which are still continuing.

Later R. J. Clifton and S. R. Bodner [21] studied elastic-plastic unloading in plastic waves for both semi-infinite and finite bars under a pressure pulse of short duration. The stress-strain behavior was based upon the assumption that the tensile stress-strain behavior was independent of any previous compression and agrees, except for sign, with initial compression behavior. By using the method of characteristic,

the general shape of boundaries in the x-t plane, which separate regions governed by the dynamic elastic equations from regions governed by the dynamic plastic equations, was presented. The main features of their solution are in agreement with some experimental results.

In treating unloading waves, a more recent work was carried out by Wood analytically [22]. In addition to considerations of lower yield and strain-rate effects, he also explored many cases of unloading such as sudden elastic unloading and gradual elastic-plastic unloading. Comparisons were made considering and not considering lower yield and rate effects. Based upon this work, Wood and Phillips [23] concluded that the failure of Malvern's [12,13] rate-dependent theory to show a distinct strain plateau was due to the fact that the load had not been applied long enough. They also showed that the degree of plasticity plays a significant role in forming the plateau.

Because of some uncertainty in the dynamic plastic properties of materials, research continues in this area. Some investigators have proposed modified constitutive relations for the theory. Lubliner [24] formulated a more general quasi-linear constitutive equation. It was shown that strain-rate-independent and strain-rate-dependent theories are special cases of the general theory. Under certain conditions, one or the other may be valid. It should be noted that, Lubliner did not consider lower yield and the Bauschinger effect. A year later, N. Cristescu [25], presented a loading/unloading criteria for rate-sensitive materials in order to describe more clearly mechanical properties of materials in one-dimensional dynamic problems. He indicated that the static yield stress never increases up to the

magnitude of the instantaneous dynamic yield stress. That means when the stress decreases, the plastic strain will first continue to increase, and only after the stress falls below a certain limit, will the plastic strain remain constant. Numerical examples were given, and some interesting plots, which gave the dynamic stress-strain history for various sections of the bar, were also presented. In Cristesu's work lower yield and Bauschinger effect were also not considered. Another investigator was Nowacki [26], who studied the propagation and reflection of a plane stress wave from a deformable support. He concluded on the basis of the examples given in the paper, that in dynamic problems with small strain rates the strain-hardening effect must be considered. Again, lower yield and the Bauschinger effect were not considered in the analysis.

For plasticity problems, Prager [27] introduced the concept of kinematic hardening based upon kinematic models. He believed that a better stress-strain relation could be provided by this model which considered the "Bauschinger effect" -- the decrease of the yield limit in compression produced by work-hardening in tension. In this case the yield surface in two-dimensional stress space is effectively translated as a rigid body instead of expanding when undergoing increased plastic strain. Therefore, it was noted that if the initial plastic strain is large enough, yield could possibly occur before zero stress is reached during unloading. This fact was confirmed experimentally by recent investigators such as Lubahn [28], Ivey [29], Phillips and Sierakowski [30] and Justusson [31]. Its effect on plastic waves was investigated analytically by Wood [22]. Wood explored, in his work, the effect of

lower yield for plastic waves in a semi-infinite bar with both rate-dependent and rate-independent materials. The favorable conclusion by considering lower yield from Prager's model can be found from his statement that "a strain plateau will result from the strain-rate theory in general agreement with experiment if yield upon unloading is introduced with unloading rate effects taken into account". It is also noted that, an excellent and comprehensive survey history on the subject of plastic waves was presented in his work.

In a relatively new series of studies by Kalaski and Wlodrczyk [1, 32, 33], the solution of stationary problems in the domain of dynamic boundary value problems of plasticity has been brought into attention. Here, an interesting problem, that of plastic resonance for longitudinal elastic-plastic waves in a finite bar was first introduced. As stated in the first of their three papers, "Such a problem, in addition to its essential theoretical interest, has also an essential practical importance. It suffices to mention, as a single example of this type, the problem of measurement of the parameters of plastic state and plastic waves, the solution of which enables the measurement to be performed under steady state, not by using the technique of instantaneous measurement of wave processes at short intervals necessitated by the wave character of the phenomenon." In their three part studies: (1) plastic resonance of elastic-plastic waves in finite bar; (2) resonance of longitudinal shock waves; and (3) resonance of elastic-visco-plastic waves in a finite bar -- the lower yield effect was included but without the Bauschinger effect (the yield limit in tension and compression are identical). The excitation frequency was limited by the dimension and the

material of the bar. An important accomplishment in their study was the presentation of an amplification coefficient of stress amplitude at the fixed end of the bar. They found (for an elastic-plastic bar) that the amplification coefficient for stress only depends on the ratio of the velocity of an elastic wave to the velocity of a plastic wave. However, for an elastic-visco-plastic bar, the amplification coefficient of stress at the fixed end depends not only on the velocities of waves, but also on the rate-dependent material constant k and the length of the bar.

This completes the historical development. This review has shown that the study of dynamic plasticity has a relatively short but interesting history. Many well-known researchers have made contributions. Still, many questions remain to be answered. Today more research needs to be done in dynamic plasticity both theoretically and experimentally in order to keep up with advanced technology.

CHAPTER II

THEORETICAL FORMULATION

1. Statement of the Problem

The problem considered is the propagation of longitudinal elastic-visco-plastic waves in thin, homogeneous, fixed-free bars. The theory is developed on the assumption that three-dimensional effects may be neglected. Therefore the problem involves only a single stress component and a single strain component, also a single spatial coordinate.

The influence of the shape of the transverse section of the rod on the propagation of the wave will be disregarded; only the area of this transverse section will be taken into account in the problem. The rod will be considered "thin" in the sense of being able to neglect lateral inertia. It is also assumed that the cross-section of the bar, which is plane before loading, remains plane after loading. Thus, the displacement of particles parallel to the axis of the bar is equal in a given transverse plane for the entire cross-section. In the case when longitudinal impact produces compression, the possibility may arise that the bar would buckle. However, if the compression occurs in a very short interval of time, the inertia force in general does not allow this to occur. Dynamic buckling then will also be disregarded.

II. The Compatibility Relation and the Equation of Motion

The analysis in this dissertation is presented in terms of material Lagrangian coordinates with use of engineering stress and strain.

In the Lagrangian description, attention will be fixed on the description of the state of convected particles themselves, rather than the state of a system of particles observed to pass through fixed geometrical points. Let the ξ-axis and the bar axis coincide. The independent variables are taken as the initial coordinate x of a typical particle P and the time t. The dependent variables are displacement $u(x,t)$, velocity $v(x,t)$, engineering stress $\sigma(x,t)$ and engineering strain $\epsilon(x,t)$.

Now consider a particle P in the bar. Initially, at $t = 0$, it is defined by a coordinate at $X = x(P)$, and at a later time t, it is given by the coordinate $X = \xi\ (P,t)$. Therefore the particle is identified either by the initial value x or by the current value ξ. Obviously, $x(P) = \xi$, $(P,0) = \xi_o$, $(P) = \xi$, $(x,0)$ and x is a Lagrange coordinate. (See Figure 2-1). The displacement of particle P, initially at x, is

$$u(x,t) = \xi(x,t) - \xi(x,0) = \xi(x,t) - x \ . \qquad (2\text{-}1)$$

Consequently, the particle velocity $v(x,t)$ and acceleration $a(x,t)$ are given by

$$v(x,t) = \frac{\partial \xi(x,t)}{\partial t} = \frac{\partial u(x,t)}{\partial t} \qquad (2\text{-}2)$$

and

$$a(x,t) = \frac{\partial v(x,t)}{\partial t} = \frac{\partial^2 u(x,t)}{\partial t} \ . \qquad (2\text{-}3)$$

The engineering strain is,

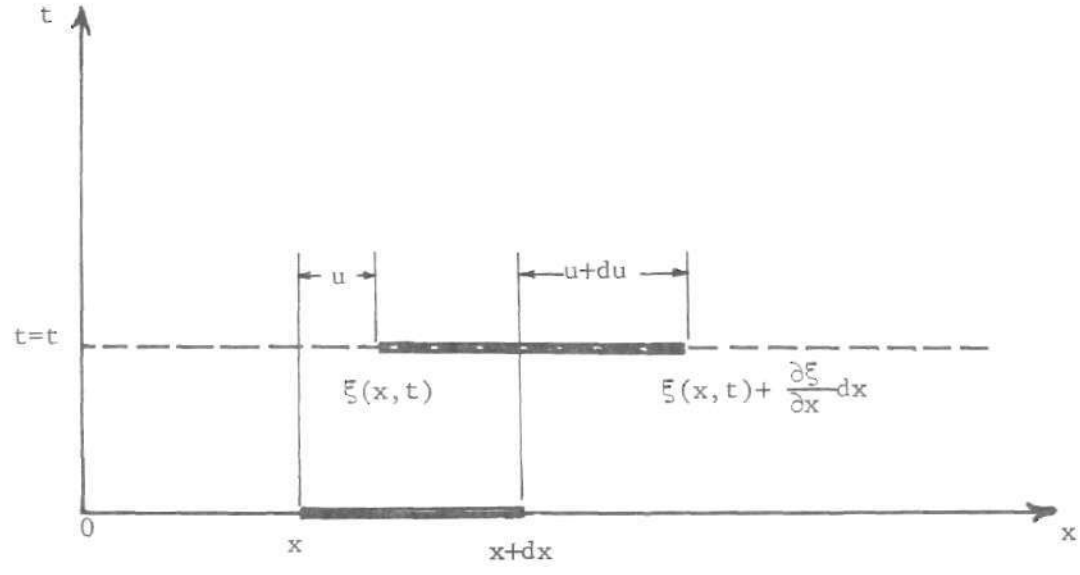

Figure 2-1. Geometric Representation of a Particle at Lagrange Coordinate.

$$\varepsilon(x,t) = \lim_{\Delta x \to 0} \left\{ \frac{[\xi(x+\Delta x,t) - \xi(x,t)] - [\xi(x+\Delta x,0) - \xi(x,0)]}{[\xi(x+\Delta x,0) - \xi(x,0)]} \right\}$$

$$= \lim_{\Delta x \to 0} \left\{ \frac{[\xi(x+\Delta x,t) - \xi(x,t)]}{[\xi(x+\Delta x,0) - \xi(x,0)]} - 1 \right\}$$

$$= \frac{\left[\xi(x,t) + \frac{\partial \xi(x,t)}{\partial x}\, dx\right] - \xi(x,t)}{dx} - 1$$

$$= \frac{\partial \xi(x,t)}{\partial x} - 1$$

or with the aid of equation (2-1),

$$\varepsilon(x,t) = \frac{\partial u(x,t)}{\partial x} \quad . \tag{2-4}$$

Also the engineering stress is denoted by the instantaneous axial force $F(x,t)$ divided by the initial cross-sectional area $A(x,0) = A_o(x)$,

$$\sigma(x,t) = \frac{F(x,t)}{A(x,0)} = \frac{F(x,t)}{A_o(x)} \quad . \tag{2-5}$$

From equations (2-2) and (2-4), in order to ensure that velocity $v(x,t)$ and strain $\varepsilon(x,t)$ are derivable from $u(x,t)$. The velocity and strain

must satisfy the following compatibility relation,

$$\frac{\partial v(x,t)}{\partial x} = \frac{\partial \varepsilon(x,t)}{\partial t} \quad . \tag{2-6}$$

Next, let $\rho(x,t)$ be the mass density per unit volume; then the initial density is $\rho(x,0) = \rho_o(x) =$ constant. Also $A(x,t)$ be the cross-section area of the bar; then the initial cross-section area is $A(x,0) = A_o(x) =$ constant. Furthermore, let $m(x)$ be the total mass between the cross-section x and some arbitrary fixed reference cross-section $x = a$; then $m(x) = \rho_o A_o x +$ constant is independent of time t, as a particular value x defines a fixed particle P(x). The equation of conservation of mass, then, can be written in the form,

$$\begin{aligned} m(x) &= \int_a^x \rho(x',t)A(x',t)\,\frac{\partial \xi}{\partial x'}\,dx' \\ &= \int_a^x \rho_o\, A_o\, dx' \\ &= \rho_o\, A_o\, x + \text{constant} \end{aligned} \tag{2-7}$$

where $\frac{\partial \xi}{\partial x}$ is the Jacobian in one dimensional form, or in differential expression,

$$\rho_o A_o = \rho A\,\frac{\partial \xi}{\partial x} = \rho A\left(1 + \frac{\partial u}{\partial x}\right) \tag{2-8}$$

with the use of equation (2-1). The equation of motion is

$$\frac{dm}{dx}\,\frac{\partial v}{\partial t} = \frac{\partial F}{\partial x} \tag{2-9}$$

for m is independent of time variable t. Taking the advantage of equations (2-7) and (2-8) with above equation one gets,

$$\rho_o A_o \frac{\partial v}{\partial t} = A_o \frac{\partial \sigma}{\partial x}$$

or

$$\rho_o \frac{\partial v(x,t)}{\partial t} = \frac{\partial \sigma(x,t)}{\partial x} \quad . \tag{2-10}$$

III. Formulation of the Constitutive Equation

There are two general theories can be applied for the propagation of stress waves in solids when the material is loaded into the plastic region. One is a strain-rate-independent theory, the other is a strain-rate-dependent theory. For the rate-independent theory, sometimes known as the Karman-Taylor Theory, it is assumed that the dynamic response of the material can be adequately expressed by using stress-strain relations which are invariant to rate effects. This means that static or quasi-static stress-strain data may be applied to characterize the material's response to high rates of loading. For the rate-dependent theory, on the other hand, the instantaneous strength and energy absorption of a material will increase with rate of strain for a given strain increment. Tests show that the magnitude of this change can be significant for many materials--certain polymers, metals and alloys. For example, the dynamic properties of mild steel have been studied by J. D. Campbell and Duby [34] where it was concluded that the dynamic yield stress can be 2.5 times larger than the static value. Thus, the dynamic yield stress is certainly not a characteristic constant of the material. In other words, for a

given material with various loading histories, one obtains various dynamic yield stresses. Finally, it has been shown by experiments that for nearly all technological materials under a wide range of conditions, an increase of the rate of the strain produces an increase of the dynamic yield stress.

Many authors have proposed various constitutive equations in order to describe the mechanical behavior of materials that exhibit time rate effects. However, the author intends here to propose a more complete constitutive equation for plastic wave propagation in rate-dependent, work-hardening material, under plastic cyclic loading and unloading. The following works provide the basis for derivation of the constitutive equation.

(A). Prager's Kinematic Model:

In considering plasticity problems, Prager [27] introduced the concept of kinematic hardening based on kinematic models, that represent stresses by displacements. He used five dynamic models to represent five types of mechanical behavior under uniaxial stress (Fig. 2-2). He concluded from the stress-strain diagram of Fig. (2-2e) that "the decrease of the yield limit in compression produced by working hardening in tension is known as the Bauschinger effect. For the solid considered here, work hardening and the Bauschinger effect counterbalance each other in such a manner that the gap between the yield limits in tension and compression is independent of the permanent deformation". Therefore, both work hardening and the Bauschinger effect, which are considered qualitatively important in characterizing the material dynamic properties based upon recent experimental evidence have been included

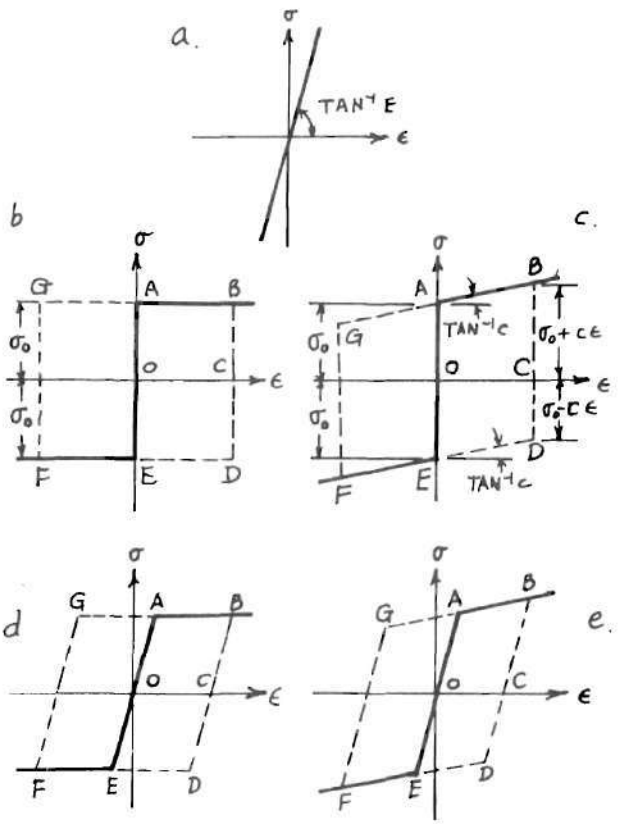

Figure 2-2. Prager's Dynamic Models.

in his model. And, one learns, from his model, that between the two yield limits (tension and compression or upper and lower), there exists an elastic region. In other words, the yield surface in two dimensional stress space is effectively translated as a rigid body when undergoing increased plastic strain.

(B). Bauschinger Effect:

Johann Bauschinger [35], using a mirror extensometer to probe stress-strain characteristics of metals, observed that if a mild steel speciman is stretched beyond its yield point in tension, then its yield point in compression is lowered. This characteristic of certain material carries his name and is called the "Bauschinger Effect". As one sees here, Prager's model from the last section can analytically represent this effect.

(C). Malvern's Model of Rate-Dependent Material:

Sokolovski [36] and Malvern [12] developed theories of plastic wave propagation in bars, taking account of the dependence of strain rate. If the material is work-hardening, and if the conventional quasi-static stress-strain relation is $\sigma = f(\epsilon)$, then Malvern [12,13] proposed the constitutive equation in following form

$$\sigma = f(\epsilon) + a \ln(1+b\ \dot{\epsilon}^p) \tag{2-11}$$

where a, b are characteristic constants for the material considered, and $\dot{\epsilon}^p$ represents plastic strain rate. An alternate form of the above equation can be written as

$$\dot{\epsilon}^p = \frac{1}{b}\left[\exp\left(\frac{\sigma - f(\epsilon)}{a}\right) - 1\right] \quad . \tag{2-12}$$

An important fact can be seen from this expression. The plastic rate of strain must be a function of dynamic overstress σ-f(ε), that is, for a certain corresponding plastic strain value, strain rate depends upon the difference between dynamic instantaneous stress σ and static yield stress f(ε). After some substitutions, Malvern obtained a constitutive equation in the form

$$E_o \frac{\partial \varepsilon}{\partial t} = \frac{\partial \sigma}{\partial t} + g(\sigma, \varepsilon) \qquad (2\text{-}13)$$

where

$$g(\sigma, \varepsilon) = E_o \frac{\partial \varepsilon^p}{\partial t} = k[\sigma - f(\varepsilon)]$$

where ε^p is plastic strain, k is a material constant specifying the magnitude of the strain-rate effect, provided by the experimental data. As Wood [22] discussed in his work, k takes values between $0 \leq k \leq \infty$ for rate-dependent material. In the limit, when k=0 the material behaves as purely elastic, for $k = \infty$, it behaves as a time-independent elastic-plastic material. Also E_o is Young's modulus and the function $g(\sigma, \varepsilon)$ expresses the plastic strain rate multiplied by Young's modulus.

(D). Lower Yield Effect Upon Unloading:

In the study of plastic wave propagation in solids, not until very recently have authors considered a lower yield effect. But results of recent experiments, directed at better definition of stress-strain relations, confirm not only Prager's model qualitatively but lower yield as well. In particular, those of Lubahn [28], Ivey [29], Phillips and Sierakowski [30], and Justusson [31] show that for large strains, yield

occurs upon unloading before zero stress is reached. Next, the question is raised, what new effects are contributed to the plastic wave propagation problem by introducing a lower yield concept? Wood [22] has explored the effect of lower yield for plastic waves in a semi-infinite bar with both rate-dependent and rate-independent materials. The favourable conclusion in considering the lower yield effect can be found from his statement that "a strain plateau will result from the strain-rate theory in general agreement with experiment if yield upon unloading is introduced with unloading rate effects taken into account." Earlier, Malvern had failed to predict the plateau. A possible explanation could be that lower yield was not considered in his work.

With this understanding of related works as discussed above for a basis, a more general constitutive equation can be postulated. The equation will be based upon Prager's dynamic model as the static stress-strain relation and upon Malvern's rate-dependent theory, but extended to the lower yield stress region (See Fig. 2-3).

In Fig. (2-3) the functions $f_1(\epsilon)$ and $f_2(\epsilon)$ denote static stress-strain relations, which are time independent. In the σ-ϵ plane, the area where stresses are greater than $f_1(\epsilon)$ is called the upper yield region, the area where the stresses fall between lines $f_1(\epsilon)$ and $f_2(\epsilon)$ is called the elastic region. In this region the stress-strain relation will follow the elastic equation which is independent of plastic strain. The area below the line $f_2(\epsilon)$ is called the lower yield region.

In order to give a better mathematical expression of this proposed constitutive equation, one starts from Malvern's equation,

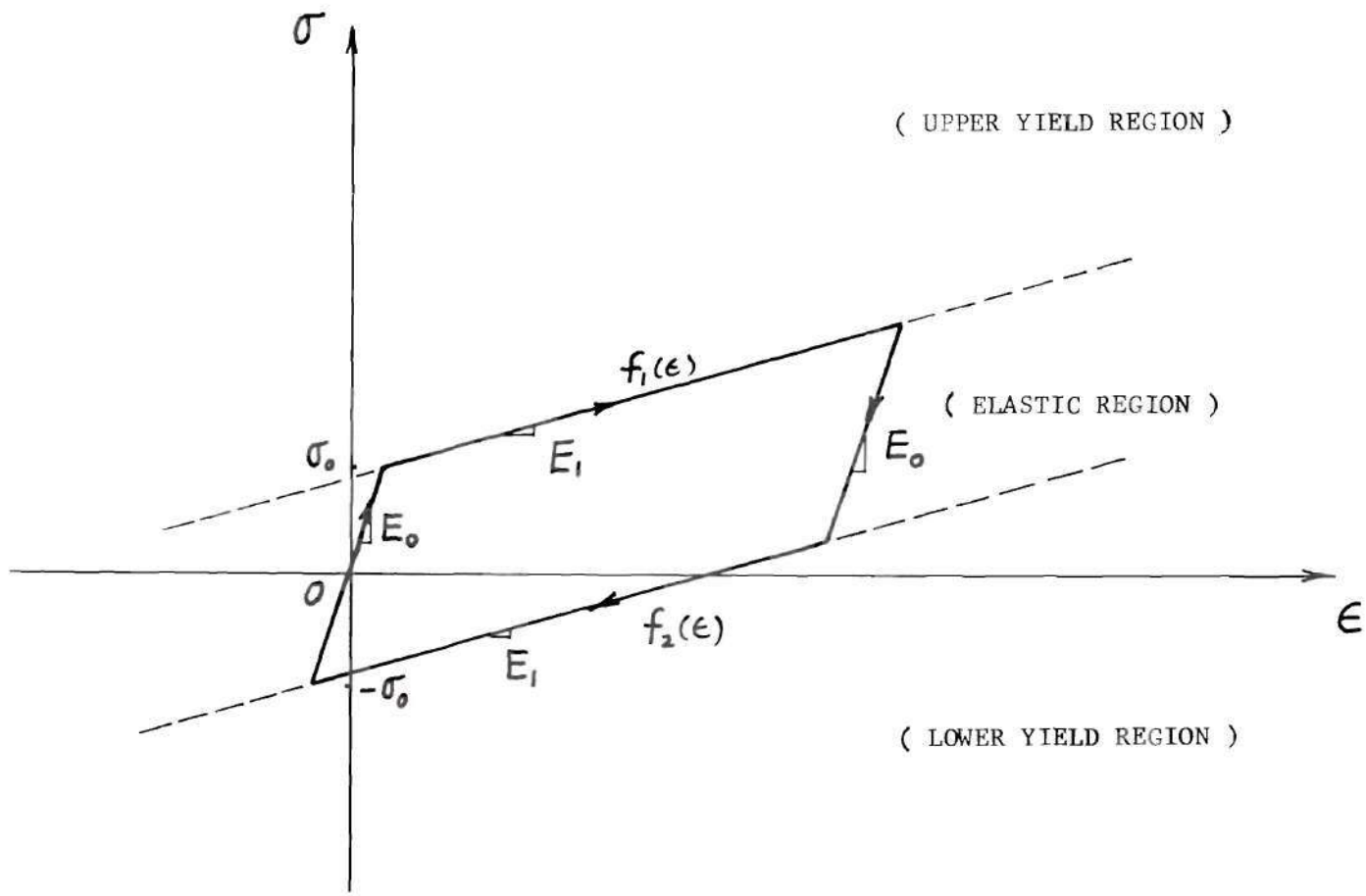

Figure 2-3. Static Stress-Strain Relations from Prager's Model.

$$E_o \frac{\partial \varepsilon}{\partial t} = \frac{\partial \sigma}{\partial t} + g(\sigma, \varepsilon)$$

$$= \frac{\partial \sigma}{\partial t} + k[\sigma - f(\varepsilon)] \ . \qquad (2\text{-}14)$$

It is understood that Malvern assumes that strain rate is proportional to the excess of the instantaneous stress over the stress at the strain in a static test only for the upper yield region. In other words, he assumes that,

$$E_o \frac{\partial \varepsilon^p}{\partial t} = g_1(\sigma, \varepsilon) = k[\sigma - f_1(\varepsilon)] \qquad (2\text{-}15)$$

where $f_1(\varepsilon)$, as we know, defines the static upper yield stress. Since the "Bauschinger effect" is included, consequently a static lower yield stress $f_2(\varepsilon)$ must also be presented. One may postulate similarly, in the lower yield region,

$$E_o \frac{\partial \varepsilon^p}{\partial t} = g_2(\sigma, \varepsilon) = k[\sigma - f_2(\varepsilon)] \qquad (2\text{-}16)$$

where $f_2(\varepsilon)$ defines the static lower yield stress, $[\sigma - f_2(\varepsilon)]$ is the excess of the instantaneous stress in a negative sense. In other words, $[\sigma - f_2(\varepsilon)]$ can only be either less than zero or equal to zero. Thus, it is clear that a constitutive equation for loading and unloading can be written as,

$$E_o \frac{\partial \varepsilon}{\partial t} = \frac{\partial \sigma}{\partial t} + \langle g(\sigma, \varepsilon) \rangle \qquad (2\text{-}17)$$

where

$$\langle g(\sigma,\epsilon)\rangle \equiv \begin{cases} g_1(\sigma,\epsilon) & \text{for } \sigma > f_1(\epsilon) \\ 0 & \text{for } f_2(\epsilon) \le \sigma \le f_1(\epsilon) \\ g_2(\sigma,\epsilon) & \text{for } \sigma < f_2(\epsilon) \end{cases}$$

where g_1 and g_2 are defined in Equations (2-15) and (2-16).

It should be noted that the value of $\langle g(\sigma,\epsilon)\rangle$ in this equation will be decided by the location of instantaneous stress on the σ-ϵ plane rather than by the process of loading or unloading, since $g(\sigma,\epsilon)$ exhibits any of three different values depending upon the region of instantaneous stress. In other words, as long as the instantaneous stress and strain are known in any of the three regions, a proper value of $\langle g(\sigma,\epsilon)\rangle$ is provided by the above expression for both loading and unloading. The loading and unloading are defined mathematically as,

loading: $\frac{\partial\sigma}{\partial t} > 0$ at $[0,\ell]$

unloading: $\frac{\partial\sigma}{\partial t} \le 0$ at $[0,\ell]$.

It is interesting to note that if one traces a continuous dynamic stress-strain curve as proposed in this dissertation and governed by equation (2-17), various stages of stress rate and strain rate are shown during a complete cycle of loading and unloading. Fig. (2-4) will give us a clear picture for this point.

If one intends to load further from I, then, after passing the elastic region and upper yield region boundary J, the dynamic stress-strain curve will meet its previous history curve at point K. (see Fig. (2-4)) This illustrates the fact that stress-strain hysteresis loops will appear

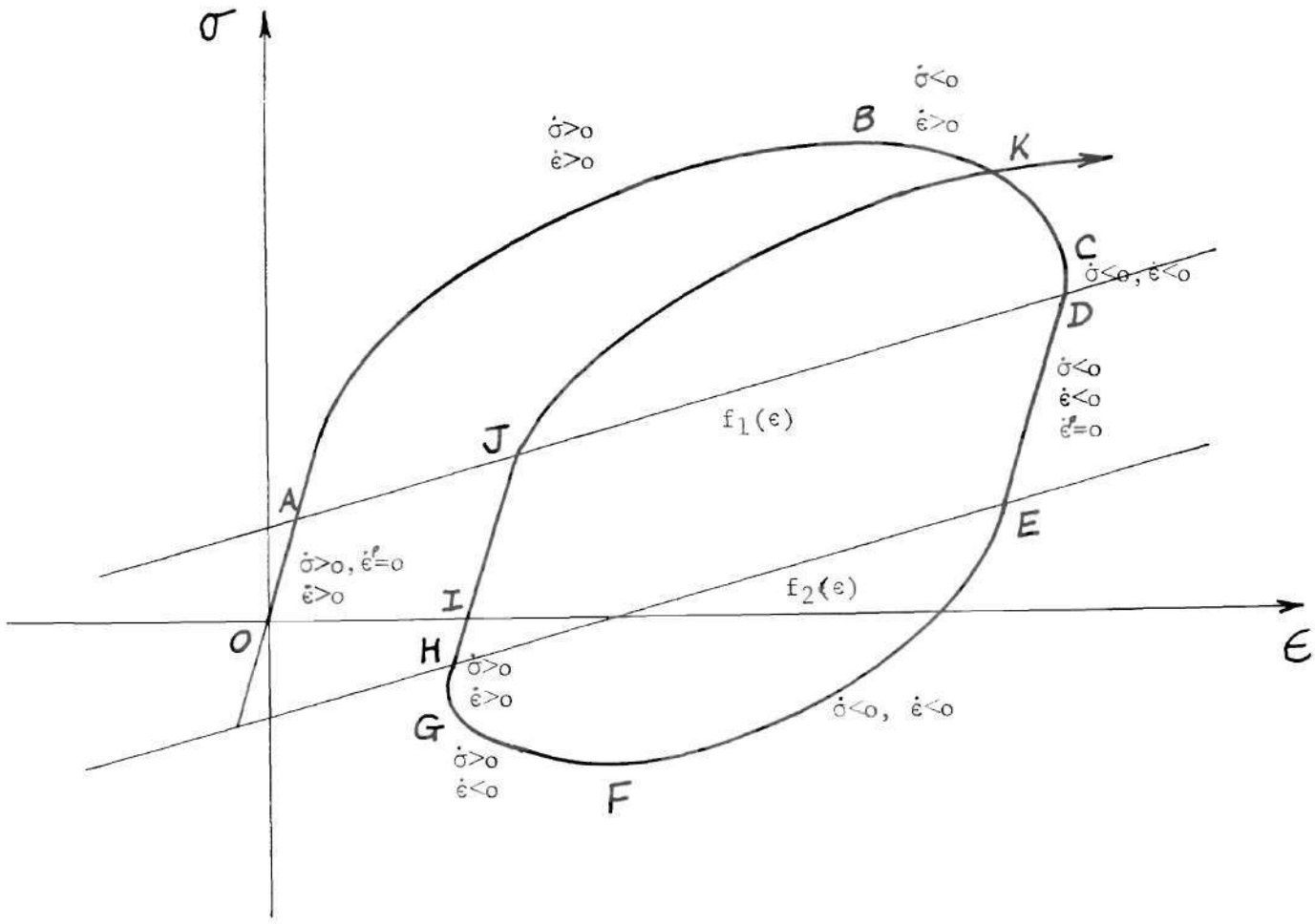

Figure 2-4. Dynamic Loading/Unloading Curve (with the Lower Yield and Bauschinger Effect).

if the amplitude of cyclic loading is so large that the dynamic stress-strain curve will alternate back and forth between upper and lower yield regions. It can also be seen that the size of this hysteresis loop will depend on the frequency of the cyclic stress for a specified material.

IV. Another Mechanical Model -- Without Lower Yield and the Bauschinger Effect

It should be pointed out that a second mechanical model, which is different from the one defined in last section by the failure of considering the lower yield and the Bauschinger effect, will be considered here. The purpose of introducing this model is purely for the achievement of a comparison between these two models. This second model had been used already by Cristescu [24], Lubliner [25], Wood and author [37] in their earlier works. The characteristic of this mechanical model can be expressed mathematically as,

$$E_o \frac{\partial \epsilon}{\partial t} = \frac{\partial \sigma}{\partial t} + \langle g(\sigma,\epsilon) \rangle \tag{2-18}$$

where

$$\langle g(\sigma,\epsilon) \rangle = \begin{cases} g_1(\sigma,\epsilon), & \text{for } \sigma > f_1(\epsilon) \\ 0, & \text{for } \sigma \leq f_1(\epsilon) \end{cases}$$

where $f_1(\epsilon)$ and $g_1(\sigma,\epsilon)$ are defined in equations (2-15) and (2-16). It is noted that the function $\langle g(\sigma,\epsilon) \rangle$ in equation (2-18) is deviated from the one in equation (2-17) only by the fact that $g_2(\sigma,\epsilon)$ is equal to zero in the lower yield region. A dynamic loading/unloading curve for this model can be shown in Figure (2-5).

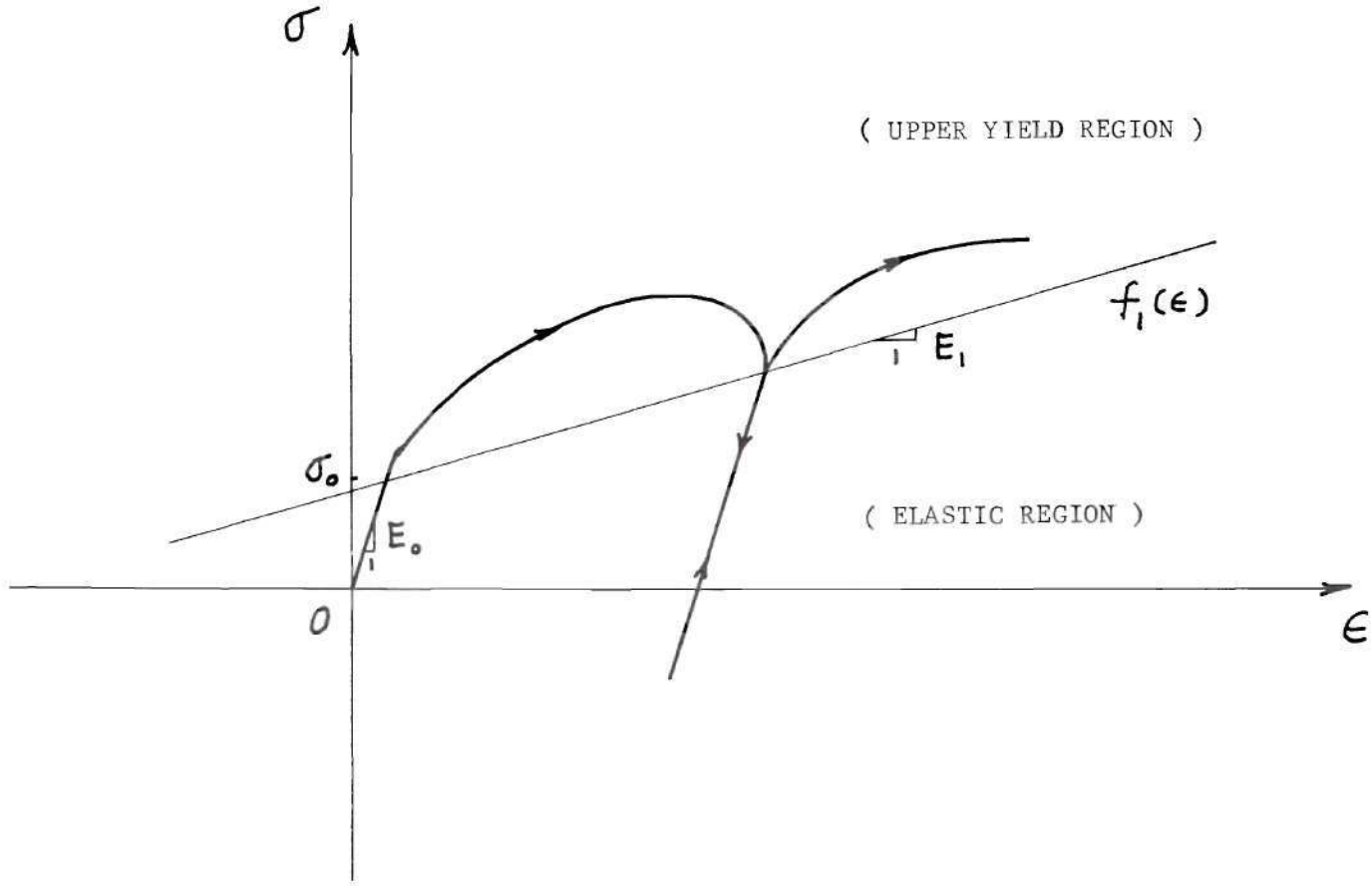

Figure 2-5. Dynamic Loading/Unloading Curve (without the Lower Yield and Bauschinger Effect).

From this figure, it is clear that the plastic hysteresis loop will no longer exist. This is due to the fact that the absence of the lower yield effect makes the trace of loading and unloading stay in the same line in both elastic and lower yield region of σ-ϵ plane.

V. Boundary Conditions and Initial Conditions

As stated in Section (I) of this chapter, the problem considered here is a homogeneous fixed-free bar, as shown in Fig. (2-6). The free end of the bar will be subjected to an axially applied oscillating load, (Fig. (2-7)), whose magnitude can be varied to well beyond the yield limit. In Fig. (2-6), ℓ is the bar's original length, x is the distance from the origin, where the origin represents the undisturbed position of the free end of the bar (Lagrangian coordinate description) and P(t) is the applied loading function. The function P(t), in Fig. (2-7) or $\sigma(t)$ as one wishes, at free end $x = 0$ is a sine function plus a constant. This can be also expressed as $\sigma(t)/\sigma_o = B + A \sin(\omega t)$ in dimensionless form, where σ_o represents the yield stress, ω is the loading frequency, A and B are loading parameters.

With this understanding, one can write the boundary conditions of the bar mathematically as follows, if one lets the applied stress $\sigma(t) = P(t)/A_0$,

(i) at free end:

$$\sigma(0,t) = \sigma(t) \qquad \text{for } t > 0 \tag{2-19}$$

(ii) at fixed end:

$$v(\ell,t) = 0 \qquad \text{for } t > 0 \tag{2-20}$$

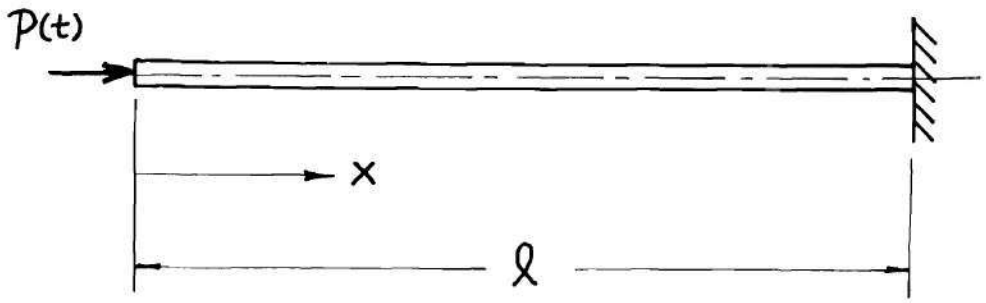

Figure 2-6. Geometric Configuration of a Fixed-Free Bar.

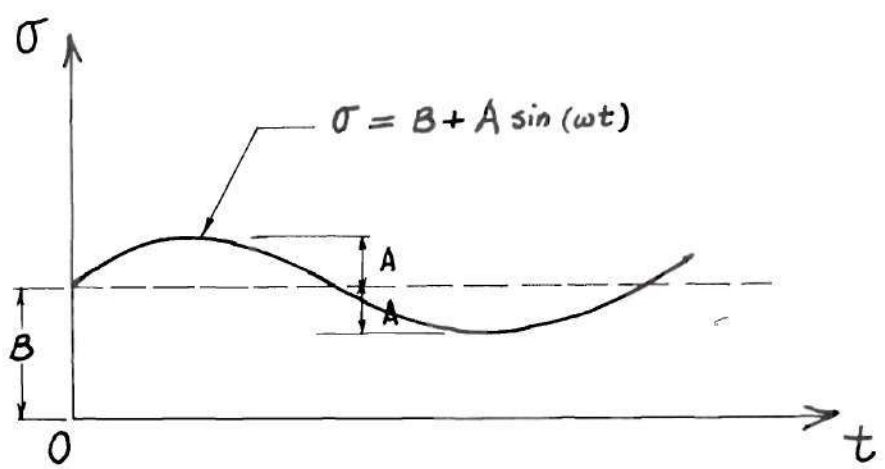

Figure 2-7. The Loading Function at the Free End.

It also should be pointed out that the strain $\epsilon(0,t)$ and velocity $v(0,t)$ at the free end, and the stress $\sigma(\ell,t)$ and strain $\epsilon(\ell,t)$ at the fixed end are all unknown quantities. Since the bar is initially at rest, the initial conditons can be prescribed as,

(iii) at $t = 0$,

$$\sigma(x,0) = \epsilon(x,0) = v(x,0) = 0 \quad \text{for } 0 \leq x \leq \ell \ . \tag{2-21}$$

VI. Summary

In conclusion, the analysis used in this dissertation for plastic waves in a fixed-free homogeneous bar under longitudinal cyclic stress will be based upon the following set of quasi-linear partial differential equations,

$$\frac{\partial \sigma}{\partial x} = \rho_o \frac{\partial v}{\partial t}$$

$$\frac{\partial \epsilon}{\partial t} = \frac{\partial v}{\partial x}$$

$$E_o \frac{\partial \epsilon}{\partial t} = \frac{\partial \sigma}{\partial t} + \langle g(\sigma,t) \rangle \tag{2-22}$$

where, the first is the equation of motion, the second is the kinematic equation and the third is the constitutive equation, and each are derived in the previous sections. Finding solutions of this set of equations with proper boundary and initial conditions as shown in section (V) will be discussed and presented in detail in the next chapter.

CHAPTER III

NUMERICAL SOLUTION

I. The Method of Solution

From the theoretical formulation of the last chapter, one arrives at the following set of quasi-linear partial differential equations for the propagation of elastic-plastic waves in solids by the rate-dependent theory.

$$\frac{\partial \sigma}{\partial x} = \rho_o \frac{\partial v}{\partial t}$$

$$\frac{\partial \varepsilon}{\partial t} = \frac{\partial v}{\partial x}$$

$$E_o \frac{\partial \varepsilon}{\partial t} = \frac{\partial \sigma}{\partial t} + \langle g(\sigma, \varepsilon) \rangle \qquad (3\text{-}1)$$

where

$$\langle g(\sigma,\varepsilon) \rangle \equiv \begin{cases} g_1(\sigma,\varepsilon) & \text{for} \quad \sigma > f_1(\varepsilon) \\ 0 & \text{for} \quad f_2(\varepsilon) \le \sigma \le f_1(\varepsilon) \\ g_2(\sigma,\varepsilon) & \text{for} \quad \sigma < f_2(\varepsilon) \end{cases}$$

where $g_1(\sigma,\varepsilon)$ and $g_2(\sigma,\varepsilon)$ are given as equations (2-15) and (2-16) in the last chapter. The above equations describe motion, kinematic and stress-strain behavior respectively. The equations involve two independent variables -- the Lagrangian spatial coordinate x and the time

t; and three dependent variables stress σ, strain ϵ and velocity v. This system of equations represents a hyperbolic type of quasi-linear partial differential equations. Observe that different partial differential equations are to be satisfied depending on whether the material is in the plastic or elastic state. These will be referred to later as plastic or elastic regions in the σ-ϵ plane. The state at any material point (or point in the bar) depends on the dependent variables σ and ϵ. This makes the problem complicated to solve since the regions of application of the different differential equations must be determined from instantaneous condition of the neighbouring points as the solution is developed. In plastic wave propagation only a limited number of closed-form solutions have been achieved and these are for special cases. However, it is well known from Malvern [12,13], Wood [22], and Hopkins [39], that numerical solutions can be obtained in solving a broad range of these problems using the method of characteristic. The method of characteristics will be employed in this dissertation as follows:

Combining equations (3-1) and reducing them to total differentials along characteristic lines, one obtains,

$$\text{on} \quad \frac{dx}{dt} = + c_o \; ; \qquad d\sigma - \rho_o c_o dv = - g(\sigma,\epsilon)dt$$

$$\text{on} \quad \frac{dx}{dt} = - c_o \; ; \qquad d\sigma + \rho_o c_o dv = - g(\sigma,\epsilon)dt$$

$$\text{on} \quad \frac{dx}{dt} = 0 \; ; \qquad E_o d\epsilon = d\sigma + g(\sigma,\epsilon)dt \qquad (3\text{-}2)$$

where $c_o = (E_o/\rho_o)^{\frac{1}{2}}$ represents the acoustic elastic wave speed.

The three families of characteristics are fixed families of parallel straight lines defined by the equations,

$$x - c_o t = \text{constant} ;$$

$$x + c_o t = \text{constant} ;$$

$$x = \text{constant} .$$

(see Fig. 3-1). These three families are designated C+, C- and C_o, respectively, and they correspond to particle paths and tracks of linear elastic disturbances. It is understood that an easier probelm results since the characteristics are fixed in the x-t plane and do not vary with the solution. However, equations (3-2) are still not analytically integrable. This is due to the presence of the nonlinearity of the stress-strain relation. Therefore numerical integration is required in obtaining a solution.

II. The Solution in the Network

The general method of analysis for initiating the numerical integration of equation (3-2) is discussed by Wood and Phillip [23]. A step-by-step finite difference solution is obtained throughout a network formed by the characteristics $\frac{dx}{dt} = \pm C_o$. (see Fig. 3-1). It is assumed that the net can be selected fine enough so that the interval may be approximated by trapezoidal rule. Based upon this assumption, it is important to note that any discontinuity, resulted from wave interactions of wave fronts and reflections at the boundaries will be smoothed out within a finite difference grid. Or more specifically, if the

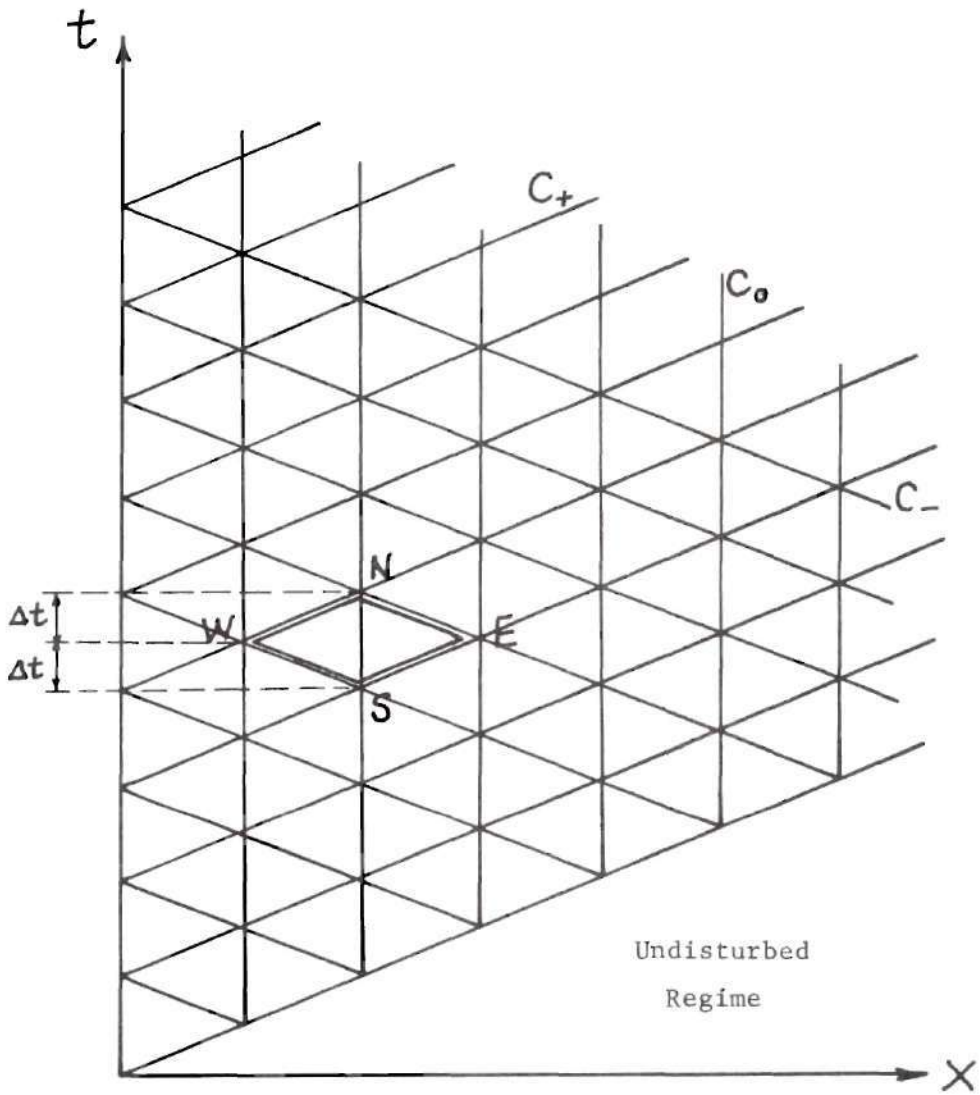

Figure 3-1. Characteristics Lines in x-t Plane.

finite difference grid is selected fine enough in the time interval, then a possible discontinuity in that interval can be replaced by putting in a straight line. As the selected interval approaches to zero as a limit, the discontinuity will reappear. This is an important aspect of using finite difference method in calculating the solution. Also, this answers the possible doubt of how complicated discontinuities are treated in plastic wave propagation problems with rate effects. It is also understood that one has the freedom to select the grid size as small as he wants. However, for the practical reason, the grid size should be determined according to the desired accuracy of the results and the economy of the digital computation.

Within a net, the total differentials of equation (3-2) resulted in the finite difference forms,

along $x = c_o t$:

$$\sigma_N - \sigma_W - \rho_o C_o (v_N - v_W) = - \frac{1}{2} (g_N + g_W) \Delta t$$

$$\sigma_E - \sigma_S - \rho_o C_o (v_E - v_S) = - \frac{1}{2} (g_E + g_S) \Delta t$$

along $x = - c_o t$:

$$\sigma_N - \sigma_E + \rho_o C_o (v_N - v_E) = - \frac{1}{2} (g_N + g_E) \Delta t$$

$$\sigma_W - \sigma_S + \rho_o C_o (v_W - v_S) = - \frac{1}{2} (g_W + g_S) \Delta t \qquad (3\text{-}3)$$

along x = constant:

$$E_o\epsilon_N - E_o\epsilon_S = \sigma_N - \sigma_S + \frac{1}{2}(g_N + g_S)(2\Delta t)$$

where E, W, N, S are referred as four locations in the x-t plane as shown in Fig. (3.1). These equations can be combined in such a way that an equation entirely in terms of stresses and $g(\sigma,\epsilon)$ is obtained, (refer to Fig. 3-1),

$$\sigma_N = \sigma_E + \sigma_W - \sigma_S - (g_N - g_S)\frac{\Delta t}{2} \tag{3-4}$$

or alternately stress may be eliminated and an equation written in terms of velocities and $g(\sigma,\epsilon)$;

$$v_N = v_E + v_W - v_S + \frac{1}{2\rho_o c_o}(g_W - g_E)\Delta t \quad . \tag{3-5}$$

The corresponding strain equation is given by the finite difference form of equation (3-3) also,

$$E_o\epsilon_N = E_o\epsilon_S + \sigma_N - \sigma_S + (g_N + g_S)\Delta t \quad . \tag{3-6}$$

Equations (3-4) through (3-6) provide the basic relations by which numerical integration is carried out in the network of the x-t plane for a given time interval Δt. Observe that to solve for stress, strain, and velocity at any point (designated here as the north point, N) in the x-t plane requires first obtaining solutions for three neighboring points (designated as east E, west W, and south point, S), see also Fig. (3-1). It should be emphasized that these relations are only valid for the proper value of $g(\sigma,\epsilon)$, to be chosen according to equation (2-17). For instance,

if the corresponding stress and strain of a south point happens to be in the lower yield region of Fig. (2-3), Chapter II, then the value of $g_S(\sigma,\epsilon)$ will take $g_2(\sigma,\epsilon)$. Because of this, the problem becomes complicated for calculations. One might question when one calculates the solution for the north point as to the proper value of $g(\sigma,\epsilon)$ to be used in g_E, g_W and g_S? However, the required information, which is needed from E,W, and S, in order to obtain the solution at N by equations (3-4), (3-5) and (3-6), can be determined since the solutions at these points are known.

Moreover, if one looks at these equations closely, one finds that those terms on the right-hand side of equations (3-4), (3-5), and (3-6) are not completely independent of σ_N and ϵ_N since $g_N = g_N(\sigma_N,\epsilon_N)$. In other words, what is the proper value for $g_N(\sigma,\epsilon)$ among the three values of $g_1(\sigma,\epsilon)$, 0, and $g_2(\sigma,\epsilon)$? Since we do not know σ_N and ϵ_N, therefore we don't know which region point N belongs to. Certainly there are only three possible answers to this question. First is $g_N(\sigma,\epsilon) = g_1(\sigma,\epsilon)$, second, $g_N(\sigma,t) = 0$, and third, $g_N(\sigma,\epsilon) = g_2(\sigma,\epsilon)$. However, there is no better way to select one from the three except by trial and error. For example, if the known south point S is located in upper yield region (see Fig. (2-3), last chapter). It is first to be assumed that the north point is also located in the upper yield region. But, there are also possibilities that the north point will be located in the elastic region if the south point is very close to the elastic-plastic boundary, or in the lower yield region if some kind of jump phenomenon exists (because of wave reflections or interactions). A logical method that involves trial and error to some degree has been developed in this

dissertation to make the proper selection possible. Here is how we handle the three possibilities: (a complete flow-diagram shown in Appendix A tells how solutions at the north point can be determined.) (i) Since the south point is in the upper yield region, a upper yield value of $g_1(\sigma,\varepsilon)$ is used to calculate the first trial values of stress and strain at the north point N for a given small increment of time. (ii) If these first calculated values of stress and strain at N turn out to be in the upper yield region, then these first calculated values are the true values of stress and strain at north. (iii) If these first calculated values of stress and strain turn out to be in the elastic region, this indicates that a situation of crossing regions occurs. This will be discussed in more detail in the next paragraph. (iv) If these first calculated values of stress and strain are found to be in the lower yield region, this means there is a large jump in stress and strain that occurs during a small time interval. Consequently, three values of $g(\sigma,\varepsilon)$, (g_1,o,g_2) should be used in the calculations but we have not yet determined how to divide the time interval into three corresponding subintervals. We do conclude that since the time interval in a single net $2\Delta t$ is too large, a smaller value of Δt must be used.

While to increase the accuracy of calculation with this finite difference method, a narrower grid size (smaller Δt,) would certainly do the job, it also means that more computing time and computer storage in the machine would be required. Thus, computer costs will quickly build up. But if one can find a way to reduce errors due to the finite difference method without narrowing the net size it will be of considerable help as far as accuracy is concerned.

We find that a source of major error is introduced when a wave crosses the elastic-plastic boundary. This was mentioned as the situation of crossing regions in the last paragraph. Refer to Fig. (3-2), and suppose the south point is in the upper yield region and the north point is in the elastic region. There are two ways of crossing the elastic-plastic boundary from S. First, following the elastic relations during the time interval $2\Delta t$ (i.e. use $g(\sigma,\epsilon) = 0$) one will get the north point at N_e in the stress-strain diagram of Fig. (3-2). Second, following the upper yield relation (i.e. $g(\sigma,\epsilon) = g_1(\sigma,\epsilon)$), one will obtain the north point at N_p. Obviously these two routes are not true, since the real path should pass through P and end at N. In order to avoid errors of this type, it was found by the author that a finer time interval should be used for grid sectors that contain an elastic-plastic boundary. Within such a grid, the time interval between S and N was subdivided into 20 subintervals, (see Fig. 3-3), and solutions of the resulting 400 points in the diamond shape sector were carried out to determine values at the north point. We observe that the known conditions are along the lines SW and SE, which can be interpolated by knowing solutions at points S,W,E and some previous points.

With this understanding to the problem, our interest here will be to find the finite difference solutions of stress σ, strain ϵ and velocity v in the network of the characteristic plane. Since the constitutive equation has three different forms for three different regions, it is advisable to divide the following derivations into three parts: (i) upper yield region, (ii) elastic region and (iii) low yield region.

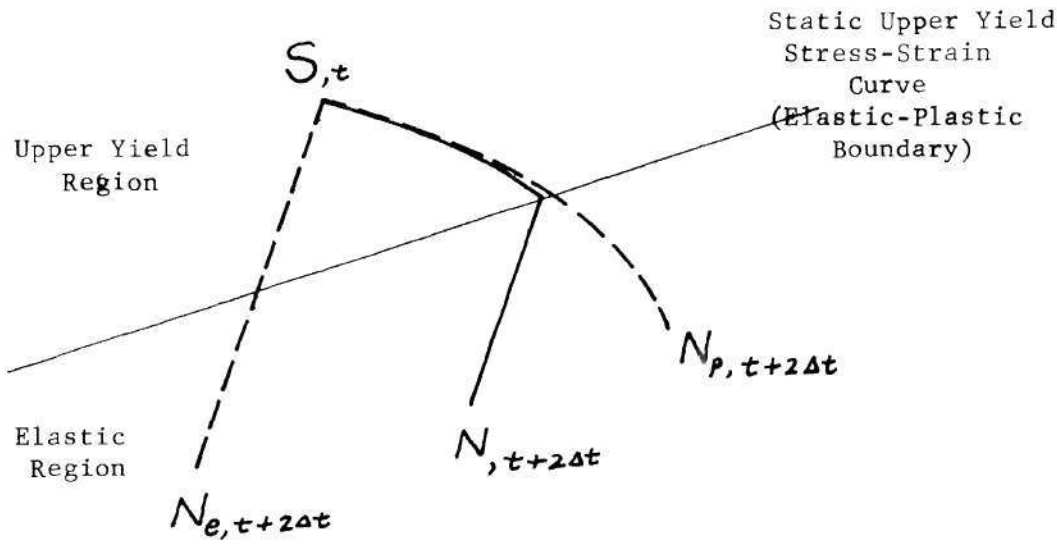

Figure 3-2. Elastic-Plastic Boundary at σ-ε Plane.

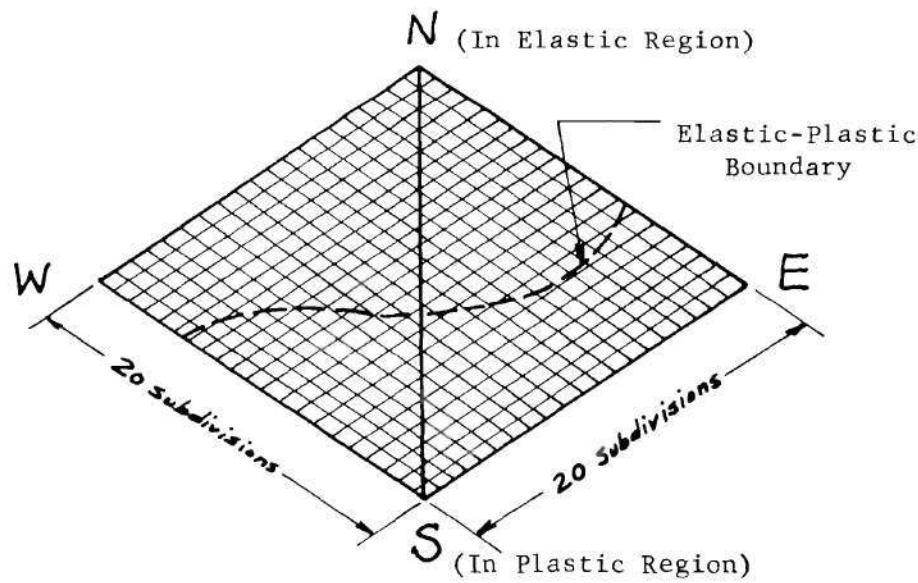

Figure 3-3. Elastic-Plastic Boundary within a Single Net of x-t Plane.

(A) Solutions in the Upper Yield Region

In the upper yield region, the function $g_1(\sigma,\epsilon)$ can be expressed,

$$g_1(\sigma,\epsilon) = k[\sigma - f_1(\epsilon)] = k \cdot H \tag{3-7}$$

where $f_1(\epsilon)$ defines the static upper yield stress and H defines the instantaneous dynamic over-stress in the upper yield region. It is assumed in this dissertation that a bilinear static upper yield stress-strain curve after that of Kolsky [38] is taken. Relating the static stress-strain diagram of Fig. (2-3), chapter II to equation (3-7), one observes that

$$f_1(\epsilon) = \sigma_o + E_1(\epsilon - \epsilon_o) \tag{3-8}$$

where σ_o and ϵ_o are yield stress and yield strain, E_1 is the slope of $f_1(\epsilon)$ on the static stress-strain diagram. With the substitution of equation (3-8) for equation (3-7) and also using the fact that $\sigma_o = E_o\epsilon_o$ one finds,

$$g_1(\sigma,\epsilon) = k\left[\sigma - \sigma_o\left(1 - \frac{E_1}{E_o}\right) - E_1\epsilon\right] = k\,H \quad . \tag{3-9}$$

On the other hand, equation (3-4), (3-5) and (3-6) can be written as,

$$\sigma_N = \sigma_W + \sigma_E - \sigma_S - \frac{k\Delta t}{2}(h_N - h_S) \tag{3-10}$$

$$v_N = v_W + v_E - v_S + \frac{k\Delta t}{2\rho_o c_o}(h_W - h_E) \tag{3-11}$$

and,

$$E_o\epsilon_N = E_o\epsilon_S + \sigma_N - \sigma_S + (h_S + h_N)k\Delta t \tag{3-12}$$

by using $g(\sigma,\epsilon) = hk$ and $h = \sigma - f(\epsilon)$, the dynamic over-stress. Since h has the dimension of stress and $g(\sigma,\epsilon)$ has the dimension of stress/time, therefore k, a material constant, should have a dimension of $(\text{time})^{-1}$. With both north and south points being located in the upper yield region, in these equations, $h_S = h_N = H$ and, h_W, and h_E are predetermined values since the solutions at W and E are known, then the above three equations yield,

$$\sigma_N = \sigma_W + \sigma_E - \sigma_S - \frac{k\Delta t}{2}(H_N - H_S) \tag{3-13}$$

$$v_N = v_W + v_E - v_S + \frac{k\Delta t}{2\rho_o C_o}(h_W - h_E) \tag{3-14}$$

$$E_o\epsilon_N = E_o\epsilon_S + \sigma_N - \sigma_S + (H_S + H_N)k\Delta t \tag{3-15}$$

where

$$H_N = \sigma_N - \sigma_o\left(1 - \frac{E_1}{E_o}\right) - E_1\epsilon_N \tag{3-16}$$

$$H_S = \sigma_S - \sigma_o\left(1 - \frac{E_1}{E_o}\right) - E_1\epsilon_S \quad . \tag{3-17}$$

Substituting equation (3-16) and (3-17) into equations (3-13), (3-14) and (3-15) results in the following three non-dimensional equations

$$\frac{\sigma_N}{\sigma_o} = \frac{\alpha\left(1 + \frac{E_1}{E_o}\, k\Delta t\right) + \beta\left(\frac{E_1}{E_o}\, \frac{k\Delta t}{2}\right)}{\gamma} \tag{3-18}$$

$$\frac{\epsilon_N}{\epsilon_o} = \frac{\alpha(1 + k\Delta t) + \beta\left(1 + \frac{k\Delta t}{2}\right)}{\gamma} \tag{3-19}$$

and,

$$\frac{v_N}{v_o} = \frac{v_W}{v_o} + \frac{v_E}{v_o} - \frac{v_S}{v_o} - \frac{k\Delta t}{2}\left(\frac{h_W}{\sigma_o} - \frac{h_E}{\sigma_o}\right) \tag{3-20}$$

where,

$$\alpha = \frac{\sigma_W}{\sigma_o} + \frac{\sigma_E}{\sigma_o} - \frac{\sigma_S}{\sigma_o} + \frac{H_S}{\sigma_o}\, \frac{k\Delta t}{2} + \left(1 - \frac{E_1}{E_o}\right) \frac{k\Delta t}{2} \tag{3-21}$$

$$\beta = \frac{\epsilon_S}{\epsilon_o} - \frac{\sigma_S}{\sigma_o} + \frac{H_S}{\sigma_o}\, k\Delta t - \left(1 - \frac{E_1}{E_o}\right) k\Delta t \tag{3-22}$$

$$\gamma = 1 + \frac{1}{2}\, k\Delta t + \frac{1}{2}\, \frac{E_1}{E_o}\, k\Delta t$$

and v_o defines $-\sigma_o/(\rho_o c_o)$, where $k\Delta t$ is the incremental time in dimensionless form. Equations (3-18) through (3-20) are the non-dimensional solutions of stress, strain and velocity referred to the north point N. It is clear that all terms on the right hand side of these three equations may be predetermined.

(B) Solutions in the Elastic Region

A relatively simple case is that when $g_N(\sigma,\epsilon)$ and $g_S(\sigma,\epsilon)$ take the value of zero in the elastic region. For this case the following solutions

result from equations (3-4), (3-5) and (3-6),

$$\frac{\sigma_N}{\sigma_o} = \frac{\sigma_W}{\sigma_o} + \frac{\sigma_E}{\sigma_o} - \frac{\sigma_S}{\sigma_o} \tag{3-23}$$

$$\frac{\epsilon_N}{\epsilon_o} = \frac{\epsilon_S}{\epsilon_o} + \frac{\sigma_N}{\sigma_o} - \frac{\sigma_S}{\sigma_o}$$

$$= \frac{\epsilon_S}{\epsilon_o} + \frac{\sigma_W}{\sigma_o} + \frac{\sigma_E}{\sigma_o} - 2\frac{\sigma_S}{\sigma_o} \tag{3-24}$$

and,

$$\frac{v_N}{v_o} = \frac{v_W}{v_o} + \frac{v_E}{v_o} - \frac{v_S}{v_o} - \frac{k\Delta t}{2}\left(\frac{h_W}{\sigma_o} - \frac{h_E}{\sigma_o}\right) \quad . \tag{3-25}$$

An alternate form for velocity can be written as,

$$\frac{v_N}{v_o} = \frac{v_S}{v_o} + \frac{\sigma_W}{\sigma_o} - \frac{\sigma_E}{\sigma_o} \quad . \tag{3-26}$$

This certainly proves that the equality between equation (3-25) and (3-26) holds true.

(C) Solutions in the Lower Yield Region

A similar case to that shown in the upper yield region occurs in the lower yield region function f_2 is defined

$$f_2(\epsilon) = -\sigma_o + E_1(\epsilon + \epsilon_o) \tag{3-27}$$

and results in,

$$g_2(\sigma,\epsilon) = k[\sigma - f_2(\epsilon)]$$

$$= k\left[\sigma + \sigma_o\left(1 - \frac{E_1}{E_o}\right) - E_1\epsilon\right]$$

$$= k\,\bar{H} \tag{3-28}$$

where $f_2(\epsilon)$ defines the static lower yield stress and $\bar{H}$ defines the instantaneous dynamic under stress in the lower yield region. ($\bar{H}$ to be bounded by $\bar{H} \leq 0$). Therefore similar to equations (3-13) through (3-17) one obtains

$$\sigma_N = \sigma_W + \sigma_E - \sigma_S - \frac{k\Delta t}{2}\,(\bar{H}_N - \bar{H}_S) \tag{3-29}$$

$$v_N = v_W + v_E - v_S + \frac{k\Delta t}{2\rho_o c_o}\,(h_W - h_E) \tag{3-30}$$

$$E_o\epsilon_N = E_o\epsilon_S + \sigma_N - \sigma_S + (\bar{H}_S + \bar{H}_N)k\Delta t \tag{3-31}$$

where,

$$\bar{H}_N = \sigma_N + \sigma_o\left(1 - \frac{E_1}{E_o}\right) - E_1\epsilon_N \tag{3-32}$$

$$\bar{H}_S = \sigma_S + \sigma_o\left(1 - \frac{E_1}{E_o}\right) - E_1\epsilon_S\ . \tag{3-33}$$

Substituting equation (3-32) and (3-33) into equation (3-29), (3-30) and (3-31) the following set of equations results in dimensionless form,

$$\frac{\sigma_N}{\sigma_o} = \frac{\bar{\alpha}\left(1 + \frac{E_1}{E_o}\,k\Delta t\right) + \bar{\beta}\left(\frac{E_1}{E_o}\,\frac{k\Delta t}{2}\right)}{\gamma} \tag{3-34}$$

$$\frac{\epsilon_N}{\epsilon_o} = \frac{\bar{\alpha}(1 + k\Delta t) + \bar{\beta}\left(1 + \frac{k\Delta t}{2}\right)}{\gamma} \tag{3-35}$$

$$\frac{v_N}{v_o} = \frac{v_W}{v_o} + \frac{v_E}{v_o} - \frac{v_S}{v_o} - \frac{k\Delta t}{2}\left(\frac{h_W}{\sigma_o} - \frac{h_E}{\sigma_o}\right) \tag{3-36}$$

where,

$$\bar{\alpha} = \frac{\sigma_W}{\sigma_o} + \frac{\sigma_E}{\sigma_o} - \frac{\sigma_S}{\sigma_o} + \frac{\bar{H}_S}{\sigma_o}\frac{k\Delta t}{2} - \left(1 - \frac{E_1}{E_o}\right)\frac{k\Delta t}{2} \tag{3-37}$$

$$\bar{\beta} = \frac{\epsilon_S}{\epsilon_o} - \frac{\sigma_S}{\sigma_o} + \frac{\bar{H}_S}{\sigma_o} k\Delta t + \left(1 - \frac{E_1}{E_o}\right)k\Delta t \quad . \tag{3-38}$$

Equations (3-18), (3-19), (3-20), (3-23), (3-24), (3-25) and (3-34), (3-35), (3-36) provide the basic form of solution in the x-t plane. Numerical integration can therefore be carried out for a specified time increment $k\Delta t$ (time interval) with all the solutions of three neighboring points E, W, S known.

As was indicated in Wood's work [22], in order to initiate the solution in the x-t plane it is first necessary to apply boundary conditions along the $x = c_o t$ (wave front), $x = 0$ and $x = \ell$ axis. Corresponding derivations and calculations are given in the next three sections.

III. Solution Along the $x = c_o t$ (Wave Front Axis)

Fig. (3-4) illustrates the geometric relation between the characteristic lines $x = c_o t$ and $x = -c_o t$. We understand that any solution along $x = c_o t$ in the x-t plane implies the intersection points of line $x = c_o t$ and a family of lines of $x = -c_o t$ (as line ab in Fig. (3-4). Following the work of Wood [22] for the derivation of the solution

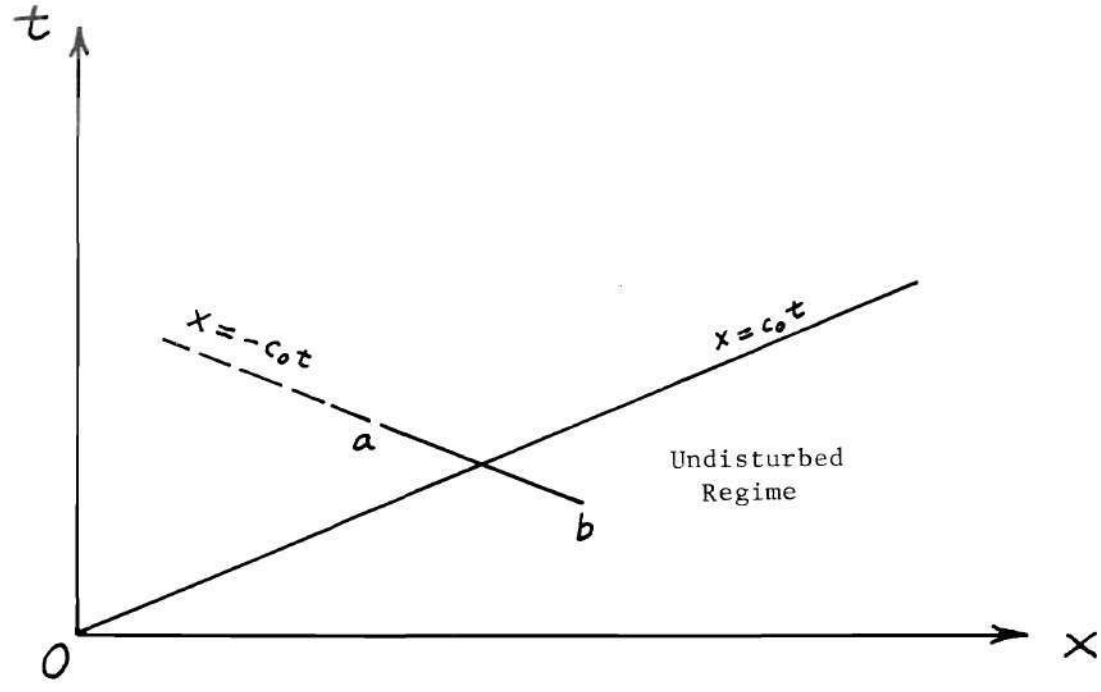

Figure 3-4. Initial Wave Front on x-t Plane.

along $x = c_o t$ we have the following set of equations:

$$\int_p^{\sigma} \frac{d\sigma}{g(\sigma)} = \int_o^t -\frac{1}{2}\, dt \tag{3-37}$$

$$\frac{\varepsilon}{\varepsilon_o} = \frac{\sigma}{\sigma_o} \tag{3-38}$$

$$\frac{v}{v_o} = \frac{\sigma}{\sigma_o} \quad . \tag{3-39}$$

Equation (3-37) gives the solution of stress along $x = c_o t$. To complete the integration of equation (3-37), it is required to know the value of P, the initially applied load at $x = 0$. The corresponding $g(\sigma)$ can be expressed separately as,

$$g_1(\sigma) = k\left[\sigma-\sigma_o\left(1 - \frac{E_1}{E_o}\right) - E_1\varepsilon\right] = k\left[(\sigma-\sigma_o)\left(1 - \frac{E_1}{E_o}\right)\right], \quad \text{for } \sigma > \sigma_o$$

$$g(\sigma) = 0, \qquad \text{for } -\sigma_o \le \sigma \le \sigma_o$$

$$g_2(\sigma) = k\left[\sigma+\sigma_o\left(1 + \frac{E_1}{E_o}\right) - E_1\varepsilon\right] = k\left[(\sigma+\sigma_o)\left(1 - \frac{E_1}{E_o}\right)\right], \quad \text{for } \sigma < -\sigma_o \quad . \tag{3-40}$$

Substituting equation (3-40) into equation (3-37) and integrating, one arrives at the following solution for stress,

$$\frac{\sigma}{\sigma_o} = \begin{cases} 1 + \left(\frac{P}{\sigma_o} - 1\right)\exp\left[-\frac{1}{2}\left(1 - \frac{E_1}{E_o}\right)k\Delta t\right], & \text{for } \sigma > \sigma_o \\ \frac{P}{\sigma_o}, & \text{for } -\sigma_o \le \sigma \le \sigma_o \\ -1 + \left(\frac{P}{\sigma_o} + 1\right)\exp\left[-\frac{1}{2}\left(1 - \frac{E_1}{E_o}\right)k\Delta t\right], & \text{for } \sigma < -\sigma_o \quad . \end{cases} \tag{3-41}$$

Equations (3-41), (3-38), and (3-39) provide all possible solutions along $x = c_o t$.

IV. Solutions at the x = 0 (Free End)

At x = 0, the stress is prescribed as a function of time by the boundary condition. Therefore the third equation of equations (3-1) can be reduced to an ordinary differential equation with dependent variable ε and independent variable, the time t,

$$E_o \frac{d\varepsilon}{dt} = \left(\frac{d\sigma}{dt}\right)_{\text{prescribed}} + \langle g(\sigma,\varepsilon)\rangle \tag{3-42}$$

where,

$$\langle g(\sigma,\varepsilon)\rangle = \begin{cases} g_1(\sigma,\varepsilon) , & \text{for } \sigma > f_1(\varepsilon) \\ 0 , & \text{for } f_2(\varepsilon) \le \sigma \le f_1(\varepsilon) \\ g_2(\sigma,\varepsilon) , & \text{for } \sigma < f_2(\varepsilon) \end{cases} .$$

It is more convenient if one transfers this equation into a non-dimensional form as

$$\frac{d\left(\frac{\varepsilon}{\varepsilon_o}\right)}{d(kt)} = \frac{d\left(\frac{\sigma}{\sigma_o}\right)}{d(kt)} + \left[\left(\frac{\sigma}{\sigma_o}\right) - 1 - \left(\frac{E_1}{E_o}\right)\left(\frac{\varepsilon}{\varepsilon_o} - 1\right)\right] , \quad \text{for } \sigma > f_1(\varepsilon) \tag{3-43}$$

$$\frac{d\left(\frac{\varepsilon}{\varepsilon_o}\right)}{d(kt)} = \frac{d\left(\frac{\sigma}{\sigma_o}\right)}{d(kt)} , \quad \text{for } f_2(\varepsilon) \le \sigma \le f_1(\varepsilon) \tag{3-44}$$

$$\frac{d\left(\frac{\varepsilon}{\varepsilon_o}\right)}{d(kt)} = \frac{d\left(\frac{\sigma}{\sigma_o}\right)}{d(kt)} + \left[\left(\frac{\sigma}{\sigma_o}\right) + 1 - \left(\frac{E_1}{E_o}\right)\left(\frac{\varepsilon}{\varepsilon_o} + 1\right)\right] , \quad \text{for } \sigma < f_2(\varepsilon) . \tag{3-45}$$

Before one tries to solve these equations for $\frac{\epsilon}{\epsilon_o}$ in each corresponding region, it should be noted that the equations hold true during any time interval. In the very general case, one may set up a time axis as shown in Fig. (3-5). Here, t is referred to the time axis beginning at the instant of each intersection point on the elastic-plastic boundary and t′ measures total time.

By doing this, a compatible and continuous relationship between successive solutions for each time interval can be obtained.

The function $\frac{\sigma}{\sigma_o}$ was defined in the last Chapter as

$$\frac{\sigma}{\sigma_o} = \bar{B} + \bar{A} \sin[\bar{\omega}(kt')] = \bar{B} + \bar{A} \sin[\bar{\omega}k(t_m + t)] \qquad (3\text{-}46)$$

where $\bar{A}$, $\bar{B}$, and $\bar{\omega}$ represent non-dimensional quantities with $\bar{\omega}$ being the input non-dimensional frequency. The time derivative of $\frac{\sigma}{\sigma_o}$ yields,

$$\frac{d}{d(kt)}\left(\frac{\sigma}{\sigma_o}\right) = \bar{\omega}\,\bar{A} \cos[\bar{\omega}k(t_m + t)] \quad . \qquad (3\text{-}47)$$

Substituting equation (3-47) into equations (3-43), (3-44) and (3-45) and solving one obtains correspondingly,

$$\frac{\epsilon}{\epsilon_o} = \begin{cases} C_1 \exp(-\bar{E}kt) + \left[\frac{\bar{A}\bar{\omega}}{\bar{E}}\left(1 - \frac{\bar{E}+\bar{\omega}^2}{\bar{E}^2+\bar{\omega}^2}\right)\right]\cos\bar{\omega}kt' + \bar{A}\left(\frac{\bar{E}+\bar{\omega}^2}{\bar{E}^2+\bar{\omega}^2}\right)\sin\omega\, kt' - \left(\frac{1-\bar{E}-\bar{B}}{\bar{E}}\right) \\ \qquad\qquad \text{for } \sigma > \sigma_o \qquad (3\text{-}48) \\ C_2 + \bar{A} \sin[\bar{\omega}kt'] \qquad\qquad \text{for } -\sigma_o \le \sigma \le \sigma_o \qquad (3\text{-}49) \\ C_3 \exp(-\bar{E}kt) + \left[\frac{\bar{A}\bar{\omega}}{\bar{E}}\left(1 - \frac{\bar{E}+\bar{\omega}^2}{\bar{E}^2+\bar{\omega}^2}\right)\right]\cos\bar{\omega}kt' + \bar{A}\left(\frac{\bar{E}+\bar{\omega}^2}{\bar{E}^2+\bar{\omega}^2}\right)\sin\omega\, kt' - \left(\frac{\bar{E}-\bar{B}-1}{\bar{E}}\right) \\ \qquad\qquad \text{for } \sigma < -\sigma_o \qquad (3\text{-}50) \end{cases}$$

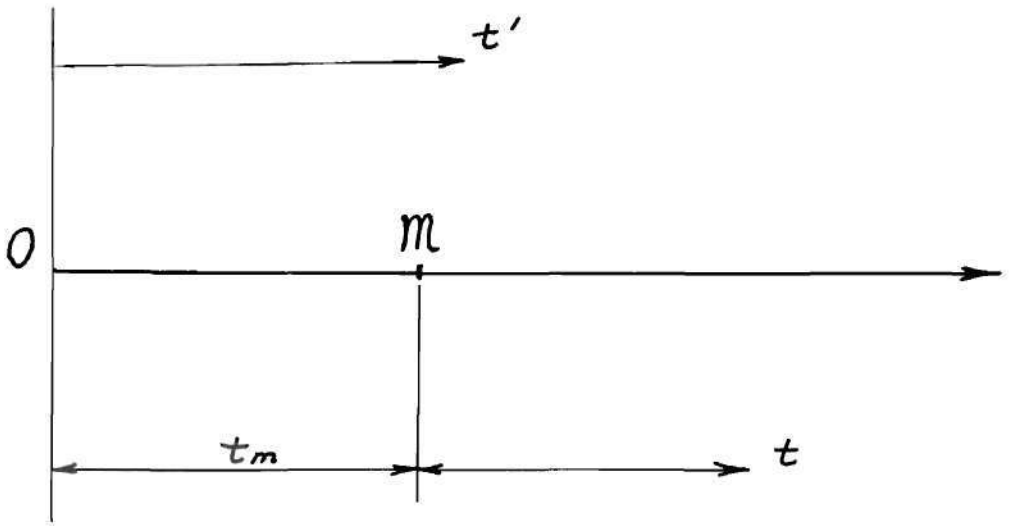

Figure 3-5. The Time-Axis.

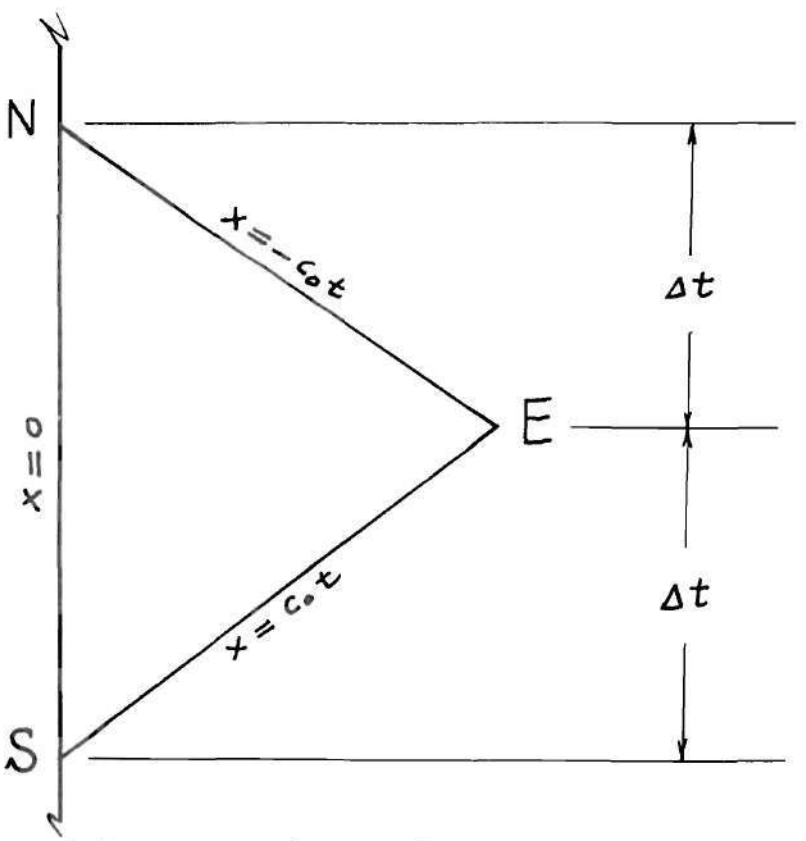

Figure 3-6. A Typical Triangle Net Near the Free End on x-t Plane.

where C_1, C_2 and C_3 are integration constants and $\bar{E} = \frac{E_1}{E_o}$. In determining these constants, the condition used here is $\frac{\epsilon}{\epsilon_o} = \frac{\epsilon_m}{\epsilon_o}$ as $t = 0$ or $t' = t_m$, where $\frac{\epsilon_m}{\epsilon_o}$ represents the value of strain at the elastic-plastic boundary. After the constants are found the final solution along $x = 0$ becomes

$$\frac{\epsilon}{\epsilon_o} = \begin{cases} \left\{\frac{\epsilon_m}{\epsilon_o} - \left[\frac{\bar{A}\bar{\omega}}{\bar{E}}\left(1 - \frac{\bar{E}+\bar{\omega}^2}{\bar{E}^2+\bar{\omega}^2}\right)\right]\cos(\bar{\omega}kt_m) - \bar{A}\left(\frac{\bar{E}+\bar{\omega}^2}{\bar{E}^2+\bar{\omega}^2}\right)\sin(\bar{\omega}kt_m)\right. \\ \qquad \left. + \left(\frac{1-\bar{E}-\bar{B}}{\bar{E}}\right)\right\}\exp(-\bar{E}kt) + \left[\frac{\bar{A}\bar{\omega}}{\bar{E}}\left(1 - \frac{\bar{E}+\bar{\omega}^2}{\bar{E}^2+\bar{\omega}^2}\right)\right]\cos(\bar{\omega}kt') \\ \qquad + \bar{A}\left(\frac{\bar{E}+\bar{\omega}^2}{\bar{E}^2+\bar{\omega}^2}\right)\sin(\bar{\omega}kt') - \left(\frac{1-\bar{E}-\bar{B}}{\bar{E}}\right) \quad \text{for } \sigma > \sigma_o \qquad (3\text{-}51) \\ \bar{B} + \bar{A}\sin(\bar{\omega}kt') = \frac{\sigma}{\sigma_o} \quad \text{for } -\sigma_o \le \sigma \le \sigma_o \qquad (3\text{-}52) \\ \left\{\frac{\epsilon_m}{\epsilon_o} - \left[\frac{\bar{A}\bar{\omega}}{\bar{E}}\left(1 - \frac{\bar{E}+\bar{\omega}^2}{\bar{E}^2+\bar{\omega}^2}\right)\right]\cos(\bar{\omega}kt_m) - \bar{A}\left(\frac{\bar{E}+\bar{\omega}^2}{\bar{E}^2+\bar{\omega}^2}\right)\sin(\bar{\omega}kt_m)\right. \\ \qquad \left. + \left(\frac{\bar{E}-\bar{B}-1}{\bar{E}}\right)\right\}\exp(-\bar{E}kt) + \left[\frac{\bar{A}\bar{\omega}}{\bar{E}}\left(1 - \frac{\bar{E}+\bar{\omega}^2}{\bar{E}^2+\bar{\omega}^2}\right)\right]\cos(\omega kt') \\ \qquad + \bar{A}\left(\frac{\bar{E}^2+\bar{\omega}^2}{\bar{E}^2+\bar{\omega}^2}\right)\sin(\bar{\omega}kt') - \left(\frac{\bar{E}-\bar{B}-1}{\bar{E}}\right) \quad \text{for } \sigma < -\sigma_o \,. \qquad (3\text{-}53) \end{cases}$$

It should be remarked that equations (3-51) through (3-53) represent the analytical solution for strain along $x = 0$. Adding this to the boundary condition of prescribed stress, the only unknown is velocity. Since no closed form solution can be found for velocity, one applies numerical integration by the finite difference method on the characteristic plane. In order to understand how this numerical integration is carried out along $x = 0$, we examine a typical triangular net which appears

in the neighborhood of the axis x = 0 as shown in Fig. (3-6). Point S (south) and E (east) are two previous points where the solutions are known. At the north point N, stress is given by the prescribed boundary condition and strain can be calculated by one of the equations (3-51), (3-52) and (3-53). From equation (3-3), combining the corresponding equations between SE and NE and eliminating $g_E(\sigma,\varepsilon)$, one has

$$v_N = v_S - \frac{1}{\rho_o c_o}\left[\sigma_N - 2\sigma_E + \sigma_S + \frac{1}{2}(g_N - g_S)\Delta t\right] \tag{3-54}$$

or in dimensionless form, (using the fact that $g(\sigma,\varepsilon) = k\cdot h(\sigma,\varepsilon)$)

$$\frac{v_N}{v_o} = \frac{v_S}{v_o} + \frac{\sigma_N}{\sigma_o} - 2\frac{\sigma_E}{\sigma_o} + \frac{\sigma_S}{\sigma_o} + \frac{1}{2}\left(\frac{h_N}{\sigma_o} - \frac{h_S}{\sigma_o}\right)(k\Delta t) \tag{3-55}$$

where h_N and h_S are known functions because the arguments of these functions, stresses and strains, are precalculated. In order to put equation (3-55) into a readily used form, the expressions for $h(\sigma,\varepsilon)$'s are substituted into the equation. From this a solution for velocity $\frac{v_N}{v_o}$ results,

$$\frac{v_N}{v_o} = \frac{v_S}{v_o} + \frac{\sigma_N}{\sigma_o} - \frac{2\sigma_E}{\sigma_o} + \frac{\sigma_S}{\sigma_o} + \frac{k\Delta t}{2}\langle D\rangle \tag{3-56}$$

where D takes the following values

(i) Both N and S are in the upper yield region, or both in the lower region:

$$\langle D\rangle = \frac{\sigma_N}{\sigma_o} - \frac{\sigma_S}{\sigma_o} - \frac{E_1}{E_o}\frac{\varepsilon_N}{\varepsilon_o} + \frac{E_1}{E_o}\frac{\varepsilon_S}{\varepsilon_o} \quad .$$

(ii) Both N and S are in the elastic region:

$$\langle D \rangle = 0 \quad .$$

(iii) S is in the upper or lower yield region but N is in the elastic region:

$$\langle D \rangle = - \frac{\sigma_S}{\sigma_o} + \frac{E_1}{E} \frac{\epsilon_S}{\epsilon_o} \quad .$$

(iv) N is in the upper or lower yield regions but N is in the elastic region:

$$\langle D \rangle = \frac{\sigma_N}{\sigma_o} - \frac{E_1}{E_o} \frac{\epsilon_N}{\epsilon_o} \quad .$$

V. Solutions at $x=\ell$ (fixed end)

The boundary condition requires that the velocity be zero at the fixed end in the entire time domain. This leaves the unknowns, stress $\sigma(\ell,t)$ and strain $\epsilon(\ell,t)$, to be determined. From equation (3-1) we are unable to find an analytical solution along $x=\ell$. Numerical integration in the characteristic net is then required to obtain the solution of stress and strain along $x=\ell$. Before one begins to find the solution, it is helpful to study Fig. (3-7) in order to understand the initial and subsequent wave reflections in a finite bar. This figure was taken from previous work by Wood and the author [37].

In initiating the solutions of stress and strain at $x=\ell$, one finds that the derivation should be presented in two parts: (A) The solution

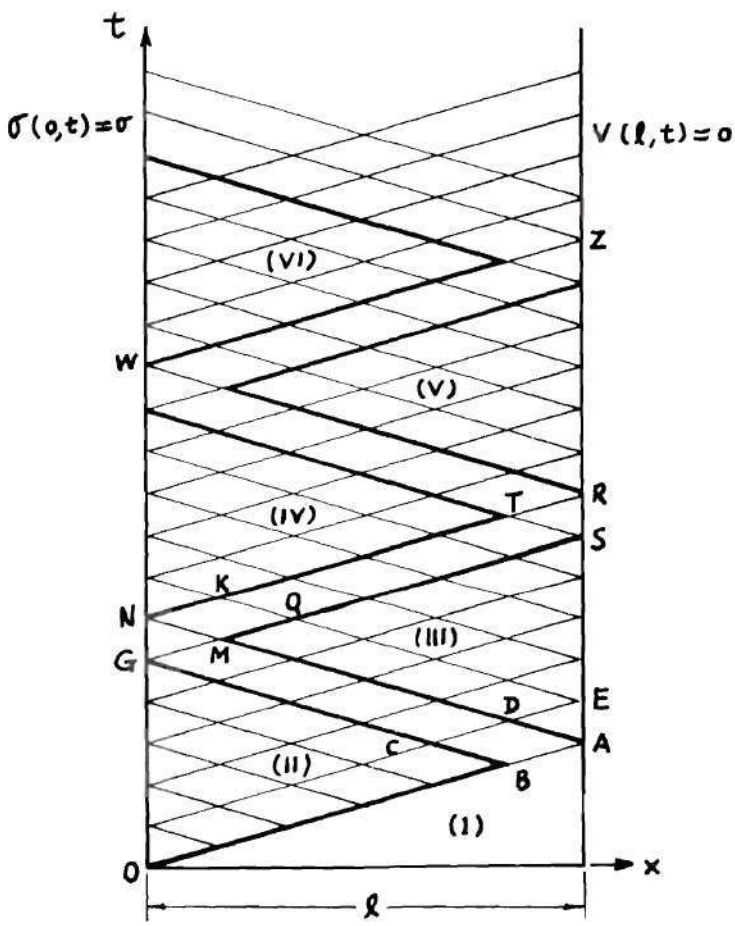

Figure 3-7. Characteristic Diagram Showing Method of Analysis for Wave Reflections.

when the stress wave just arrive at the wall (point A in Figure (3-7)).

(B) The solution at subsequent time.

(A). The Solution When the Stress Wave Just Arrive:

Fig. (3-8) shows point A on the x-t plane along with neighboring points S, W, and N. (Point A may also be considered as point E).

It is clear from equation (3 - 3) that, along the initial wave front, $x = c_o t$, one has a finite difference equation of the following form

$$\sigma_E - \sigma_S - \rho_o c_o (v_E - v_S) = -\frac{1}{2}(g_E + g_S)\Delta t \quad . \tag{3-57}$$

Introducing the boundary condition ($v_E = 0$), this becomes,

$$\sigma_E - \sigma_S + \rho_o c_o v_S = -\frac{1}{2}(g_E + g_S)\Delta t \quad . \tag{3-58}$$

From Section (III) of this chapter the stress-strain relation is seen to be elastic across the initial wave front $x = c_o t$. Thus,

$$\sigma_E = E_o \epsilon_E \quad . \tag{3-59}$$

Non-dimensionalizing and substituting between equations (3-58) and (3-59) we obtain with the proper selection of $g(\sigma,\epsilon)$, the following set of equations for stress, strain, and velocity at point A.

$$\frac{\sigma}{\sigma_o} = \begin{cases} \left(\frac{\sigma_S}{\sigma_o} + \frac{V_S}{V_o} + \frac{k\Delta t}{2} \cdot \alpha_1\right) \Big/ \delta & \text{for } \sigma_S > \sigma_o \\ \frac{\sigma_S}{\sigma_o} + \frac{V_S}{V_o} & \text{for } -\sigma_o \le \sigma_S \le \sigma_o \\ \left(\frac{\sigma_S}{\sigma_o} + \frac{V_S}{V_o} + \frac{k\Delta t}{2} \cdot \alpha_2\right) \Big/ \delta & \text{for } \sigma_S < -\sigma_o \end{cases} \tag{3-60}$$

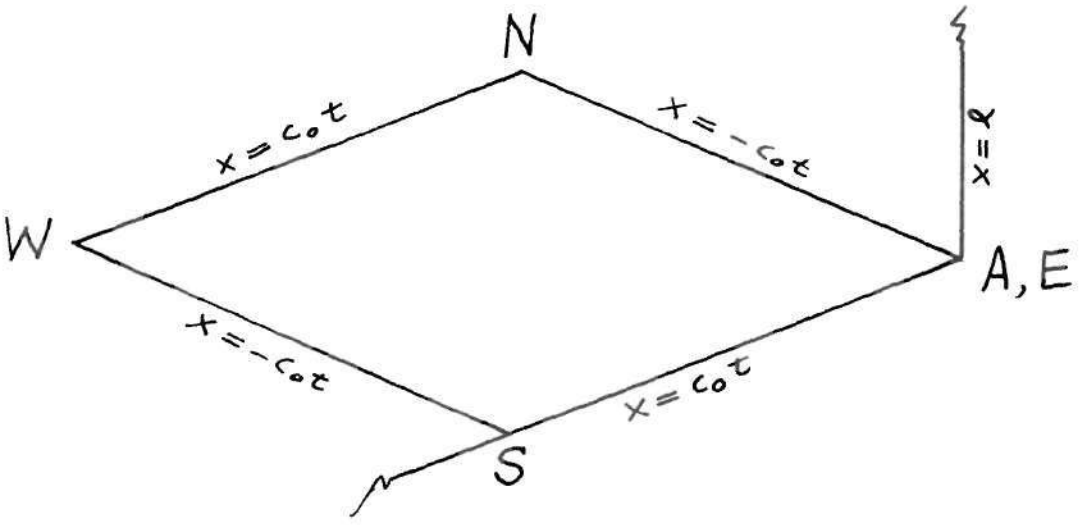

Figure 3-8. A Typical Characteristic Net Near the Fixed End on x-t Plane for Showing the Wave First Reaches Fixed End.

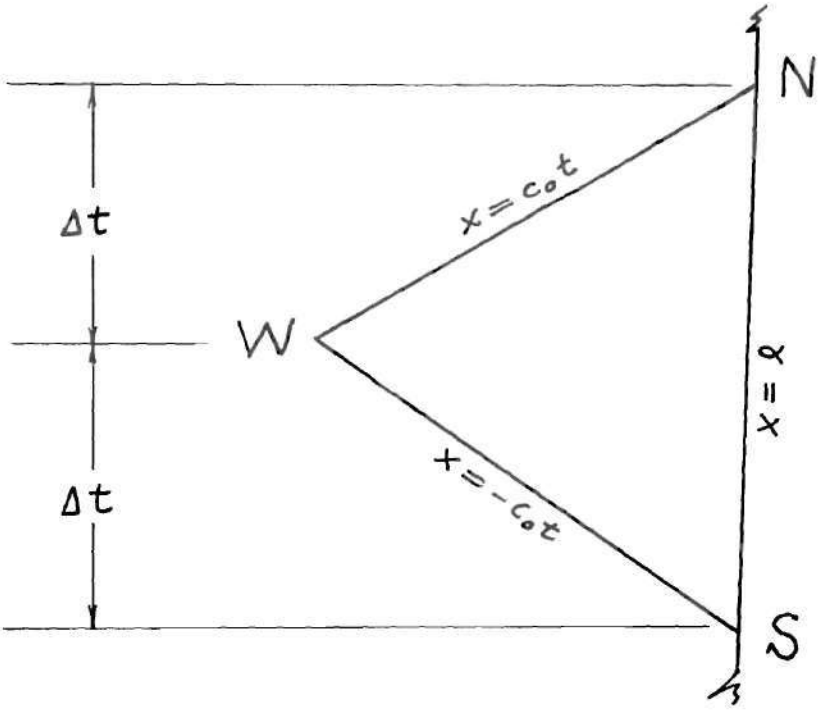

Figure 3-9. A Typical Triangle Net Near Fixed End on x-t Plane.

$$\frac{\epsilon}{\epsilon_o} = \frac{\sigma}{\sigma_o}$$

$$\frac{v}{v_o} = \frac{\sigma}{\sigma_o}$$

where

$$\alpha_1 = 2 - 2\frac{E_1}{E_o} - \frac{\sigma_S}{\sigma_o} + \frac{E_1}{E_o}\frac{\epsilon_S}{\epsilon_o} ,$$

$$\alpha_2 = 2\frac{E_1}{E_o} - 2 - \frac{\sigma_S}{\sigma_o} + \frac{E_1}{E_o}\frac{\epsilon_S}{\epsilon_o} ,$$

$$\delta = 1 + \frac{1}{2}k\Delta t - \frac{1}{2}k\Delta t\frac{E_1}{E_o} .$$

(B). The Solution at Subsequent Time at $x = \ell$:

One observes from Fig. (3-7) that a triangular shaped net composed of neighboring points forms the finite difference solutions at any later time after the wave has arrived at the wall. From Fig. (3-9), we obtain the equation along the characteristic line $x = c_o t$,

$$\sigma_N - \sigma_W - \rho_o c_o(v_N - v_W) = -\frac{1}{2}(g_N + g_W)\Delta t \qquad (3\text{-}61)$$

where $v_N = 0$, and another equation along $x=\ell$,

$$E_o(\epsilon_N - \epsilon_S) = \sigma_N - \sigma_S + (2\Delta t)\cdot\left(\frac{g_N+g_S}{2}\right) . \qquad (3\text{-}62)$$

These can be solved simultaneously in order to give the two sought solutions σ_N and ϵ_N. Because of the unknown character of the function $g_N(\sigma,\epsilon)$, it also becomes necessary to use a method of trial and error as mentioned in Section (II) to seek corresponding solutions. According to the procedure used in Section (II), one finds first a trial solution based upon

an assumed region for $g_N(\sigma,t)$. If this trial solution (at N) happens to be located in the same region (in σ-ϵ plane) as the South point S, this trial solution is the actual solution. However, if the location of this solution differs from that of S, a case of crossing a region or jumping from one region to another region results. For crossing regions, twenty subdivisions along SW and SN are formed, and the same procedure for calculation is used as in Section (II) to find the solution at the north point N. For jumping regions, a smaller increment of time interval ($k\Delta t$) should be applied instead.

To avoid repeating the explanation, the author will present here only the final solution along $x=\ell$ in each corresponding region.

(i) For Solutions in the Upper Yield Region:

$$\frac{\sigma_N}{\sigma_o} = \frac{\left[2 + 2\frac{E_1}{E_o}k\Delta t\right]\frac{\sigma_w}{\sigma_o} - \left[1 - \frac{1}{2}k\Delta t + \frac{3}{2}k\Delta t\frac{E_1}{E_o} - (k\Delta t)^2\frac{E_1}{E}\right]\frac{\sigma_S}{\sigma_o}}{1 + \frac{1}{2}k\Delta t + \frac{1}{2}\frac{E_1}{E_o}k\Delta t}$$

$$\frac{- (k\Delta t)^2\left(\frac{E_1}{E_o}\right)^2\frac{\epsilon_S}{\epsilon_o} - \left(1 - \frac{E_1}{E_o}\right)\frac{E_1}{E_o}(k\Delta t)^2}{1 + \frac{1}{2}k\Delta t + \frac{1}{2}\frac{E_1}{E_o}k\Delta t}$$

$$\frac{\epsilon_N}{\epsilon_o} = \frac{\left[2 + 2k\Delta t\right]\frac{\sigma_w}{\sigma_o} + \left[k\Delta t\right)^2 - 2\right]\frac{\sigma_S}{\sigma_o} + \left[1 + \frac{k\Delta t}{2} - \frac{3}{2}(k\Delta t)\frac{E_1}{E_o} - (k\Delta t)^2\frac{E_1}{E_o}\right]\frac{\epsilon_S}{\epsilon_o}}{1 + \frac{1}{2}k\Delta t + \frac{1}{2}\frac{E_1}{E_o}k\Delta t}$$

$$- \left(1 - \frac{E_1}{E_o}\right)\left[2k\Delta t + (k\Delta t)^2\right]$$

$$1 + \frac{1}{2}\, k\Delta t + \frac{1}{2}\,\frac{E_1}{E_o}\, k\Delta t \qquad (3\text{-}63)$$

$$\frac{v_N}{v_o} = 0 \quad .$$

(ii) For Solutions in the Elastic Region:

$$\frac{\sigma_N}{\sigma_o} = 2\,\frac{\sigma_W}{\sigma_o} - \frac{\sigma_S}{\sigma_o}$$

$$\frac{\epsilon_N}{\epsilon_o} = \frac{\epsilon_S}{\epsilon_o} + \left(\frac{\sigma_N}{\sigma_o} - \frac{\sigma_S}{\sigma_o}\right) \qquad (3\text{-}64)$$

$$\frac{v_N}{v_o} = 0 \quad .$$

(iii) For Solutions in the Lower Yield Region:

$$\frac{\sigma_N}{\sigma_o} = \frac{\left[2 + 2\,\frac{E_1}{E_o}\, k\Delta t\right]\frac{\sigma_W}{\sigma_o} - \left[1 - \frac{1}{2}\, k\Delta t + \frac{3}{2}\, k\Delta t\,\frac{E_1}{E_o} - (k\Delta t)^2\,\frac{E_1}{E_o}\right]\frac{\sigma_S}{\Delta_o}}{1 + \frac{1}{2}\, k\Delta t + \frac{1}{2}\,\frac{E_1}{E_o}\, k\Delta t}$$

$$\frac{- (k\Delta t)^2\left(\frac{E_1}{E_o}\right)^2\,\frac{\epsilon_S}{\epsilon_o} + \left(1 - \frac{E_1}{E_o}\right)(k\Delta t)^2\,\frac{E_1}{E_o}}{1 + \frac{1}{2}\, k\Delta t + \frac{1}{2}\,\frac{E_1}{E_o}\, k\Delta t}$$

$$\frac{\epsilon_N}{\epsilon_o} = \frac{\left[2 + 2k\Delta t\right]\frac{\sigma_W}{\sigma_o} + \left[(k\Delta t)^2 - 2\right]\frac{\sigma_S}{\sigma_o} + \left[1 + \frac{k\Delta t}{2} - \frac{3}{2}(k\Delta t)\right]\frac{E_1}{E_o}}{1 + \frac{1}{2}k\Delta t + \frac{1}{2}\frac{E_1}{E_o}k\Delta t}$$

$$- \frac{(k\Delta t)^2\frac{E_1}{E_o}\Big]\frac{\epsilon_S}{\epsilon_o} + \left[\left(1 - \frac{E_1}{E_o}\right)(2k\Delta t + (k\Delta t)^2)\right]}{1 + \frac{1}{2}k\Delta t + \frac{1}{2}\frac{E_1}{E_o}k\Delta t} \qquad (3\text{-}65)$$

$$\frac{v_W}{v_o} = 0$$

VI. Total Solution of the Problem in the Characteristic Plane

The previous four sections (Sections II, III, IV and V) provide all necessary equations to be used in calculating numerical solutions throughout the entire characteristic plane. However, we have not yet mentioned how these solutions are linked. In this section, we will see how the complete solution is found in the time and space domain.

In order to obtain a clear picture of this procedure first refer back to Fig. (3-7). The figure shows, as indicated before, the initial and subsequent wave reflections in the finite bar. Once the stress is applied at the free end, it propagates toward the fixed end with the wave front moving at the elastic wave speed $(E_o/\rho_o)^{\frac{1}{2}}$. This is indicated by line OA. At point A the first wave reflection occurs at the fixed end. The process of subsequent reflections is indicated by points N, R, W and Z. One observes also from the figure that regime (I) represents the stress-free undisturbed regime, regime (II) is the initially stressed regime

with no reflected waves, whereas, regimes (III), (IV) and all subsequent regimes in the characteristic x-t plane are those where wave relfections and interactions are occurring.

Now, the procedure carried out in the analysis was to first perform numerical integration in regime (II) to determine stresses, strains and particle velocities at all points. In order to complete the solutions in regime (II) it is necessary first to initiate solutions along lines OB and OG by the corresponding equations from Sections (III) and (IV) of this chapter and then use the equations from Section (II) to calculate the solutions at the remaining points in the network of the regime. After one completes the solutions in regime (II), then one uses the solutions in Section (V) to find the solutions at point A. With A, B and C known, D is readily obtained from the basic solutions of Section (II). Then all points along AM can be found in a sequence. Regime (III) has thus been linked with regime (II). The remaining calculations for regime (III) are carried out in a routine manner by using equations alternately from Section (II) and (V). By a similar approach, regime (IV) can be joined to regime (III). First N would be found from the equations of Section (IV), then K can be determined. This makes it possible to find the values along the characteristic NT by making use of known values along the characteristic line MS.

Following this procedure, each regime can then be connected to the preceding one. It is observed that, after regime (IV) is obtained, the entire analysis repeats itself. This fact was taken into account in writing the computer program by making it a complete loop. Consequently, long time effects could be explored.

A computer program was written in the FORTRAN IV Language for calculating the solutions for the entire problem. Also a subroutine was written in order to apply the CALCOMP PLOTTER to plot many results.

CHAPTER IV

RESULTS AND DISCUSSIONS

The numerical results presented in this chapter are in non-dimensional form. This is because all the solutions developed in Chapter IV have been expressed as dimensionless quantities. For the calculations, the bar was subdivided into thirty-two equal lengths and the time increment was selected where $\Delta t = 1/k$ seconds (or in non-dimensional form $k\Delta t = 1$). This resulted in stress, strain and velocity values being determined for 528 points for each triangle regime shown by Figure (3-7), where the length of the bar was selected as $32\ c_o/k$.

There are five parameters, two independent variables, and three dependent variables for this study. The loading parameters are the amplitude of oscillating stress, its mean value and the frequency of applied load. The range for amplitude of oscillating stress was taken arbitrarily in the interval from zero to twice the yield stress. The mean stress was also considered in this interval. For the study, the loading frequency was varied between $2\pi k/32$ and $2\pi k/1300$, where the length of the bar equals $32\ c_o/k$. For the material parameters, we consider the material constant k as defined in Chapter II and the degree of strain-hardening E_1/E_o, where E_1/E_o represents the slope of the plastic region of the bilinear static stress-strain relation. The material constant k is regarded as a constant, which can be determined experimentally. No specific numerical value has been

assigned in these calculations. A study was made of the parameter E_1/E_o degree of strain-hardening. The range of this parameter is varied between zero and one. In the limit, if E_1/E_o takes the value of one then the material behaves elastically. On the other hand, if E_1/E_o takes the value of zero this results in an elastic-prefectly-plastic material. We note that the smaller E_1/E_o is, the more strain-hardening the material has, and the more plastically the material will behave.

Two independent variables are the spatial coordinate x and the time variable t. In non-dimensional analysis, the spatial variable x/ℓ may take values between zero and one. Here, when $x/\ell = 0$ it indicates a free end, and when $x/\ell = 1$ it represents a fixed end. The time variable t takes positive values.

Based upon this, the reader will find that solutions in this study are available at any of 33 positions along the bar and at any incremental instant of time after the bar is loaded. Solutions can also be obtained at any loading condition which may be specified by the ranges of the three loading parameters. With variation on E_1/E_o, solutions are also available for different degrees of strain-hardening. From these variations we examine the resulting response in terms of stress $\sigma(x,t)$ strain $\epsilon(x,t)$ and particle velocity $v(x,t)$. These will now be presented and discussed.

I. The Dynamic Stress-Strain Time History

In order to have a clearer picture of the significance of lower yield and the Bauschinger effect, Figure (4-1) and Figure (4-2) show two dynamic stress-strain relations in the σ-ϵ plane for responses with

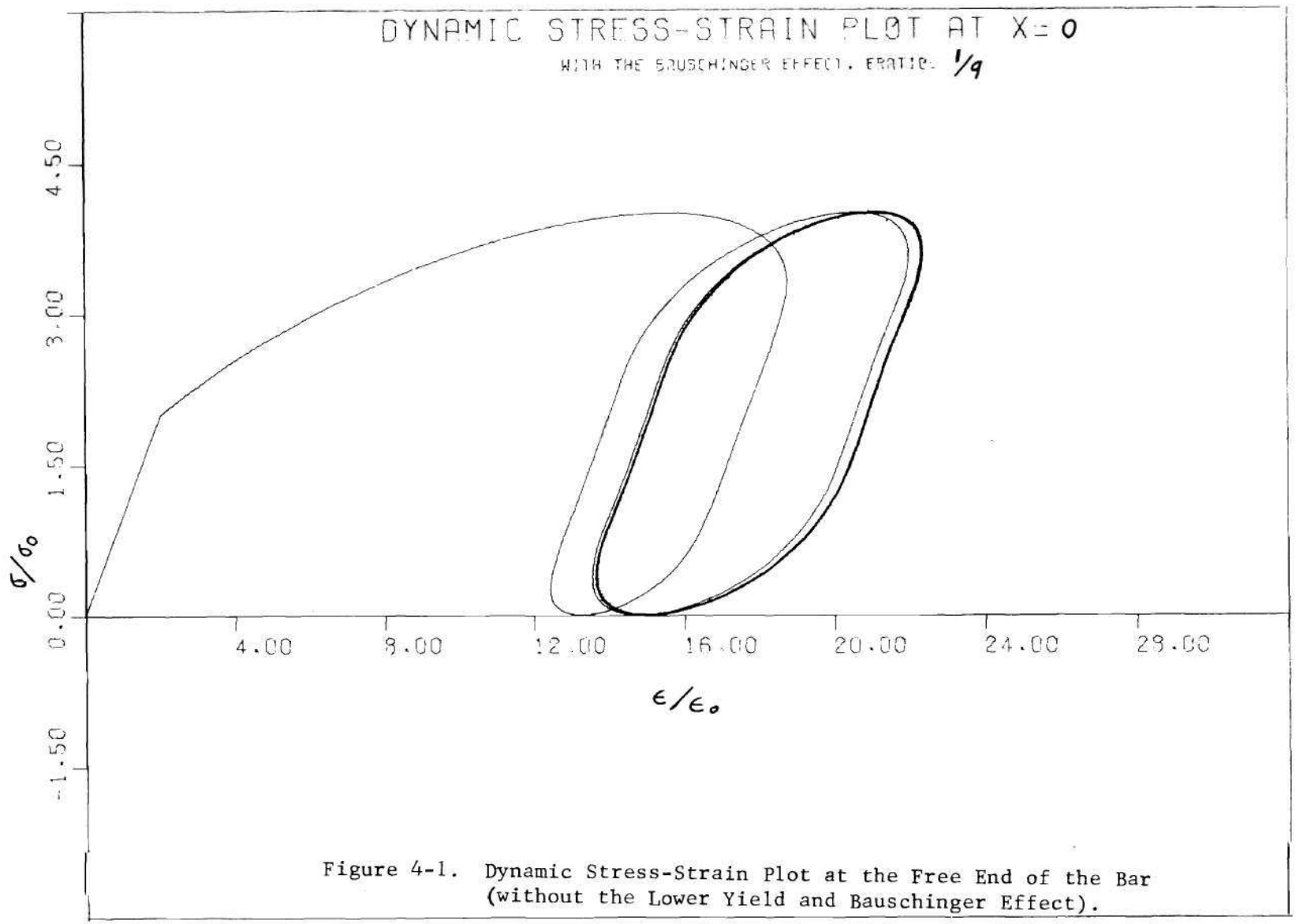

Figure 4-1. Dynamic Stress-Strain Plot at the Free End of the Bar (without the Lower Yield and Bauschinger Effect).

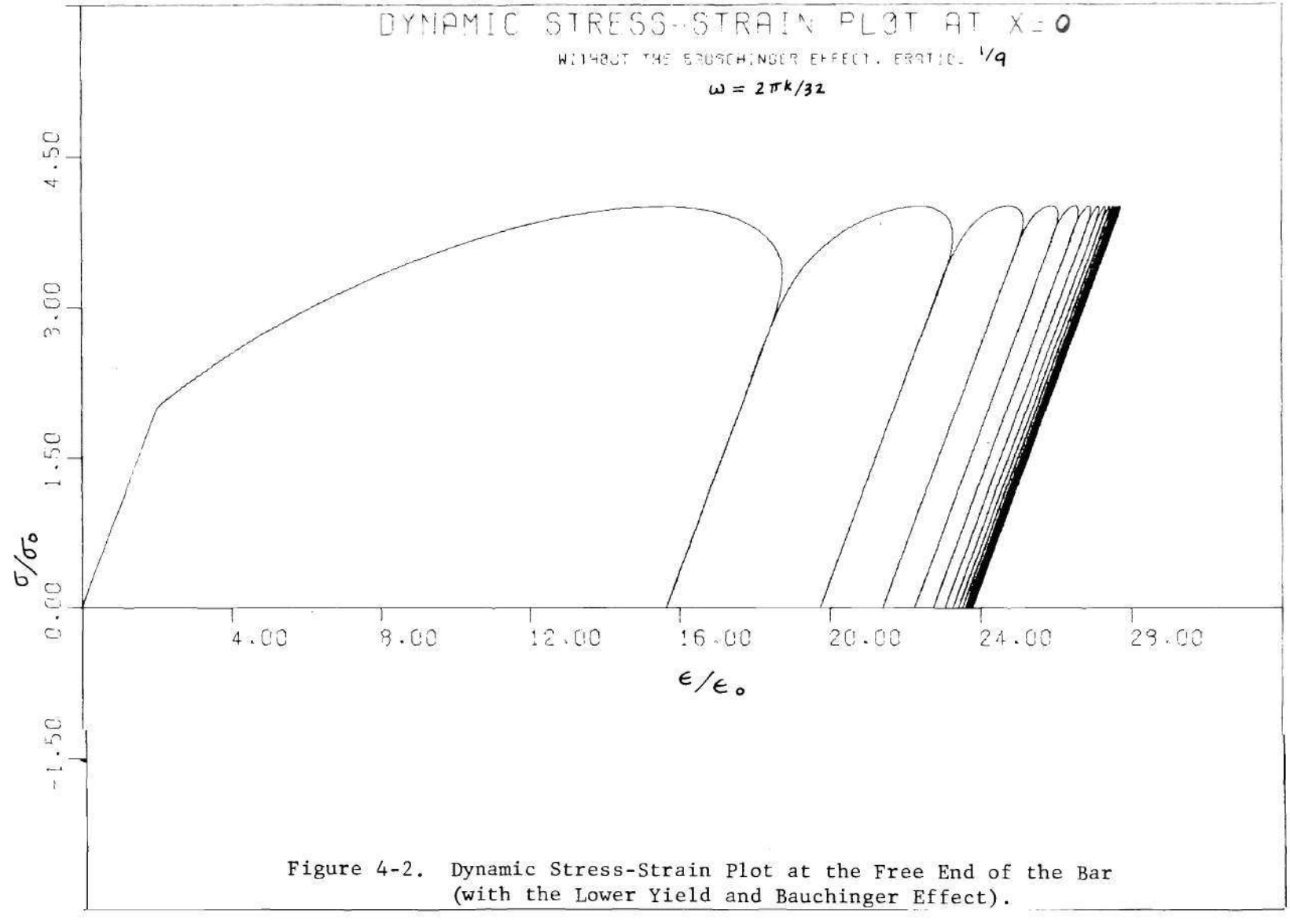

Figure 4-2. Dynamic Stress-Strain Plot at the Free End of the Bar (with the Lower Yield and Bauchinger Effect).

and without this effect respectively. The applied mean stress equals twice the yield stress and the amplitude of the alternating stress also equals twice the yield stress value. The loading frequency for both figures is equal to $2\pi k/32$, which has a corresponding period of $32/k$ second. This is about a quarter of the first fundamental period of an elastic bar under longitudinal vibration ($T_n = 128/k$). The material is selected as with E_1/E_o equal to 1/9.

Distinct hysteresis loops are formed as shown in Figure (4-1) for the case with the Bauschinger effect but not in Figure (4-2) where the Bauschinger effect has been excluded. From Figure (4-1), several important features may be noted regarding the shape of the hysteresis loops:

(1) The loop consists of two similar smooth curves or branches (loading branch and unloading branch), symmetrically located about a point somewhere along the line of mean stress.

(2) Branch curve intersections produce no corners at the loading-unloading transition points, for the type of material with constitutive equation as considered in this thesis.

(3) Most of the unloading curve is elastic, with a slope equal to E_o. However, the unloading curve in the upper and lower yield regions has a slope which depends on the corresponding value of $g(\sigma,\varepsilon)$.

The initial loading starts from $t = 0$ characterized by zero stress and zero strain. After the steady-state response has been reached, the hysteresis loops will stabilize at an unique cycle. In general, the time required to stabilize the hysteresis seems to be so short that only

a few cycles of the wave traveling between the fixed and free end are required. This may be explained by the fact that the transient response usually damps out after a short initial stage. Morrow [40] confirmed this phenomen experimentally in his strain-controlled fatigue test work, and stated that there is usually a transient change in the shape and size of the hystersis loop at the start of a cyclic test. This same conclusion has been also reached by Osiecki [20] analytically in the case of a semi-infinite bar. He noted that the process of the vibration becoming steady was relatively rapid, and stated that it can be assumed in practice that the steady process takes place after some ten to twenty cycles. On Figure (4-2), where the Bauschinger effect is not included, the transient can hardly be discerned at the loading end (free end).

It is interesting to observe that, in the case of considering lower yield and the Bauschinger effect, the highest value of residual strain after steady-state has been reached is not as great as the case of not considering this effect. The numerical values of the highest residual strains in the two cases are 22.21 ϵ_o and 27.82 ϵ_o respectively. This is quite understandable since the characteristic of lower yield would swing back the unloading curve and reduce the magnitude of the plastic strain during the process of forming each hysteresis loop. Analytically, from the constitutive equations derived in Chapter II, the difference of considering and not considering the Bauschinger effect is the presence of the rate-dependent term $g_2(\sigma,\epsilon)$ in the lower yield region. Or one can express

$$g_2(\sigma,\epsilon) = k[\sigma - f_2(\epsilon)] \qquad \text{with the Bauschinger effect}$$

$$g_2(\sigma,\epsilon) = 0 \qquad \text{without the Bauschinger effect.} \qquad (4\text{-}1)$$

In the case of the Bauschinger effect, $g_2(\sigma,\varepsilon)$ is a negative valued function since σ is defined as $\sigma < f_2(\varepsilon)$, and k is a positive constant, in the lower yield region. The contribution of this negative function $g_2(\sigma,\varepsilon)$ to plastic strain rate is given by:

$$E_o \frac{\partial \varepsilon^p}{\partial t} = g_2(\sigma,\varepsilon) \quad . \tag{4-2}$$

From this equation one notes that a decrease in plastic strain rate is produced whenever the instantaneous stress-strain curve falls into the lower yield region. Therefore, an accumulated reduction of plastic strain will result during every hysteresis loop passing through the lower yield region. In the other case, without the Bauschinger effect, since the hysteresis loop was not introduced, no plastic strain reduction will occur upon unloading. And in this case the plastic strain will continue to increase up to its limiting value, which is the intersection point of the line of maximum loading stress and the line of static upper yield stress $f_1(\varepsilon)$ in the σ-ε plane. According to Figure (4-2), the limiting value is shown about $28.0\varepsilon_o$. After that, the whole bar is cyclicly stressed elastically and the plastic strain in the bar becomes permanent strain.

Dynamic stress-strain time histories at various locations along the bar are illustrated by Figures (4-3) and (4-4) for both cases with and without the Bauschinger effect respectively. Shown are the initial loading-unloading sequence for $E_1/E_o = 1/9$ at stations $x/\ell = 0$, 1/4, 1/2 and 1, under the same loading conditions as described in the last paragraph ($\omega = 2\pi k/32$, A = 2.0, B = 2.0). In the case that accounts for the Bauschinger effect, a reduction in the amplitude of alternating stress is noticeable in any position other than the free end of the bar. But

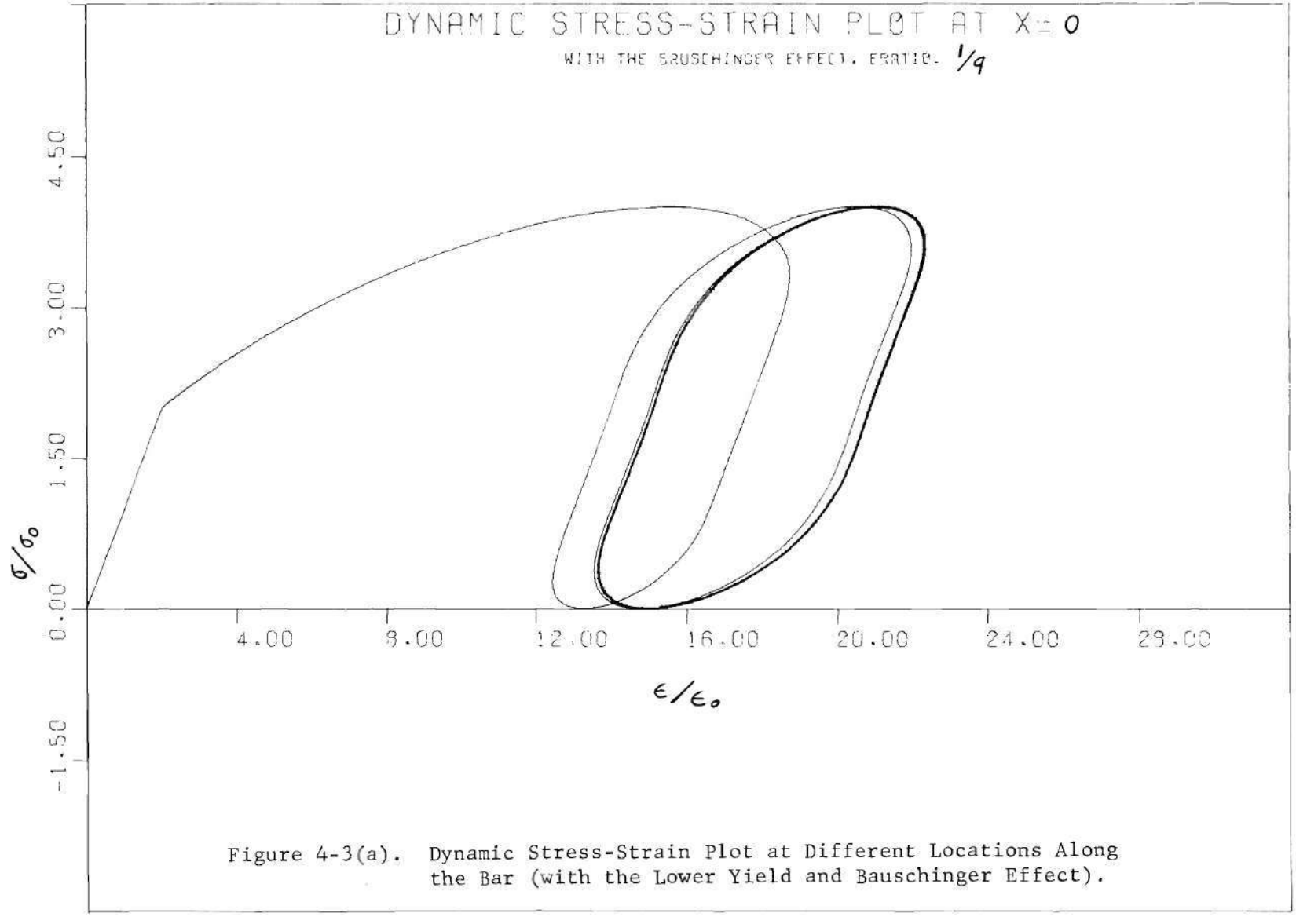

Figure 4-3(a). Dynamic Stress-Strain Plot at Different Locations Along the Bar (with the Lower Yield and Bauschinger Effect).

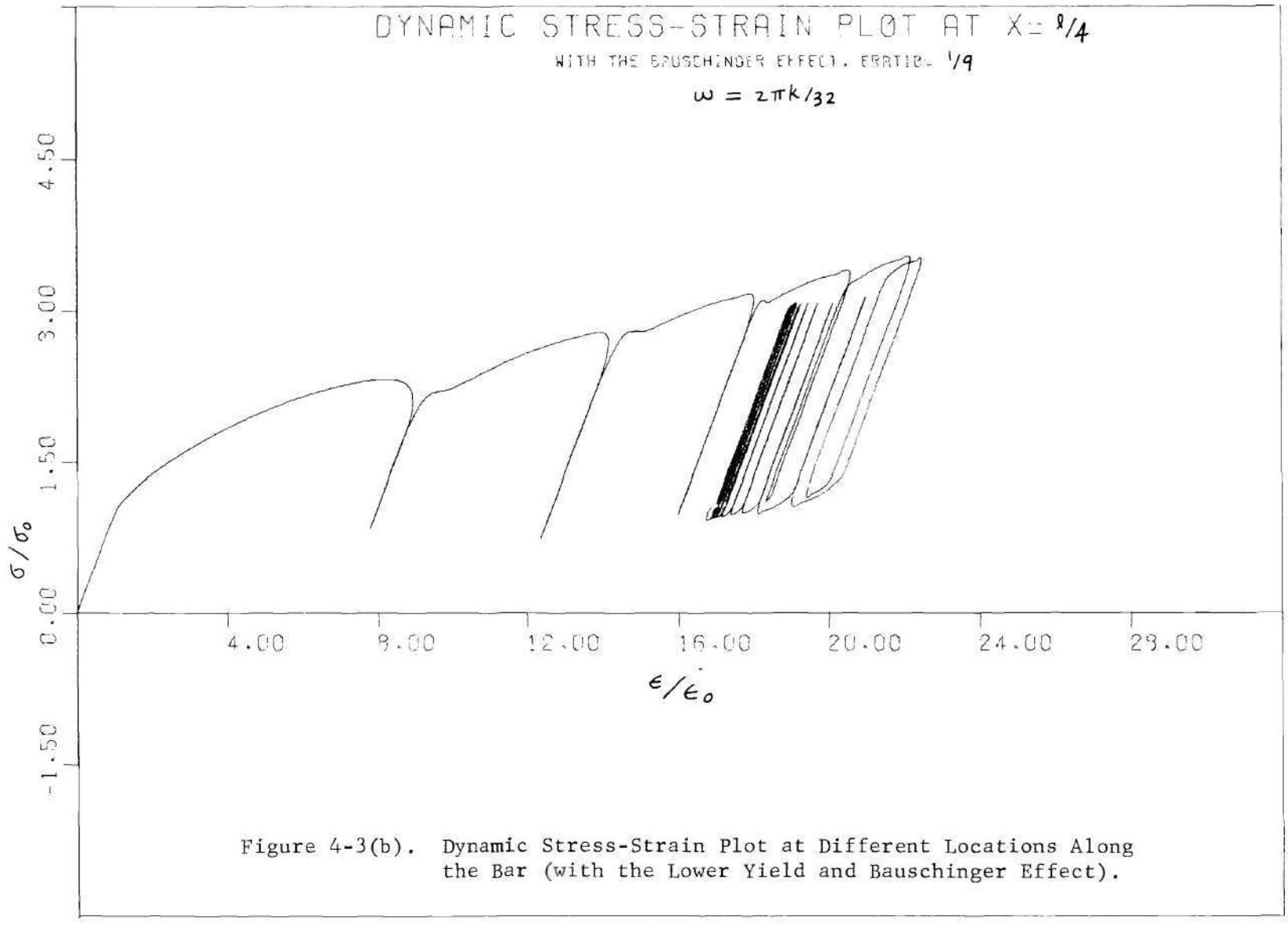

Figure 4-3(b). Dynamic Stress-Strain Plot at Different Locations Along the Bar (with the Lower Yield and Bauschinger Effect).

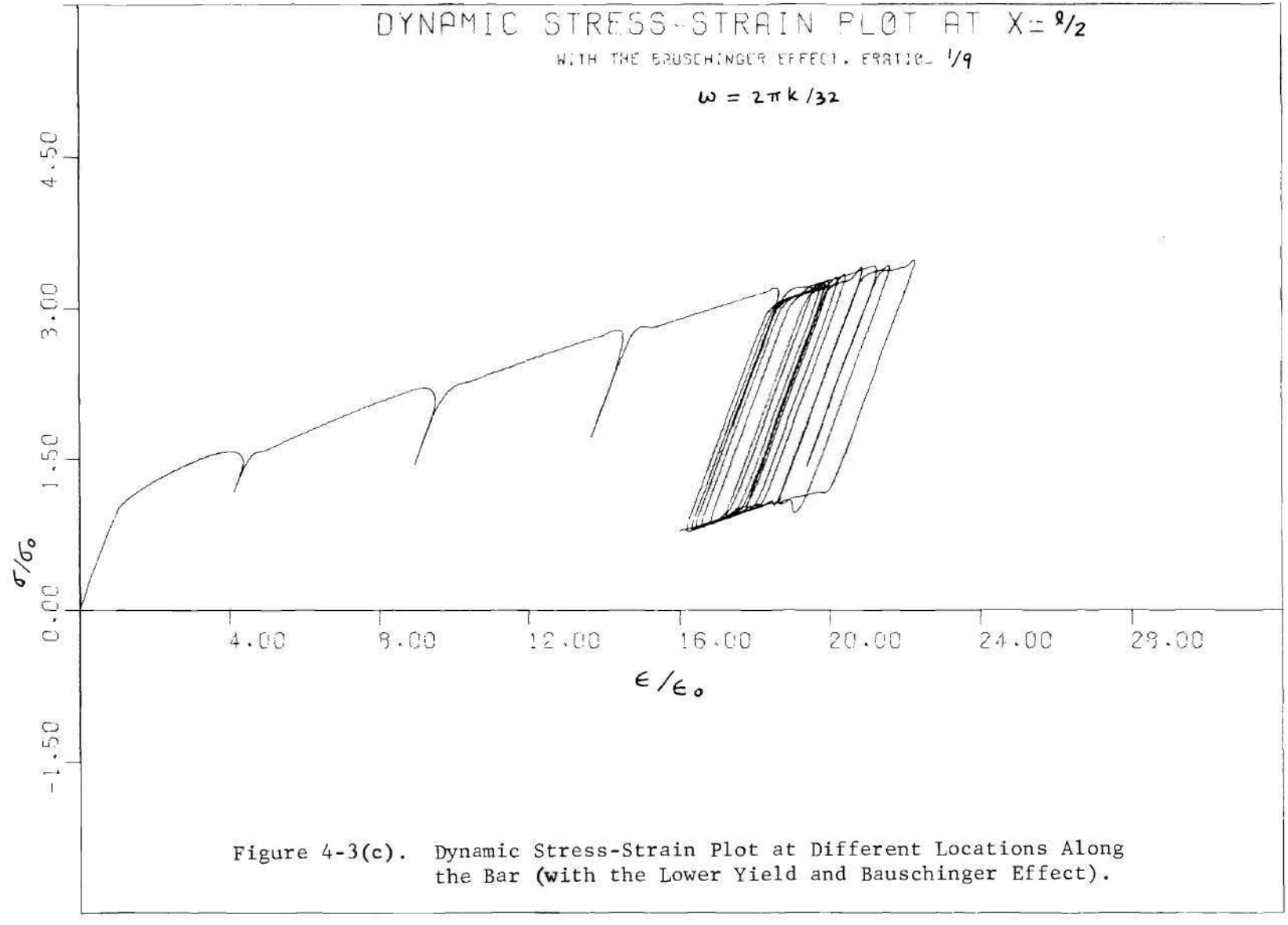

Figure 4-3(c). Dynamic Stress-Strain Plot at Different Locations Along the Bar (with the Lower Yield and Bauschinger Effect).

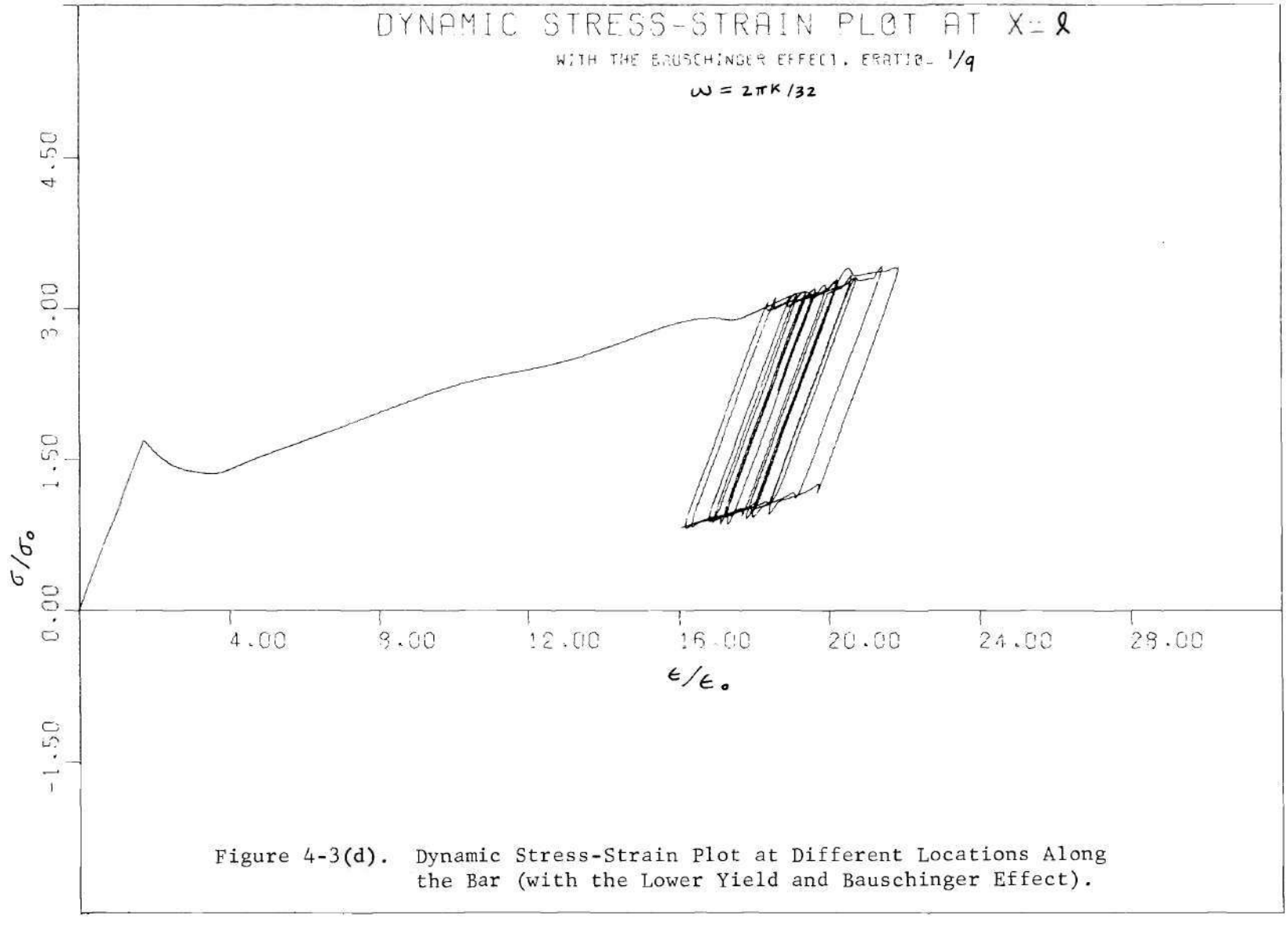

Figure 4-3(d). Dynamic Stress-Strain Plot at Different Locations Along the Bar (with the Lower Yield and Bauschinger Effect).

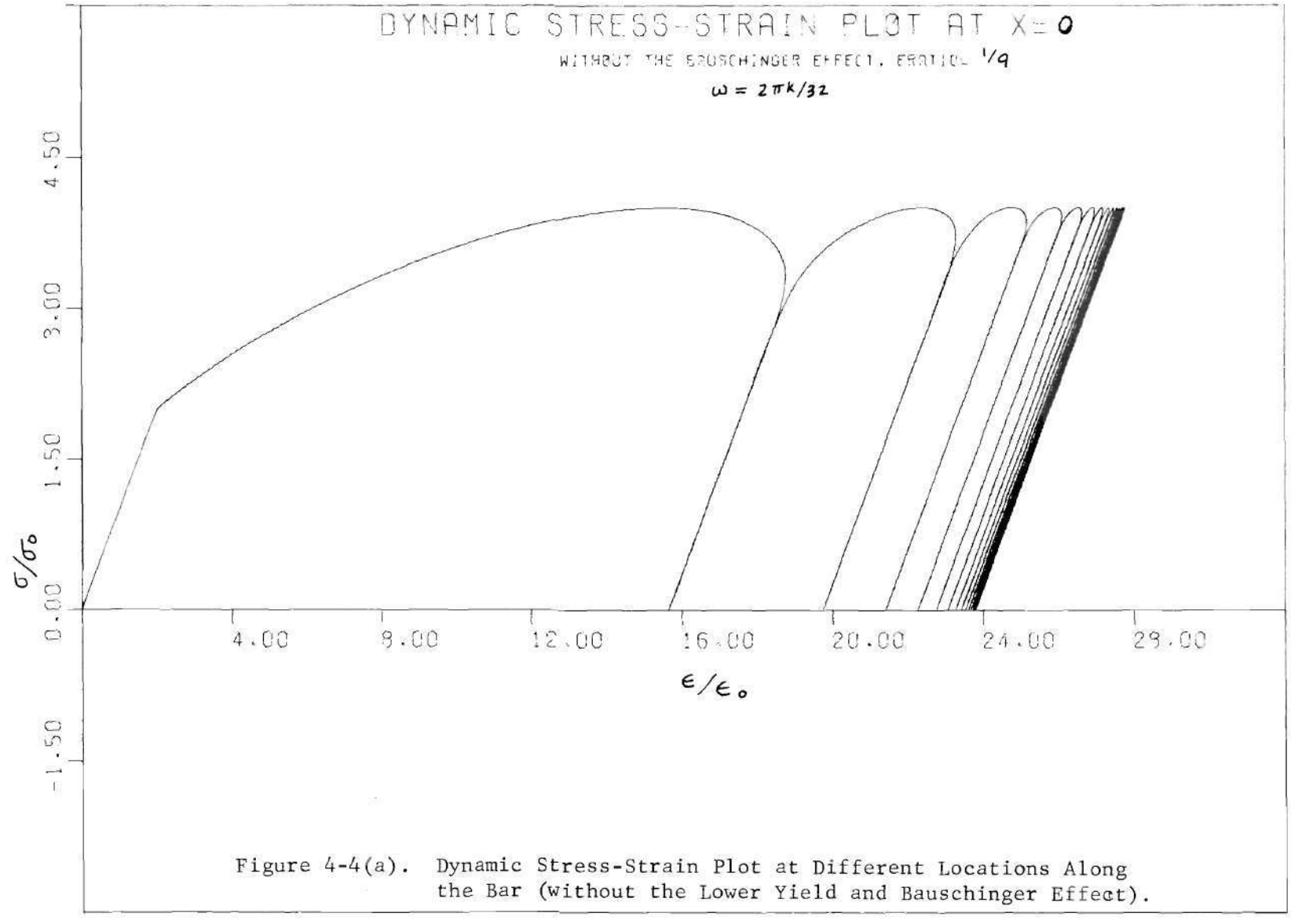

Figure 4-4(a). Dynamic Stress-Strain Plot at Different Locations Along the Bar (without the Lower Yield and Bauschinger Effect).

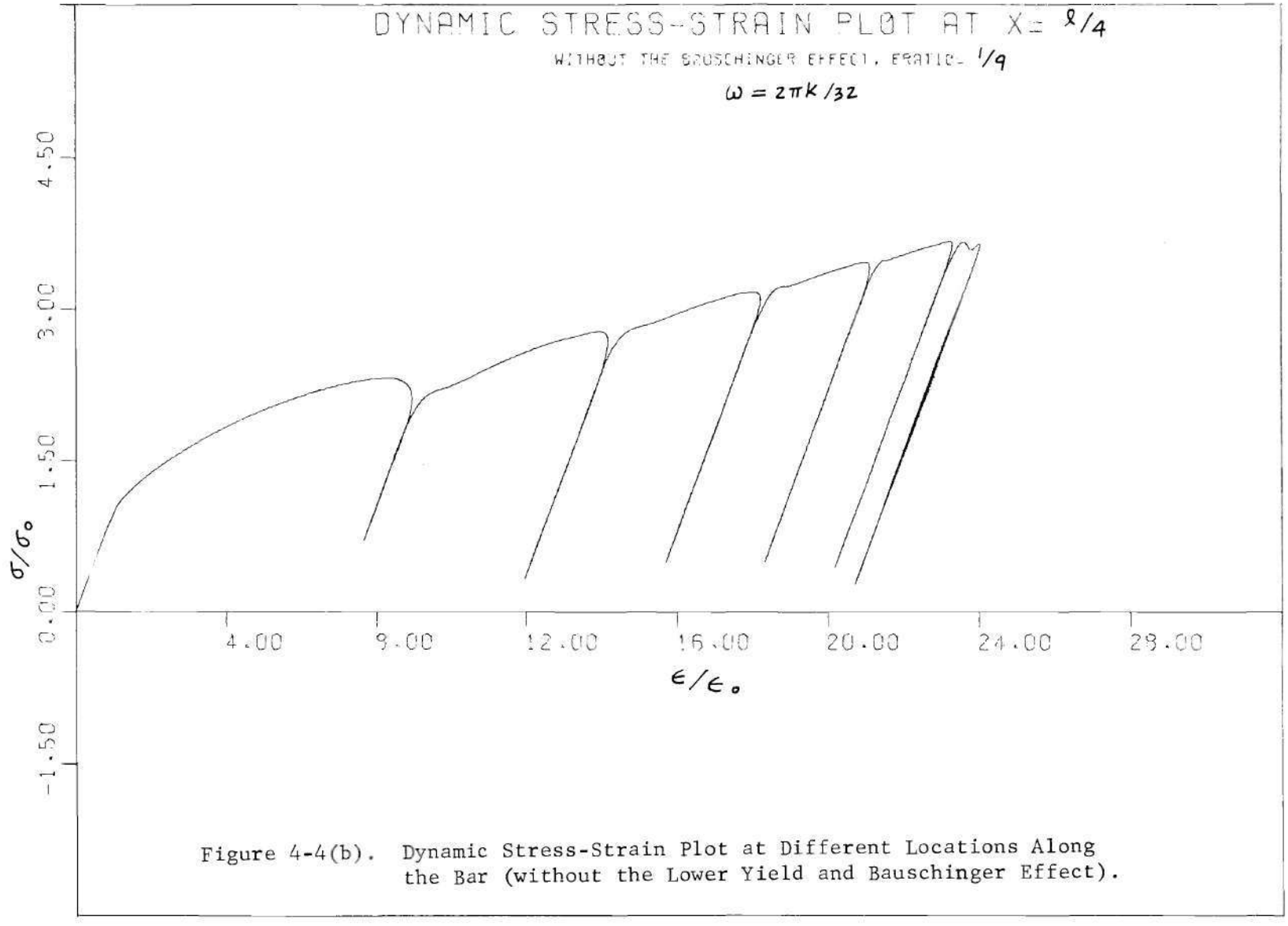

Figure 4-4(b). Dynamic Stress-Strain Plot at Different Locations Along the Bar (without the Lower Yield and Bauschinger Effect).

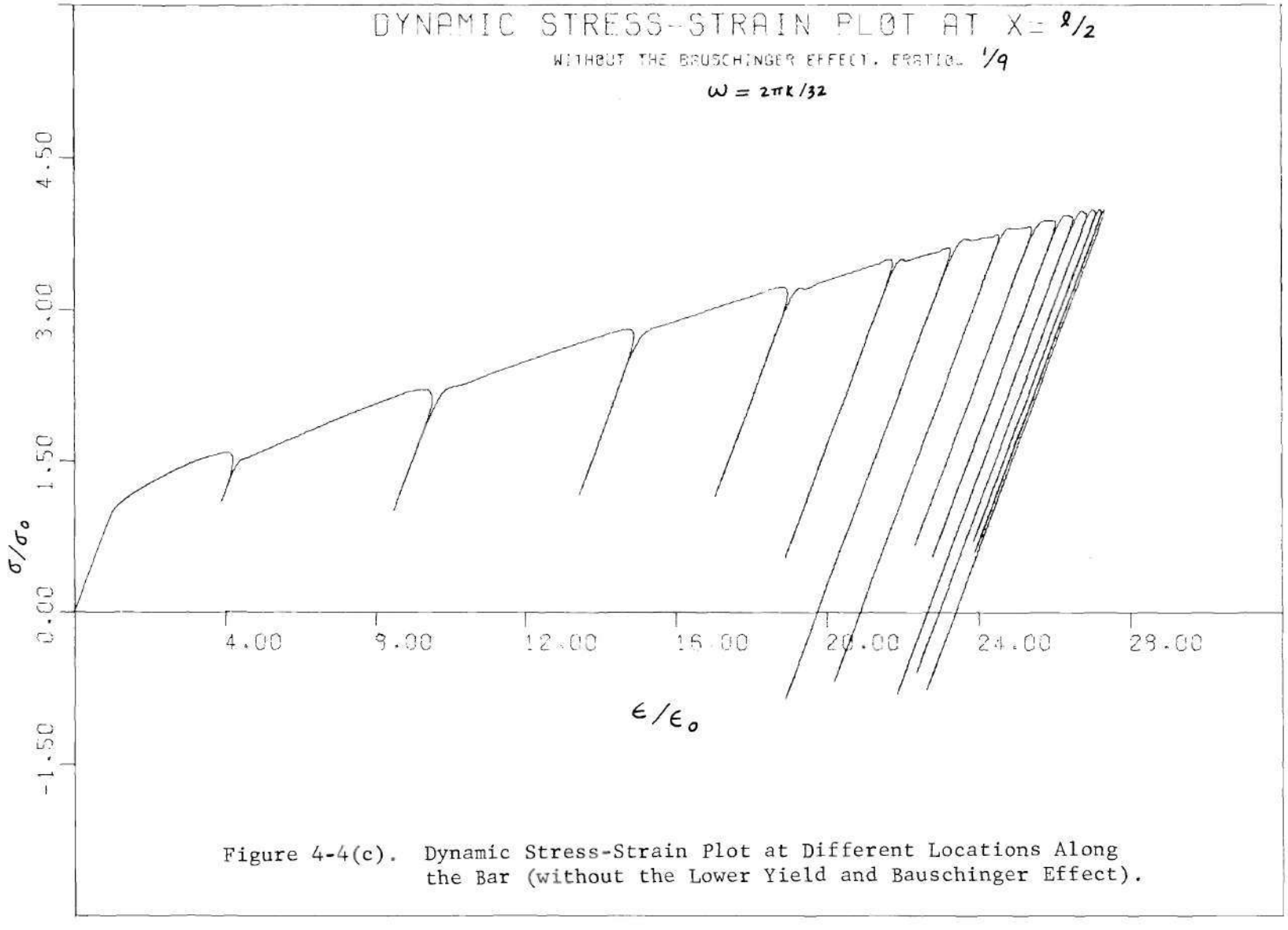

Figure 4-4(c). Dynamic Stress-Strain Plot at Different Locations Along the Bar (without the Lower Yield and Bauschinger Effect).

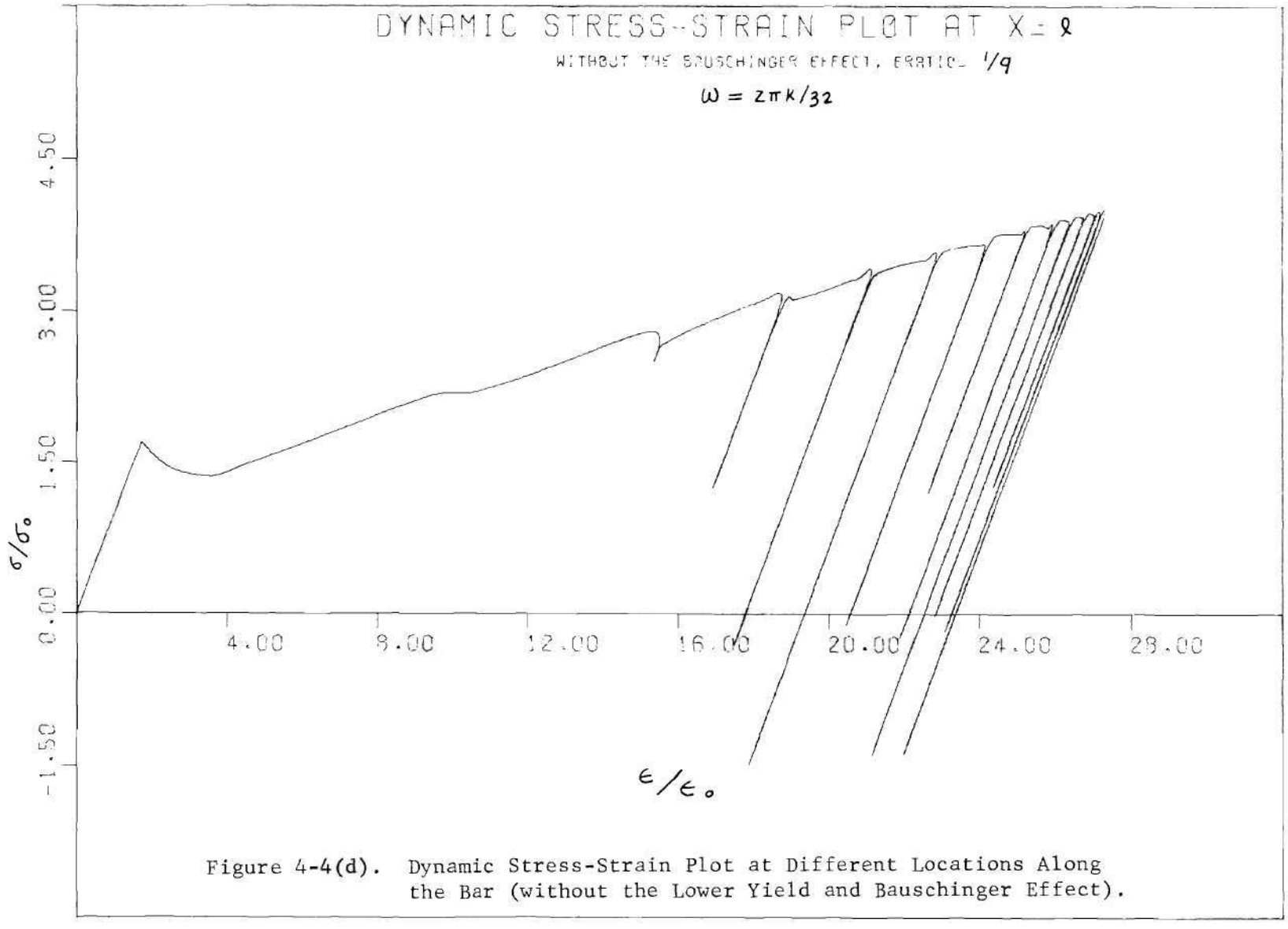

Figure 4-4(d). Dynamic Stress-Strain Plot at Different Locations Along the Bar (without the Lower Yield and Bauschinger Effect).

observe that this is not generally true for the case without the Bauschinger effect. Also note that the values of mean stress are unchanged at all stations along the bar for both cases. One sees from Figure (4-3) that the conclusion of quick stabilization in the process of forming hysteresis loops (from last paragraph) does not occur as rapidly at any other point along the bar as at the free end. In other words, it takes a longer time for the dynamic stress-strain curve to become stable at any point away from the free end of the bar. This appears due to the fact that stronger restrictions on stress are placed at the free end due to the boundary condition. Therefore, it is reasonable for the transient response to die out at any point near the free end.

Since the rate-dependent theory was applied in this study, strain-rate effects during cyclic loading become important. This is due to the fact that the rate of loading and unloading in the plastic region will affect the material's response. Unfortunately, little literature on the study of rate effects under dynamic reversed loading has been published to date in either theoretical or experimental domains of wave propagation problems. Neville and Myers [41] discuss strain-rate effects during reversed loading experimentally for conditions of a relatively long period of recovery time. Earlier, Lindholm [42] experimentally studied the effect of loading rate history on the response of aluminum and concluded that the previous strain rate history of loading affects the material's dynamic response. But the dynamic loading used was so rapid that no plastic hysteresis loop was obtained. Here, particular interest will be placed upon the effect of the rate of loading and unloading on the hysteresis loop. In other words, what is the effect on the charac-

teristic of the plastic hysteresis loop due to a rapid or slow process of loading and unloading? (corresponding high or low frequency during dynamic cycling.) Now, we shall consider two dynamic stress-strain plots, which resulted analytically from the study at the free end under two different loading frequencies. The degree of strain hardening of the bar was also $E_1/E_o = 1/9$ and the amplitude of the alternating stress and the mean stress remain the same as before. Figures (4-5) and (4-6) show the two cases which are $T = 16/k$ and $T = 176/k$. One sees distinctly from the figures that the size of the hysteresis loop is much greater for the case with a low frequency or large period. An d this is true not only at free end but also at other points along the bar. Therefore, the conclusion, usually drawn by fatigue investigators who consider a necked-down point of a bar only, that input frequency has little influence on the stress-strain relation seems not to be true here.

II. The Influence of Strain Hardening

The influence of strain hardening in the problem of plastic wave propagation in bars has been studied by Wood [22]. He concluded [37] that strain hardening does have a pronounced effect upon the shape and magnitude of stress waves in finite bars. In this study, the parameter E_1 / E_o permits us to study the dynamic response at various degrees of strain hardening.

Here, let us start by considering some interesting plots. First, given in the three dimensional plots recorded directly from a CALCOMP plotter (Figure (4-7)) are representative results of this section. Shown in Figure (4-7) is a plot of stress as a function of x, distance along the bar, and t, time for three degrees of strain hardening in the case

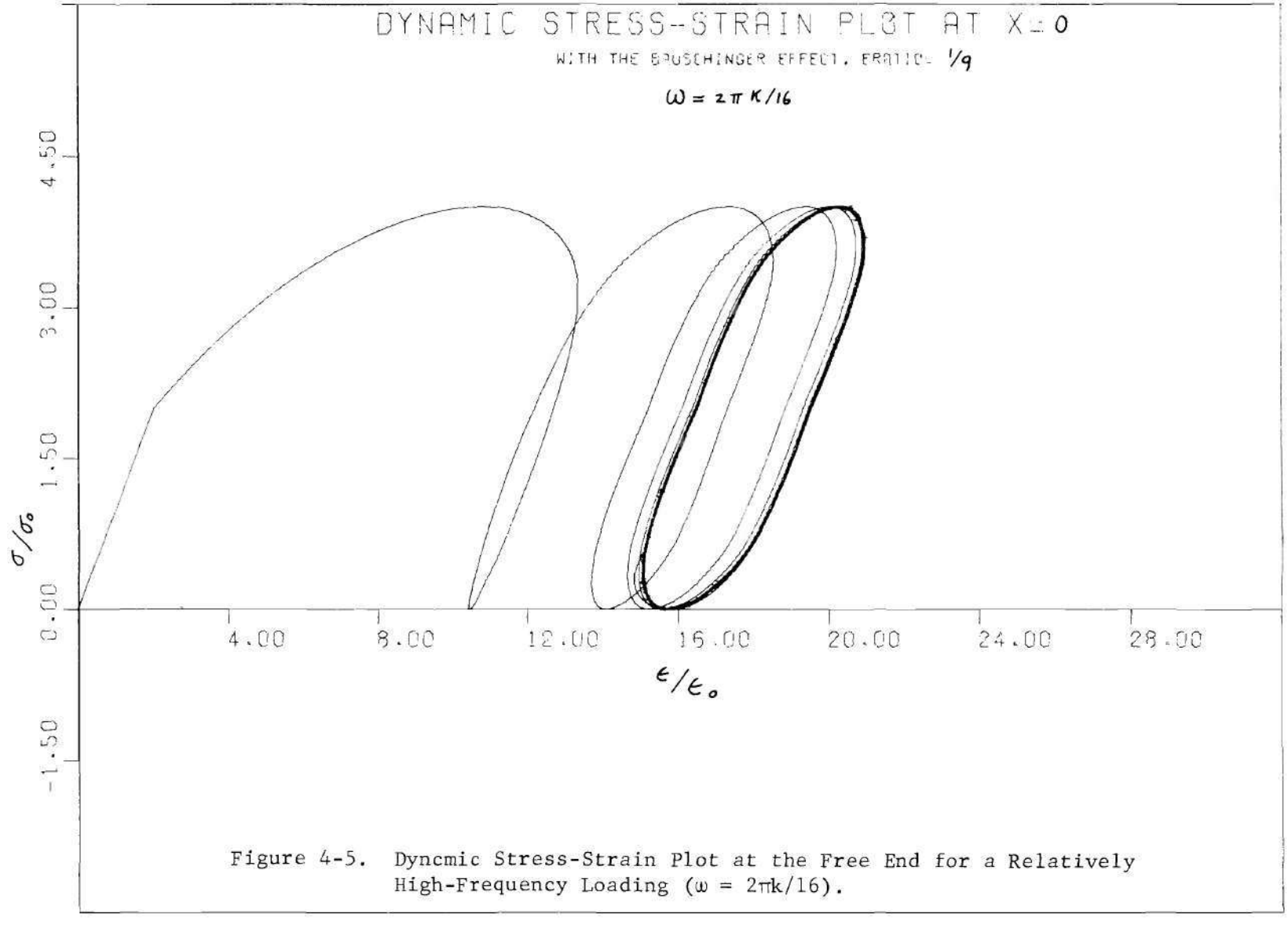

Figure 4-5. Dyncmic Stress-Strain Plot at the Free End for a Relatively High-Frequency Loading ($\omega = 2\pi k/16$).

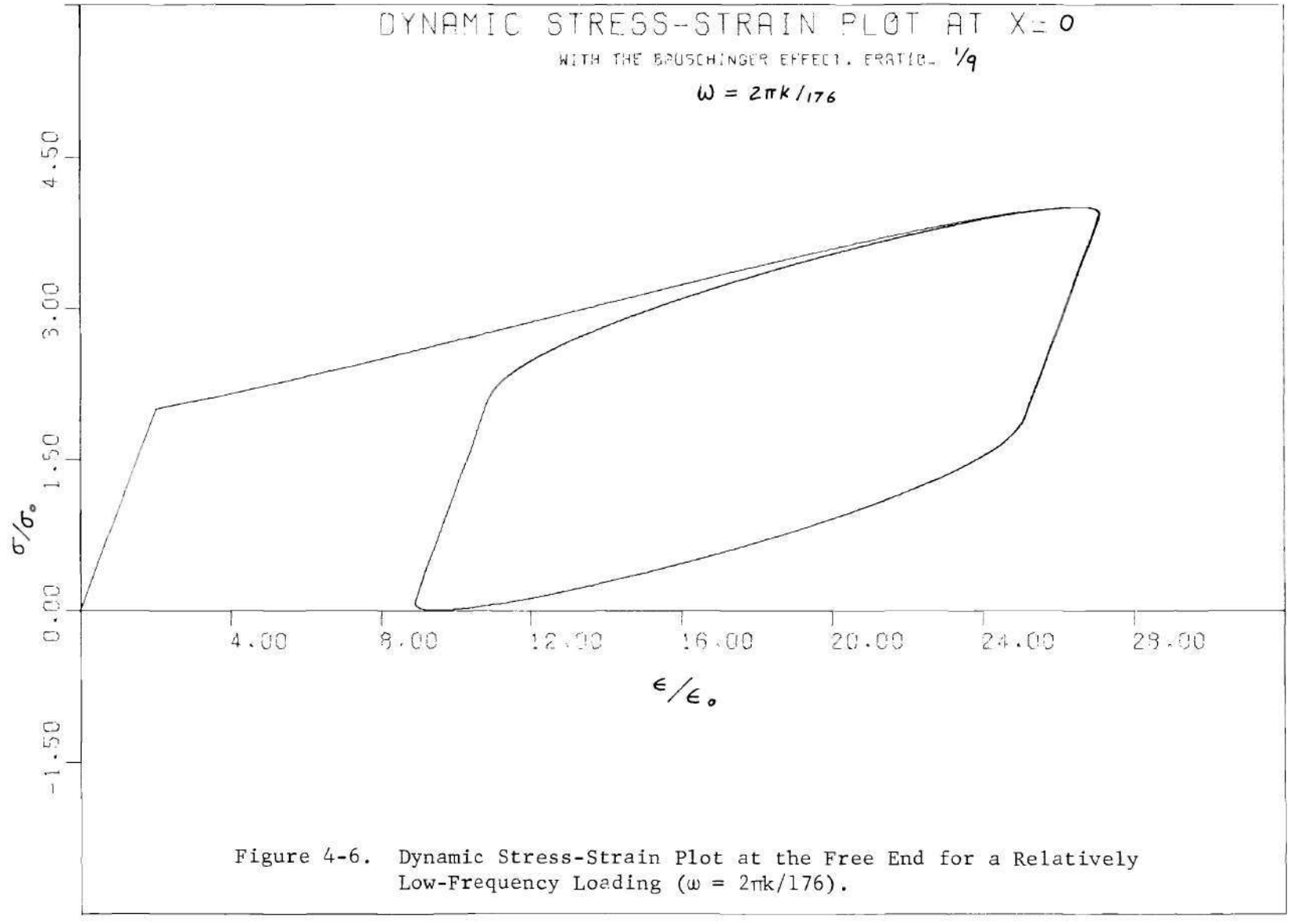

Figure 4-6. Dynamic Stress-Strain Plot at the Free End for a Relatively Low-Frequency Loading ($\omega = 2\pi k/176$).

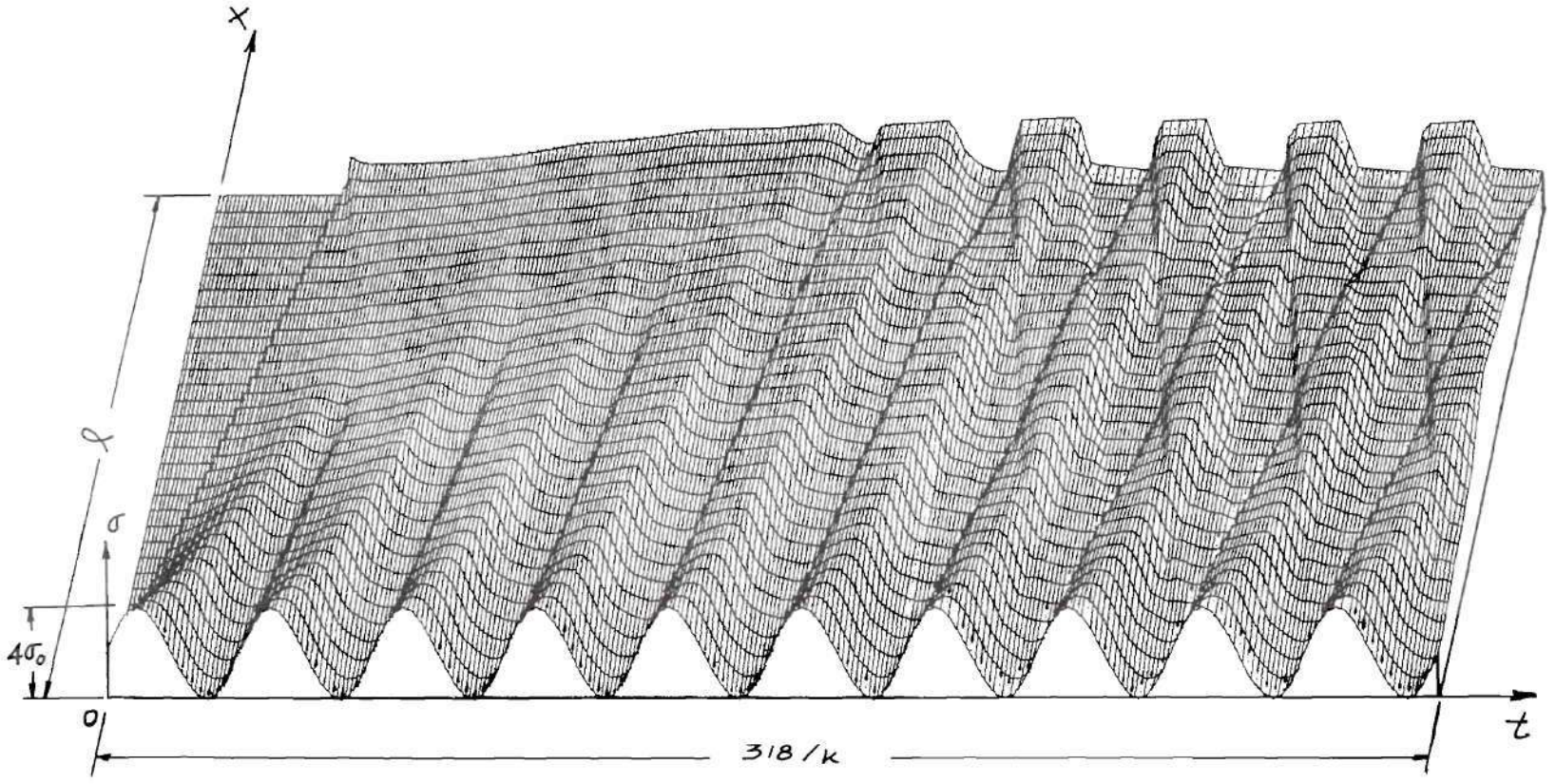

Figure 4-7(a). Three Dimensional Plot of Stress in Lagrangian x-t Plane.

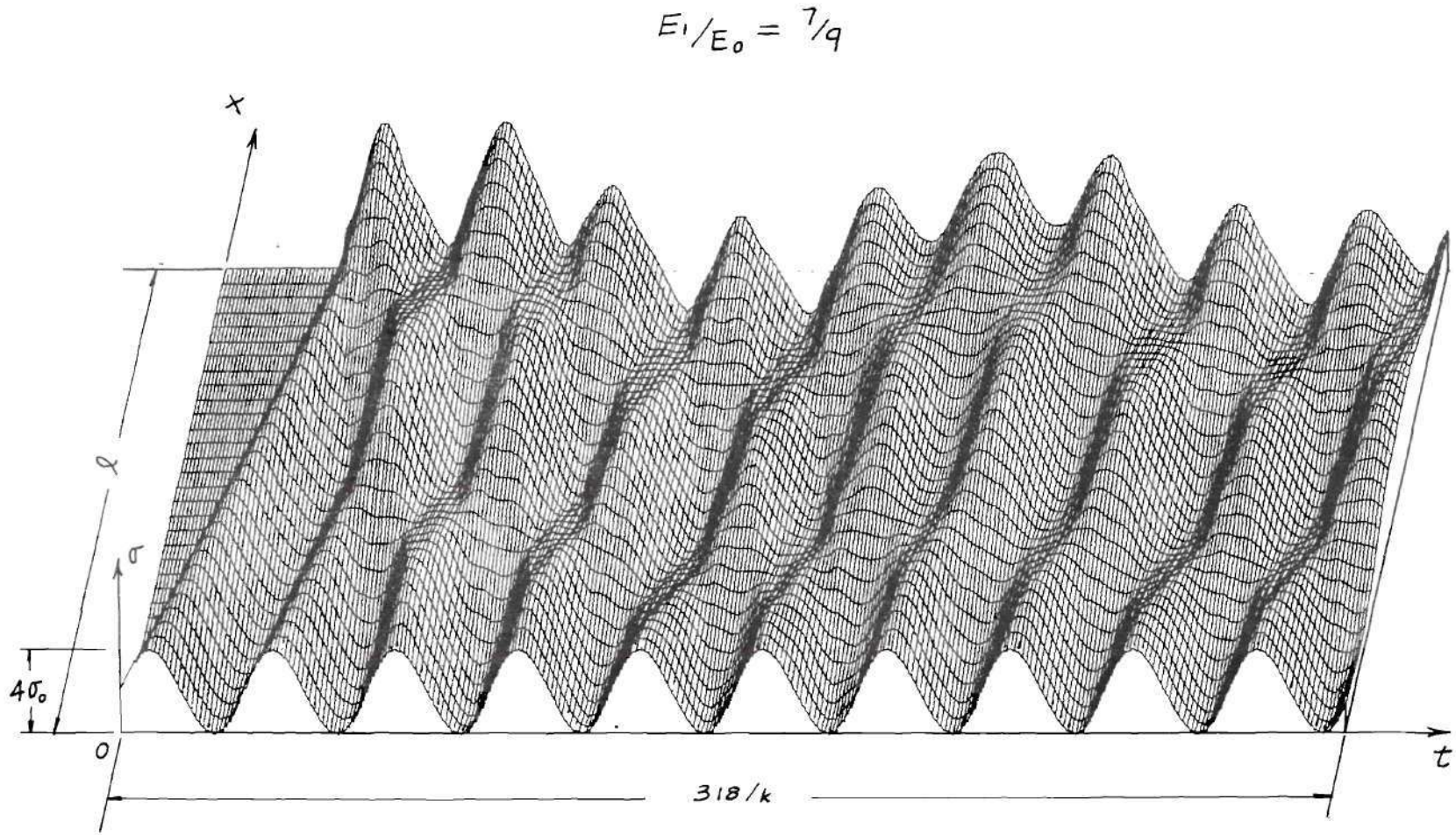

Figure 4-7(b). Three Dimensional Plot of Stress in Lagrangian x-t Plane.

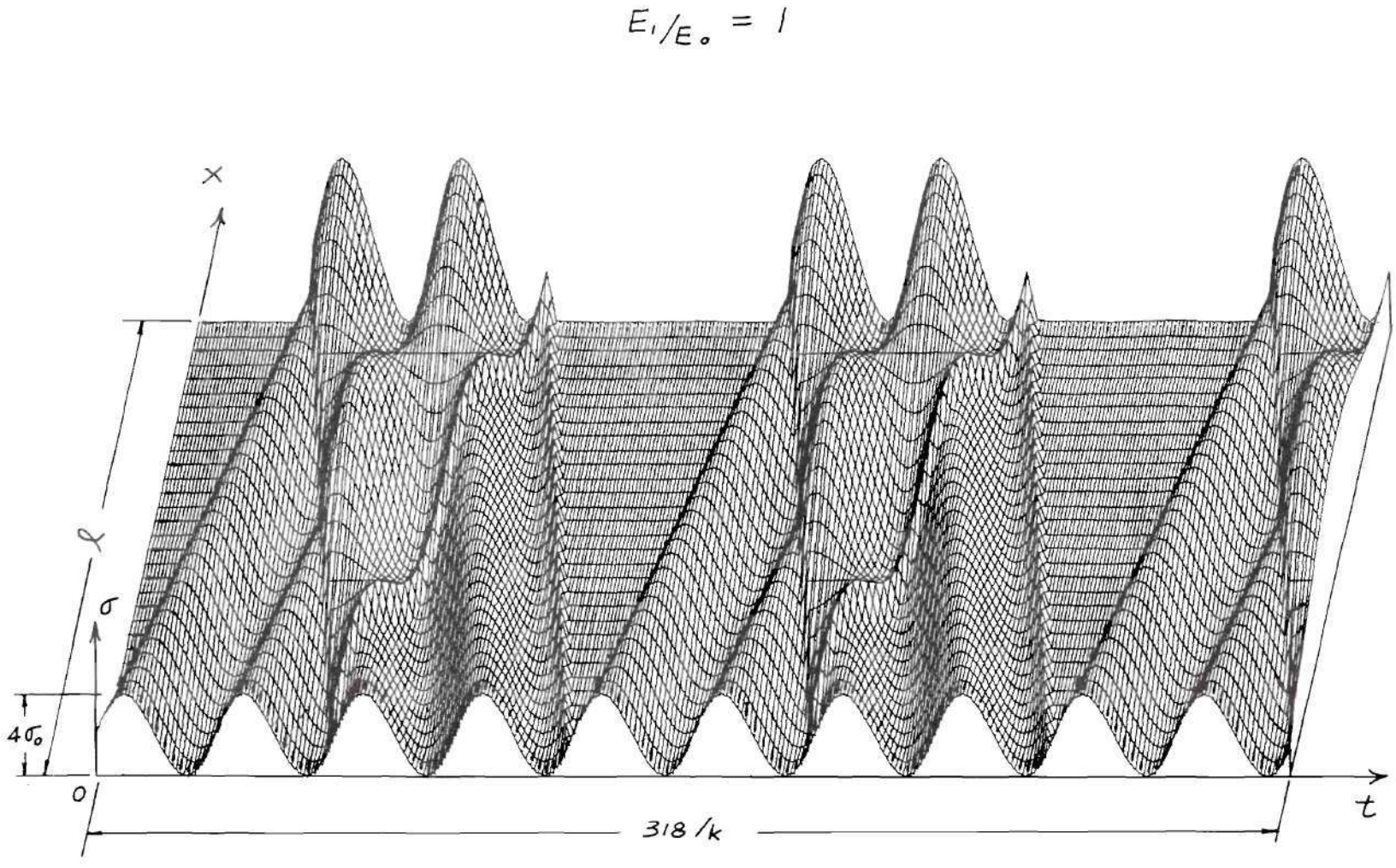

Figure 4-7(c). Three Dimensional Plot of Stress in Lagrangian x-t Plane.

with the lower yield and the Bauschinger effect. The loading parameters are the same as they were in the last section. Figure (4-7a) gives the dynamic response of stress for the case where the material is very plastic, that is $E_1/E_o = 1/9$. If one increases strain hardening such that the material is nearly elastic ($E_1/E_o = 7/9$), then one obtains the response shown in Figure (4-7b). Finally, for the elastic case ($E_1/E_o = 1$), the results are given by Figure (4-7c). By comparing the figures one finds that, for the same loading condition at the free end, the more plastically the bar behaves, the smaller magnitude of stress at the fixed end of the bar results. This can be explained physically by the fact that as a material behaves more pastically it will absorb more energy for developing plastic deformations. Therefore, less energy can be utilized and converted into stress. The elastic solution shown by Figure (4-7c) can also be readily obtained by a normal mode solution. In the case of this, one has

$$\frac{\sigma(x,t)}{\sigma_o} = \frac{2B_o}{A\ell} \sum_{n=1}^{\infty} (-1)^{n-1} \frac{1}{\omega_n} \cos\left(\frac{\omega_n x}{c_o}\right)(1 - \cos\omega_n t)$$

$$+ \frac{2C_o A_o}{A\ell} \sum_{n=1}^{\infty} (-1)^{n-1} \cos\left(\frac{\omega_n x}{c_o}\right)\left[\frac{1}{\omega^2 - \omega_n^2}(\omega \sin\omega_n t - \omega_n \sin\omega t\right] \quad (4\text{-}3)$$

where $\omega_n = \frac{n\pi c_o}{2\ell}$, $c_o = \sqrt{\frac{E_o}{\rho_o}}$ and A_o, B_o are loading parameters. (The derivation of this normal mode solution is given in Appendix B.) One check to substantiate the numerical analysis described in the proceeding chapter was to run the elastic case in which $E_1/E_o = 1$. Results were found to agree exceptionally well with those given by a normal mode solution and are as shown by Figure (4-7c). Figure (4-8) presents the

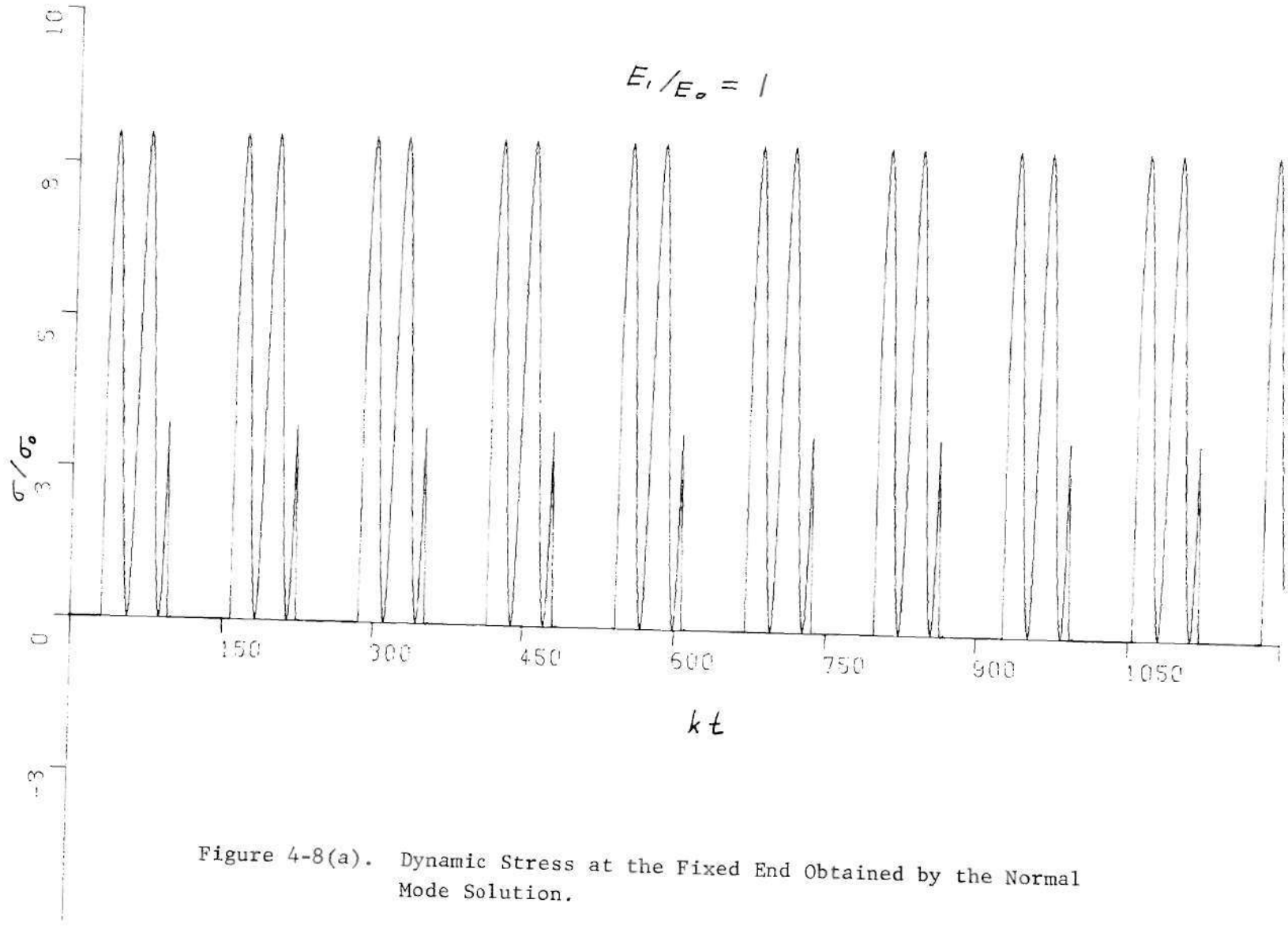

Figure 4-8(a). Dynamic Stress at the Fixed End Obtained by the Normal Mode Solution.

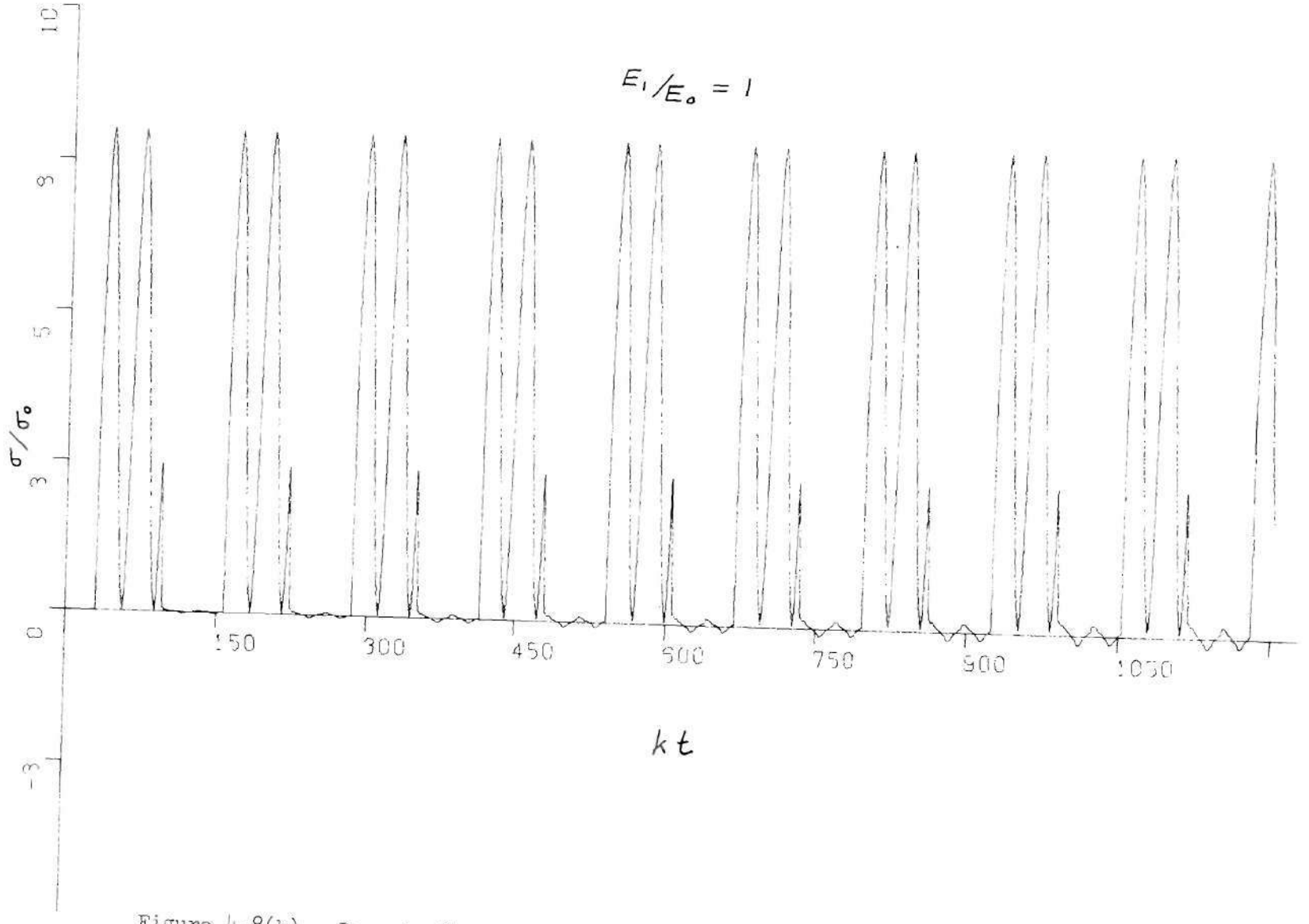

Figure 4-8(b). Dynamic Stress at the Fixed End Obtained by the Method of Characteristic.

stress-time history at the fixed end of this bar and illustrates the agreement between the two results, as found from both the method of characteristics and the method of normal modes. Study of Figure (4-7) indicates several interesting results. If one examines the time history of stress at the fixed end of the bar ($x = \ell$), one notes that there is also a time increase required for the stress to build up to its maximum value as the material becomes more plastic. In other words, the transient period, before the steady state response is obtained, is longer as the bar exhibits less strain hardening. This is due to the contributions of the strain-rate dependent term, $g(\sigma,\epsilon)$, and also the presence of a mean stress at the free end, which results in a longer period in the transient stage. Illustrated in Figure (4-9) is the stress time history at the fixed end of the bar for a time interval immediately after the bar has been stressed. Presented are results for ratios of E_1/E_o ranging from 1.0 (elastic) to 1/900 (near perfectly plastic). As shown in the figure, the steady state response, which oscillates at the input frequency $\omega = 2\pi k/32$ or period $T = 32/k$, is obtained more slowly as the material exhibits more plasticity. In fact, an infinite value of time is needed before the steady state occurs for the case of $E_1/E_o = 0$. It can also be seen from the figures that the mean value of the oscillating stress for all degrees of strain hardening has not changed and remains the same value ($\sigma_m = 2\sigma_o$) as the input mean stress. This delay (or phase shift) due to the influence of strain hardening was discussed in detail in an earlier paper by Wood and the author [37] in which a step load was applied and no Bauschinger effect was considered. This concludes the influence of strain hardening on phase of the resulting oscillating stress. The effect of

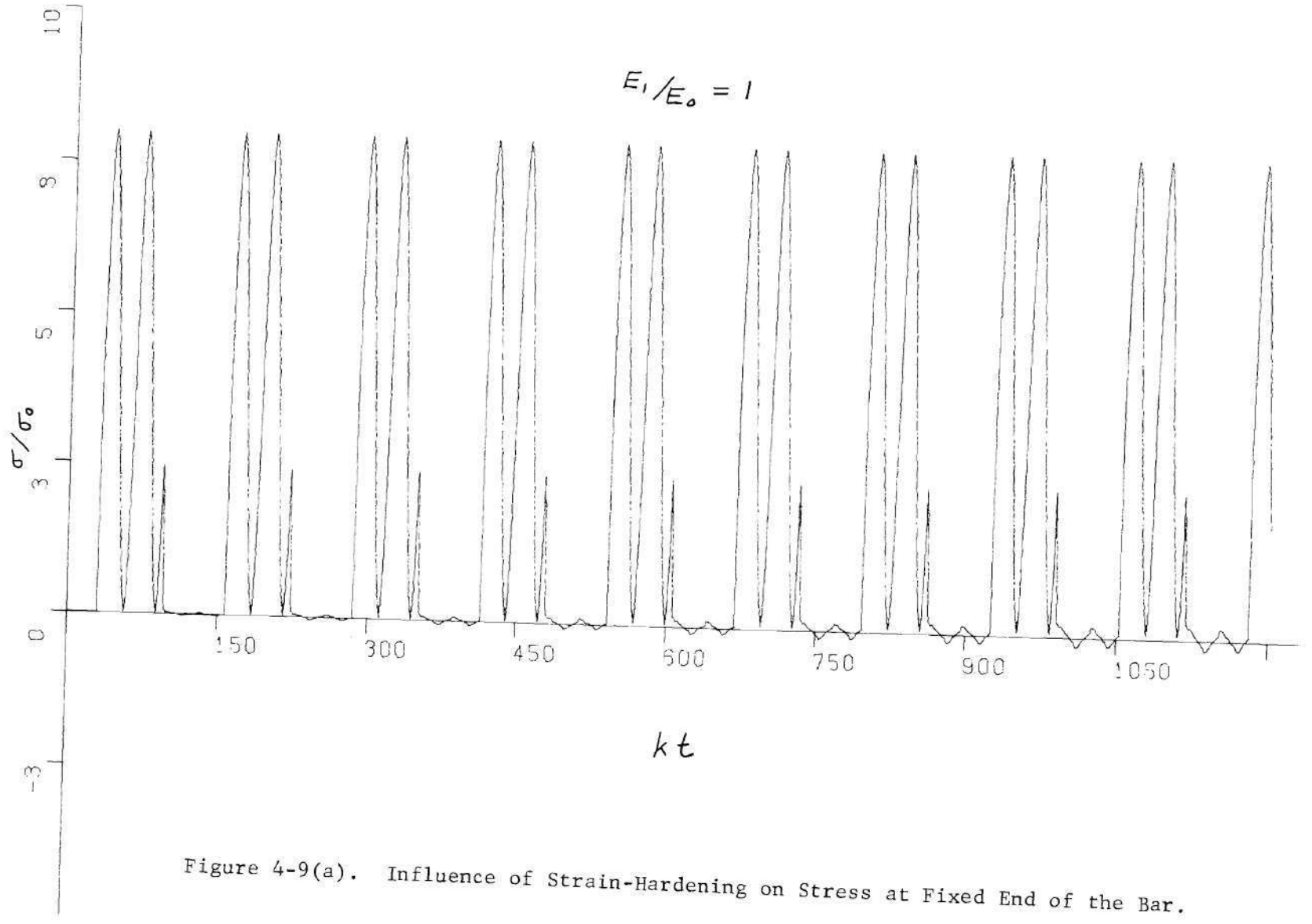

Figure 4-9(a). Influence of Strain-Hardening on Stress at Fixed End of the Bar.

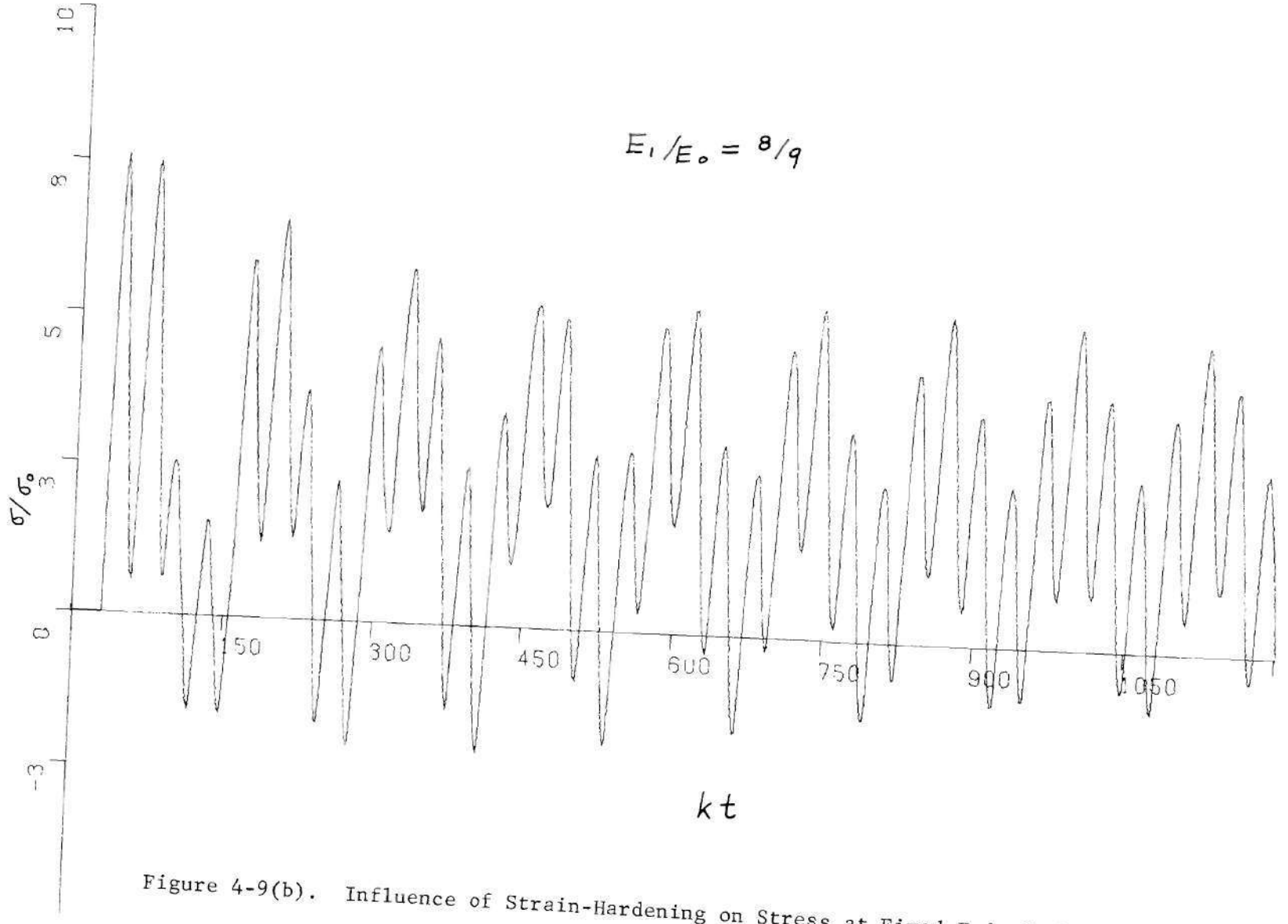

Figure 4-9(b). Influence of Strain-Hardening on Stress at Fixed End of the Bar.

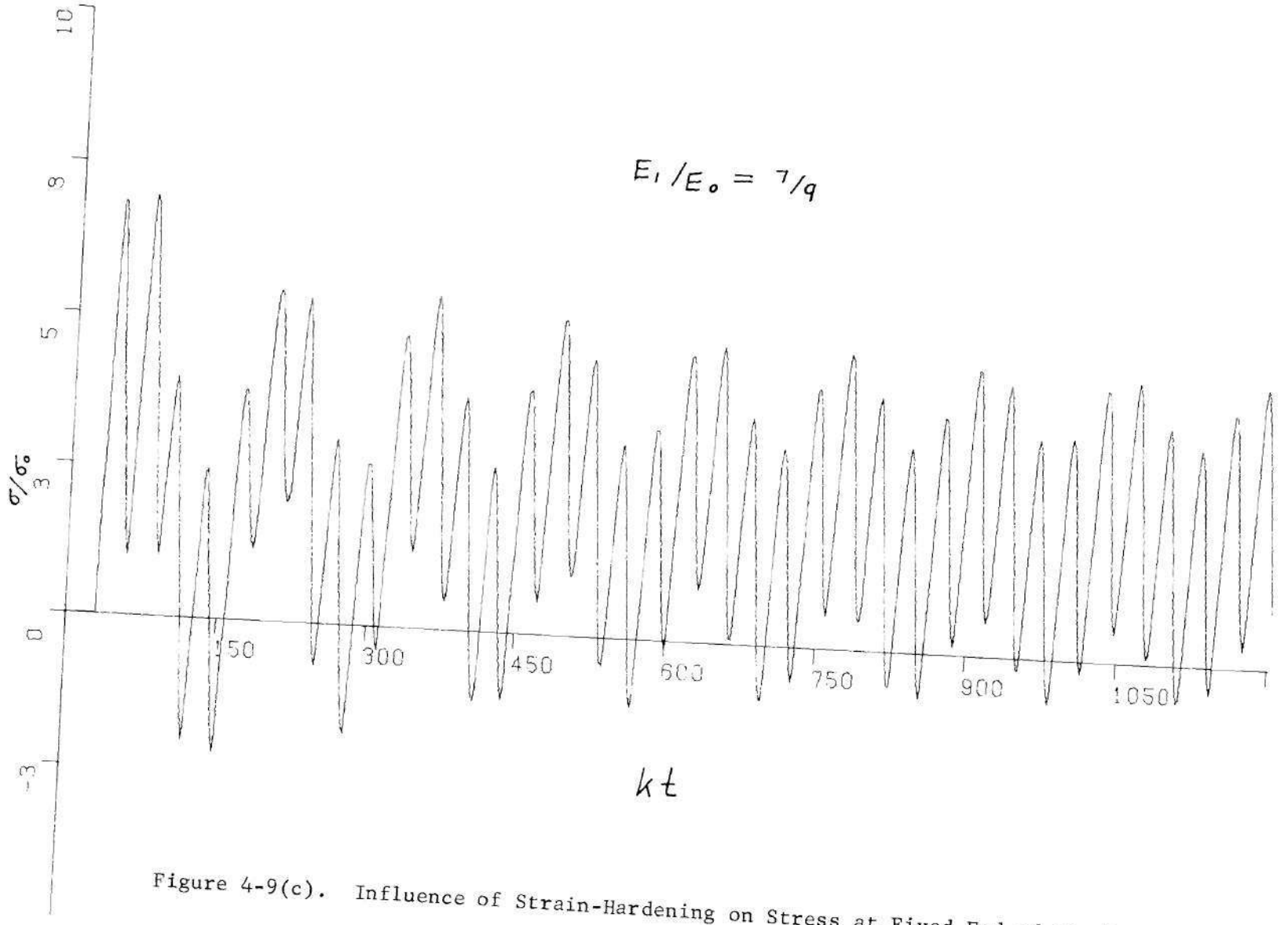

Figure 4-9(c). Influence of Strain-Hardening on Stress at Fixed End of the Bar.

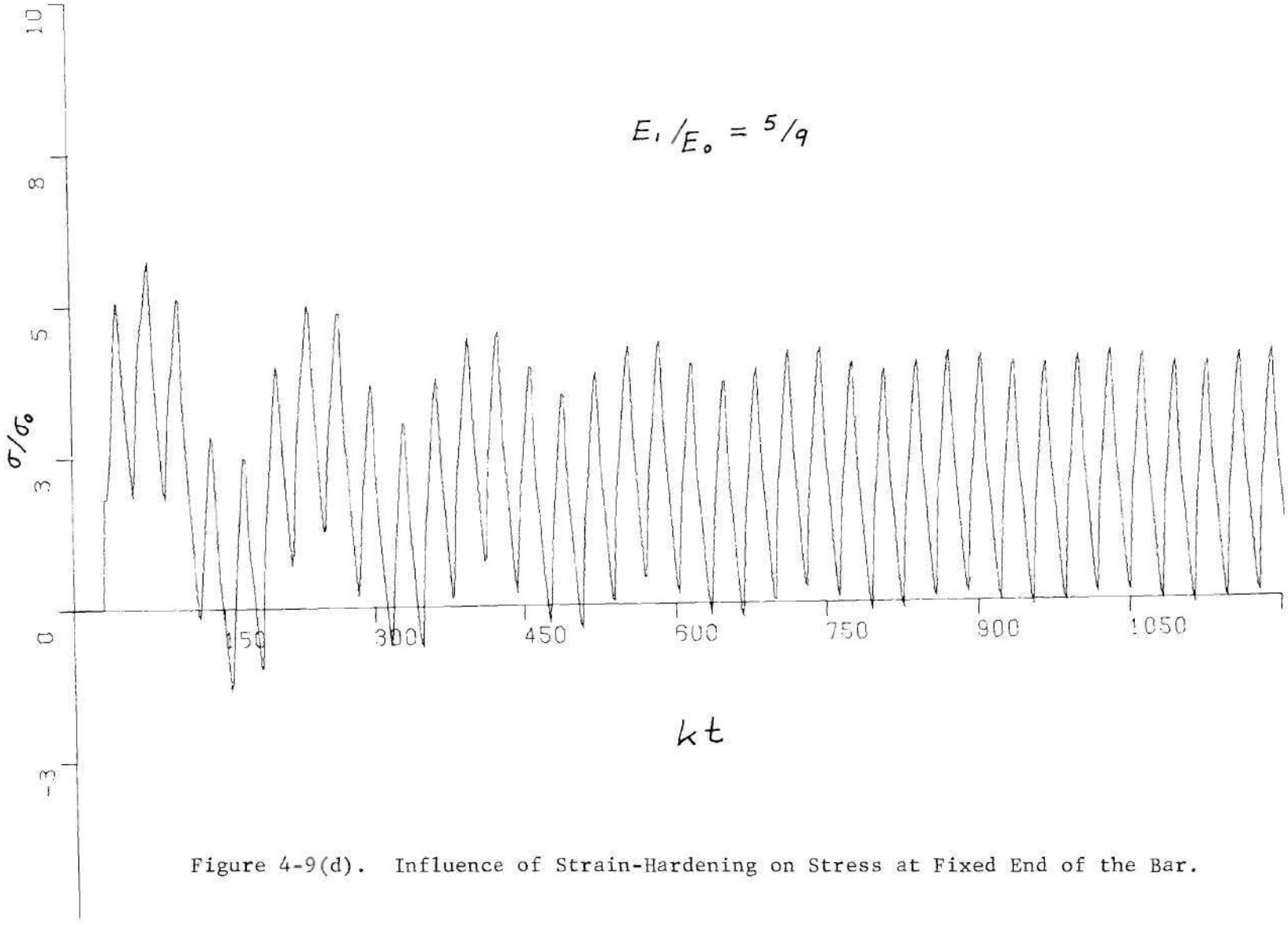

Figure 4-9(d). Influence of Strain-Hardening on Stress at Fixed End of the Bar.

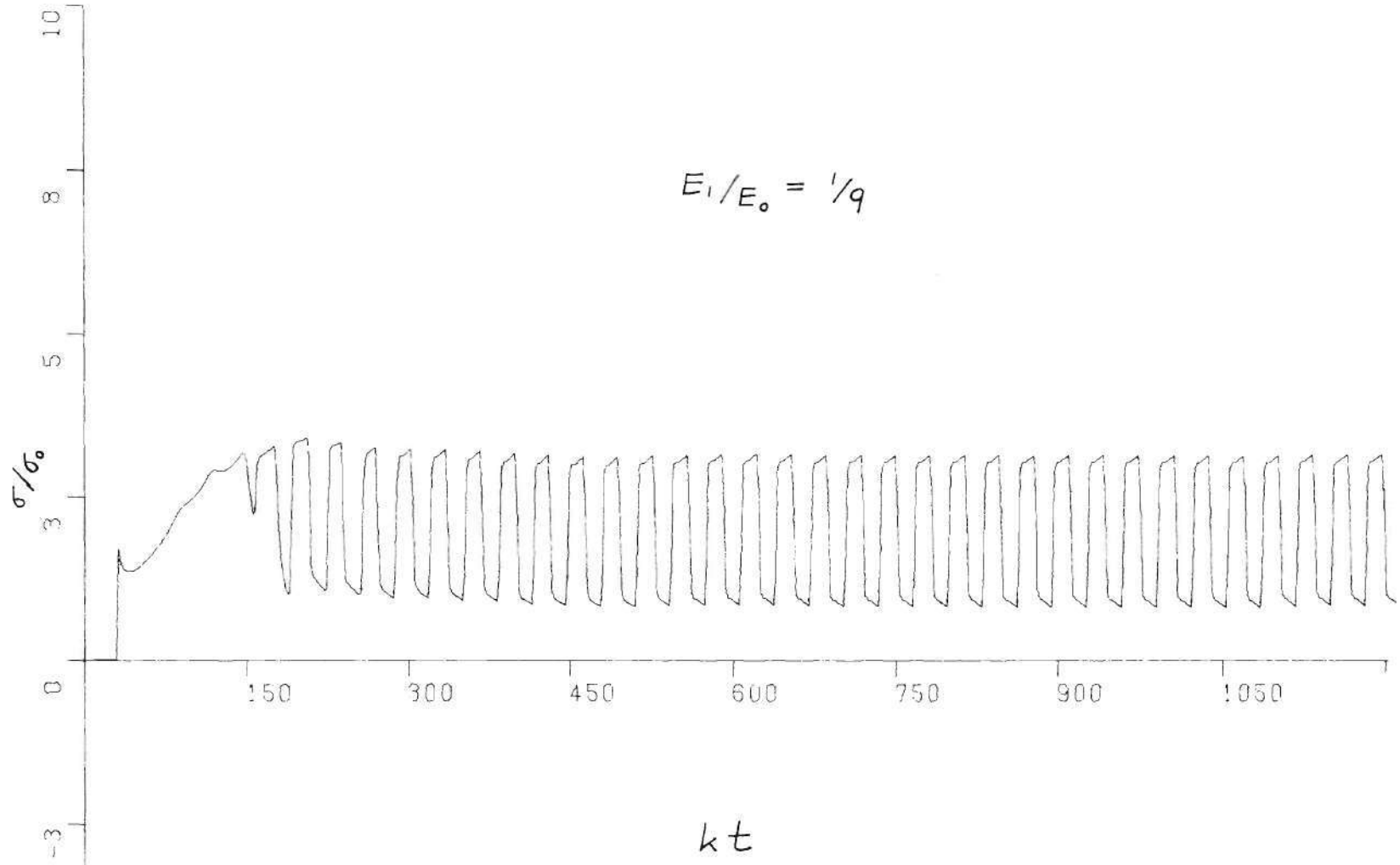

Figure 4-9(e). Influence of Strain-Hardening on Stress at Fixed End of the Bar.

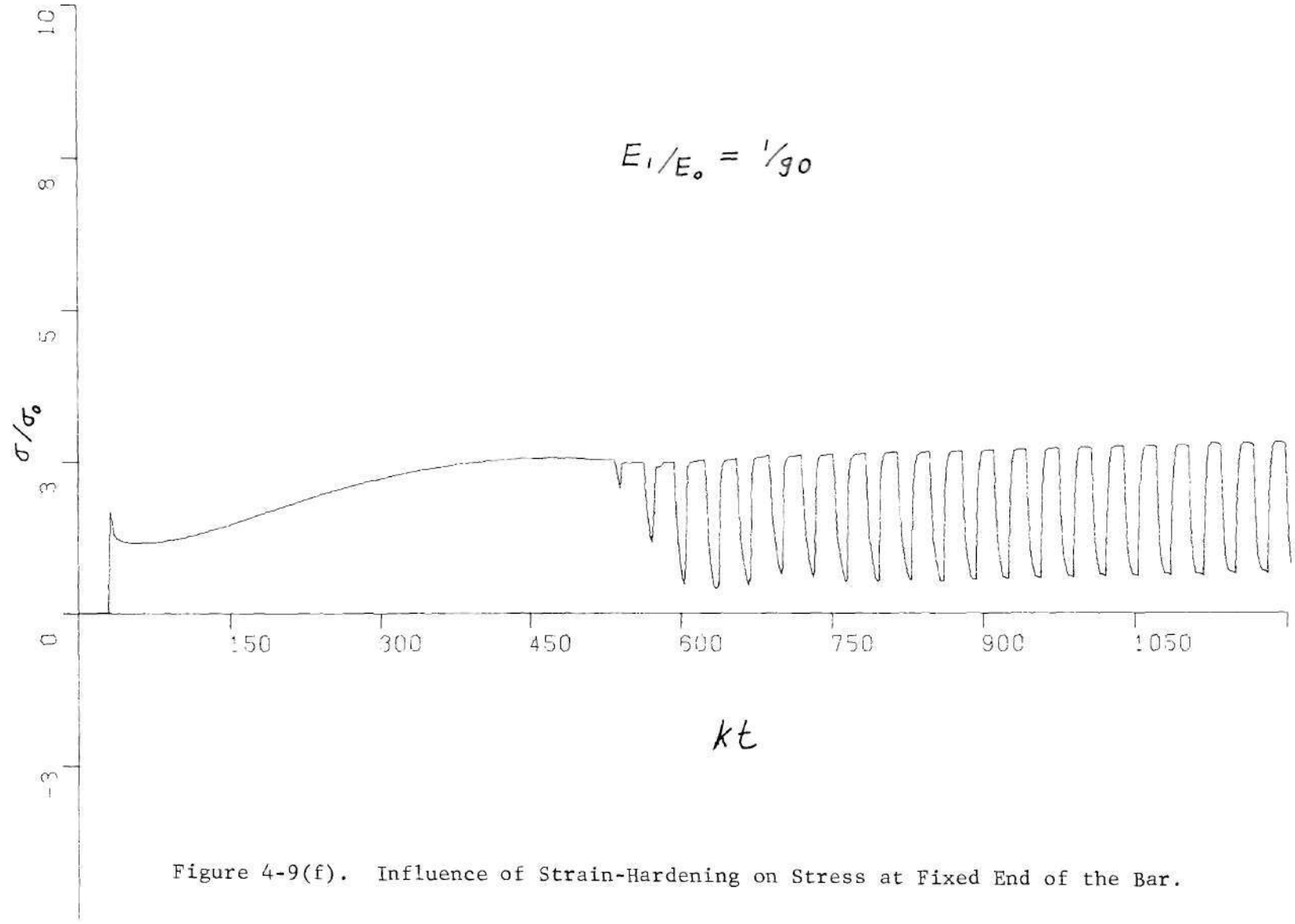

Figure 4-9(f). Influence of Strain-Hardening on Stress at Fixed End of the Bar.

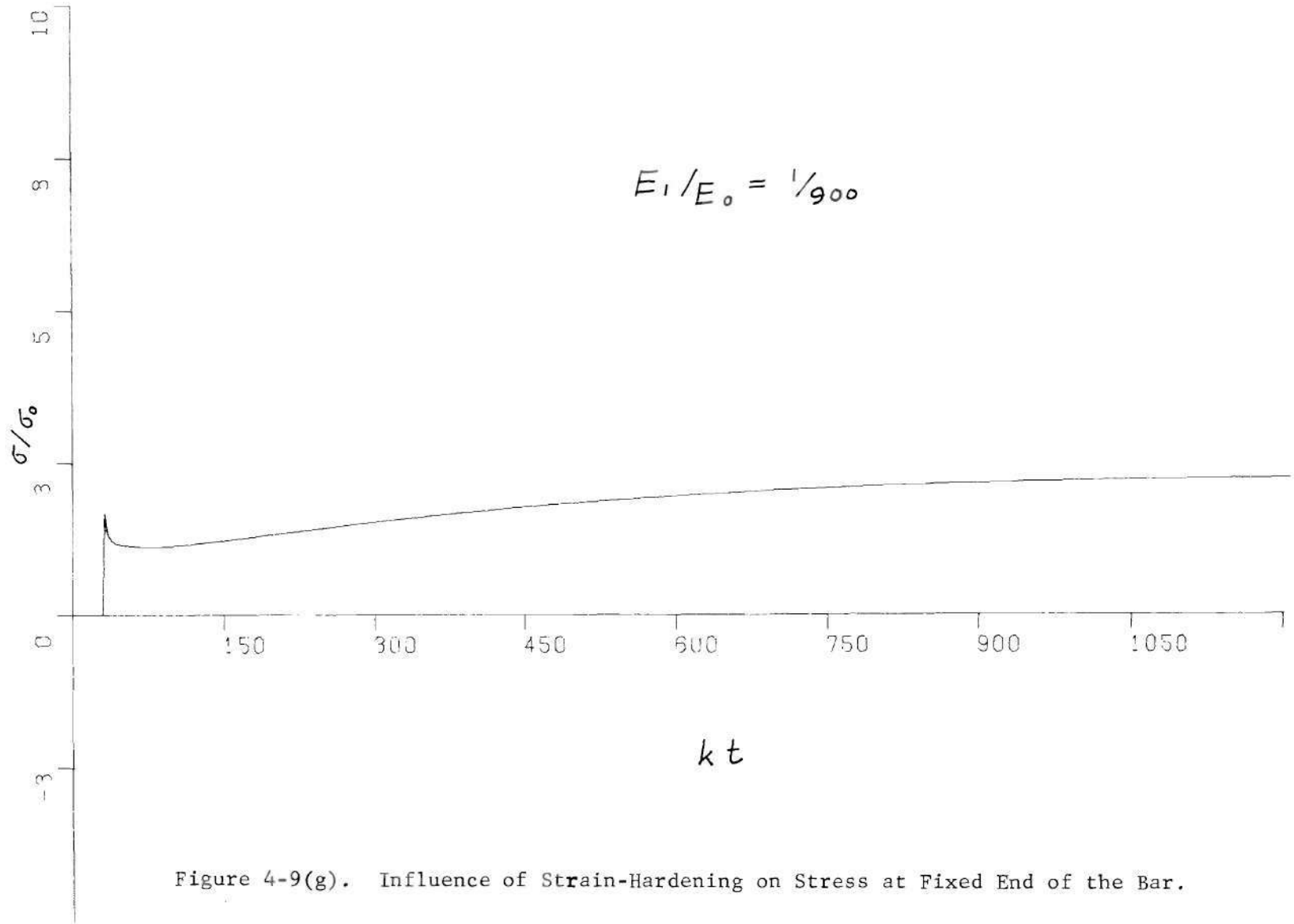

Figure 4-9(g). Influence of Strain-Hardening on Stress at Fixed End of the Bar.

strain hardening on the amplitude of the resulting oscillating stress will be discussed in more detail in a later section. We have seen some dynamic stress-strain plots with the Bauschinger effect and also at various locations of the bar. In the following figures, (Fig. (4-10) and Fig. (4-11)) one shall see the dynamic stress-strain curves under the influence of degrees of strain hardening. It is noticeable here that the degrees of strain hardening have a large effect on the dynamic stress-strain plot, especially on the size of the hysteresis loop and the permanent strain. As indicated in Figure (4-10), the less strain-hardening in the bar, the more area the hysteresis loop covers, and also the more permanent strain the bar has. Figure (4-11) shows the dynamic stress strain curve in which the Bauschinger effect was neglected. At $E_1/E_o = 1$ both cases will have the same dynamic stress strain curve, which is a straight line.

III. Time History of Stress Wave Development

In studies of elastic-plastic wave propagation, it has frequently been shown that an elastic wave front travels along a semi-infinite bar followed by a plastic wave front. This is due to the elastic wave velocity being faster than that of the plastic wave. Further, if elastic unloading is introduced, then behind the preceeding plastic wave front there comes an unloading wave front which travels at elastic wave speed. And this unloading wave will eventually overtake the plastic one. Figure (4-12) was taken from Wood's work [22] and shows some trends regarding this kind of wave interaction. The wave interaction in this study occurs from time to time since the wave velocity is a function of the slope of

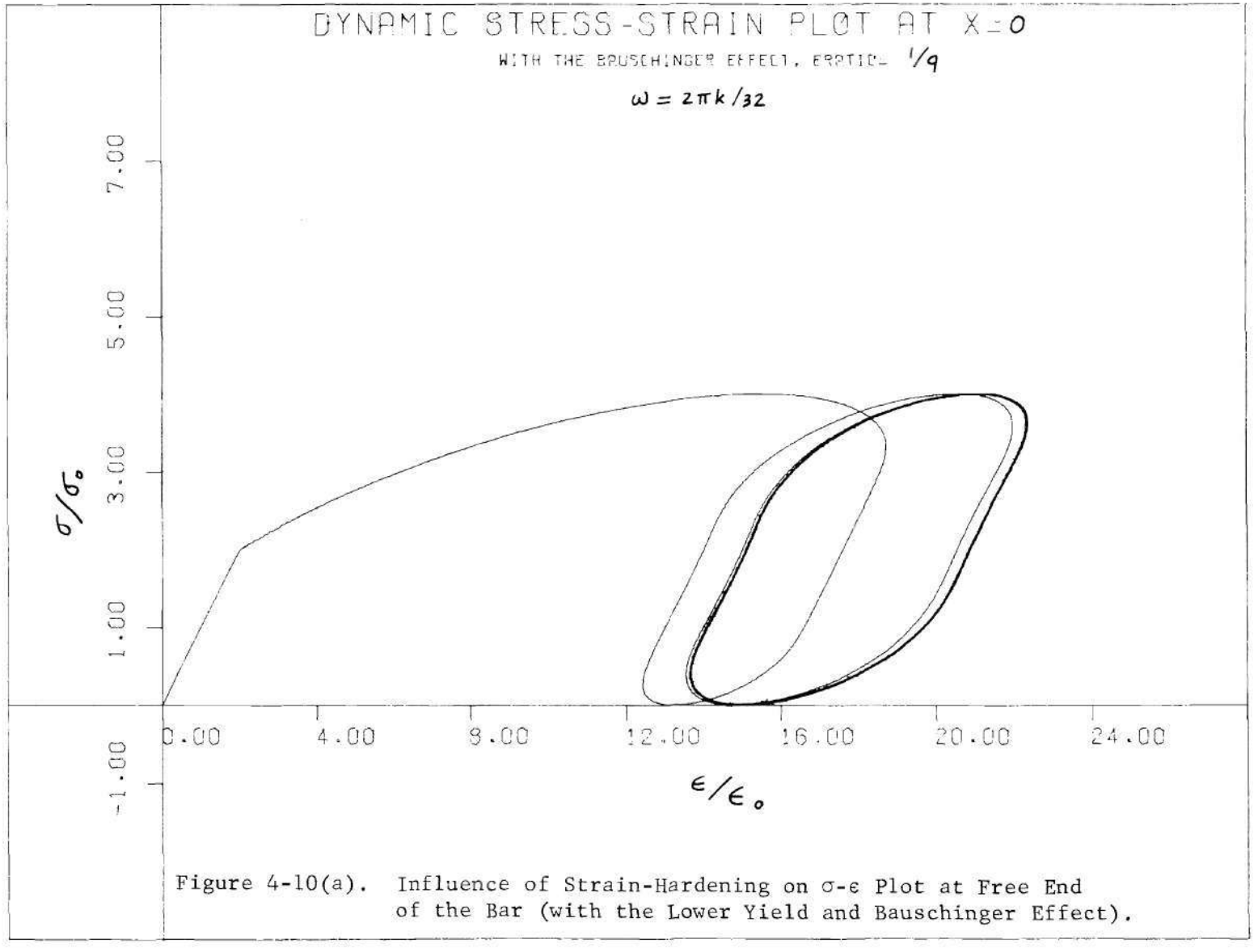

Figure 4-10(a). Influence of Strain-Hardening on σ-ε Plot at Free End of the Bar (with the Lower Yield and Bauschinger Effect).

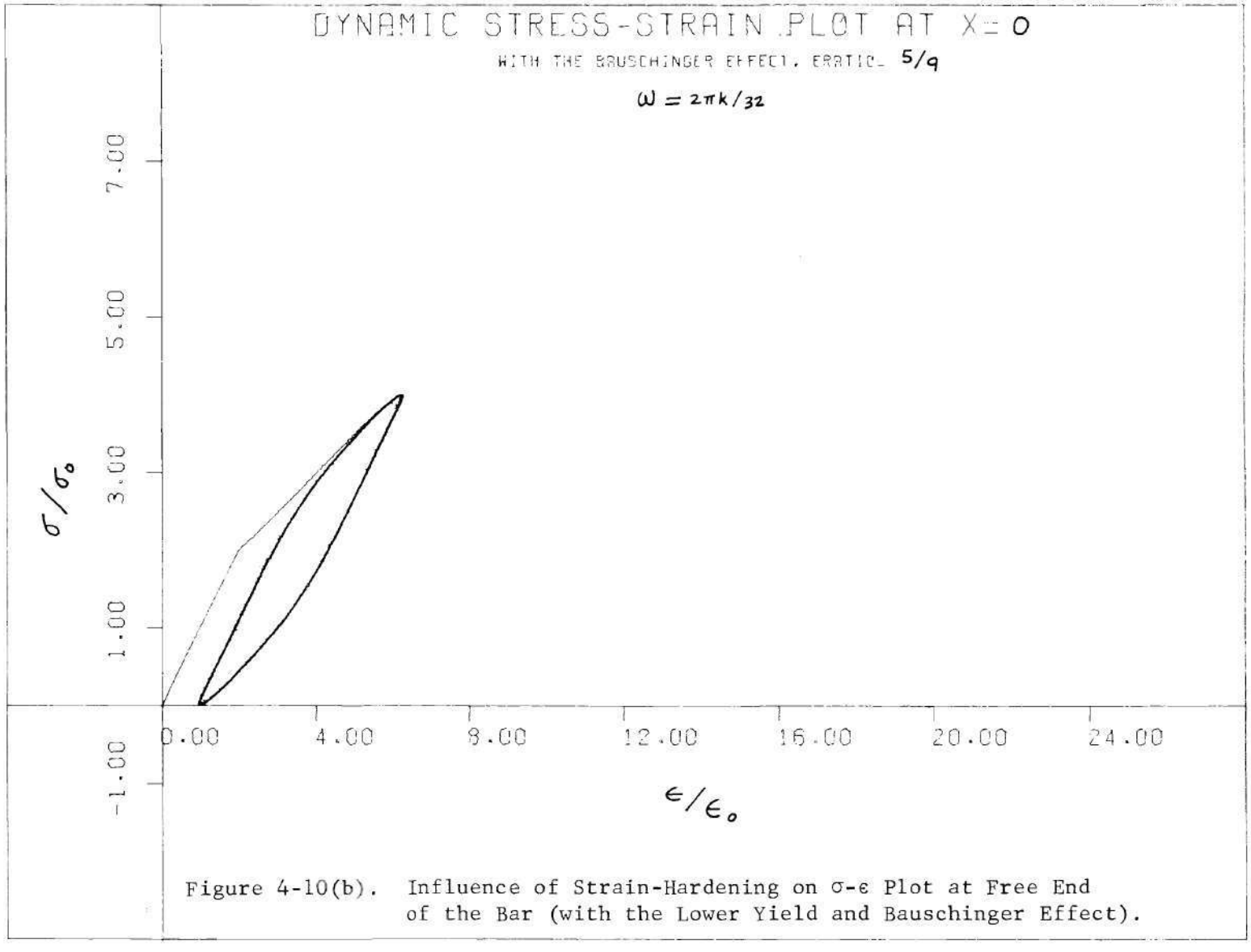

Figure 4-10(b). Influence of Strain-Hardening on σ-ε Plot at Free End of the Bar (with the Lower Yield and Bauschinger Effect).

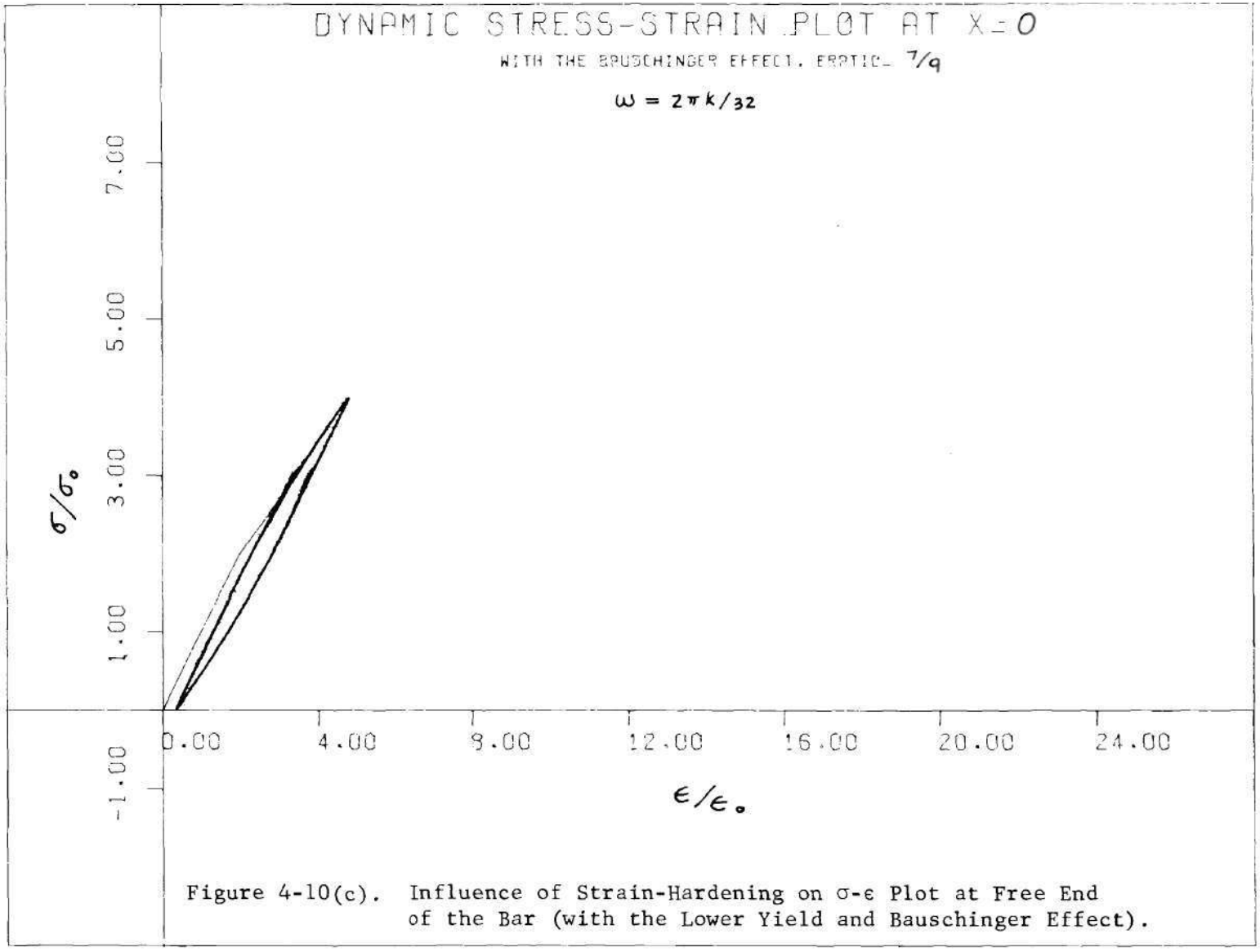

Figure 4-10(c). Influence of Strain-Hardening on σ-ε Plot at Free End of the Bar (with the Lower Yield and Bauschinger Effect).

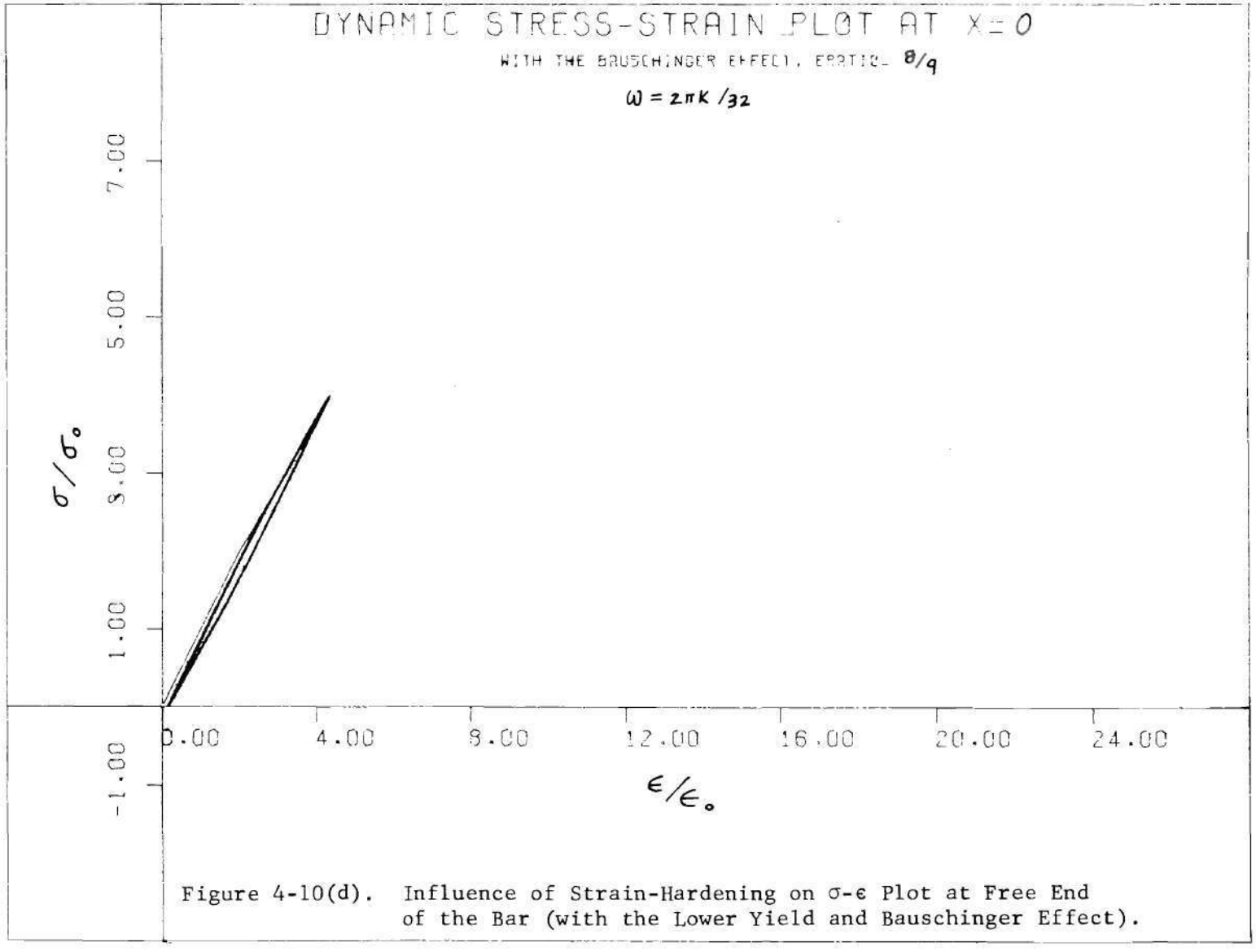

Figure 4-10(d). Influence of Strain-Hardening on σ-ϵ Plot at Free End of the Bar (with the Lower Yield and Bauschinger Effect).

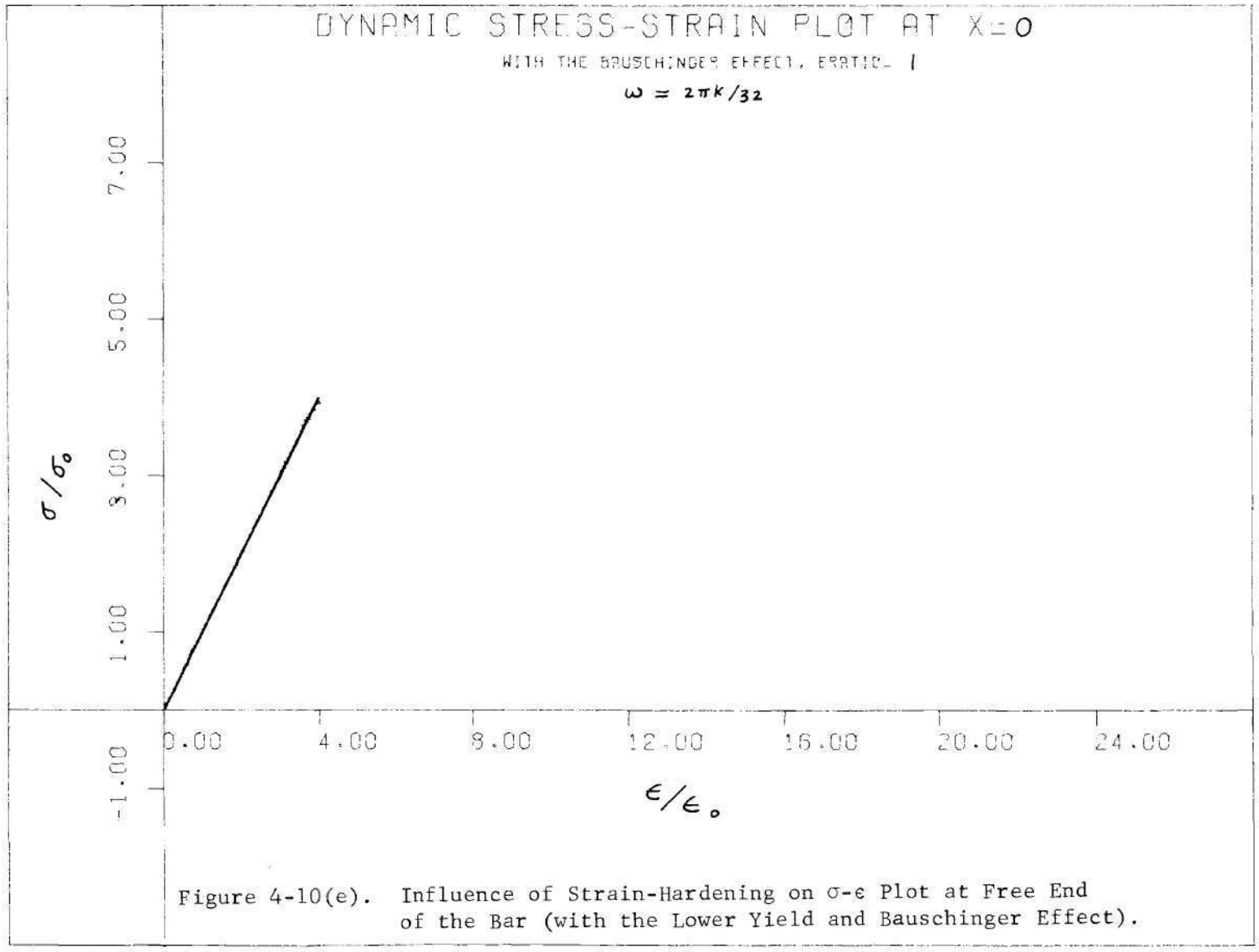

Figure 4-10(e). Influence of Strain-Hardening on σ-ε Plot at Free End of the Bar (with the Lower Yield and Bauschinger Effect).

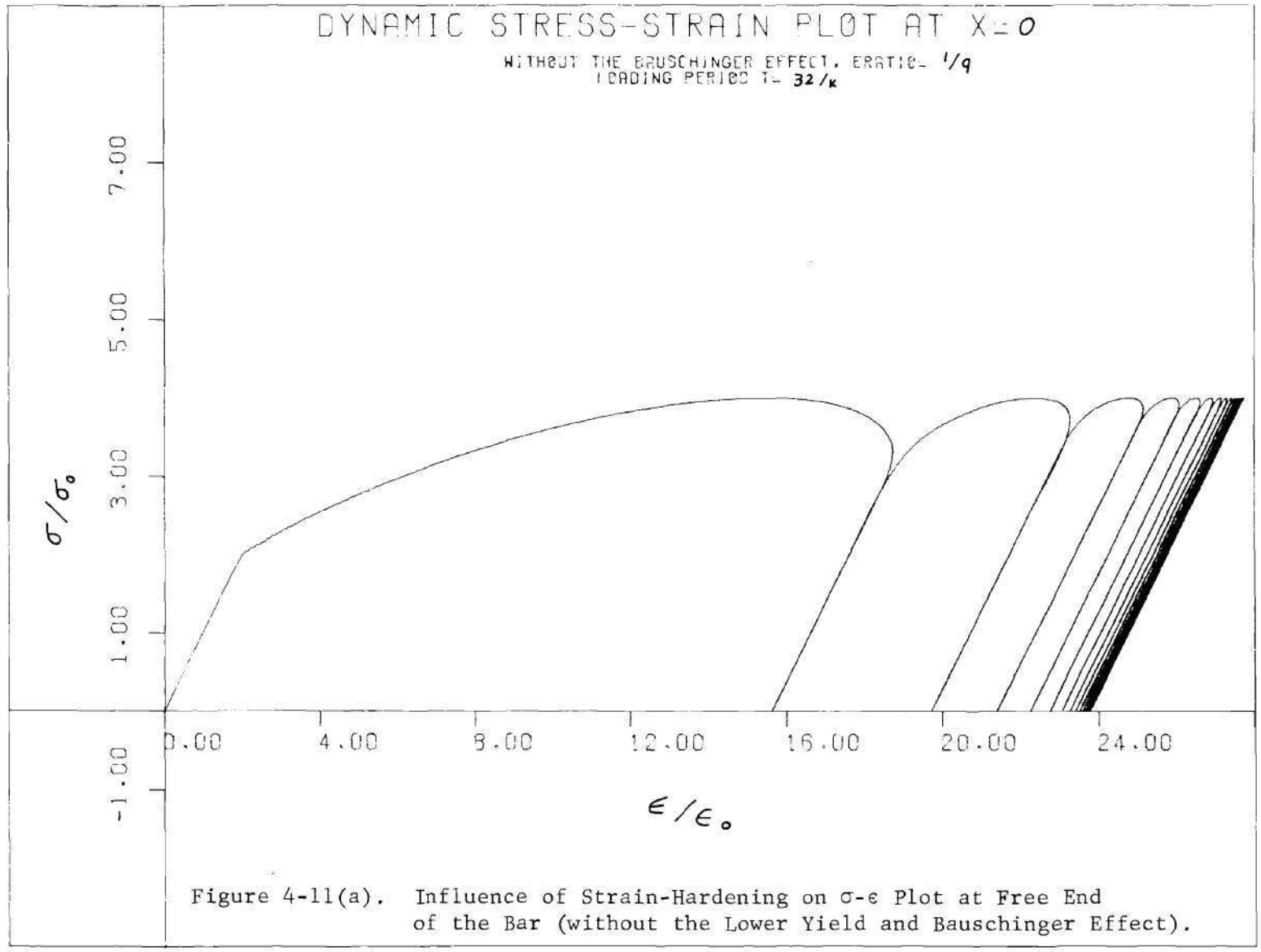

Figure 4-11(a). Influence of Strain-Hardening on σ-ϵ Plot at Free End of the Bar (without the Lower Yield and Bauschinger Effect).

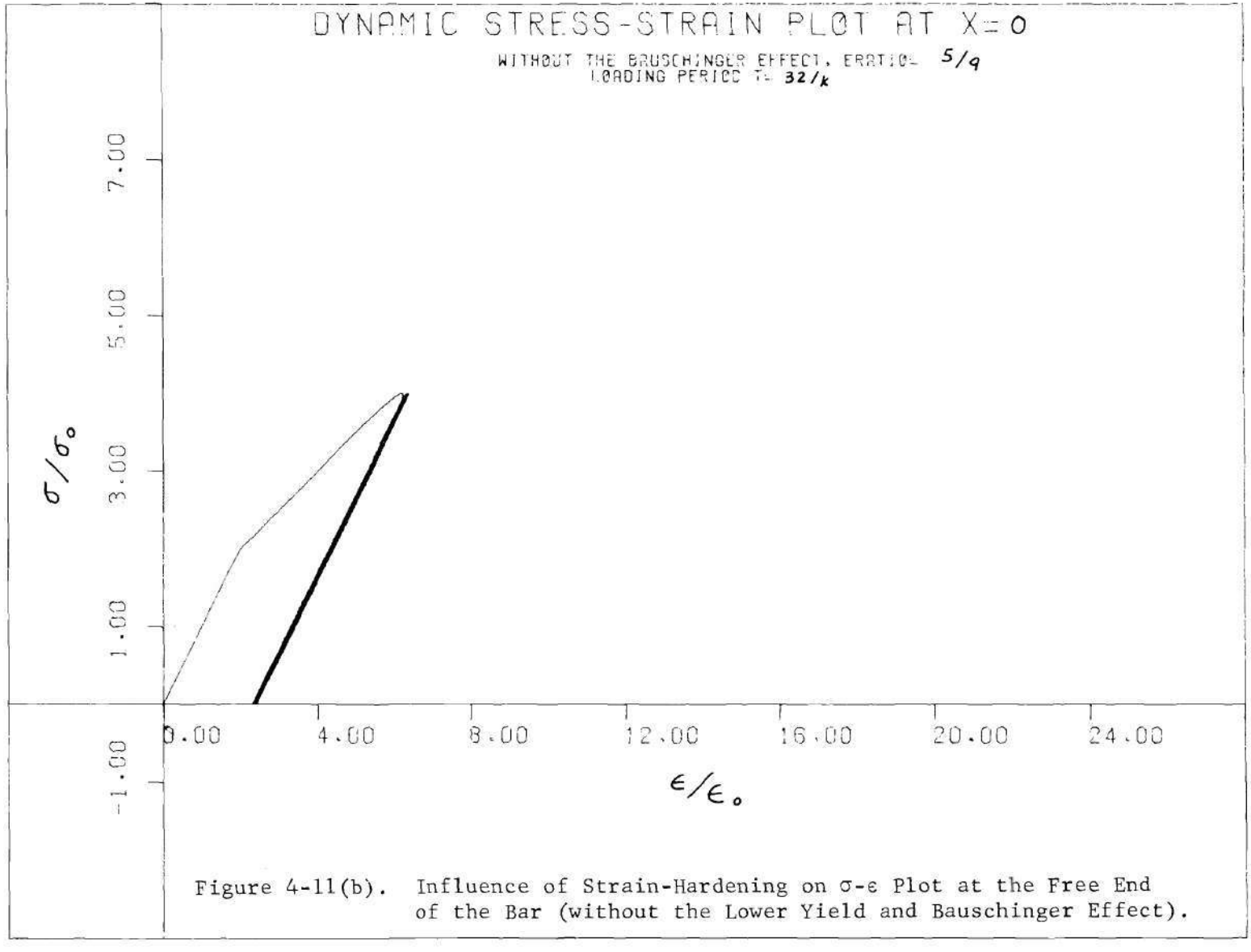

Figure 4-11(b). Influence of Strain-Hardening on σ-ε Plot at the Free End of the Bar (without the Lower Yield and Bauschinger Effect).

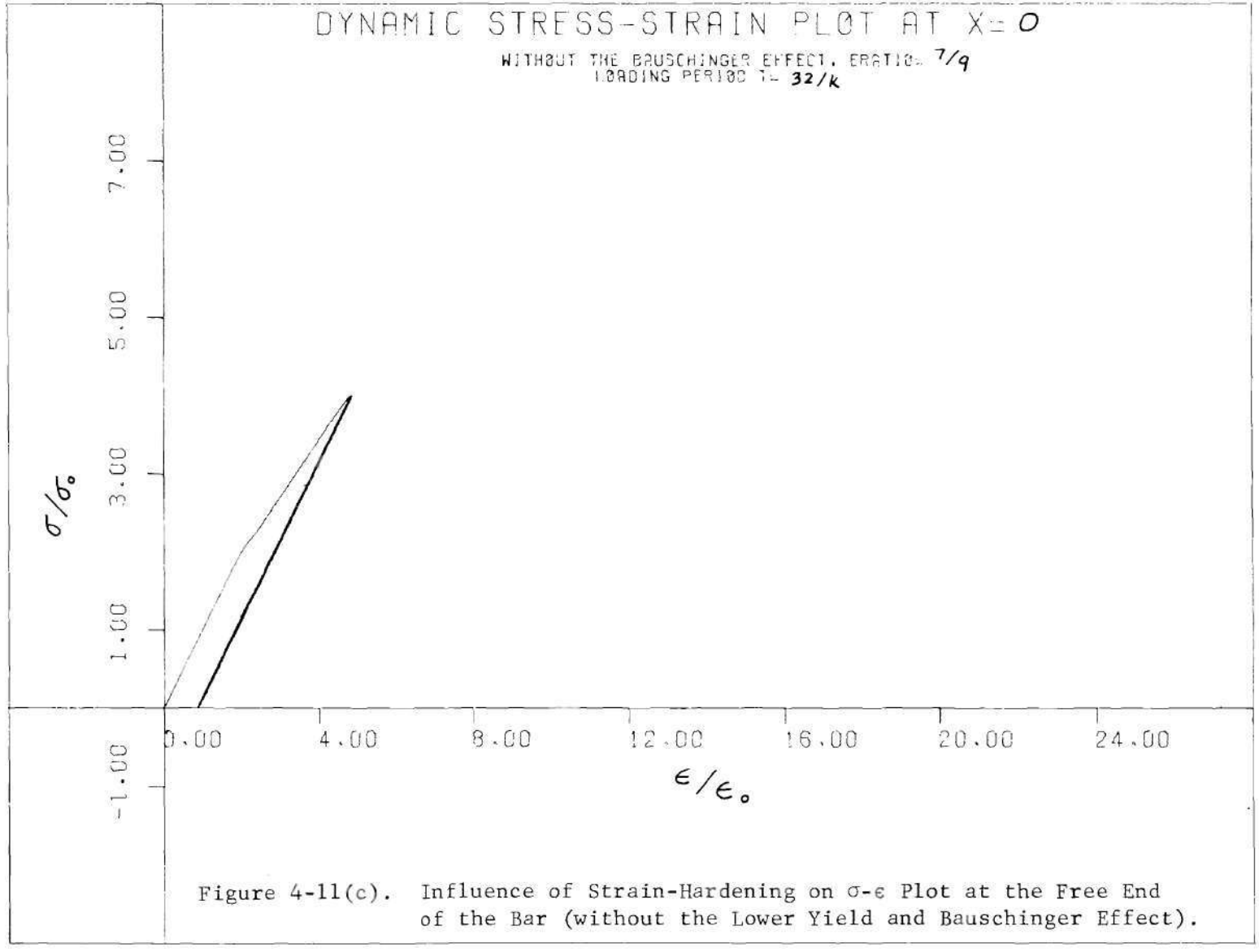

Figure 4-11(c). Influence of Strain-Hardening on σ-ε Plot at the Free End of the Bar (without the Lower Yield and Bauschinger Effect).

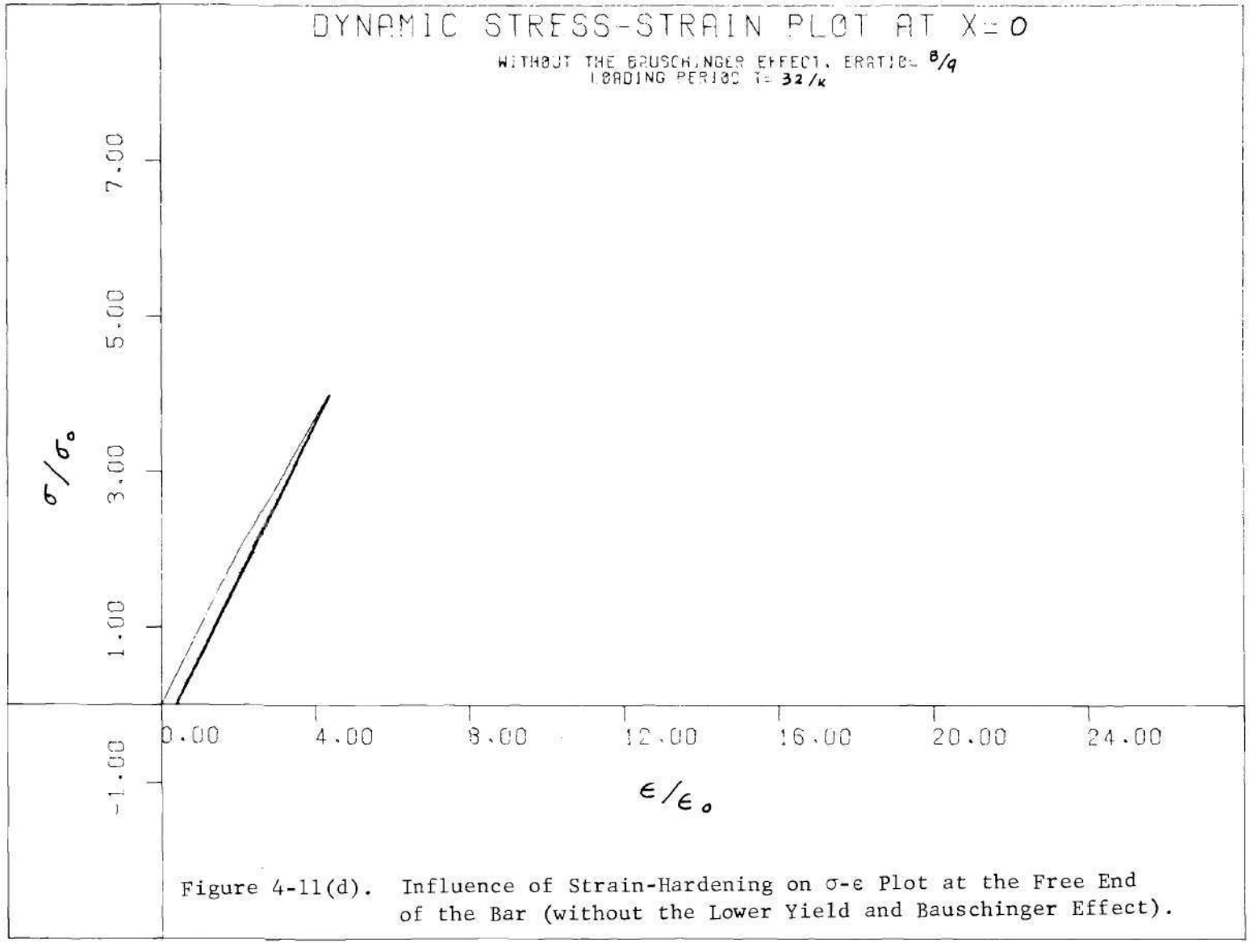

Figure 4-11(d). Influence of Strain-Hardening on σ-ε Plot at the Free End of the Bar (without the Lower Yield and Bauschinger Effect).

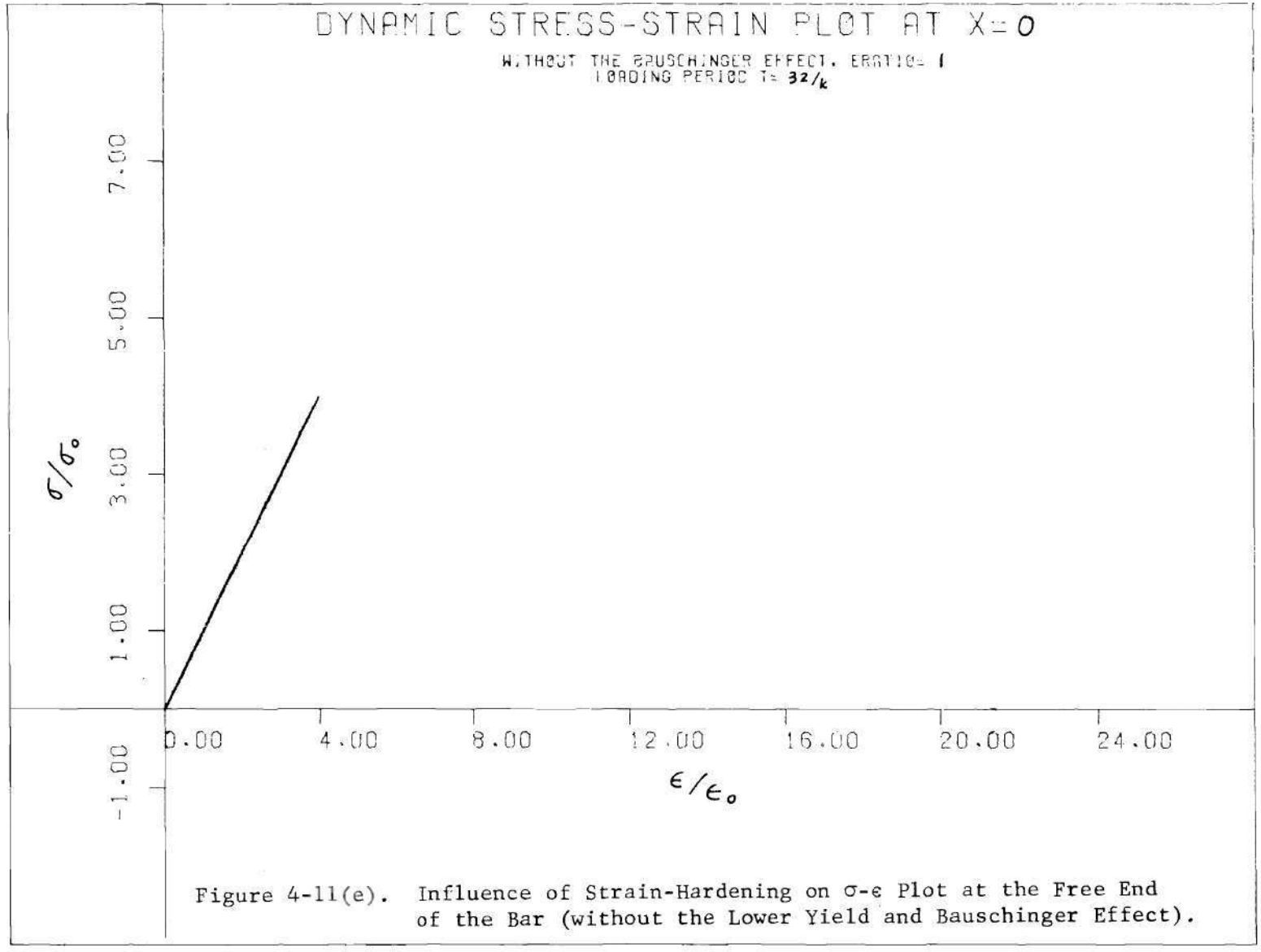

Figure 4-11(e). Influence of Strain-Hardening on σ-ε Plot at the Free End of the Bar (without the Lower Yield and Bauschinger Effect).

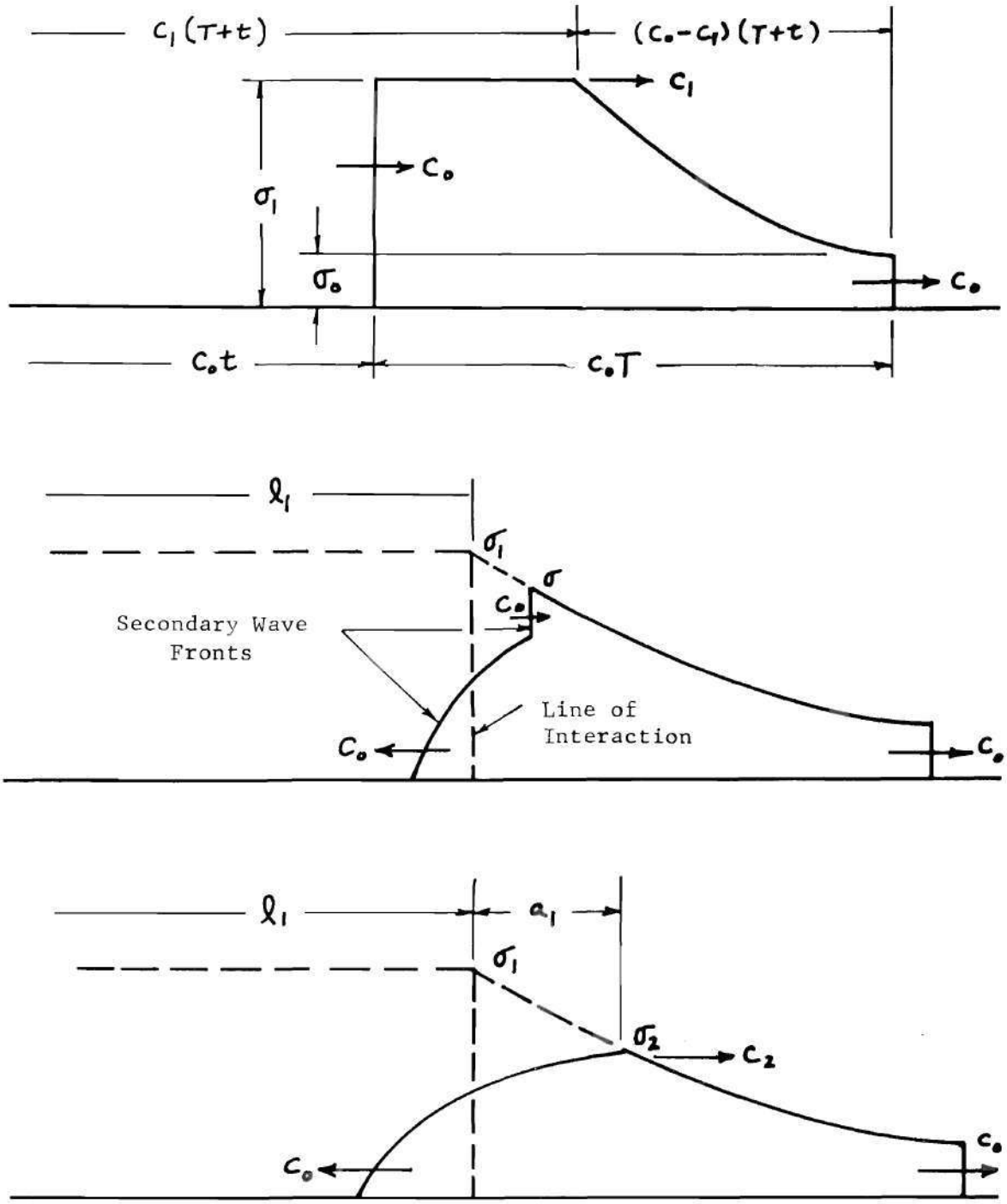

Figure 4-12. Wave Interactions after Wood's Work.

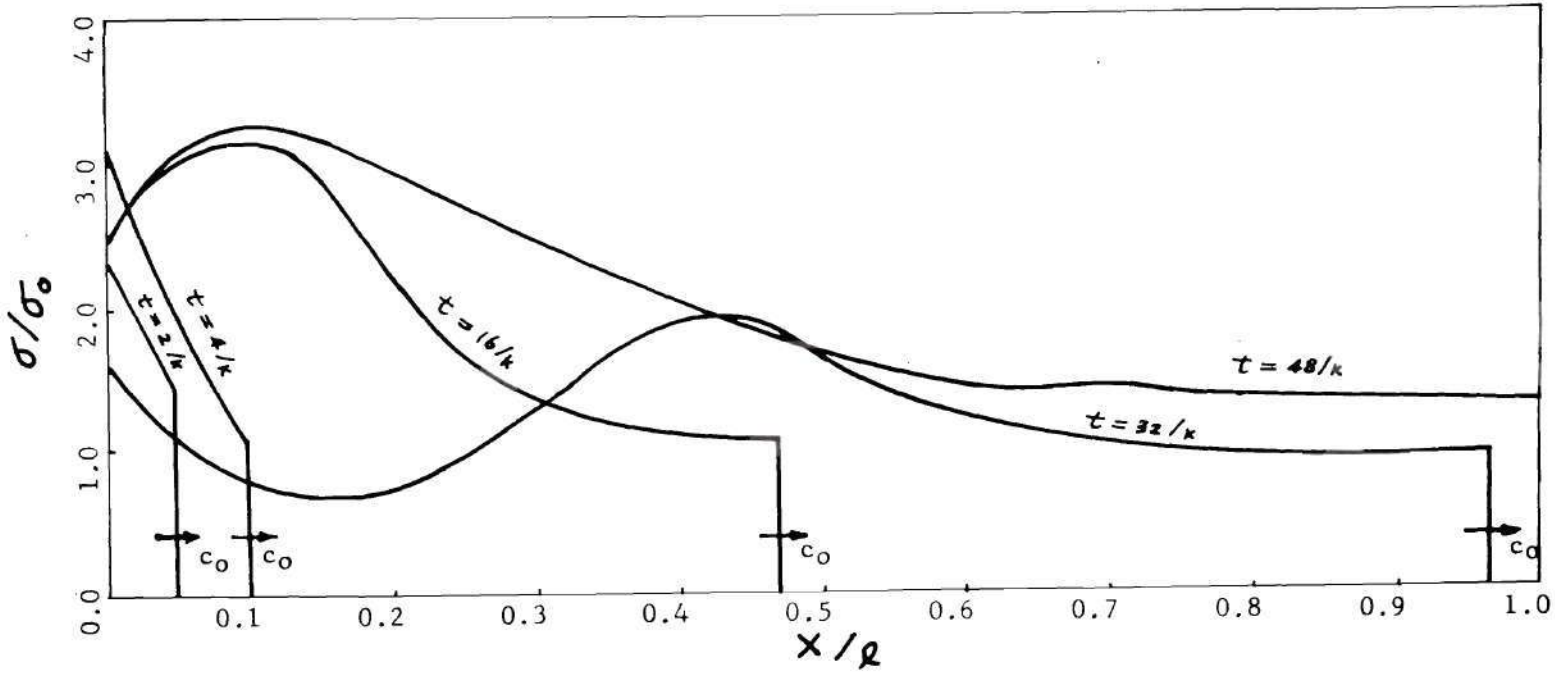

Figure 4-13. The formation of Dynamic Stress Wave Form during Different Period Along the Bar

the dynamic stress-strain relations which vary all the time. Therefore, wave velocity is different at any location of the bar and at any instant of time. It would be simpler if there was a single step pulse travelling in a semi-infinite bar. However, for a rate-dependent material under a cyclic load (for a finite bar) the multiple wave interactions and reflections give rise to a very complicated wave form along the bar. Numerical solution in this study yields all the stresses in the x-t plane (also strain and velocity). The development of the stress wave and its wave front is able to be seen in Figure (4-13).

IV. Frequency Response and Plastic Resonance

The next phase of the study considers the most important aspect of this dissertation. That is, we study the dynamic response of a bar that exhibits elastic-visco-plastic characteristics and the Bauschinger effect, acting under a sinusoidal load at various frequencies. Consequently, the amplification effect of the dynamic response of the bar can be studied closely. As mentioned in Chapter I, this amplification effect was first encountered by Kalaski and Wladarczyk [1, 32, 33], who introduced the term "plastic resonance". Because of the generality of the formulation in this study, one can see the solution of the problem from several different view points. For instance, what is the frequency responses at any location along the bar? How does the degree of strain-hardening effect the frequency response? And what is the amplification factor at plastic resonance? All of these questions will be answered in the following section. A comparison will be also made for plastic resonance, considering the Bauschinger effect and without this effect.

(A) Frequency Response

Shown in Figure (4-14) and Figure (4-15) are two frequency response plots for the bar (loaded sinusoidally at the free end with an amplitude of twice the yield stress and zero mean stress). The y-axis represents the maximum amplitude of dynamic displacement $A^u(o)/u_o$ divided by the static displacement u_{st}/u_o at the free end, or that is sometimes referred to as amplification factor. The x-axis represents the ratio of the input frequency (ω) to the first fundamental frequency of an elastic bar (ω_n). The circular frequency ω, for the bar in this study is found to be $2\pi k/128$. The dynamic displacement can be found by numerical integration of velocity with respect to time at the free end with an initial velocity of zero. Under a static bilinear stress-strain relation, the static displacement at the free end of a plastic bar is given by,

$$u^{st}(o) = \begin{cases} \dfrac{p\ell}{AE_o} & \text{for } \dfrac{P}{A} \le \sigma_o \\ \left[\dfrac{\frac{P}{A} - \sigma_o}{E_1} + \dfrac{\sigma_o}{E_o}\right]\ell & \text{for } \dfrac{P}{A} > \sigma_o \end{cases} \qquad (4\text{-}4)$$

where ℓ is the length of the bar, P/A is the applied stress, σ_o is the yield stress and E_1, E_o are respectively the modulus of plasticity and the modulus of elasticity which define the bilinear stress-strain relations. With some transformations, equation (4-4) can be written in non-dimensional form as,

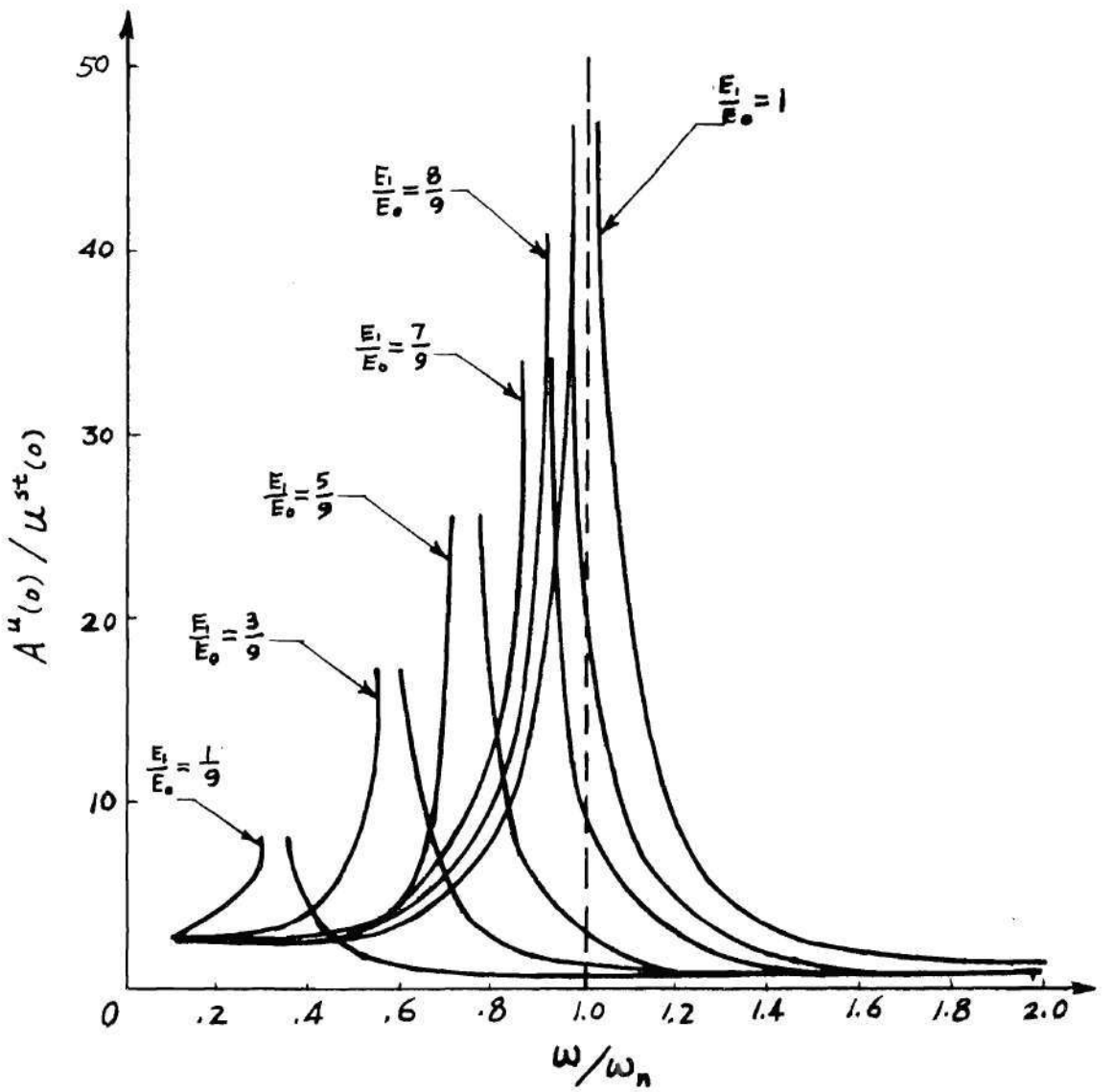

Figure 4-14. Frequency Response of Displacement at the Free End (with the Lower Yield and Bauschinger Effect).

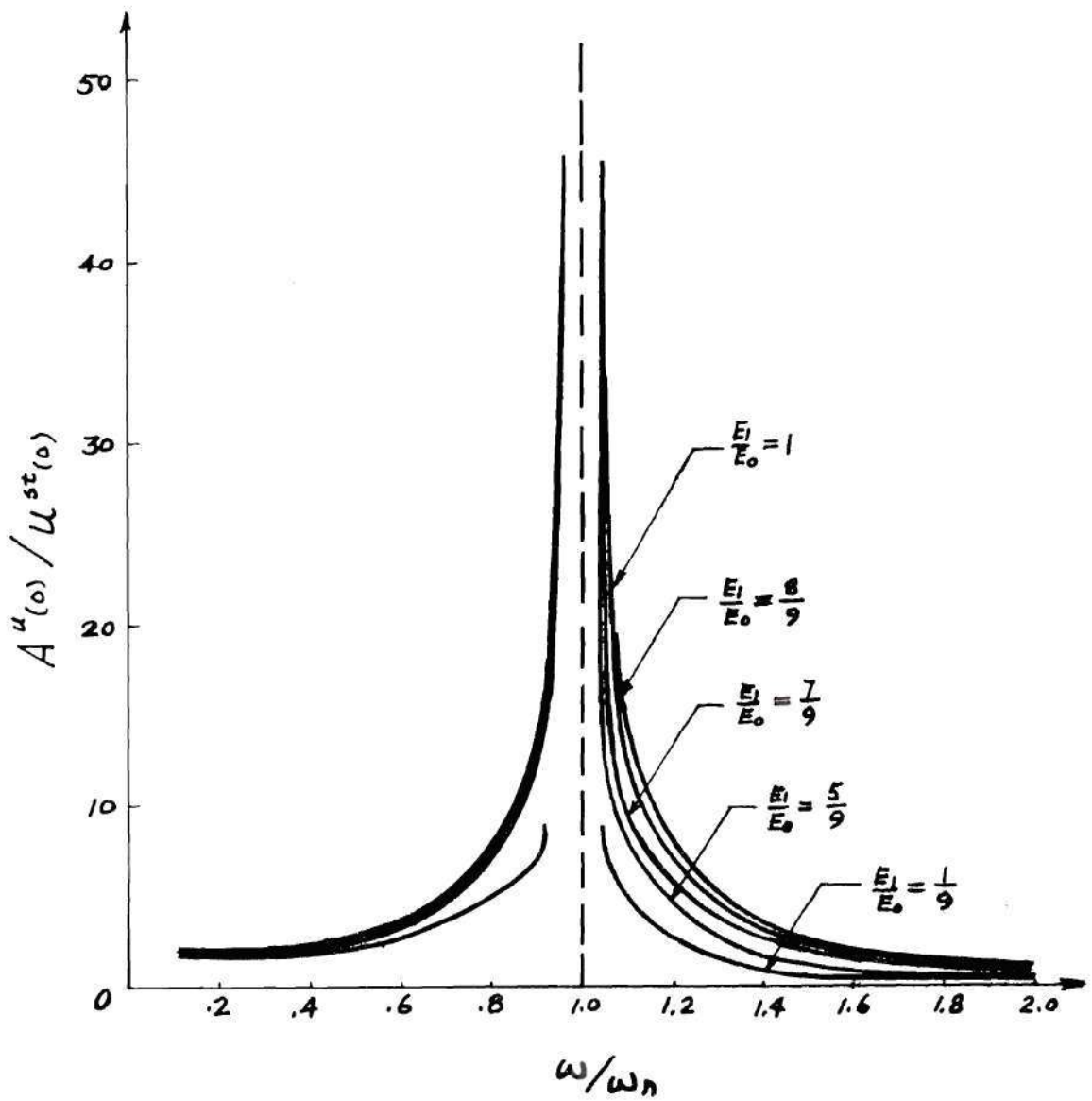

Figure 4-15. Frequency Response of Displacement at the Free End (without the Lower Yield and Bauschinger Effect).

$$\frac{u^{st}(o)}{u_o} = \begin{cases} \frac{N}{2} \cdot \bar{P} & \text{for } \bar{P} \leq 1 \\ \\ \frac{N}{2}\left[\frac{\bar{P}-1}{\frac{E_1}{E_o}} + 1\right] & \text{for } \bar{P} \geq 1 \end{cases} \qquad (4\text{-}5)$$

where $\bar{P} = P/A\sigma_o$, $N = T/2$, and $T = 2\pi/\omega_n$.

In Figure (4-14), one sees that the degree of plasticity has a pronounced effect on the resonance frequency. In the case of a more plastic bar, the resonance effect can still be seen. For $E_1/E_o = 1/9$, the resonance effect occur around $\omega/\omega_n = 0.30$ and for $E_1/E_o = 5/9$, it occurs at $\omega/\omega_n = 0.74$. In order to illustrate this fact, Figure (4-16) shows the displacement histories at the free end for several degrees of strain-hardening at a driving frequency equal to $2\pi k/172$ or $\omega/\omega_n = 0.74$ which is about 25% lower than the elastic natural frequency. When $E_1/E_o = 1$ as the limit, the resonance effect occurs at the frequency ratio of 1 as expected. The finding here tells us that, with the Bauschinger effect, the more plastically the bar behaves, the lower resonant frequency (compared to the elastic frequency) the bar has. Therefore, one can make the following statement: The resonance effect still exists for a material which behaves plastically (even for $E_1/E_o = 1/9$). However, the corresponding plastic resonance frequency is not the same as the elastic resonant frequency but instead a lower value. Another interesting plot is given in Figure (4-17) which shows the influence of strain-hardening on the resonant frequency of the bar.

On the other hand, if one looks at Figure (4-15), the case without

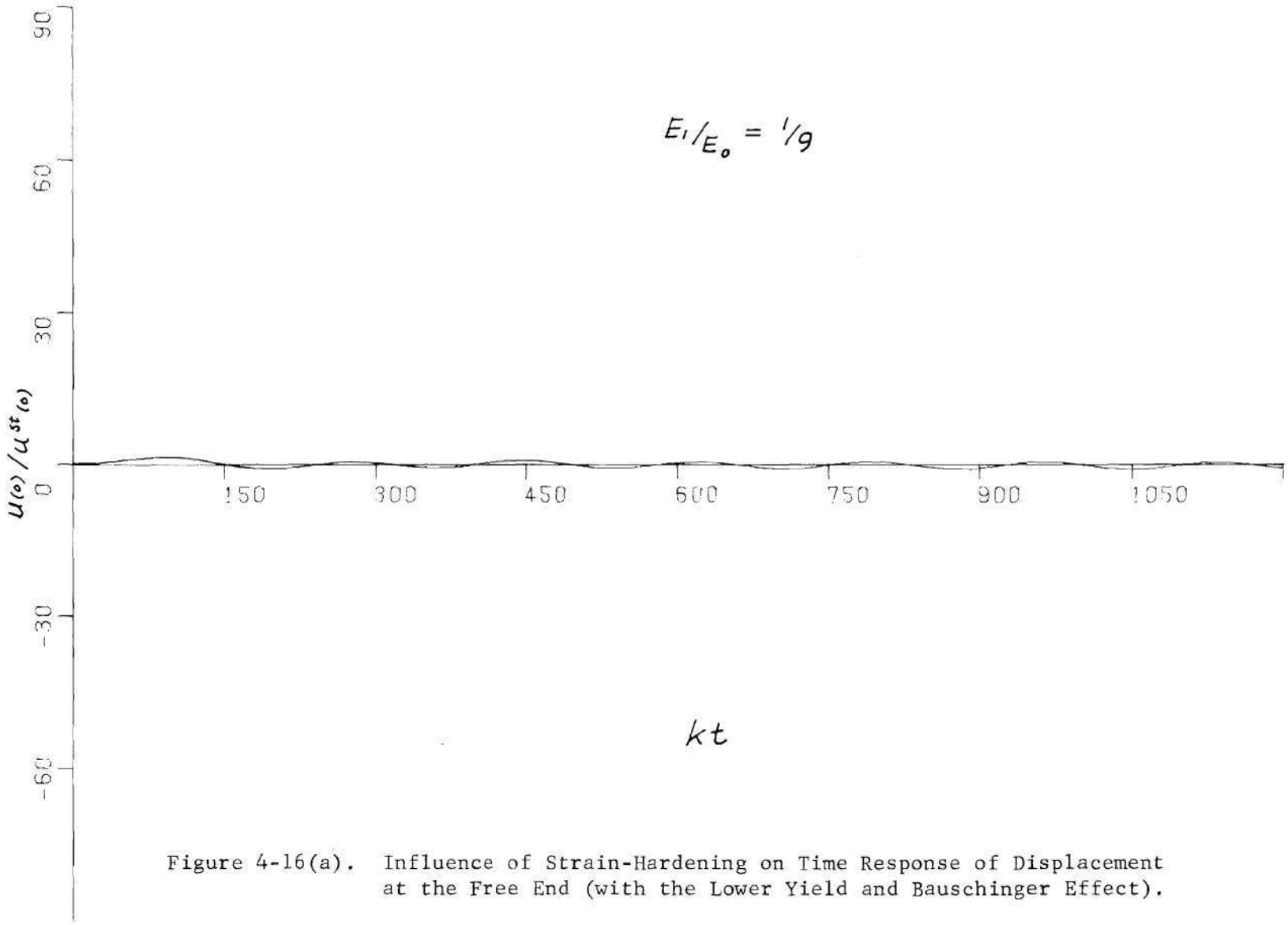

Figure 4-16(a). Influence of Strain-Hardening on Time Response of Displacement at the Free End (with the Lower Yield and Bauschinger Effect).

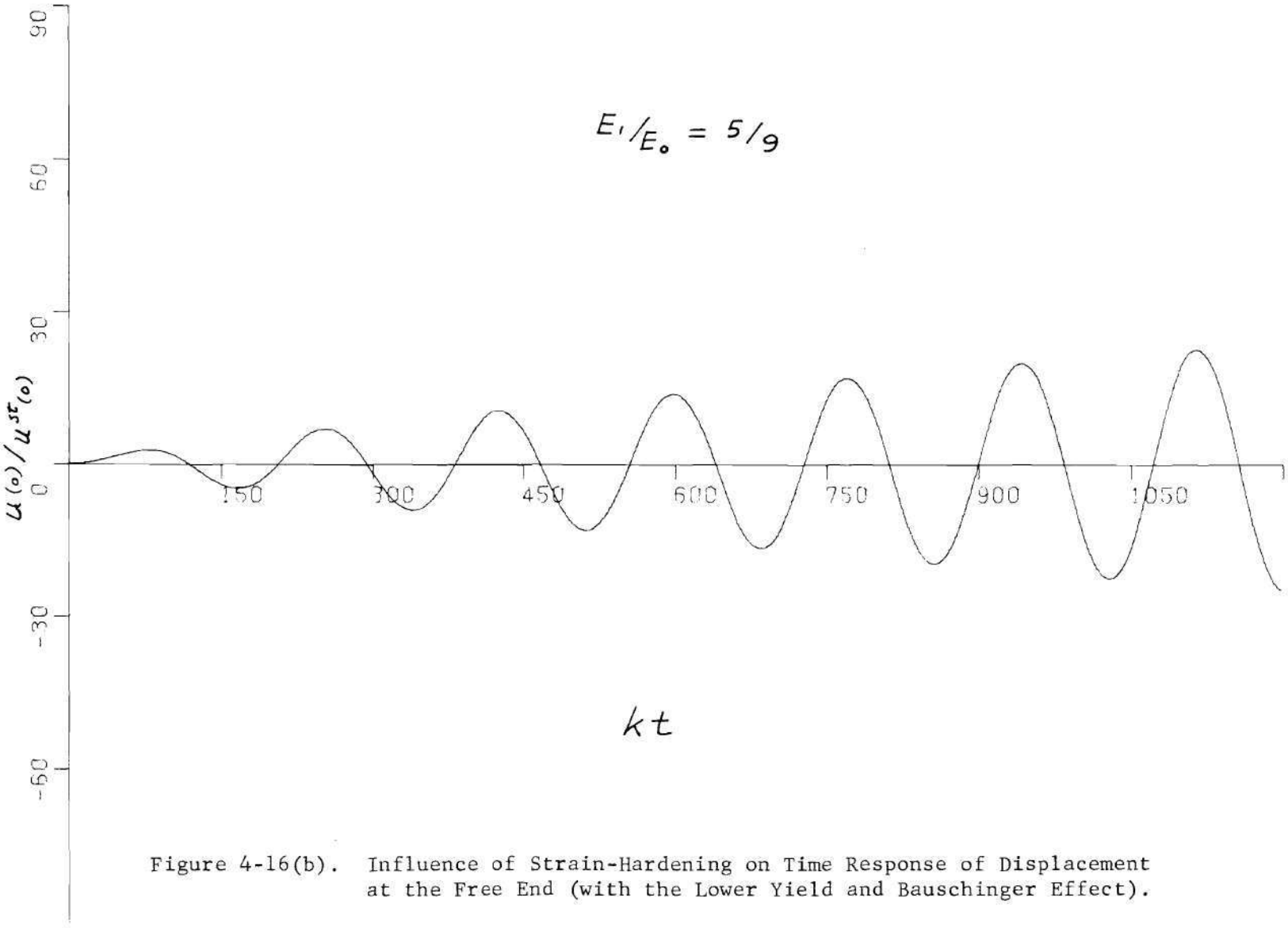

Figure 4-16(b). Influence of Strain-Hardening on Time Response of Displacement at the Free End (with the Lower Yield and Bauschinger Effect).

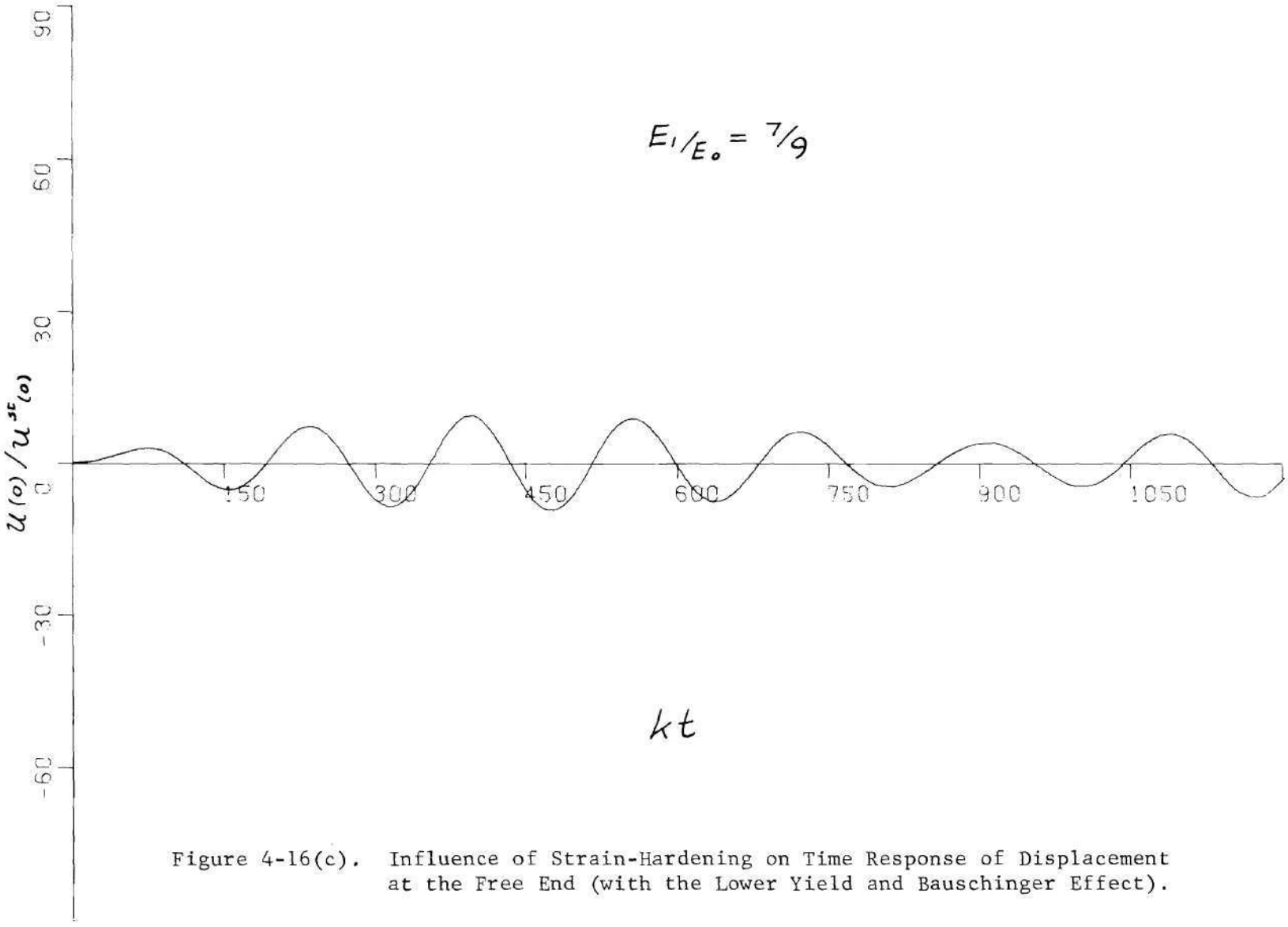

Figure 4-16(c). Influence of Strain-Hardening on Time Response of Displacement at the Free End (with the Lower Yield and Bauschinger Effect).

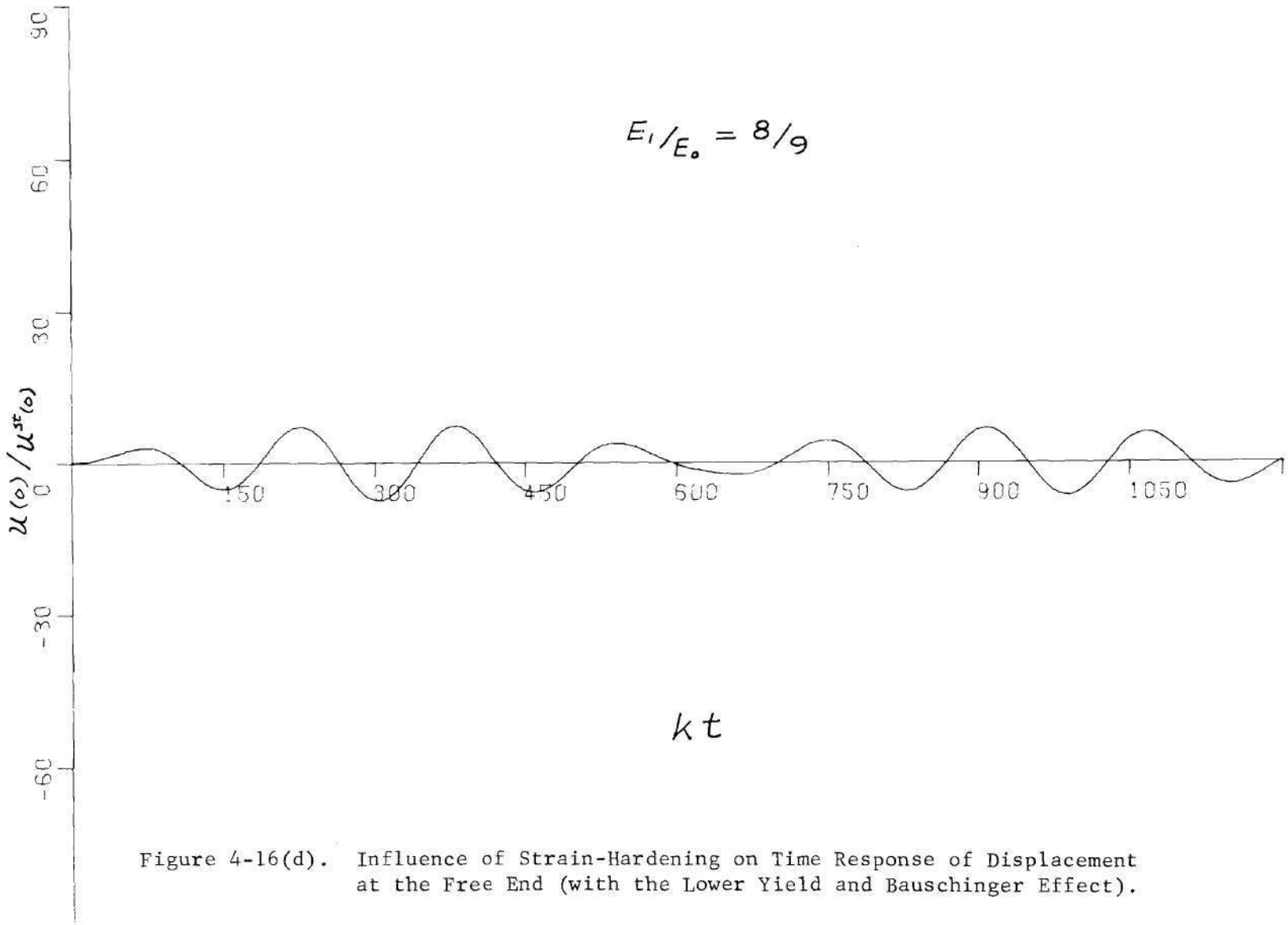

Figure 4-16(d). Influence of Strain-Hardening on Time Response of Displacement at the Free End (with the Lower Yield and Bauschinger Effect).

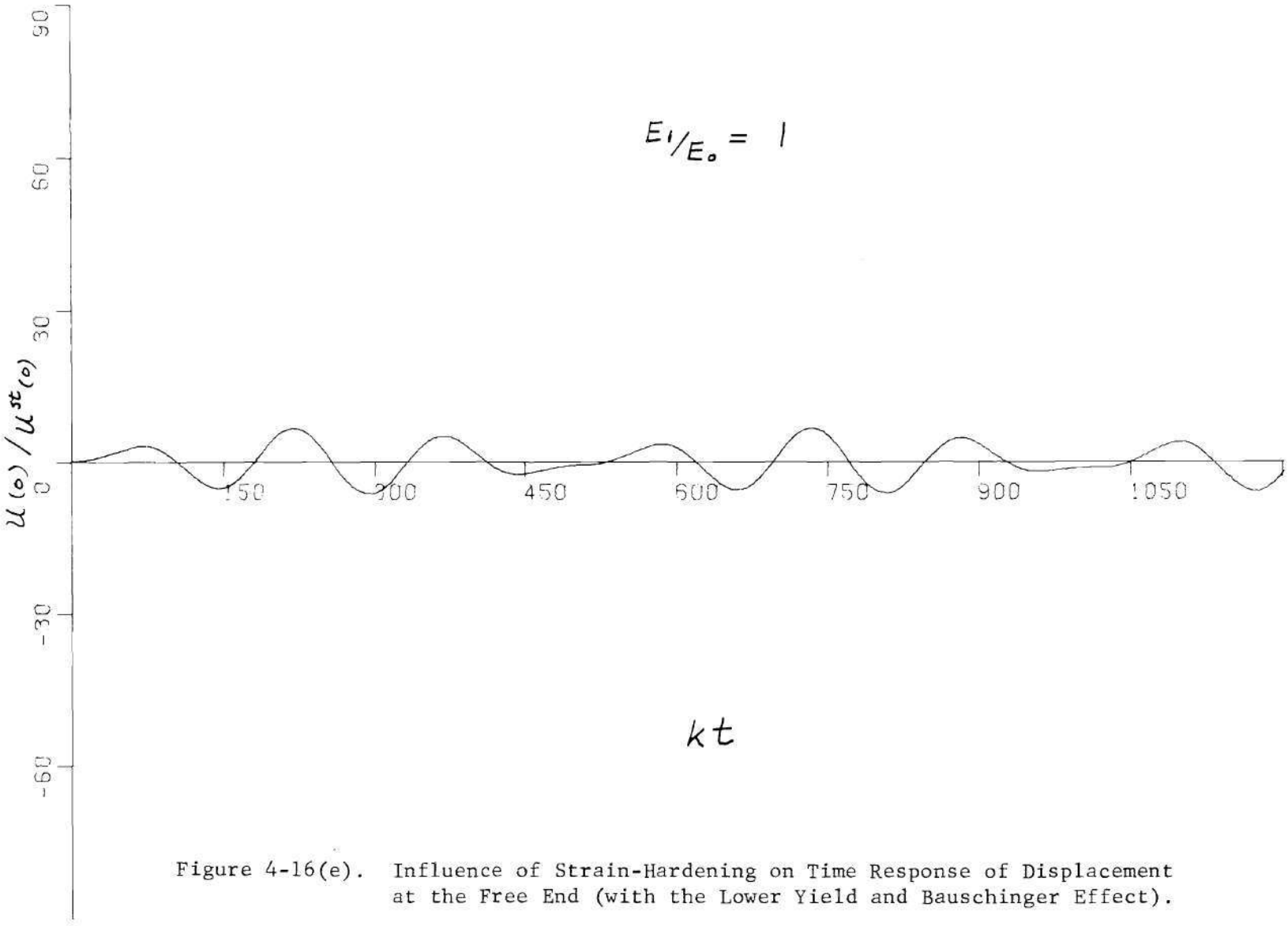

Figure 4-16(e). Influence of Strain-Hardening on Time Response of Displacement at the Free End (with the Lower Yield and Bauschinger Effect).

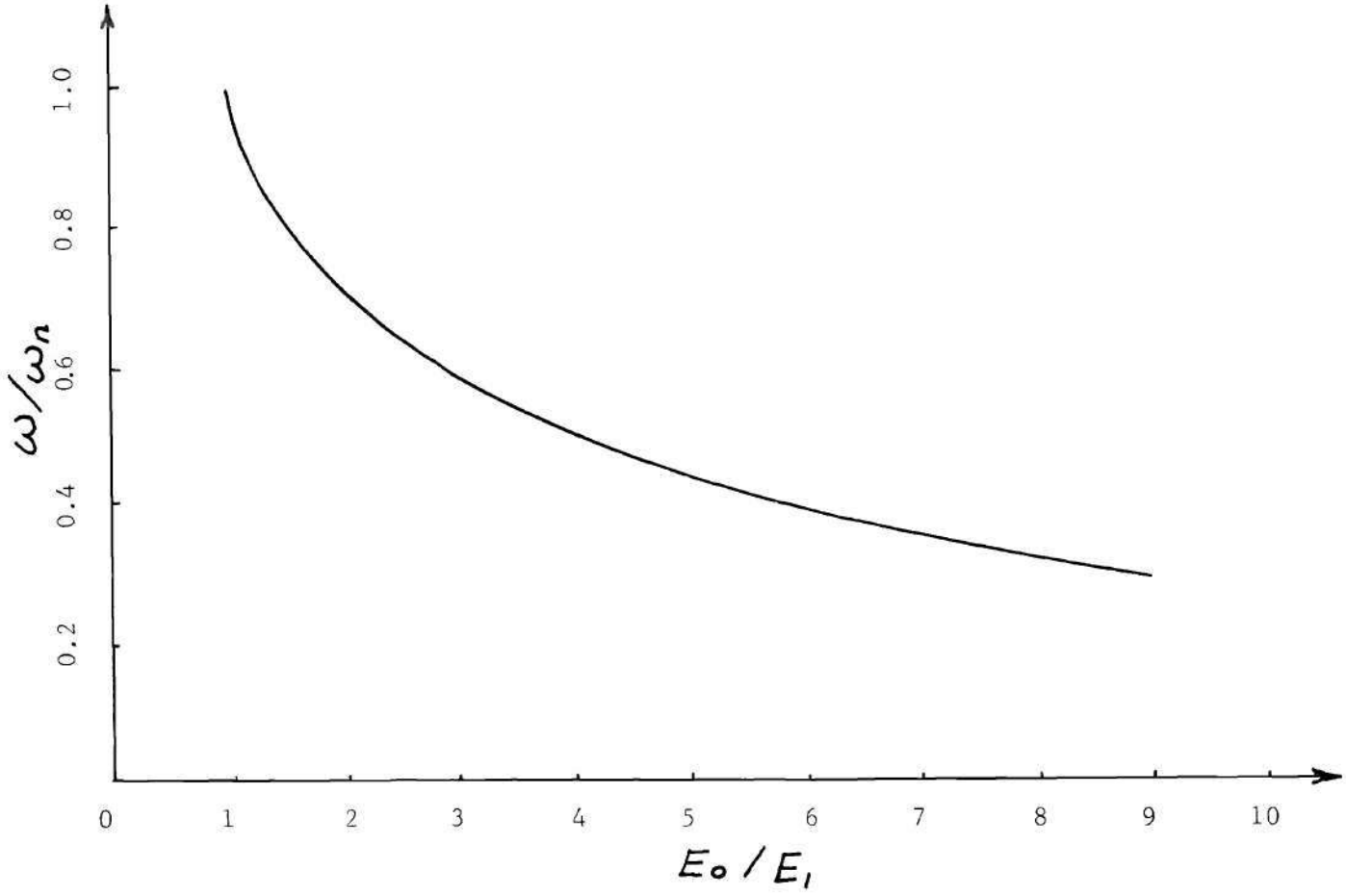

Figure 4-17. Influence of the Degree of Strain-Hardening on Resonant Frequency.

the Bauschinger effect, the degree of strain-hardening seems to have almost no effect on the resonant frequency. This is understandable by referring back to Figure (4-2). After a long period of sinusoidal loading (or at the steady-state response), the bar will reach a point where there is only an elastic wave moving back and forth along the bar. Therefore, the only resonance that can exist at this time will be elastic. However, with the Bauschinger effect, the bar experiences plastic stress and strain all the time. Consequently, the degree of plasticity will affect the natural frequency of resonance.

Caughey [43] in 1960, considered varying the input frequency in a single degree-of-freedom spring-mass system, where a bilinear hysteresis loop was included. Even though it is difficult to compare these results (continuous system) to his results (a single degree-of-freedom system), however, there are two similar conclusions from both studies: (i) from the numerical results all the curves of the frequency response are single valued, hence jump behavior, characteristic of certain nonlinear systems, is not expected to occur. (ii) The resonance phenomenon appears to move toward lower frequency values as the bar behaves more plastically. On the other hand, the plastic response of the bar loaded only at an elastic resonant frequency, was first treated analytically by Kalaski and Wlodarczyk [1,32,33], but no answer can be found from their work regarding solutions under loading frequencies other than elastic resonant frequency.

Finally, there are two related figures shown by Figures (4-18) and (4-19). These are frequency response plots of the stress at the fixed end both with and without the Bauschinger effect. The y-axis is

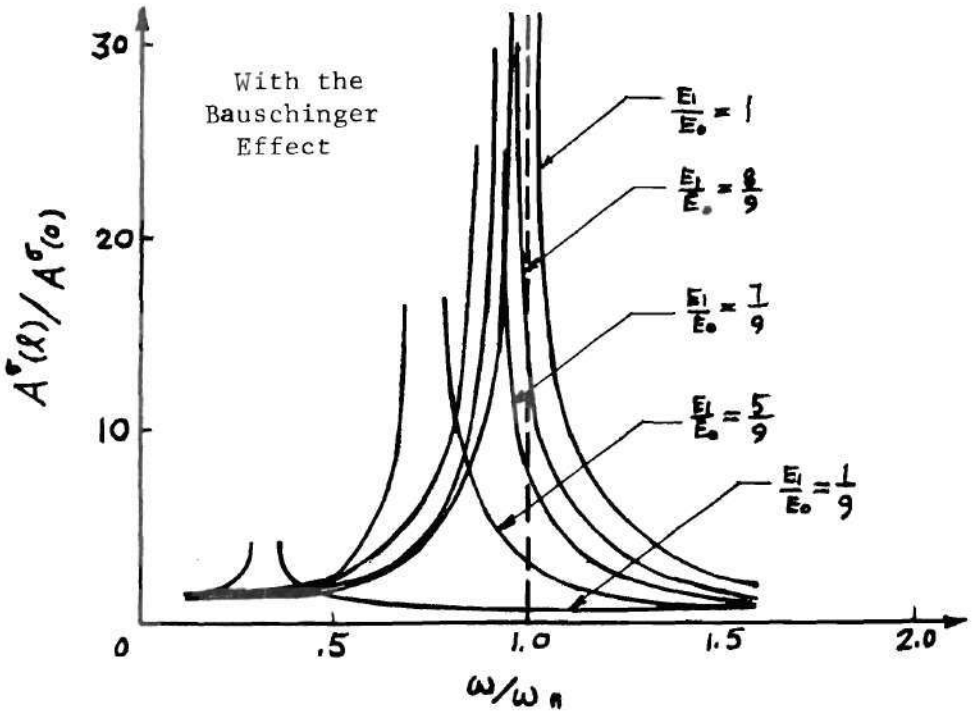

Figure 4-18. Frequency Response of Stress at Fixed End.

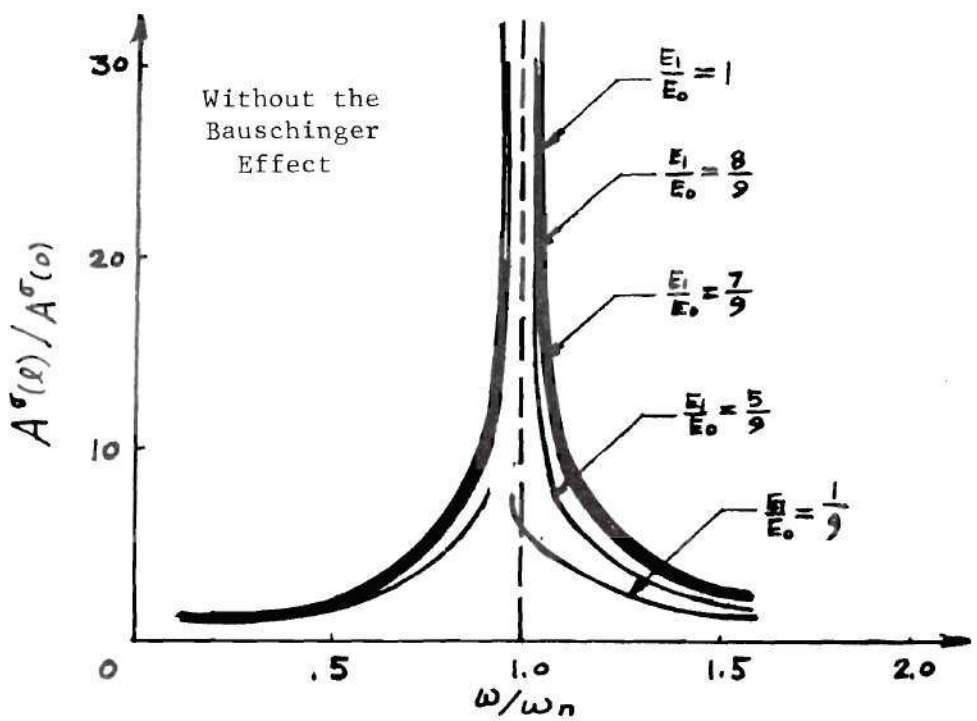

Figure 4-19. Frequency Response of Stress at Fixed End.

the ratio of the maximum amplitude of output stress at the fixed end to the amplitude of input stress at the free end. These two figures are similar to the previous Figures (4-14) and (4-15) where displacement responses were considered. The reason for considering these figures is to illustrate the amplification factor of stress in a bar.

(B) Plastic Resonance

In this section, we will investigate the dynamic response of the bar at a particular loading frequency $\omega = \omega_n = 2\pi k/128$. This is the first fundamental natural frequency for the elastic bar. Figures (4-20) and (4-21) show of displacement-time history plots at the free end and stress-time history plots at the fixed end with the Bauschinger effect considered. On the other hand, Figures (4-22) and (4-23) show corresponding plots where the Bauschinger effect is neglected. In Figures (4-20) and (4-21), the results in all elastic cases were checked by normal mode solution. Results showed good agreement (see Appendix B). It is noted here that the unbounded resonance effect only occurs at $E_1/E_o = 1$ (elastic case). This is true because the bar is being excited at the elastic first fundamental frequency (ω_n). In Figure (4-14) and Figure (4-15) all response curves are left open in the neighborhood of each corresponding resonance frequency. Frequency responses have been plotted with the maximum amplitude of steady-state response was chosen. And, in these figures, the time interval for calculating the steady state response was selected from t=0 to $t = t_1 = 1280/k$. (40 triangle-regimes in Figure (3-7)). One sees from the figures that in the neighborhood of each resonance frequency the corresponding response does not have a local maximum (bounded value) but an absolute maximum at $t = t_1$ instead.

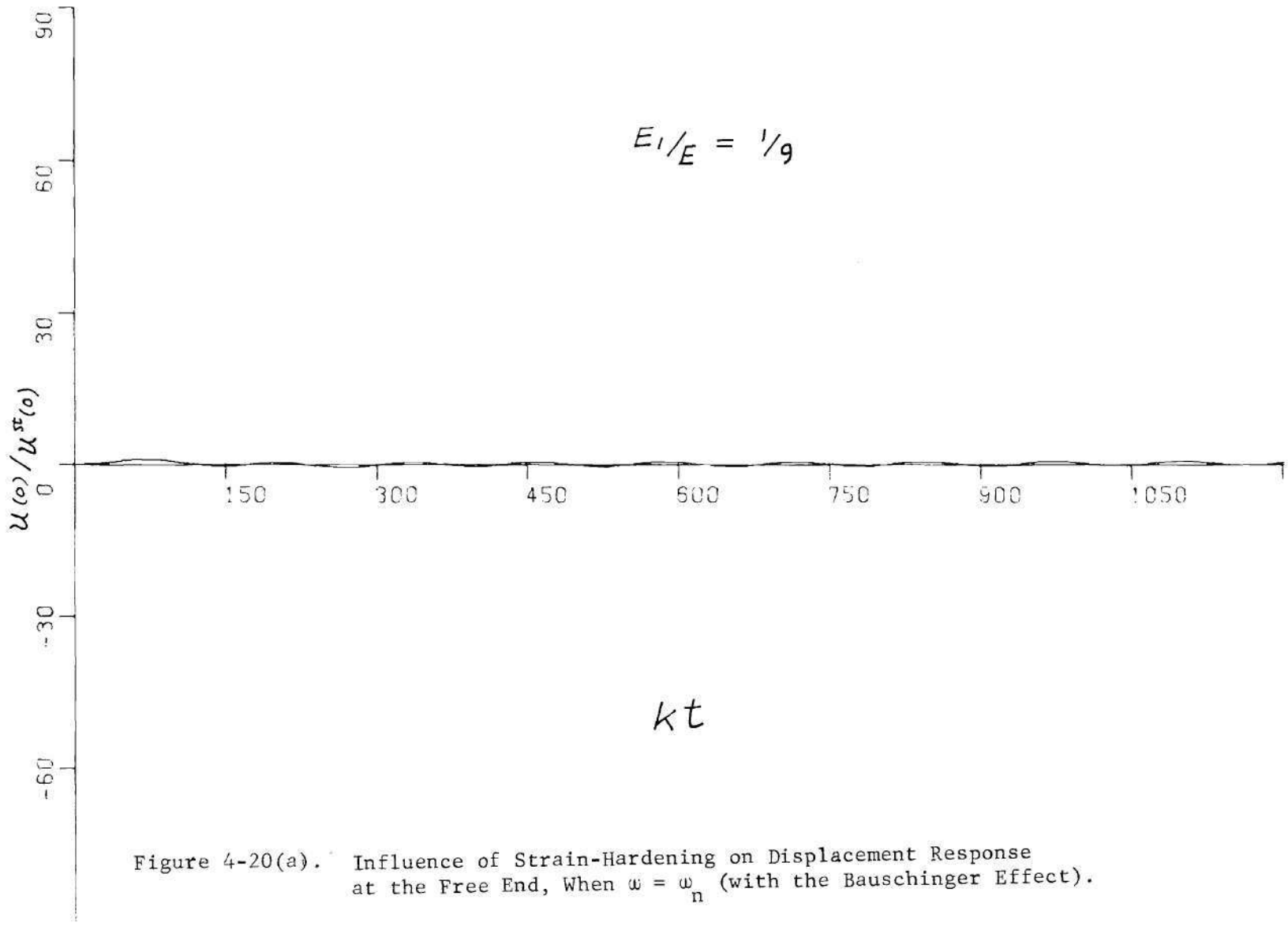

Figure 4-20(a). Influence of Strain-Hardening on Displacement Response at the Free End, When $\omega = \omega_n$ (with the Bauschinger Effect).

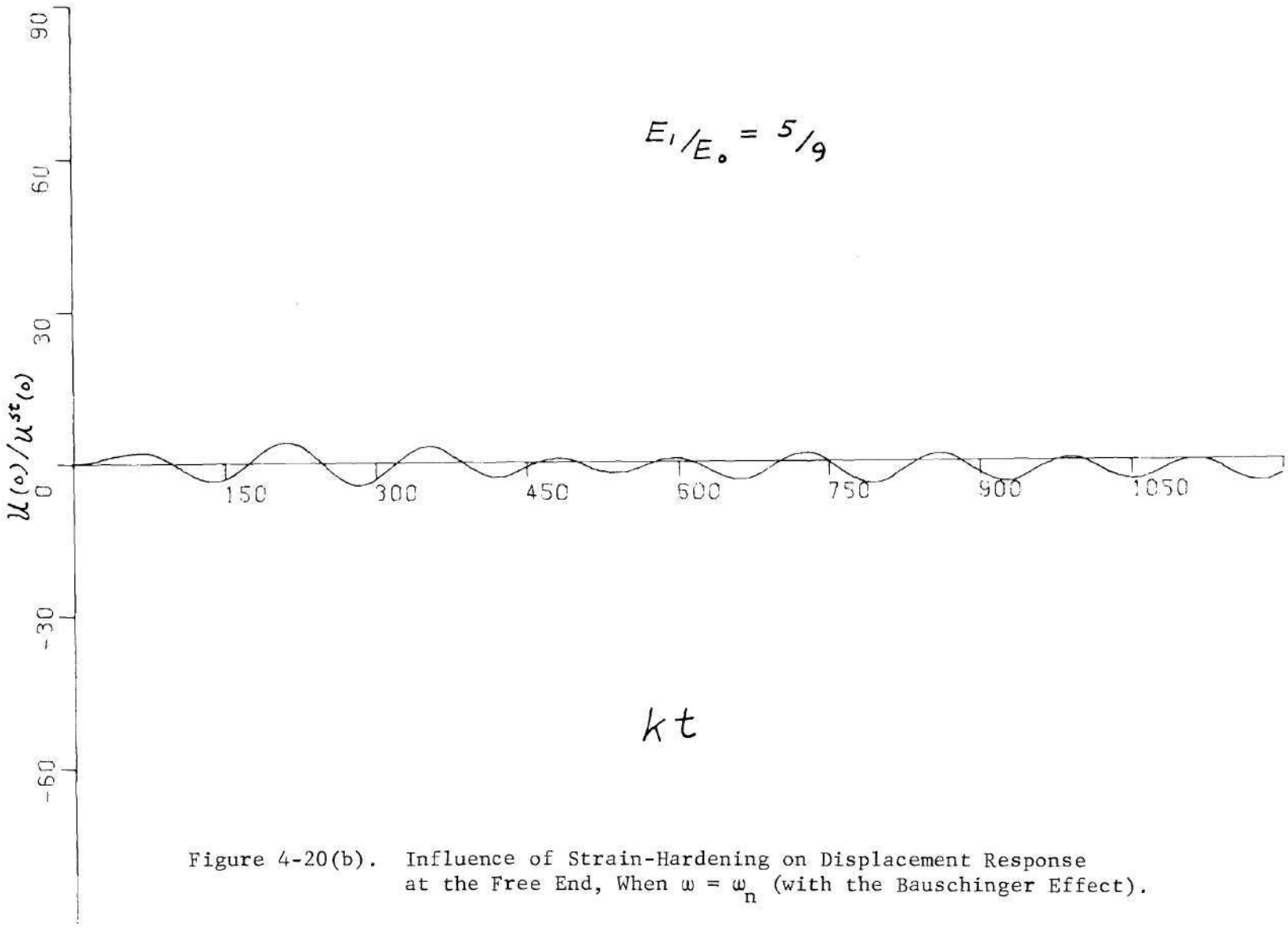

Figure 4-20(b). Influence of Strain-Hardening on Displacement Response at the Free End, When $\omega = \omega_n$ (with the Bauschinger Effect).

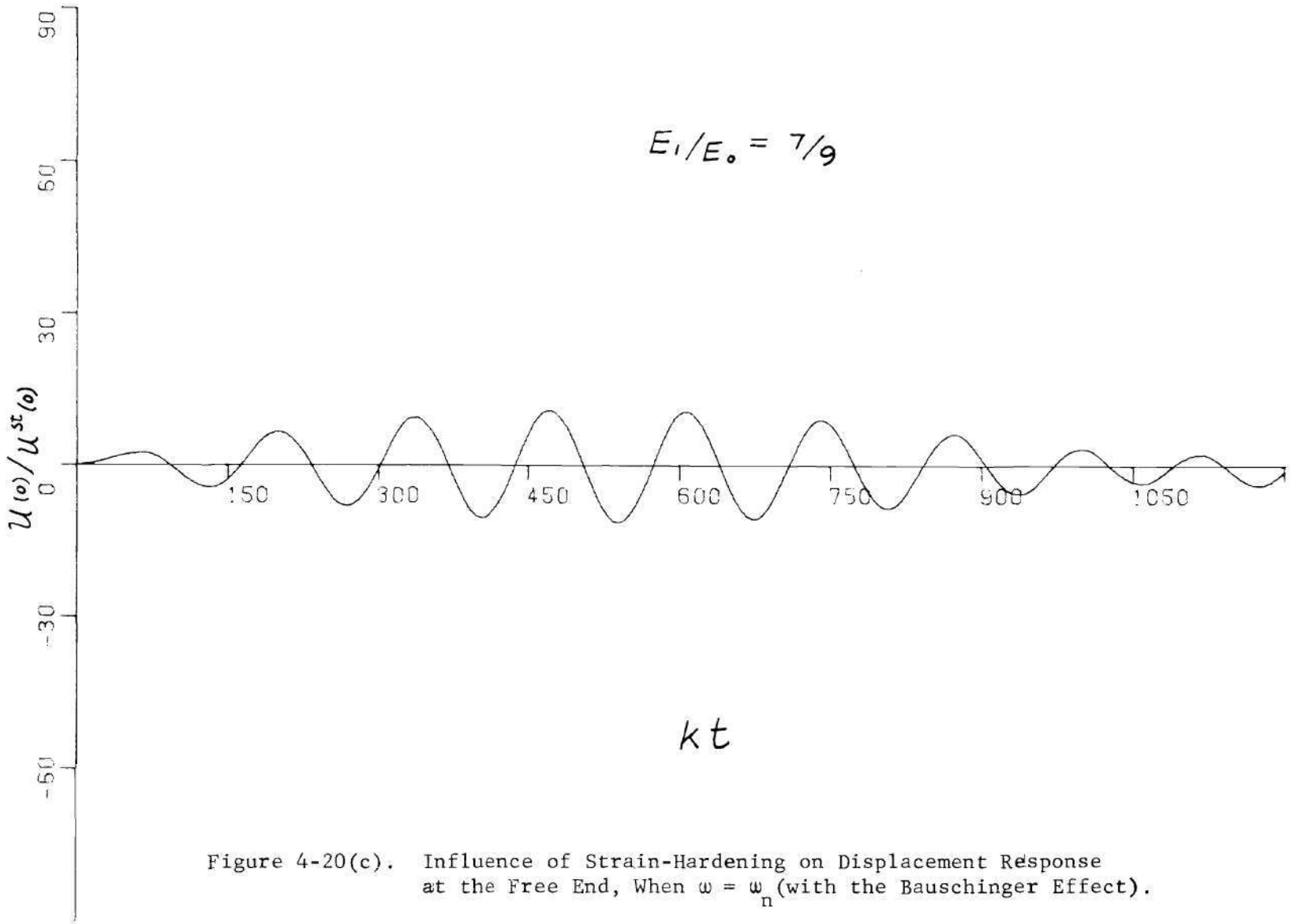

Figure 4-20(c). Influence of Strain-Hardening on Displacement Response at the Free End, When $\omega = \omega_n$ (with the Bauschinger Effect).

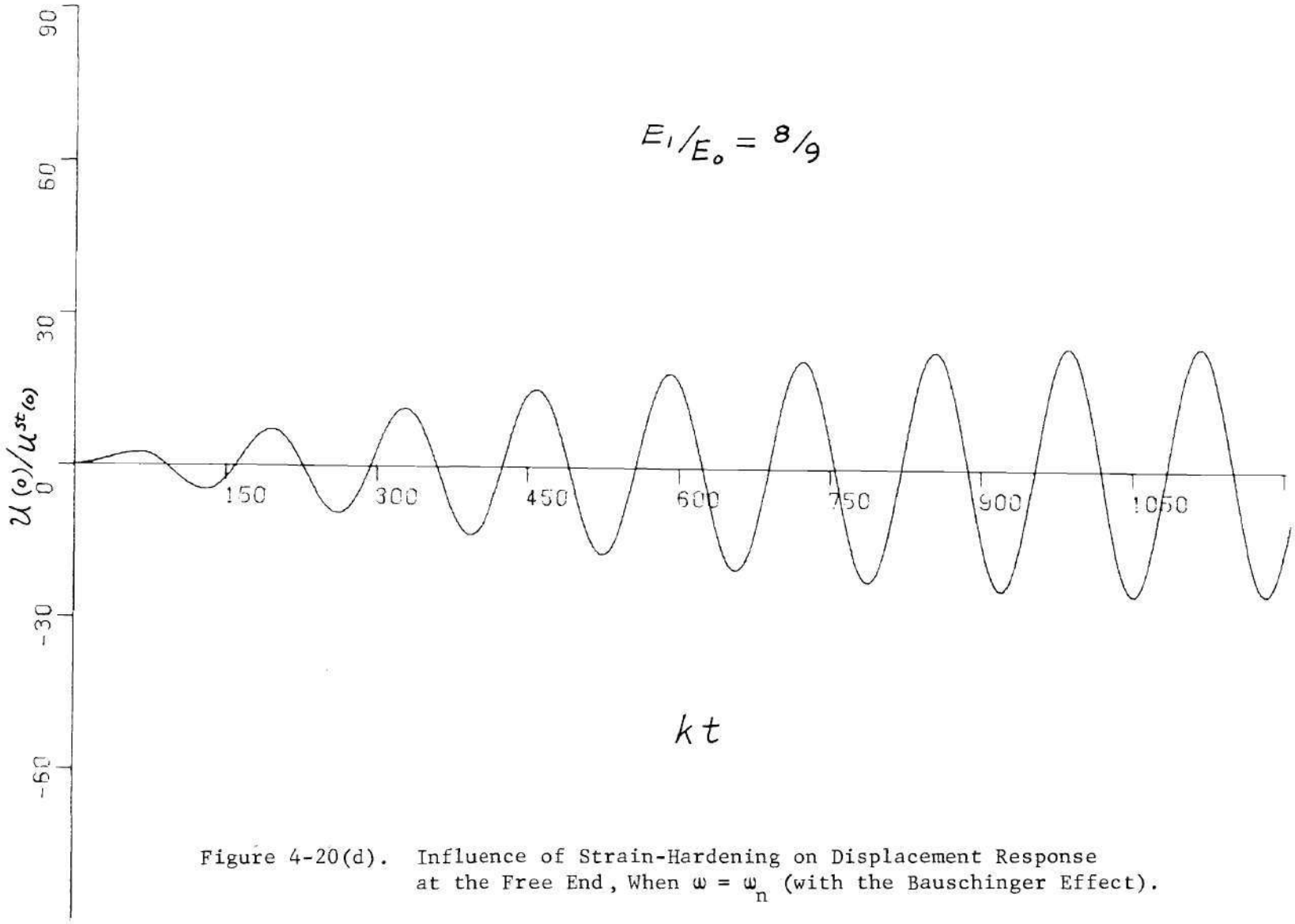

Figure 4-20(d). Influence of Strain-Hardening on Displacement Response at the Free End, When $\omega = \omega_n$ (with the Bauschinger Effect).

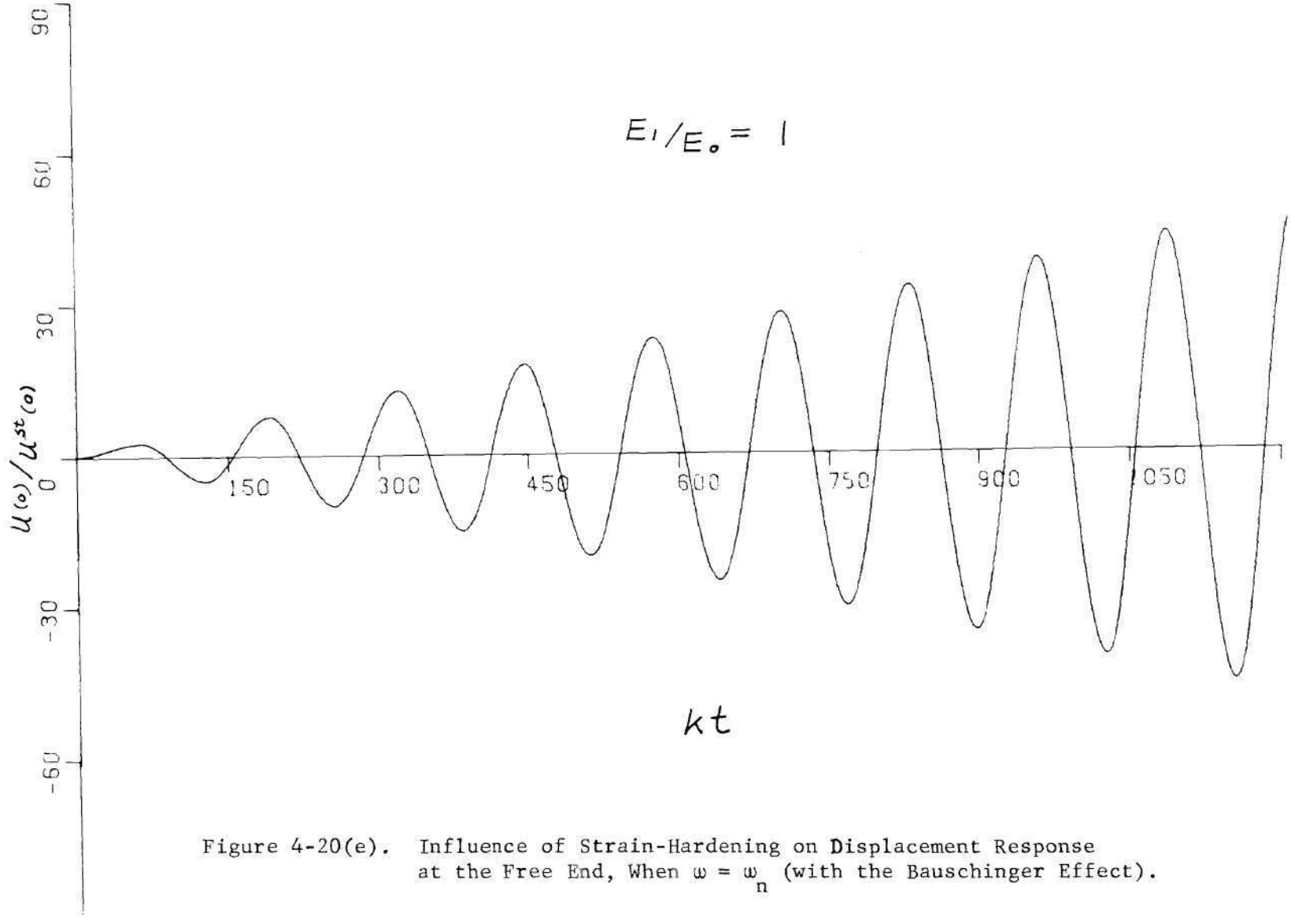

Figure 4-20(e). Influence of Strain-Hardening on Displacement Response at the Free End, When $\omega = \omega_n$ (with the Bauschinger Effect).

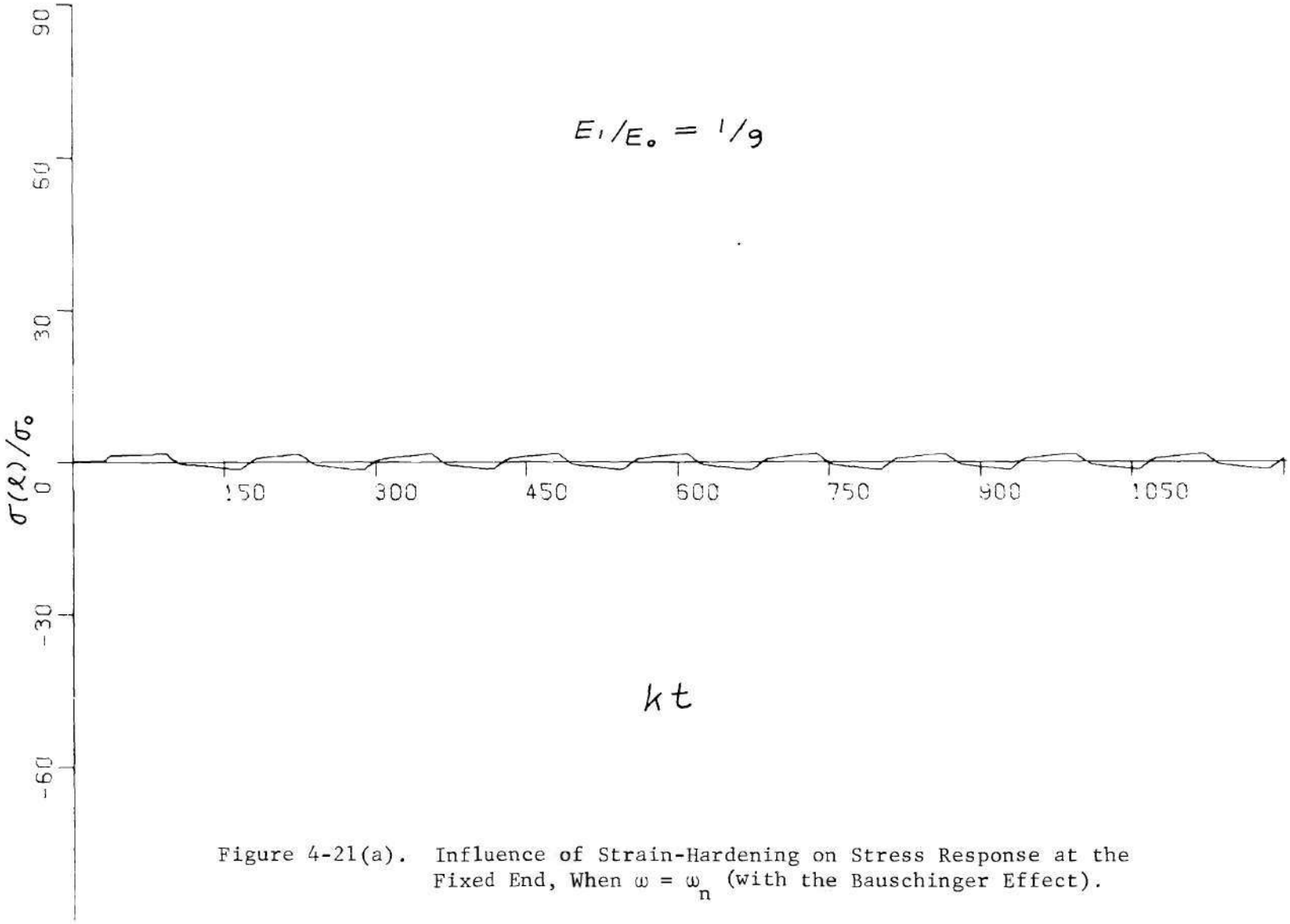

Figure 4-21(a). Influence of Strain-Hardening on Stress Response at the Fixed End, When $\omega = \omega_n$ (with the Bauschinger Effect).

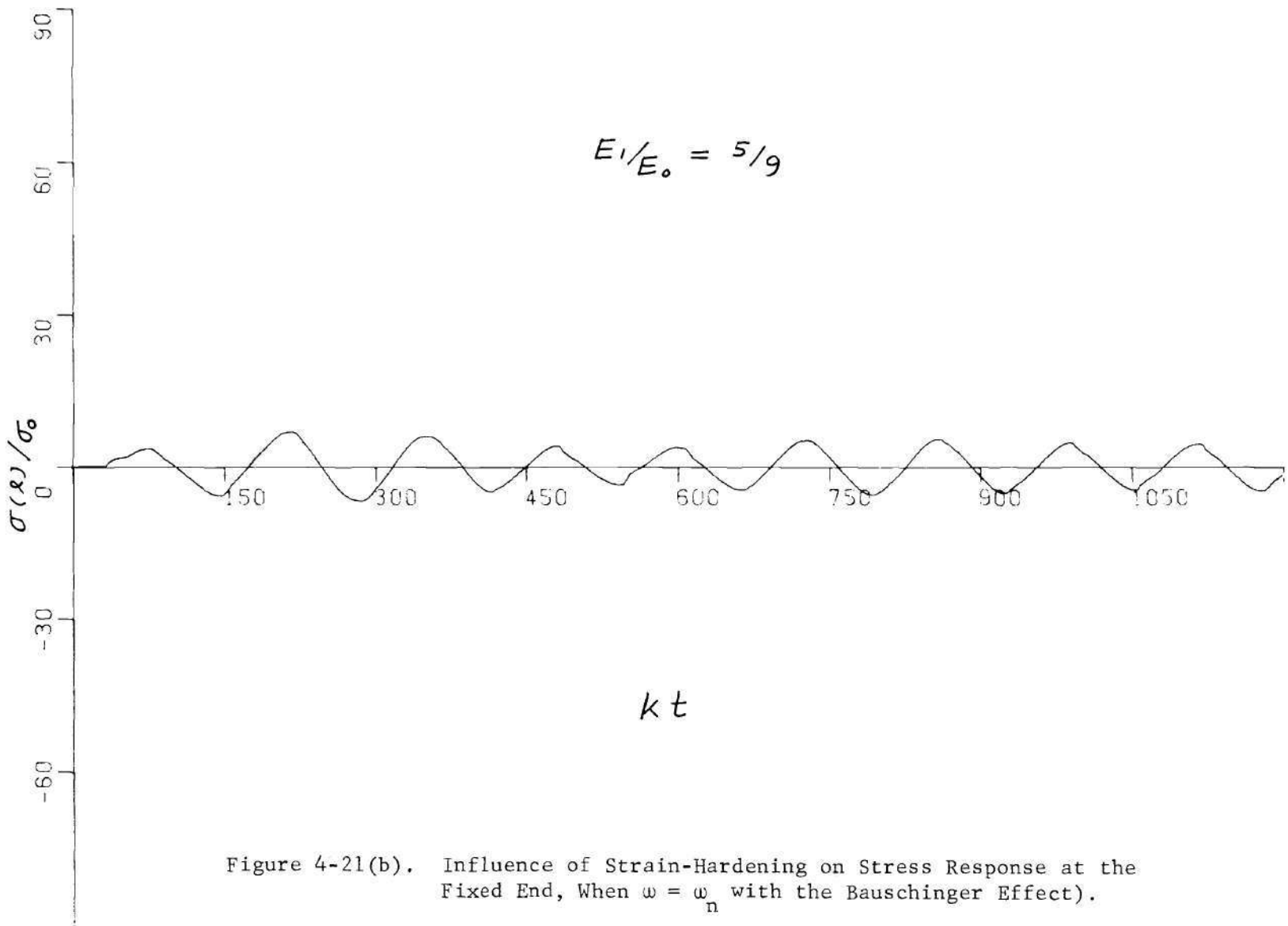

Figure 4-21(b). Influence of Strain-Hardening on Stress Response at the Fixed End, When $\omega = \omega_n$ with the Bauschinger Effect).

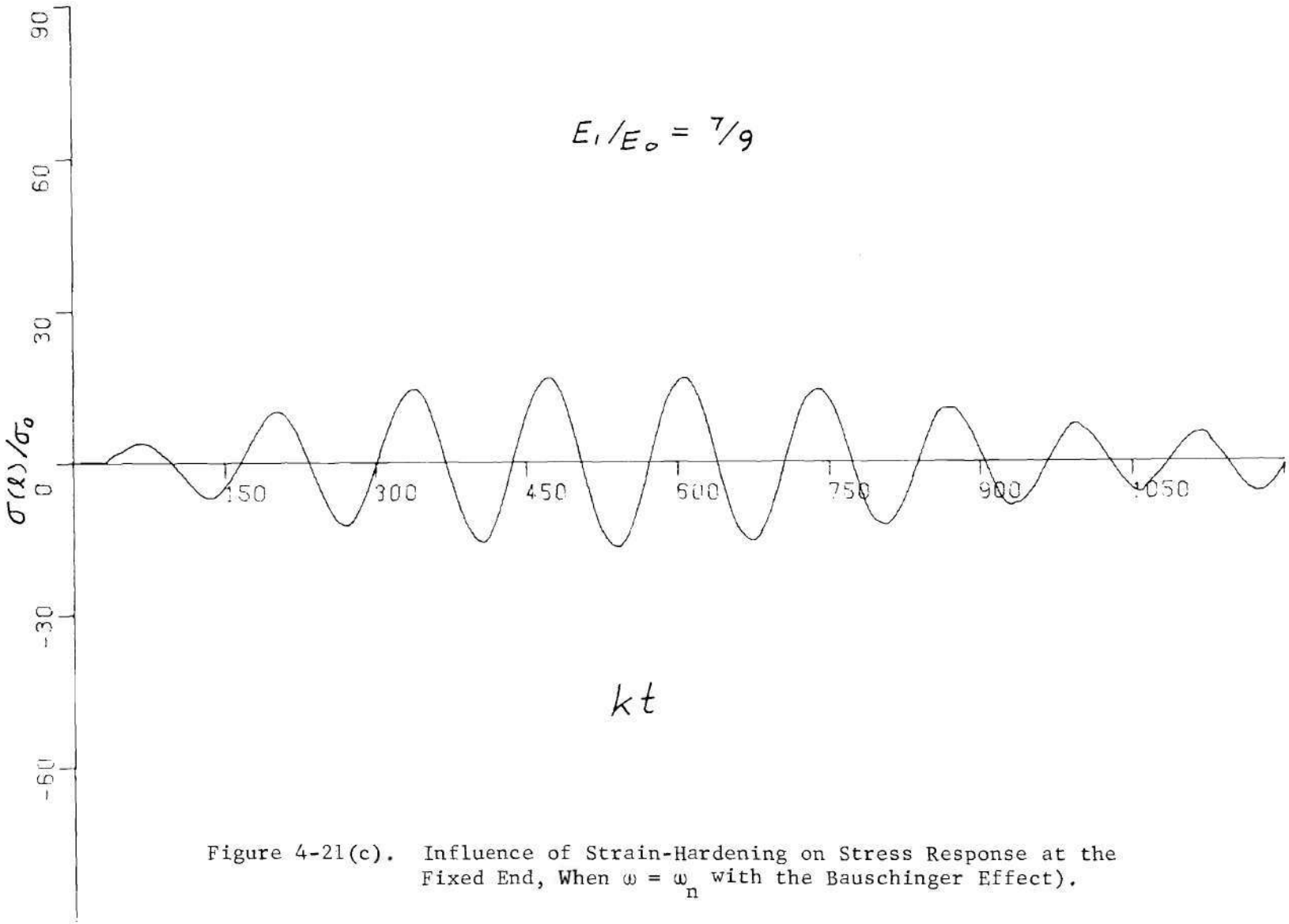

Figure 4-21(c). Influence of Strain-Hardening on Stress Response at the Fixed End, When $\omega = \omega_n$ with the Bauschinger Effect).

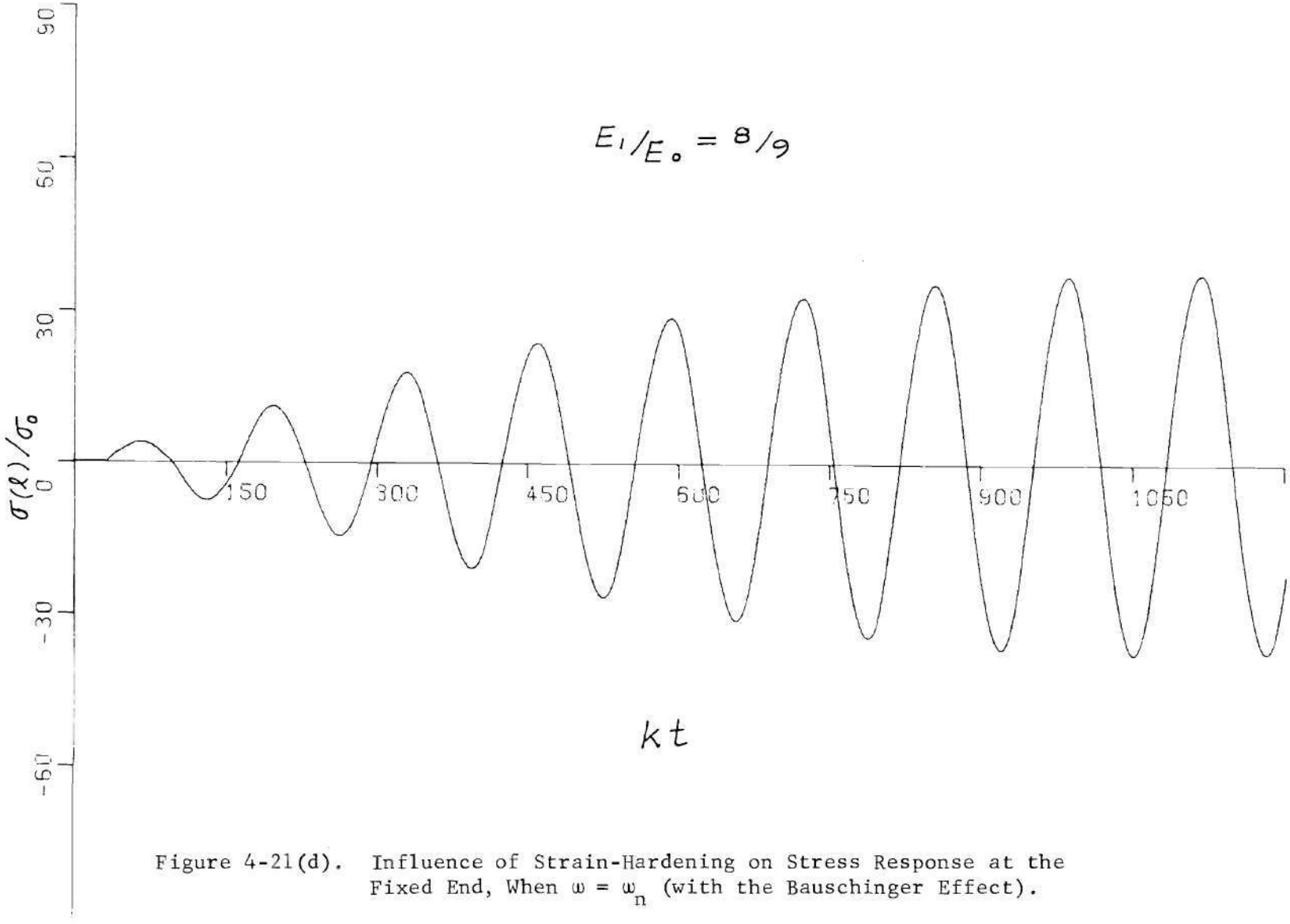

Figure 4-21(d). Influence of Strain-Hardening on Stress Response at the Fixed End, When $\omega = \omega_n$ (with the Bauschinger Effect).

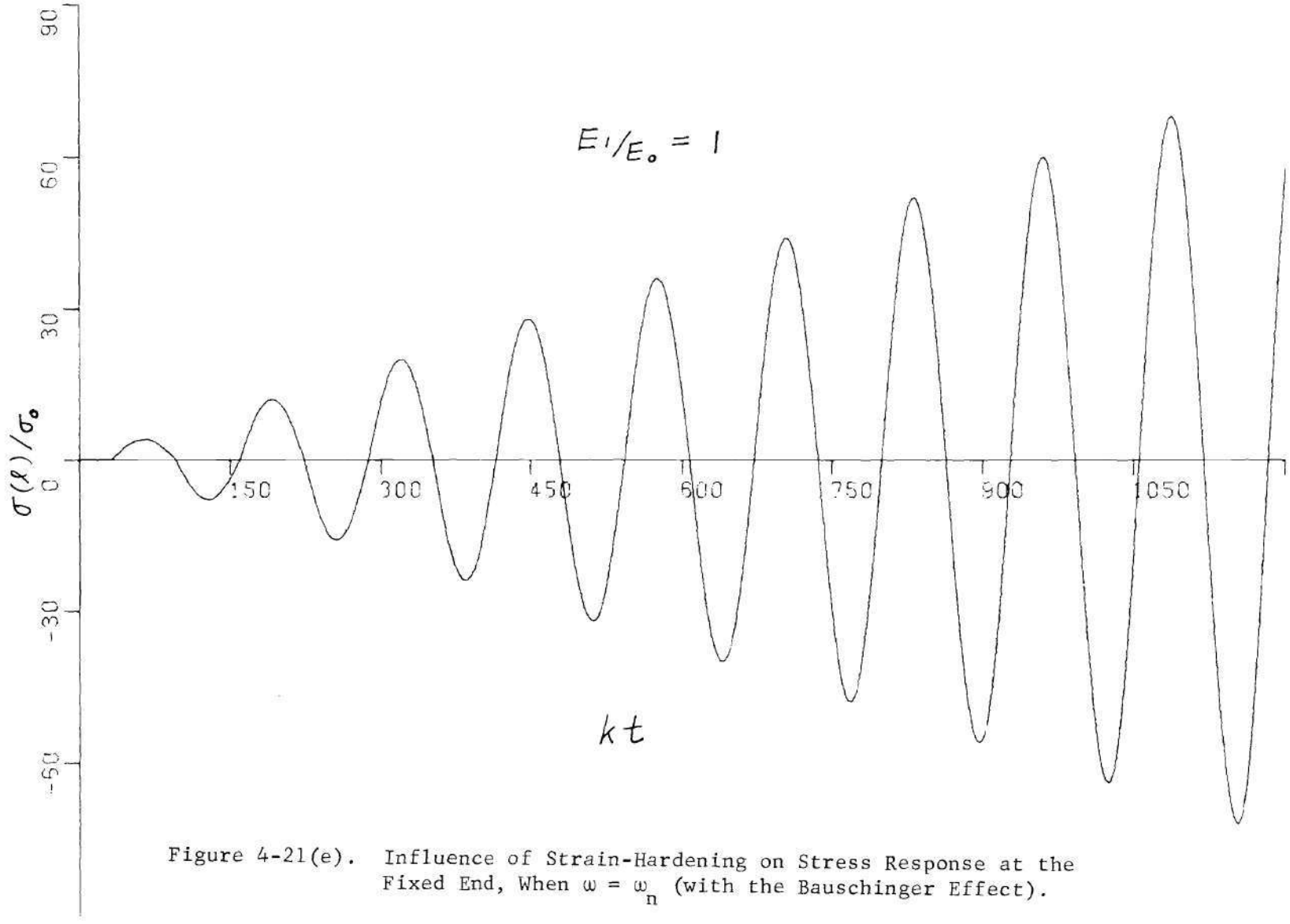

Figure 4-21(e). Influence of Strain-Hardening on Stress Response at the Fixed End, When $\omega = \omega_n$ (with the Bauschinger Effect).

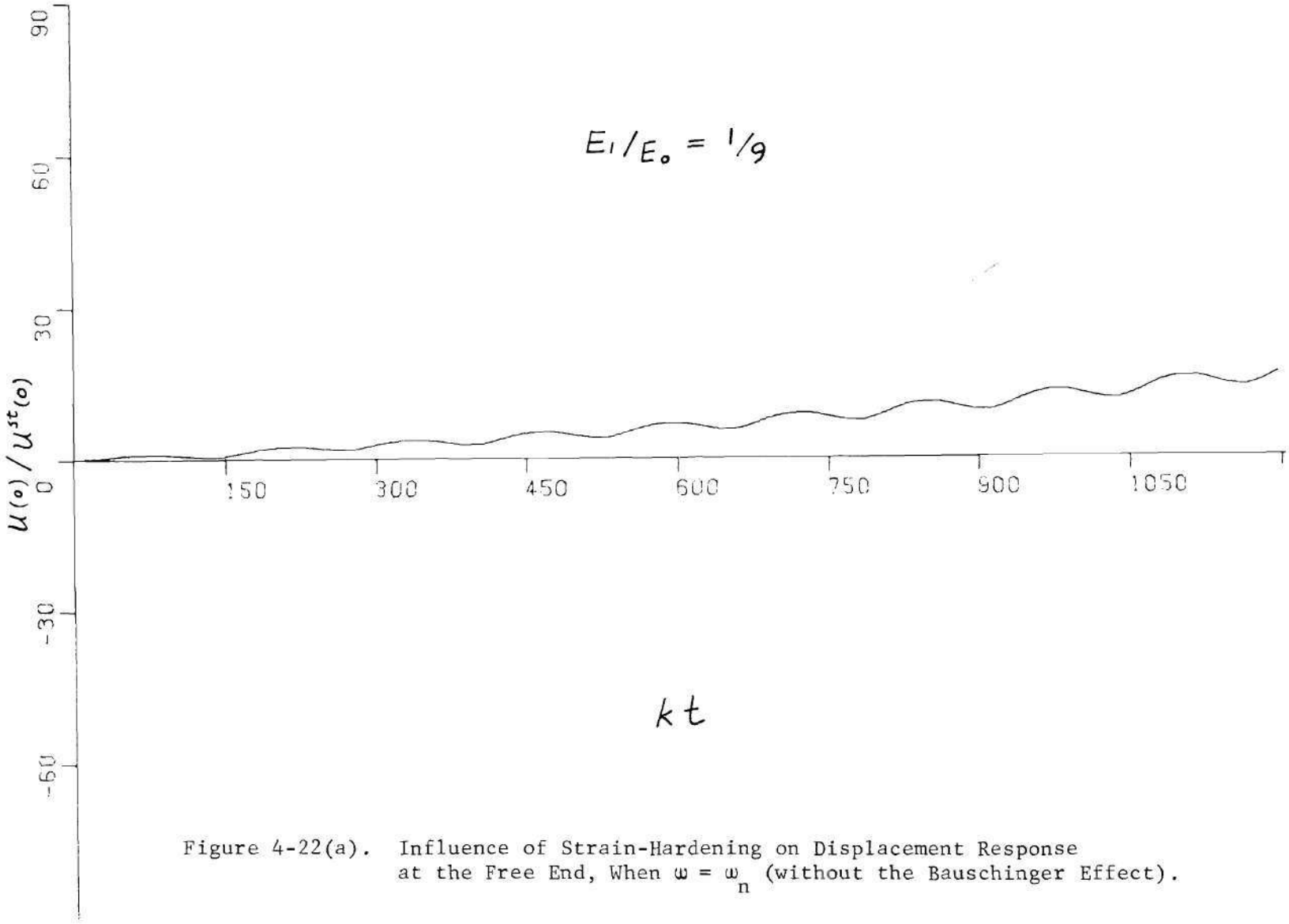

Figure 4-22(a). Influence of Strain-Hardening on Displacement Response at the Free End, When $\omega = \omega_n$ (without the Bauschinger Effect).

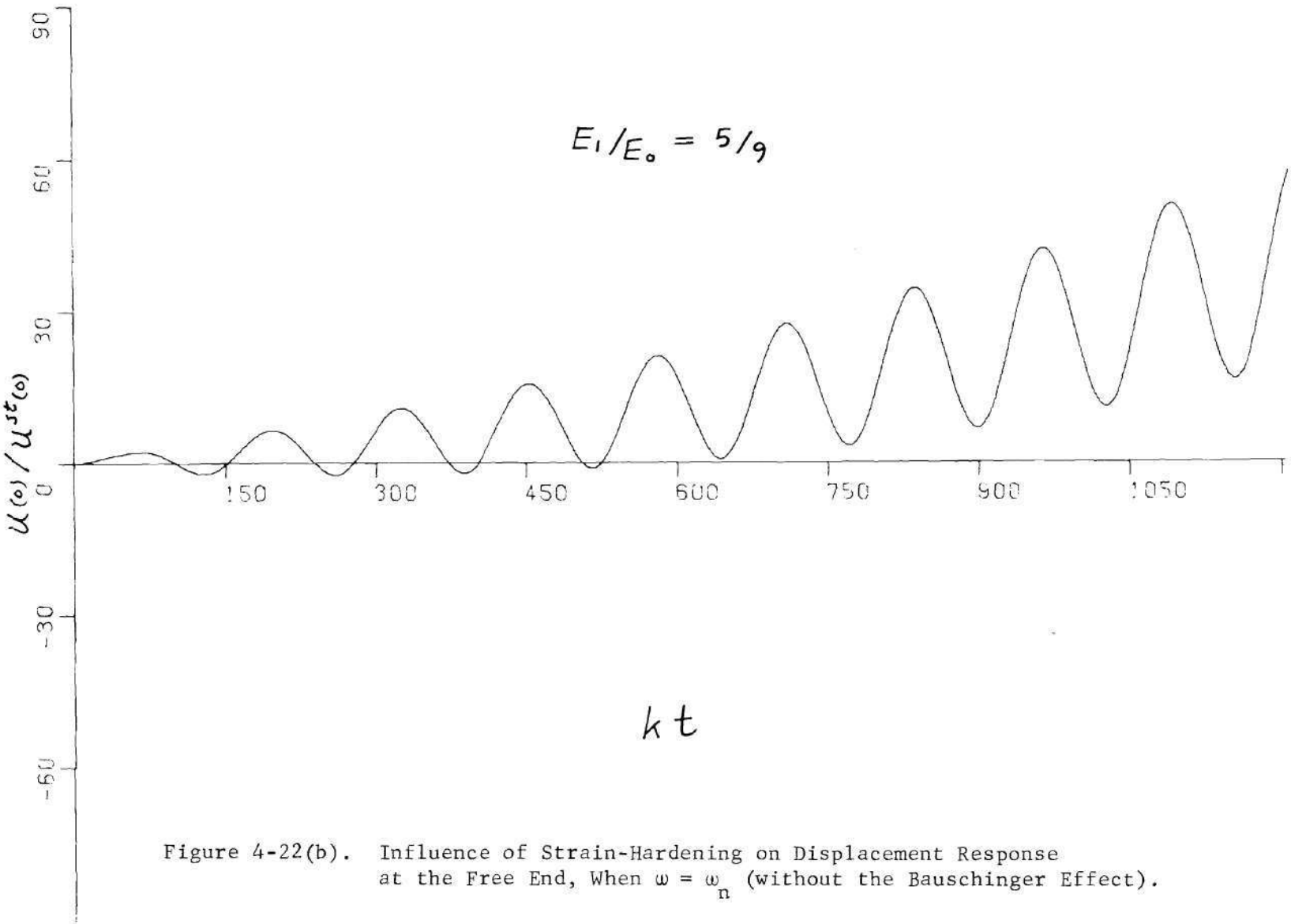

Figure 4-22(b). Influence of Strain-Hardening on Displacement Response at the Free End, When $\omega = \omega_n$ (without the Bauschinger Effect).

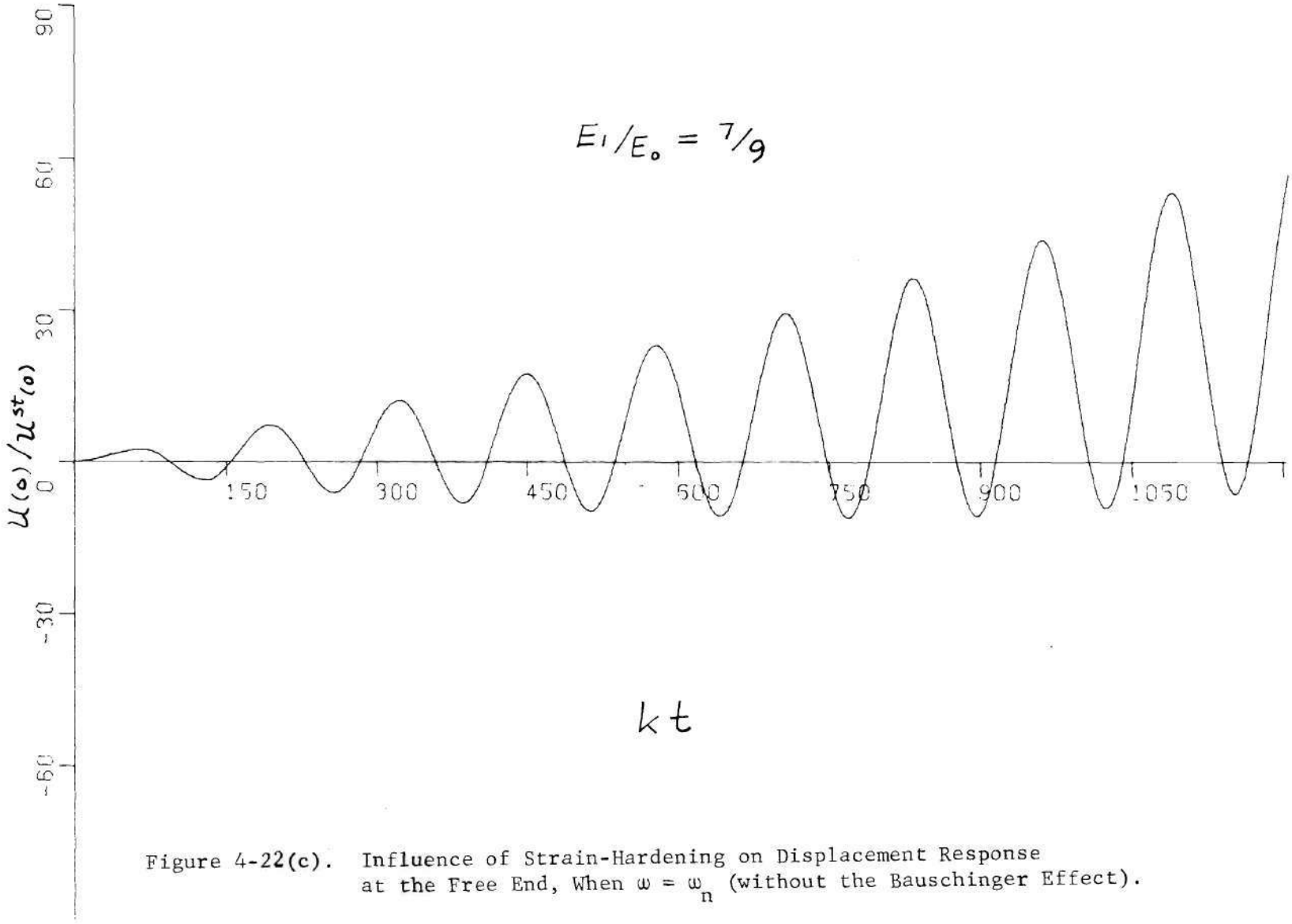

Figure 4-22(c). Influence of Strain-Hardening on Displacement Response at the Free End, When $\omega = \omega_n$ (without the Bauschinger Effect).

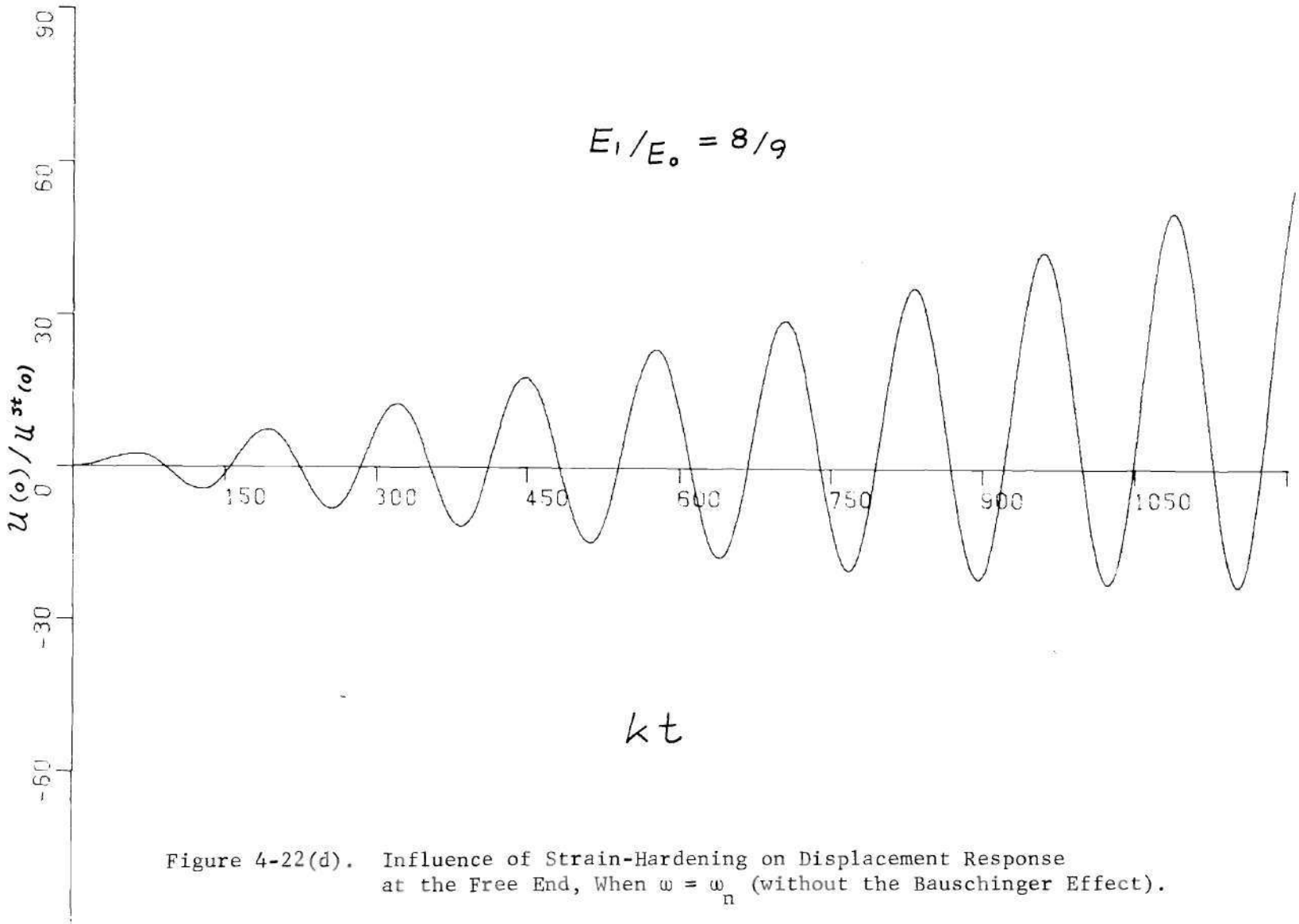

Figure 4-22(d). Influence of Strain-Hardening on Displacement Response at the Free End, When $\omega = \omega_n$ (without the Bauschinger Effect).

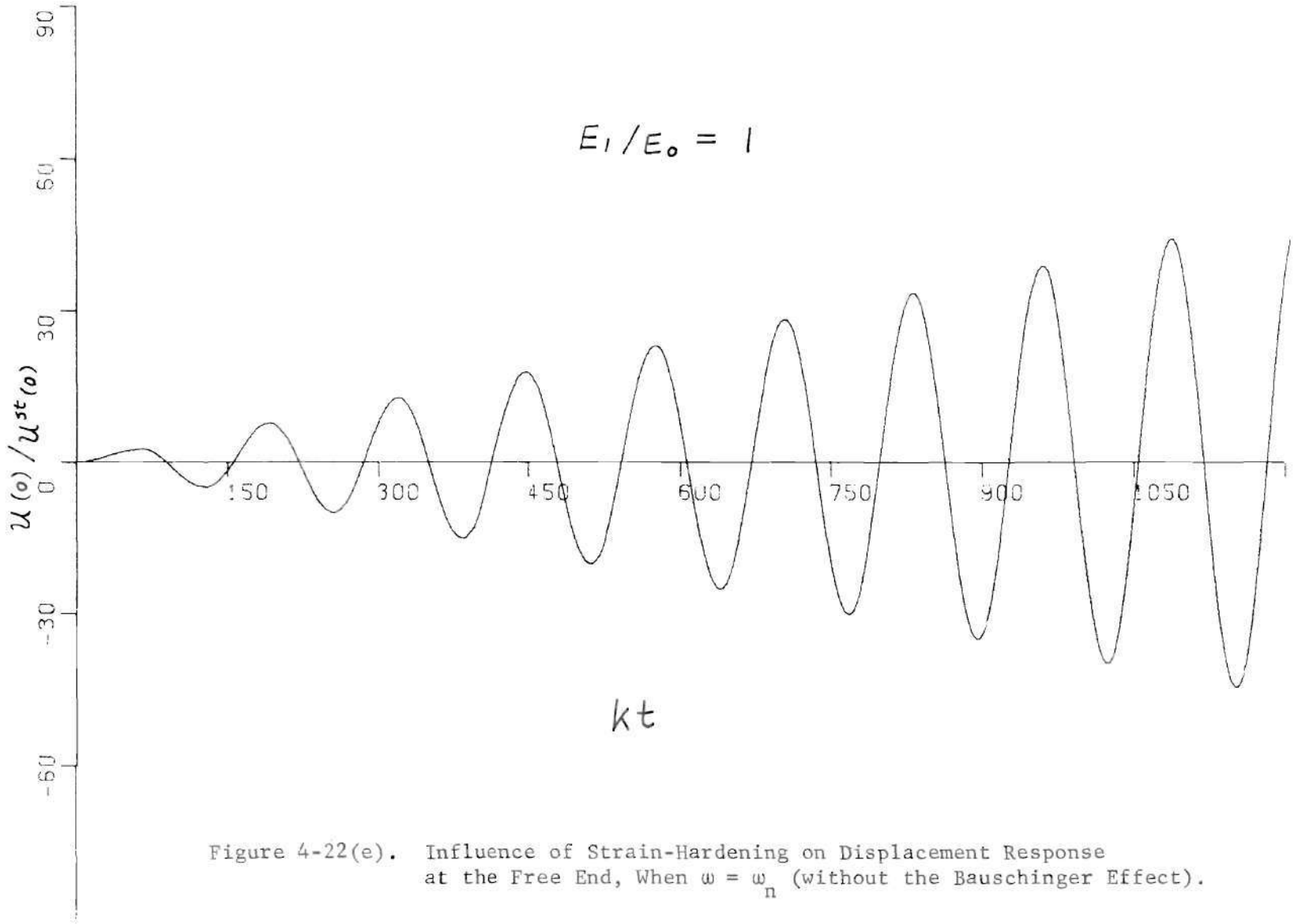

Figure 4-22(e). Influence of Strain-Hardening on Displacement Response at the Free End, When $\omega = \omega_n$ (without the Bauschinger Effect).

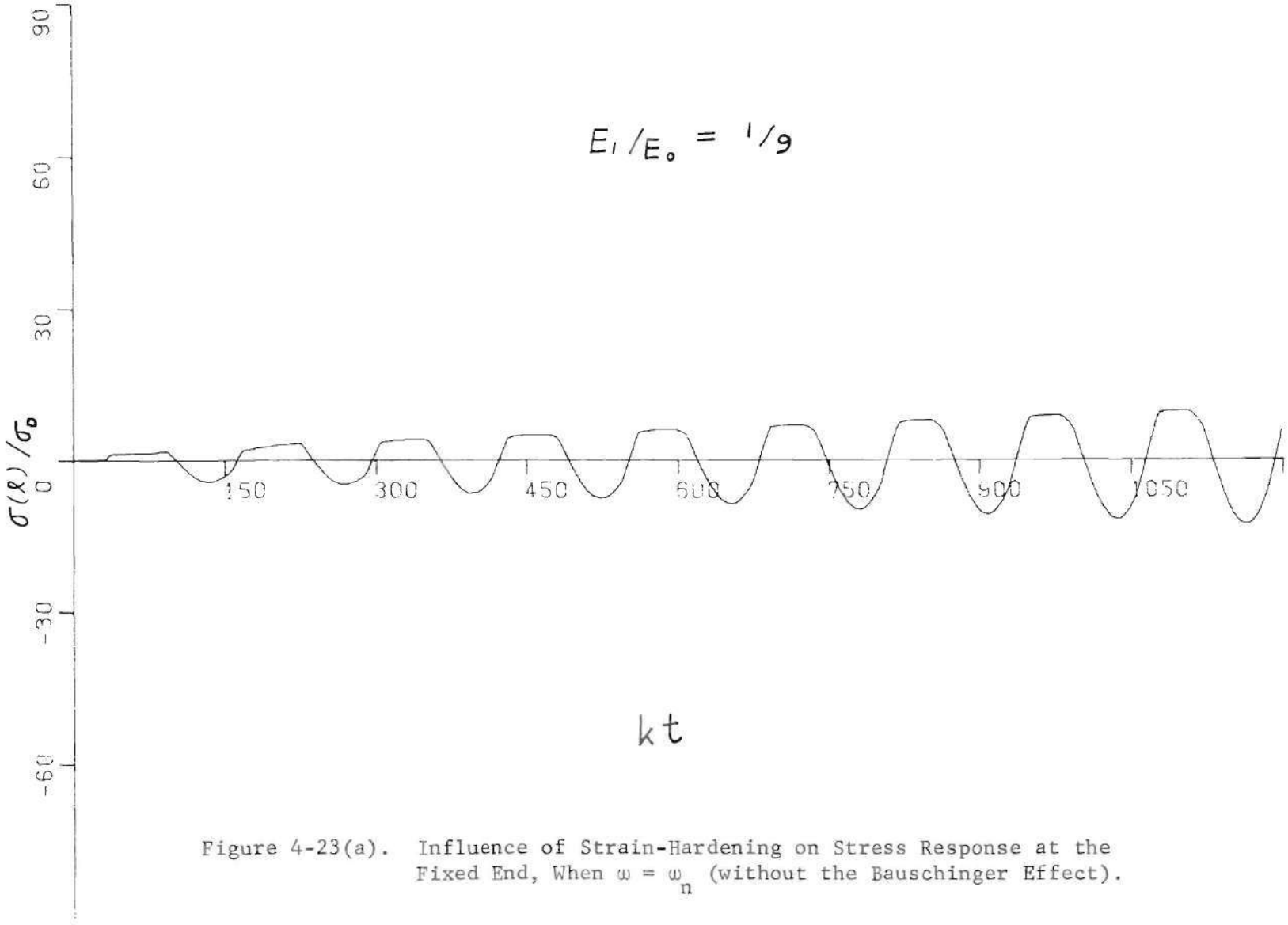

Figure 4-23(a). Influence of Strain-Hardening on Stress Response at the Fixed End, When $\omega = \omega_n$ (without the Bauschinger Effect).

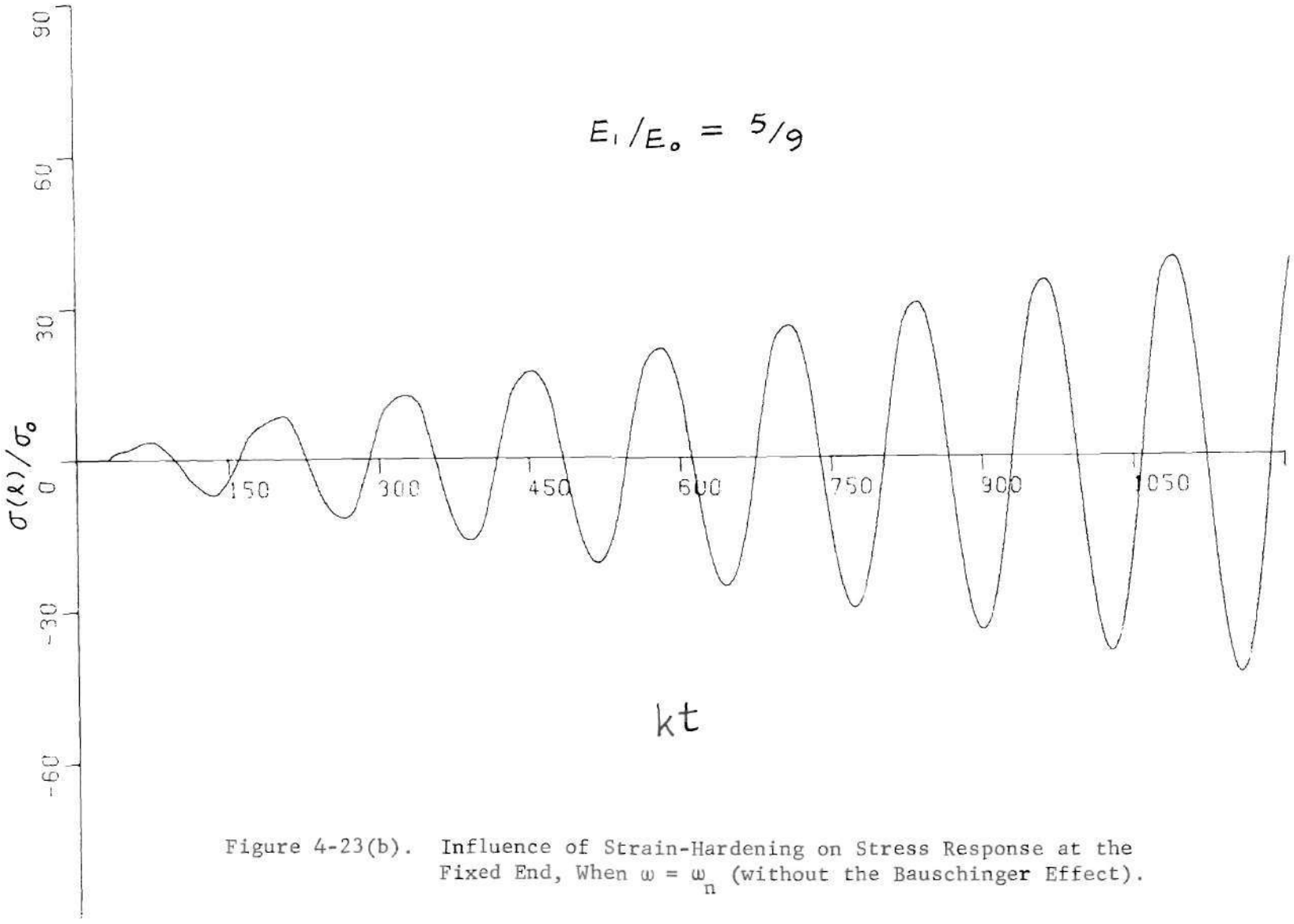

Figure 4-23(b). Influence of Strain-Hardening on Stress Response at the Fixed End, When $\omega = \omega_n$ (without the Bauschinger Effect).

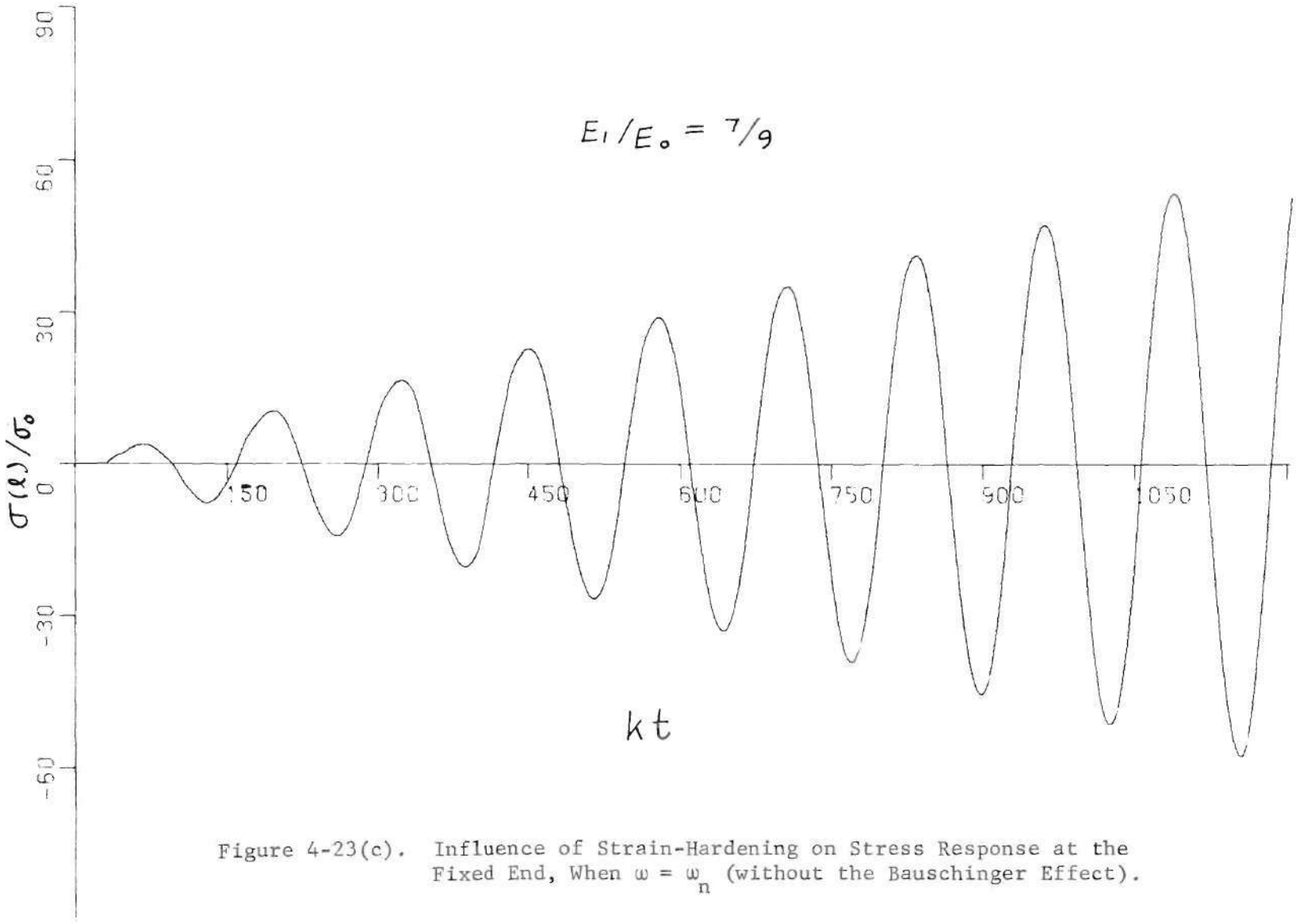

Figure 4-23(c). Influence of Strain-Hardening on Stress Response at the Fixed End, When $\omega = \omega_n$ (without the Bauschinger Effect).

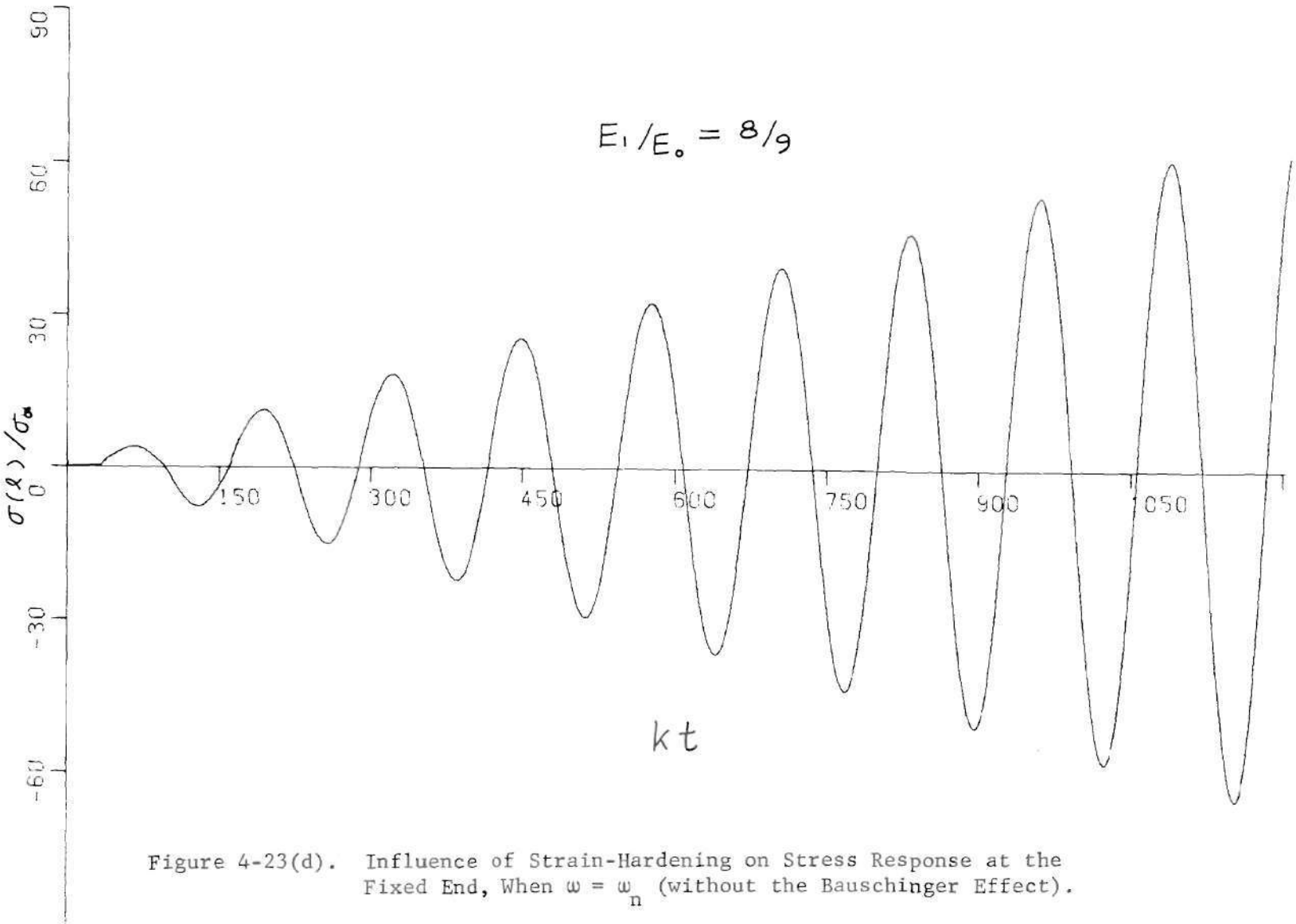

Figure 4-23(d). Influence of Strain-Hardening on Stress Response at the Fixed End, When $\omega = \omega_n$ (without the Bauschinger Effect).

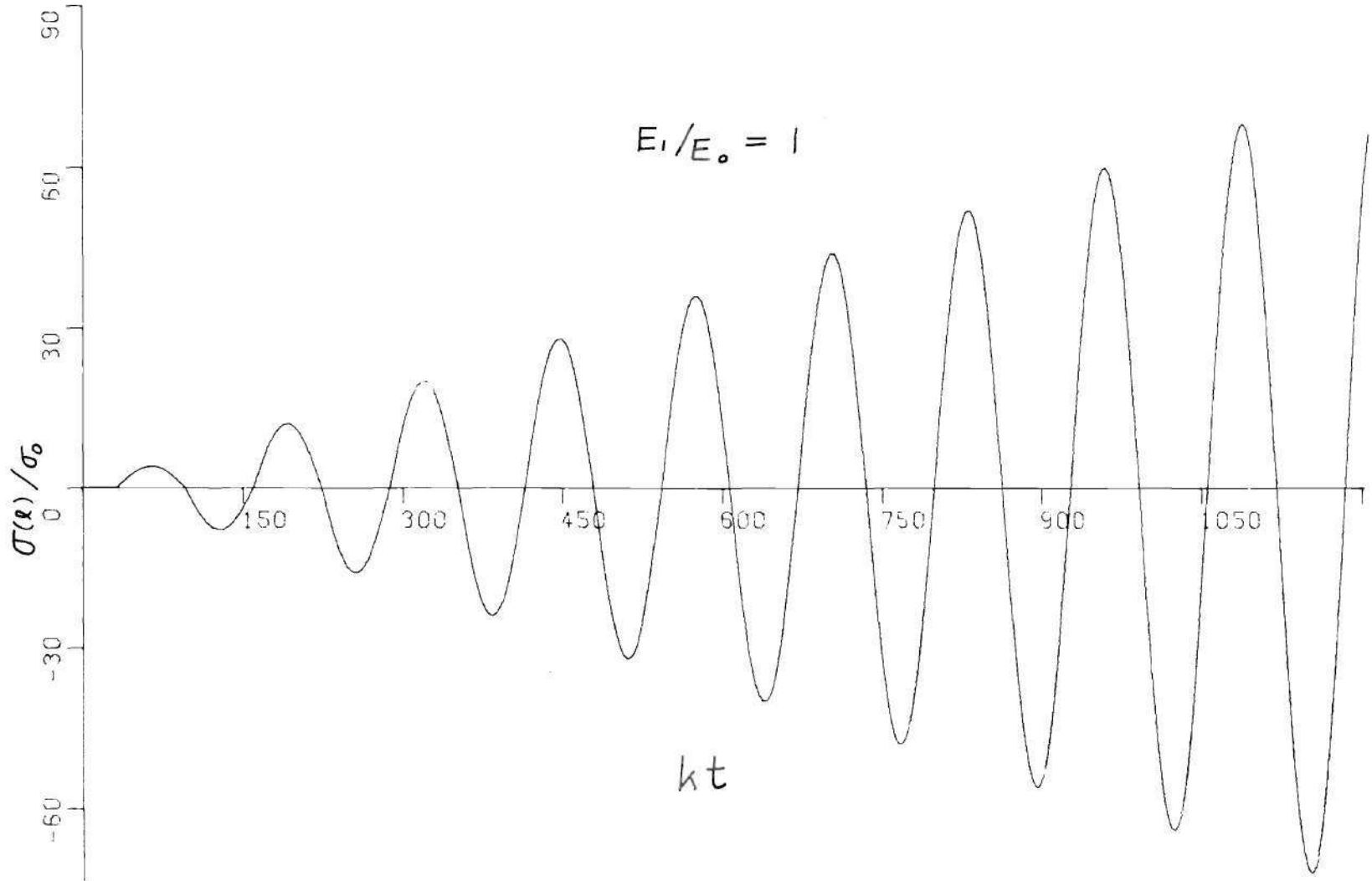

Figure 4-23(e). Influence of Strain-Hardening on Stress Response at the Fixed End, When $\omega = \omega_n$ (without the Bauschinger Effect).

In other words, $t_1 = 1280/k$ is not long enough to reach the maximum response in the neighborhood of a resonance frequency. Therefore, a very long-time response was studied in the region of resonance. (ω/ω_n = 0.74 for $E_1/E_o = 5/9$; $\omega/\omega_n = 0.89$ for $E_1/E_o = 7/9$ and $\omega/\omega_n = 0.95$ for $E_1/E_o = 8/9$). Figure (4-24) shows three displacement-time responses at the free end for $t_1 = 6400/k$ which is five times as long as $t_1 = 1280/k$. In the figure, it is shown that the response is still unbounded in this large time interval. Hence the frequency response curves in Figures (4-14) and (4-15) have to be left open for the following two reasons: (i) In order to find a local maximum in a time response curve, if there is one, it would take a large amount of machine calculating time to reach the goal. (ii) The magnitude of displacement response at the free end at $t_1 = 6400/k$ is almost 140 times the corresponding static deflection. Therefore it is not significant to define a bounded value at resonance. Due to the shift of the locations of plastic resonance frequencies for different degrees of plasticity, the amplification effect at $\omega/\omega_n = 1$ for all E_1/E_o other than 1 becomes bounded. In other words, at a frequency $\omega = \omega_n$, the frequency response corresponding to various degrees of plasticity is examined. The response decreases when the bar becomes more plastic. To illustrate this point clearly, one considers the following figure (Figure (4-25)). Here, the amplification factors for displacement at the free end is plotted against the inverse of E_1/E_o which is E_o/E_1.

A rather interesting point is noted when the bar is very plastic, say at $E_1/E_o = 1/9$ or $E_o/E_1 = 9$. In this case the amplification factor has a value less than 1. One may conclude from the figure at $\omega = \omega_n$

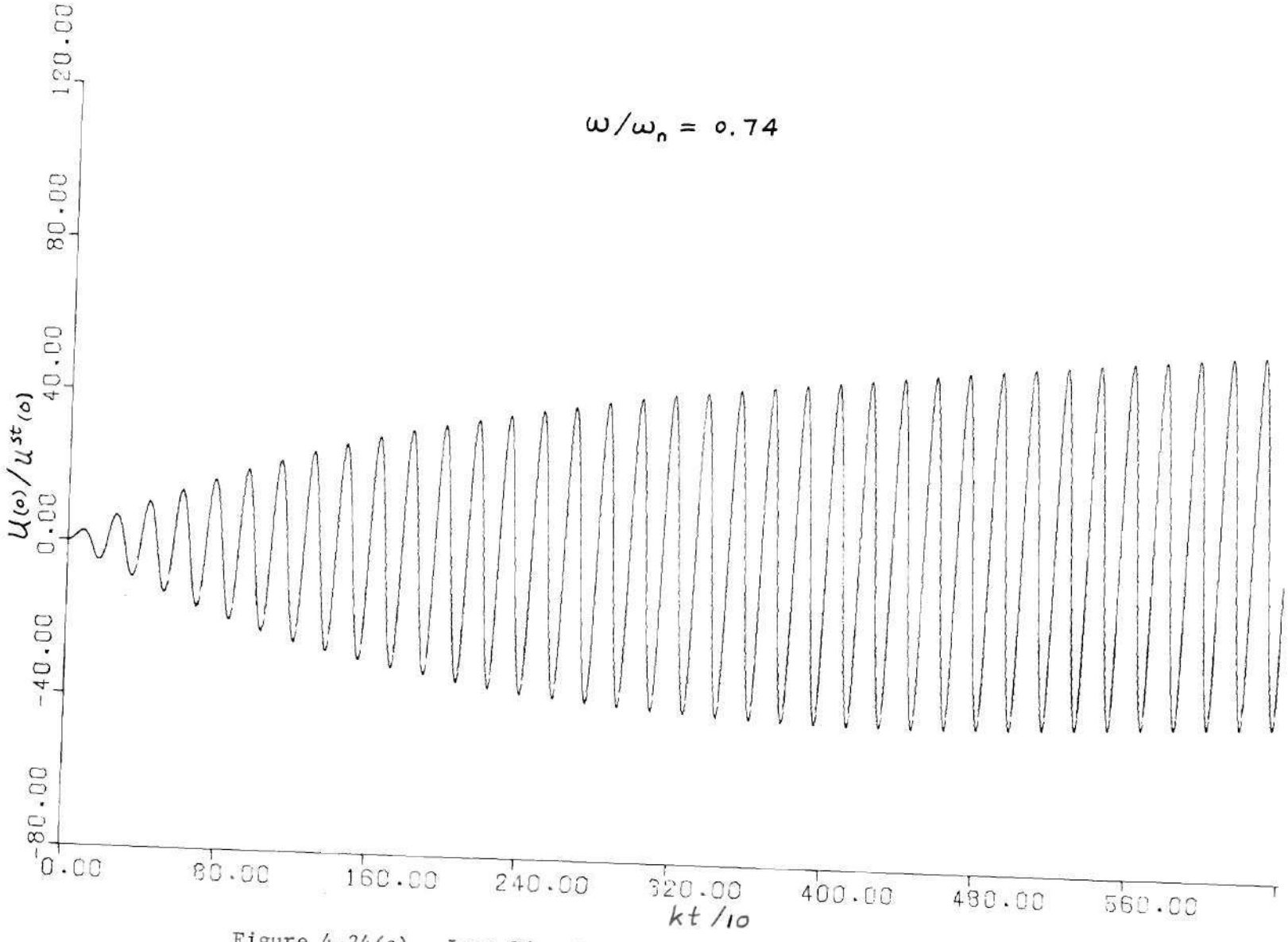

Figure 4-24(a). Long Time Response of Displacement at the Free End.

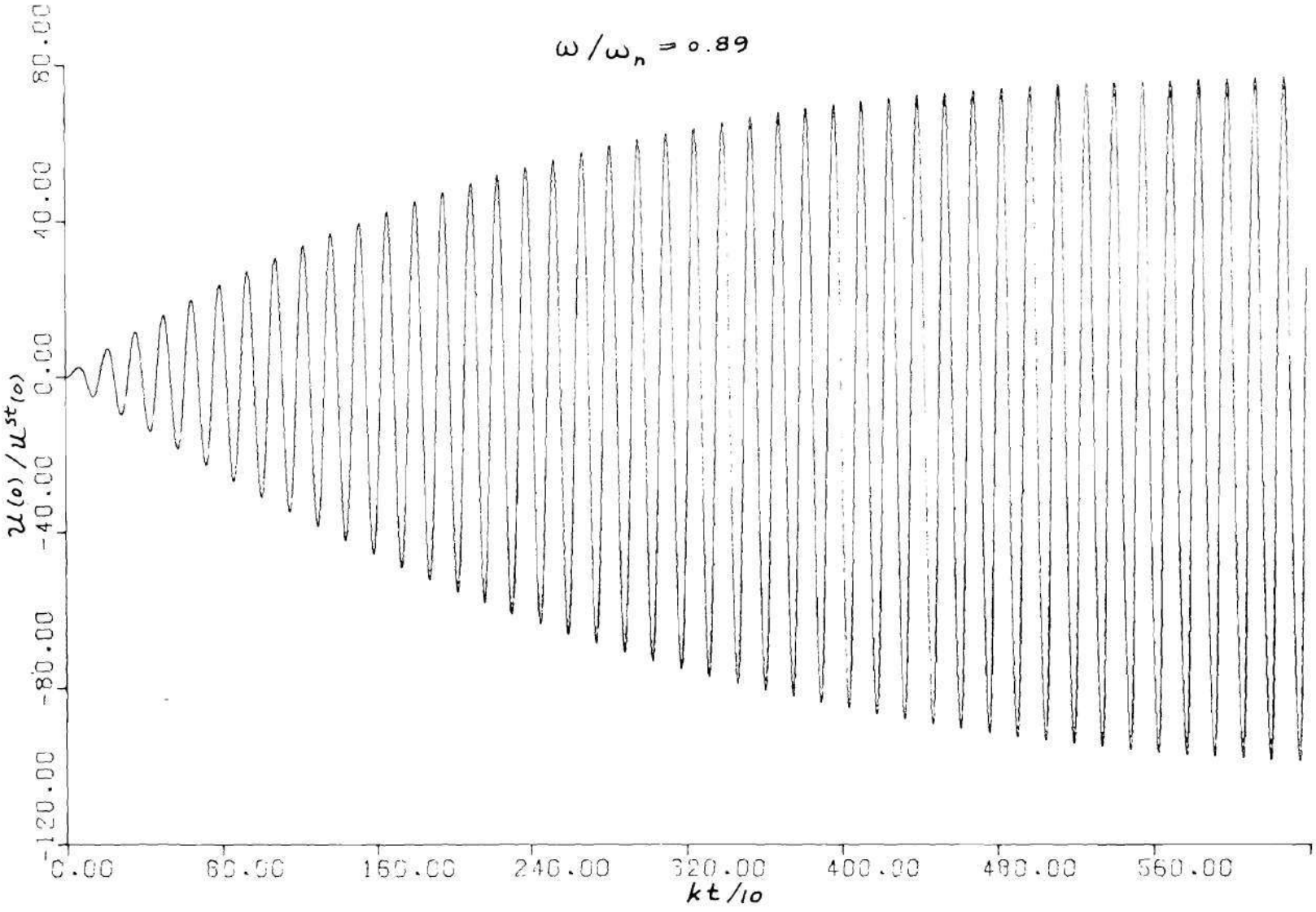

Figure 4-24(b). Long Time Response of Displacement at the Free End.

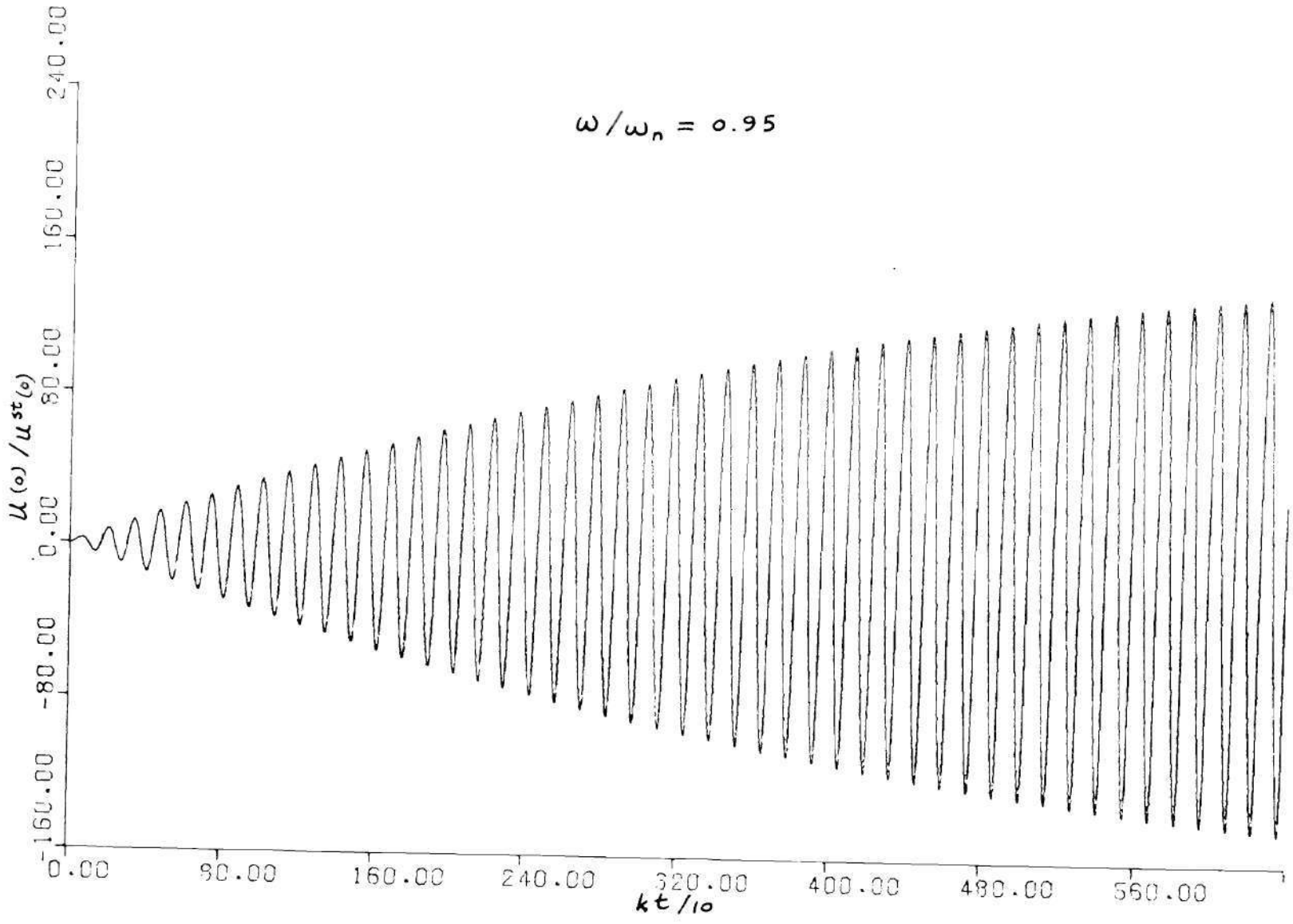

Figure 4-24(c). Long Time Response of Displacement at the Free End.

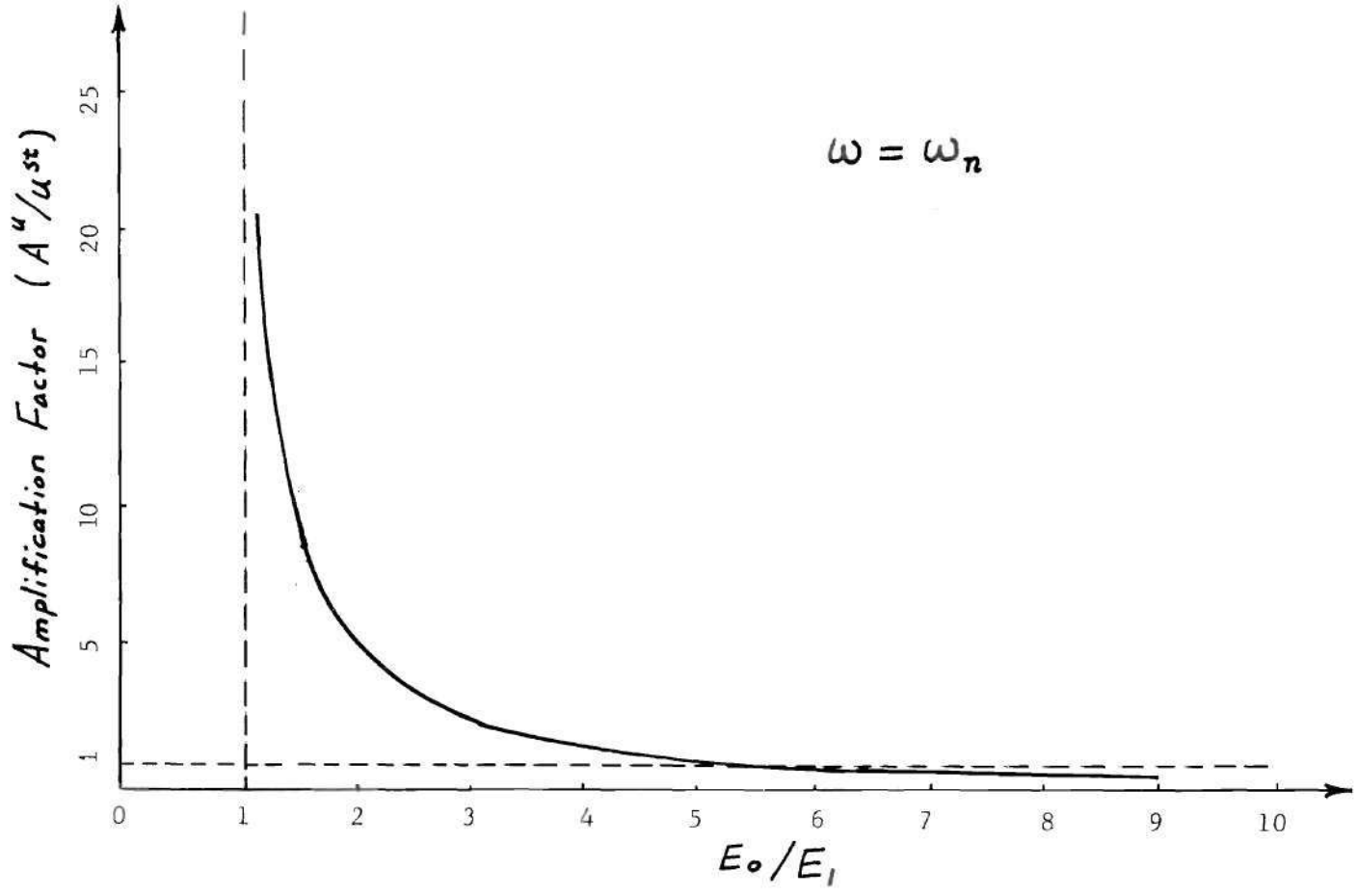

Figure 4-25. Influence of the Degree of Strain-Hardening on the Amplification Factor of Displacement at the Free End.

that for a material with $E_o/E_1 = 5.7$ or $E_1/E_o = 1.58/9$, one shall expect no amplification at all; for the material with $E_o/E_1 < 5.7$, amplification occurs, whereas for $E_o/E_1 > 5.7$ there is a reduction in amplitude. This result can be checked physically by two limiting cases, which are $E_o/E_1 = 1$ (elastic) and $E_o/E_1 \to \infty$ (perfectly plastic). First, in the elastic case, the amplification factor at resonance should approach an infinite value as the limit. This is due to the fact that for an elastic bar excited at its resonance frequency with no damping an unbounded amplification is expected. Second, in the perfectly plastic case ($E_o/E_1 \to \infty$), we cannot have any amplification because an infinite strain will be reached after the dynamic stress has exceeded the yield stress. This phenomenon was not predicted by Kalaski and Wlodarczyk [33] in their paper that first introduced the concept of plastic resonance in a plastic-visco-elastic bar.

In the case without the Bauschinger effect, referring to Figures (4-22) and (4-23), all responses are unbounded for a finite time interval $t = 1280/k$. This is to be expected since for all degrees of strain hardening, the true resonance effect only happens at $\omega/\omega_n = 1$ indicated in Figure (4-15).

Observe from Figure (4-22), where the amplitude of dynamic deflections over static deflections was plotted against time for several degrees of strain hardening, that all curves drift in the positive y-direction in all cases but the elastic. The reason for the drift can be found from the corresponding stress-strain plot. This is the case without the Bauschinger effect, and under the specific loading condition (mean stress equal to zero, and amplitude of the alternating stress equal to 2), the

dynamic stress-strain plot will build up along the positive strain axis. From the resulting strain, consequently, the displacement at any point of the bar would be expected to grow in the positive y-direction also.

(C) Beating Phenomenon

A beating phenomenon occurs when the driving frequency is near the resonant frequency. Here, the term resonant frequency represents either elastic or plastic resonance. As indicated by Jacobsen and Ayre [44], the phenomenon has little physical interest, however it exists in a mathematical sense. A proof of the results is section (A), where the plastic resonant frequencies were found from the plot in Figures (4-14), (4-15) can be reached by considering the following frequency relation:

$$\begin{aligned} \omega_N &= \omega - \omega_B \qquad \text{for} \qquad \omega > \omega_N \\ \omega_N &= \omega + \omega_B \qquad \text{for} \qquad \omega < \omega_N \end{aligned} \tag{4-6}$$

where ω_B is the beating frequency, ω_N is the resonant frequency (elastic or plastic) and ω is the driving frequency. If we transform this frequency equation to a corresponding period equation, one has

$$\begin{aligned} T_N &= \frac{T_B\, T}{T_B - T} \qquad \text{for} \qquad T_N > T \\ T_N &= \frac{T_B\, T}{T_B + T} \qquad \text{for} \qquad T_N < T \end{aligned} \tag{4-7}$$

where T_B, T_N and T are the corresponding periods. In Figure (4-26) and Figure (4-27), there are some results involving the beating phenomena. The following table shows good agreement between the resonant period

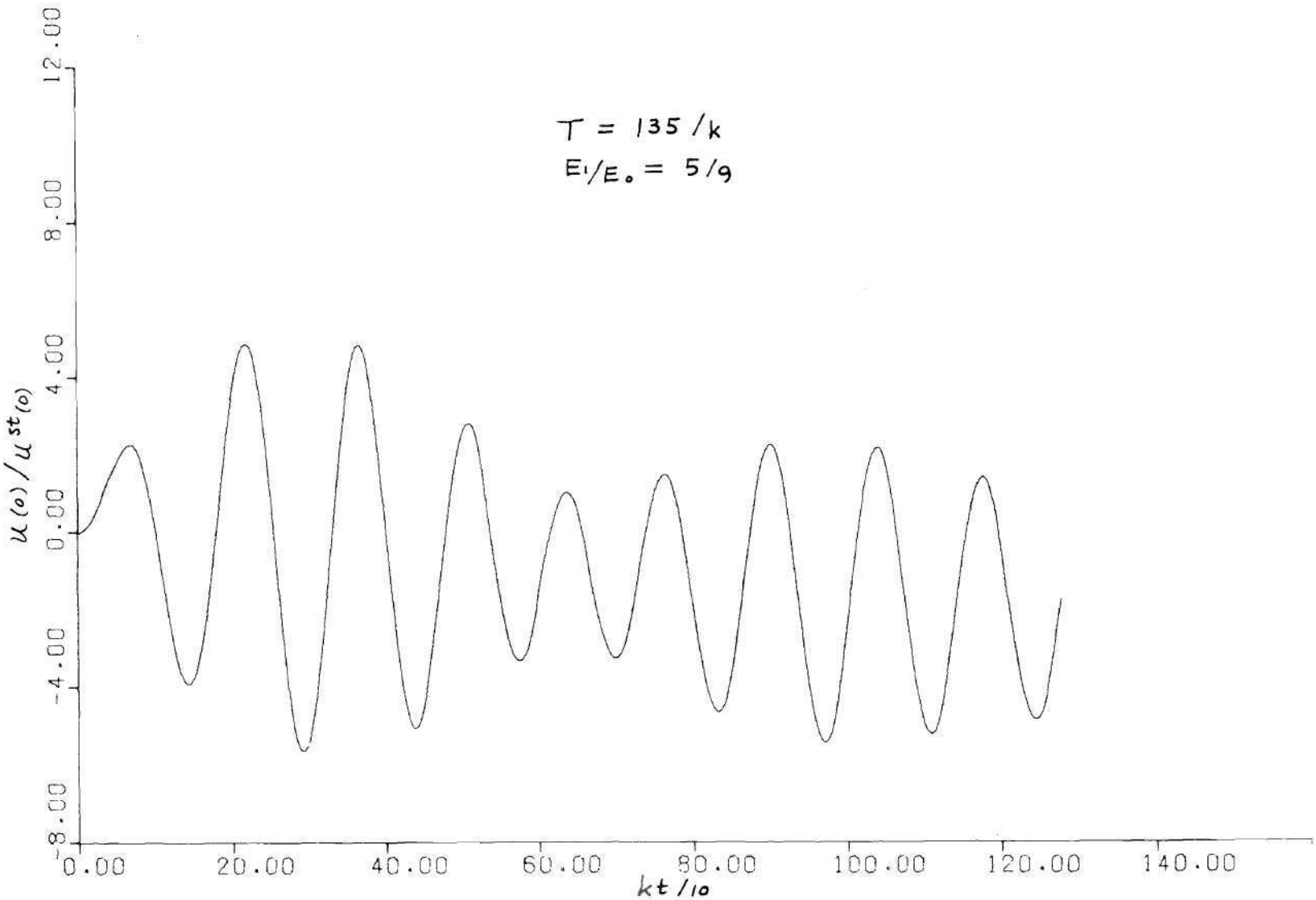

Figure 4-26(a). Beating Phenomenon on Displacement Response at the Free End (With the Bauschinger Effect).

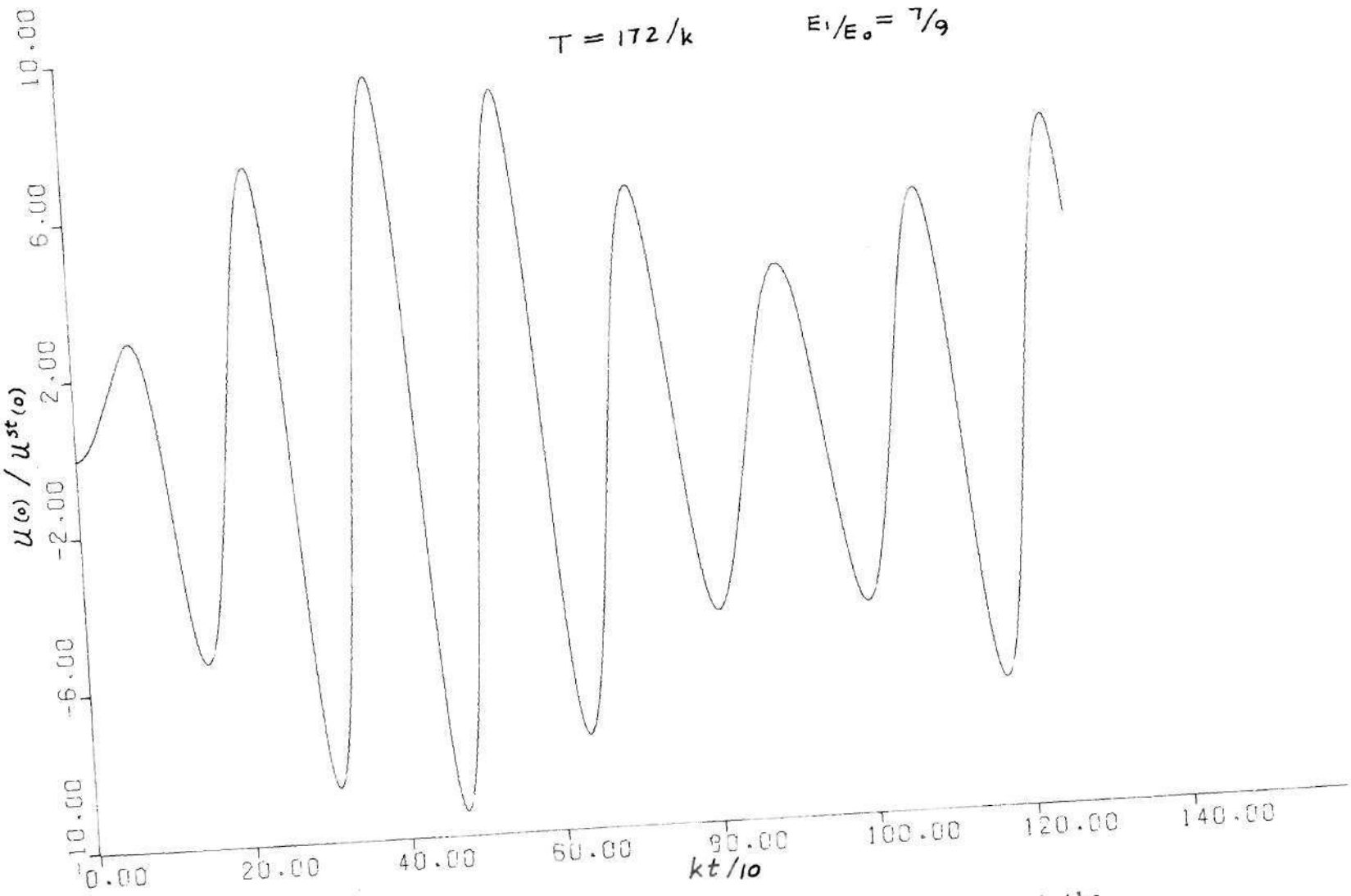

Figure 4-26(b). Beating Phenomenon on Displacement Response at the Free End (With the Bauschinger Effect).

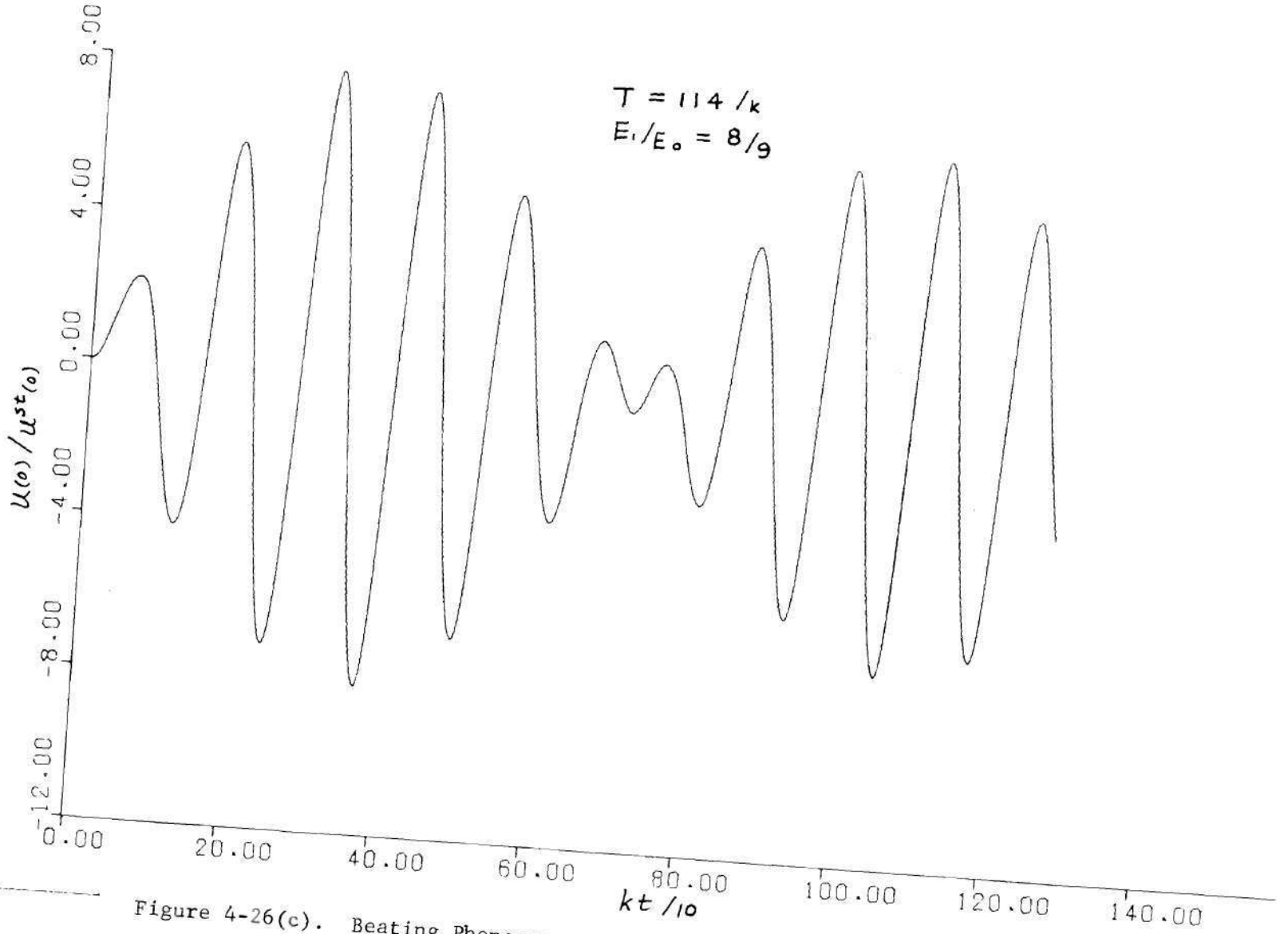

Figure 4-26(c). Beating Phenomenon on Displacement Response at the Free End (With the Bauschinger Effect).

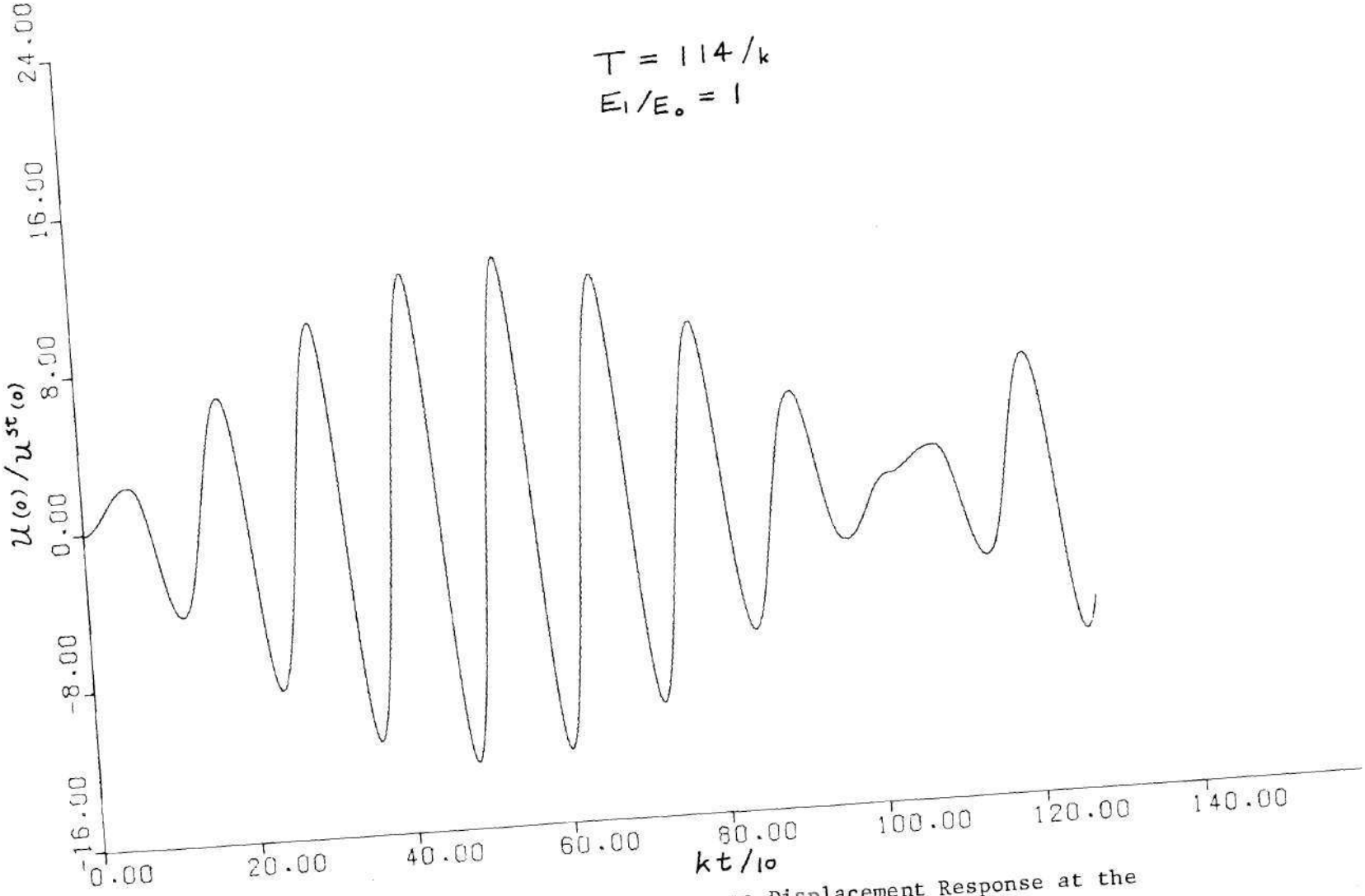

Figure 4-26(d). Beating Phenomenon on Displacement Response at the Free End (With the Bauschinger Effect).

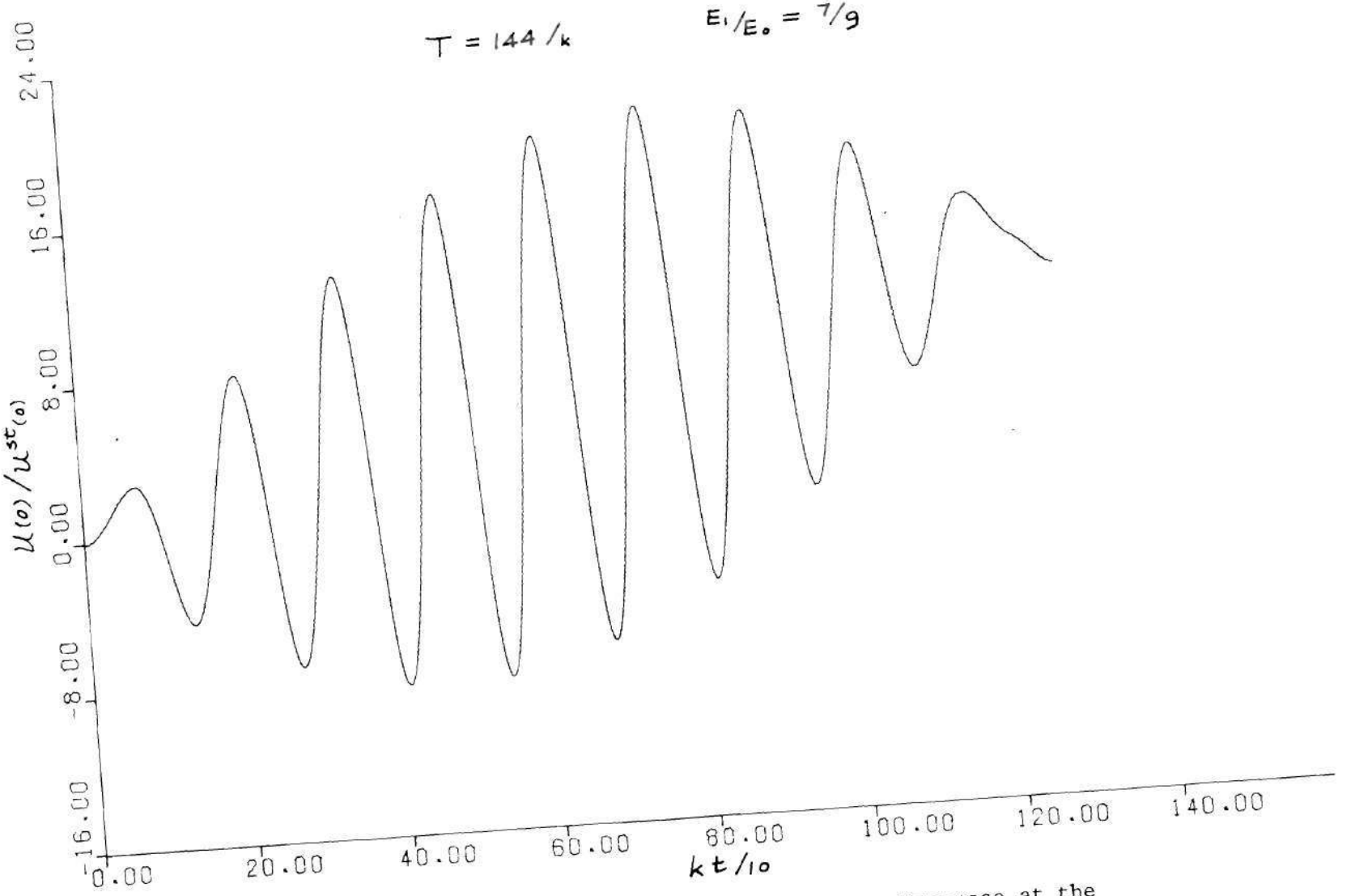

Figure 4-27(a). Beating Phenomenon on Displacement Response at the Free End (without the Bauschinger Effect).

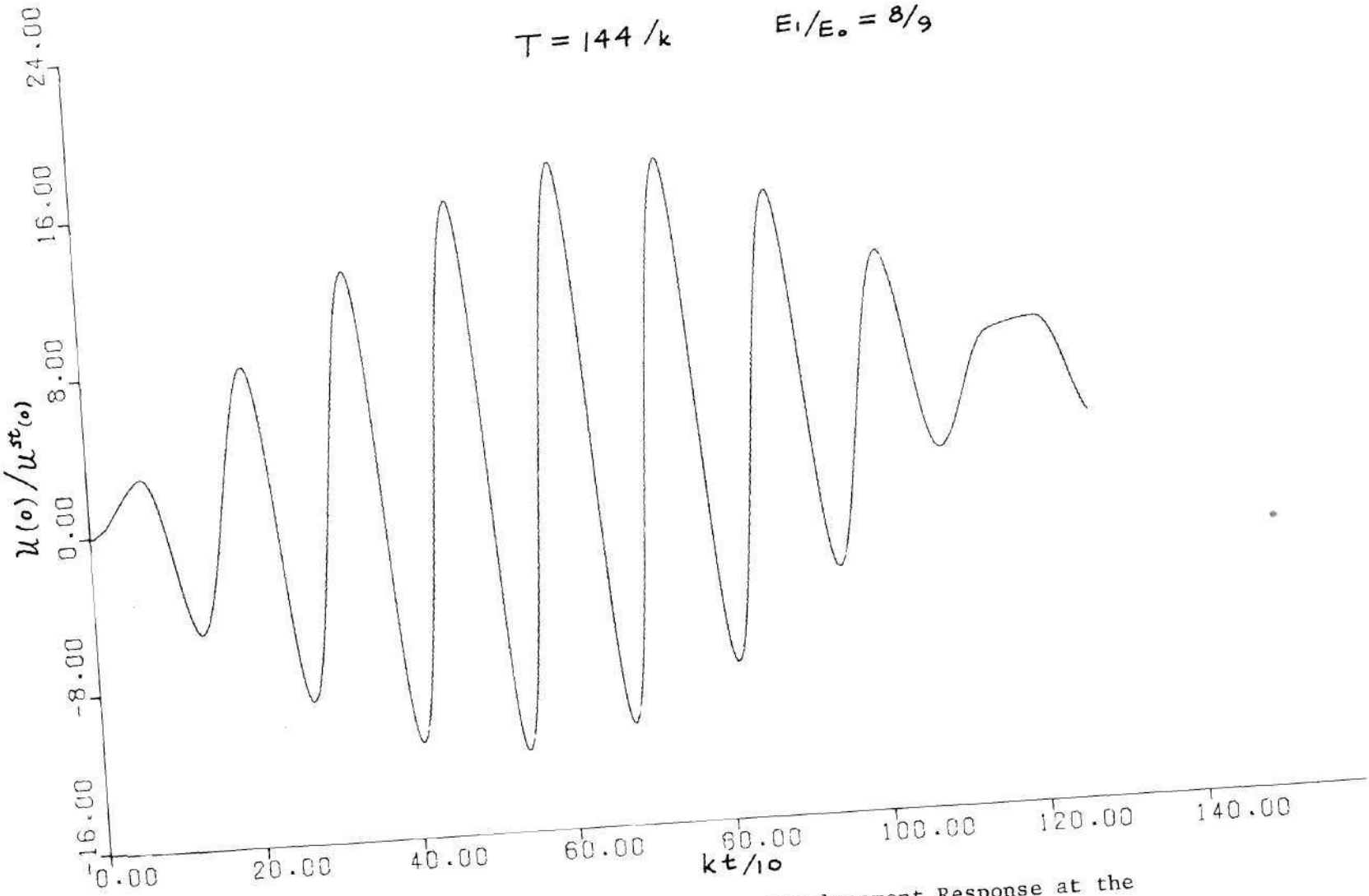

Figure 4-27(b). Beating Phenomenon on Displacement Response at the Free End (Without the Bauschinger Effect).

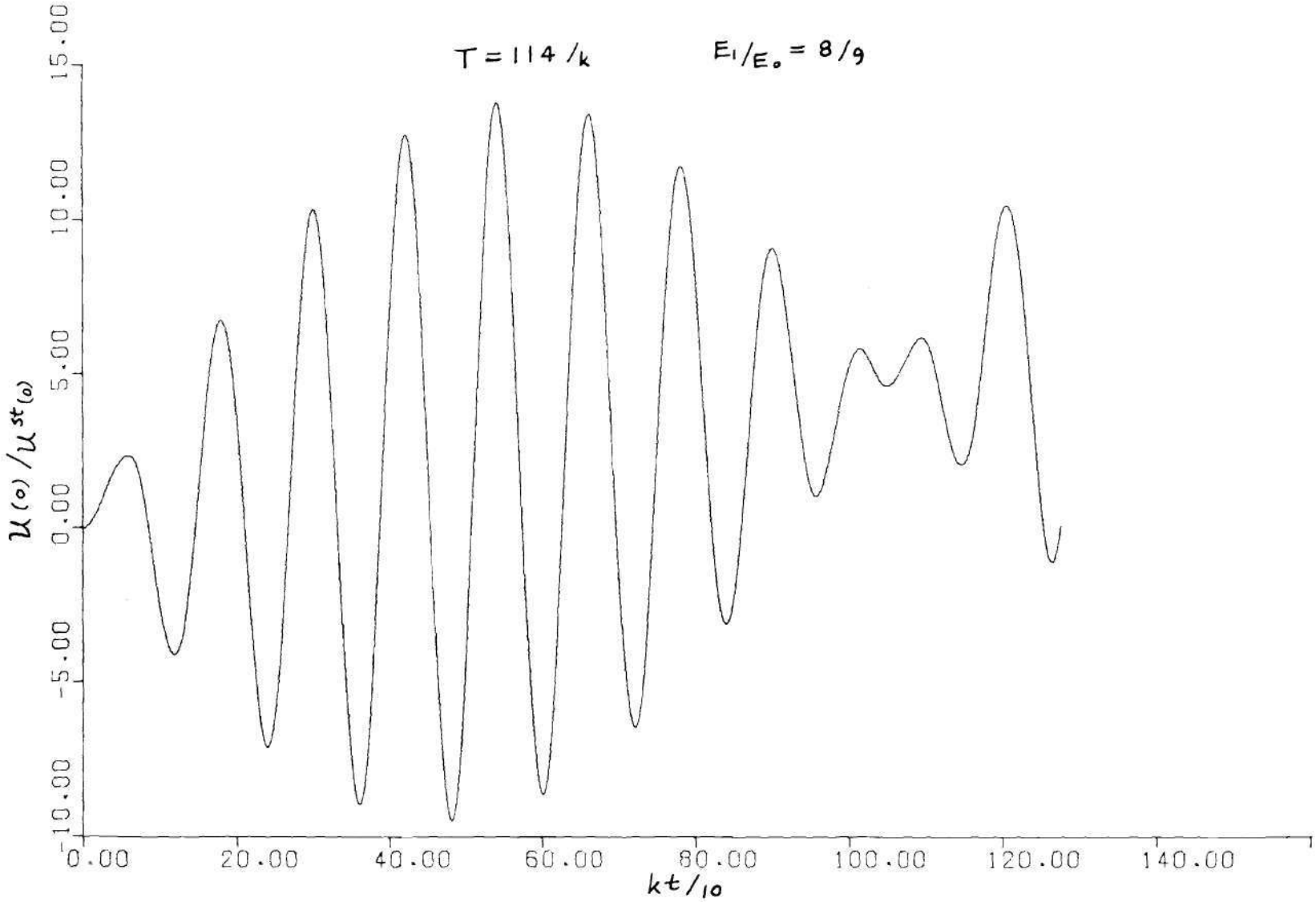

Figure 4-27(c). Beating Phenomenon on Displacement Response at the Free End (Without the Bsuschinger Effect).

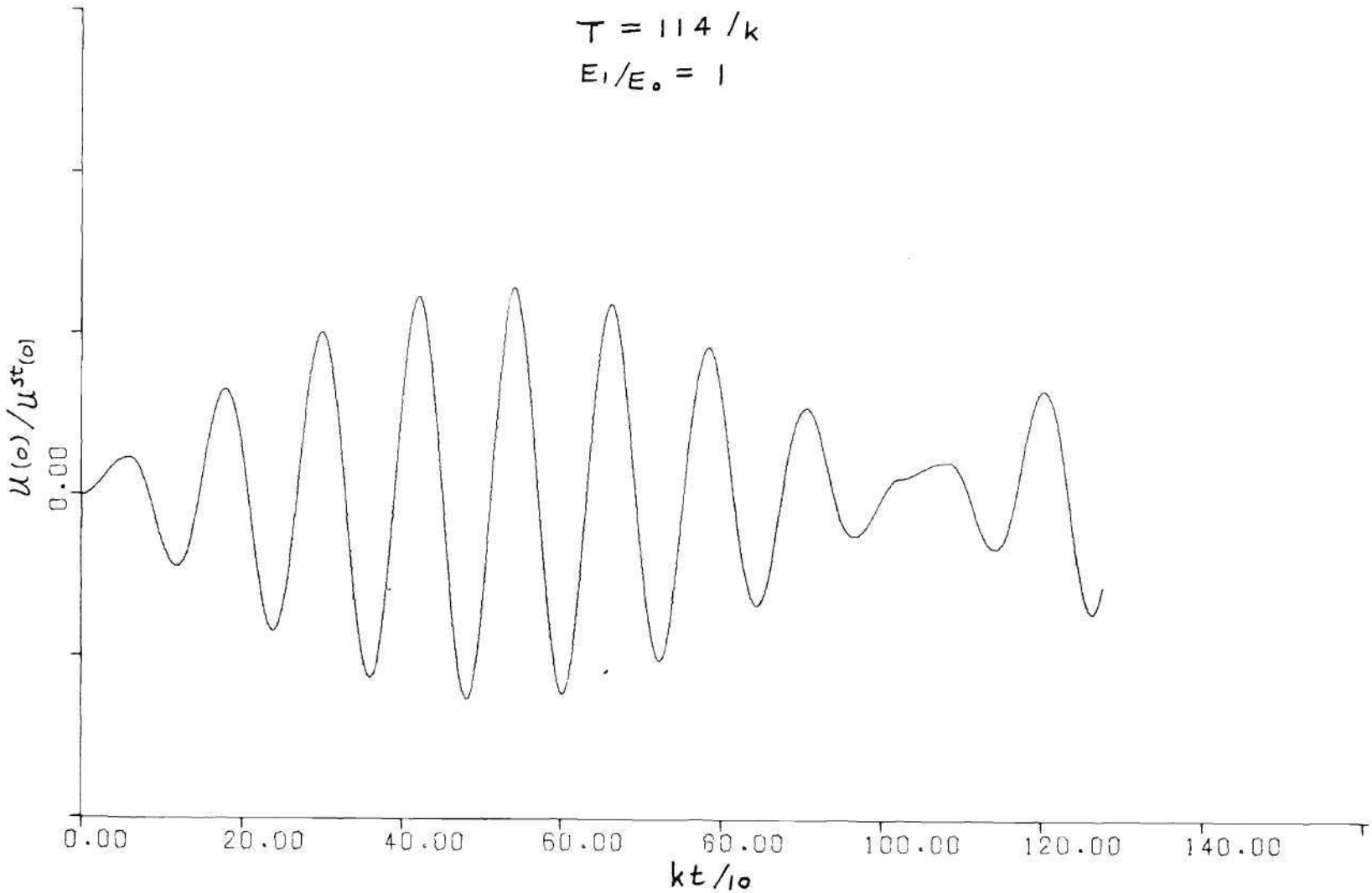

Figure 4-27(d). Beating Phenomenon on Displacement Response at the Free End (Without the Bauschinger Effect).

found by Figure (4-15) or Figure (4-16) and the resonant period found by Equation (4-7).

V. Elastic Plastic Boundaries on x-t Plane

An interesting aspect to be presented in this section are the development of elastic-plastic boundaries in the characteristics plane (x-t plane). These boundaries divide the x-t plane into many domains in which the upper yield portion, elastic portion and lower yield portion of a bar are located in during certain intervals of time. Shown by Figures (4-28) through (4-30) are x-t planes for three different loading frequencies, $2\pi k/64$, $2\pi k/96$, and $2\pi k/128$, with the Bauschinger effect. No Bauschinger effect was considered in Figure (4-31) where the loading frequency takes a value of $2\pi k/64$. For these figures the mean stress was taken equal to zero, the amplitude of alternating stress equals $2\sigma_o$ and E_1/E_o equals 1/9. We observe that after passing the initial elastic and upper yield stress domains in Figure (4-28) (which included the Bauschinger effect), the upper yield-elastic-lower yield domains appear alternately at both ends of the bar. However, the mid-point of the bar stays elastic all the time. This fact can also be seen from Figure (4-32), where the corresponding stress-strain plots at the free end, mid-point and fixed end of the bar are shown. It is also seen from Figure (4-28) that both ends of the bar experience more plastic deformation than the middle portion of the bar since they remain plastic most of the time.

Table 4.1. Comparison of the Resulting Resonant Frequencies Found Between Section (A) and Section (C).

	Degree of Strain-hardening E_1/E_o	Loading Parameters			Beating Period T_B	Plastic Resonant Period T_N	
		Mean Stress	Amplitude of Alternating Stress	Period T		by Fig. (5-12) and Fig. (5-13)	by Eq. (5-7)
with the Bauschinger effect	5/9	0.0	2.0	135.0	656.37	172.0	171.10
	7/9	0.0	2.0	172.0	888.03	144.0	144.13
	8/9	0.0	2.0	114.0	702.70	135.0	135.65
	1	0.0	2.0	114.0	1019.30	128.0	127.68
without the Bauschinger effect	7/9	0.0	2.0	144.0	1175.0	128.0	128.11
	8/9	0.0	2.0	144.0	1183.3	128.0	128.20
	8/9	0.0	2.0	114.0	1058.0	128.0	127.76
	1	0.0	2.0	114.0	1060.0	128.0	127.74

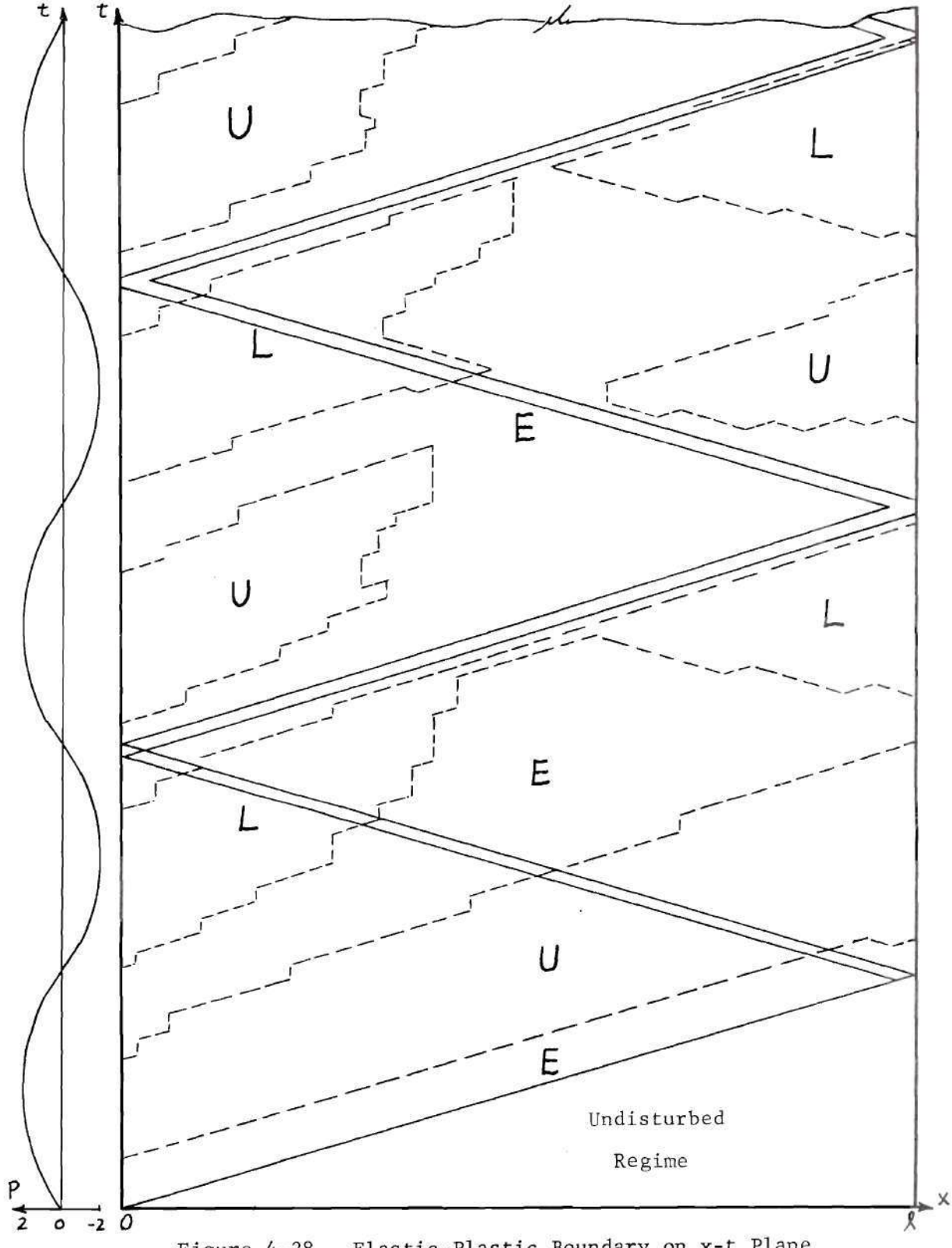

Figure 4-28. Elastic-Plastic Boundary on x-t Plane (With the Bauschinger Effect).

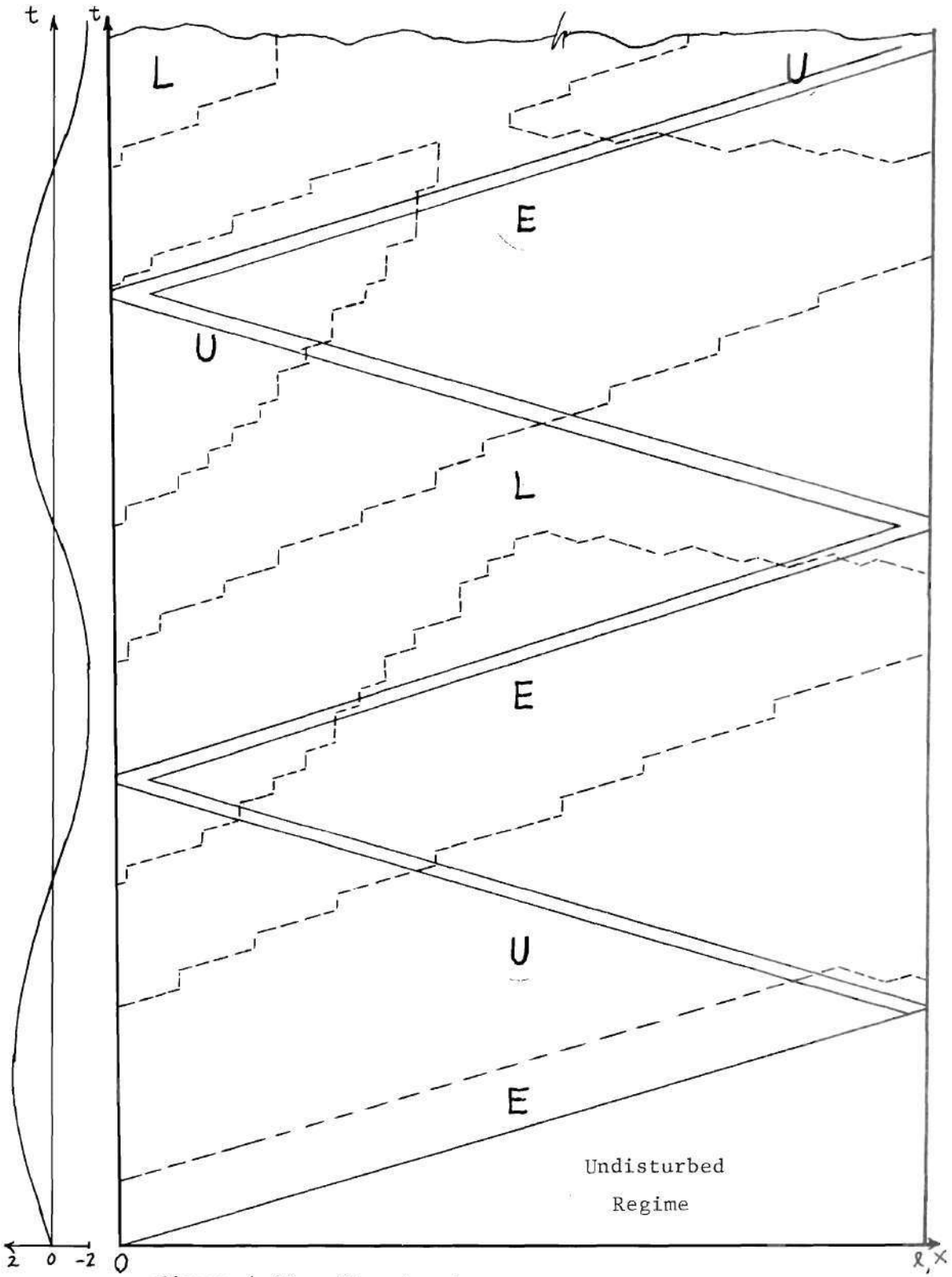

Figure 4-29. Elastic-Plastic Boundary on x-t Plane (With the Bauschinger Effect).

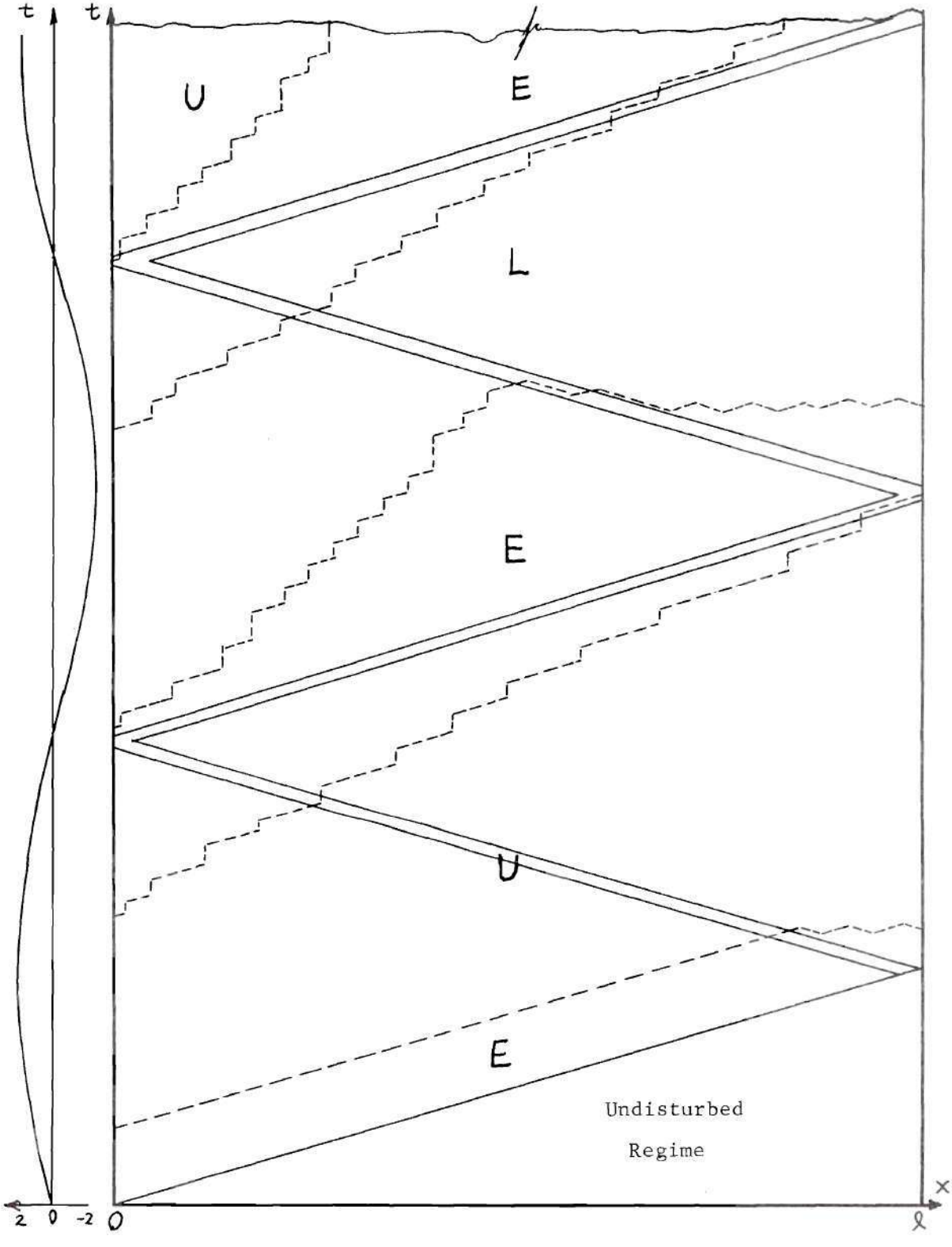

Figure 4-30. Elastic-Plastic Boundary on x-t Plane (With the Bauschinger Effect).

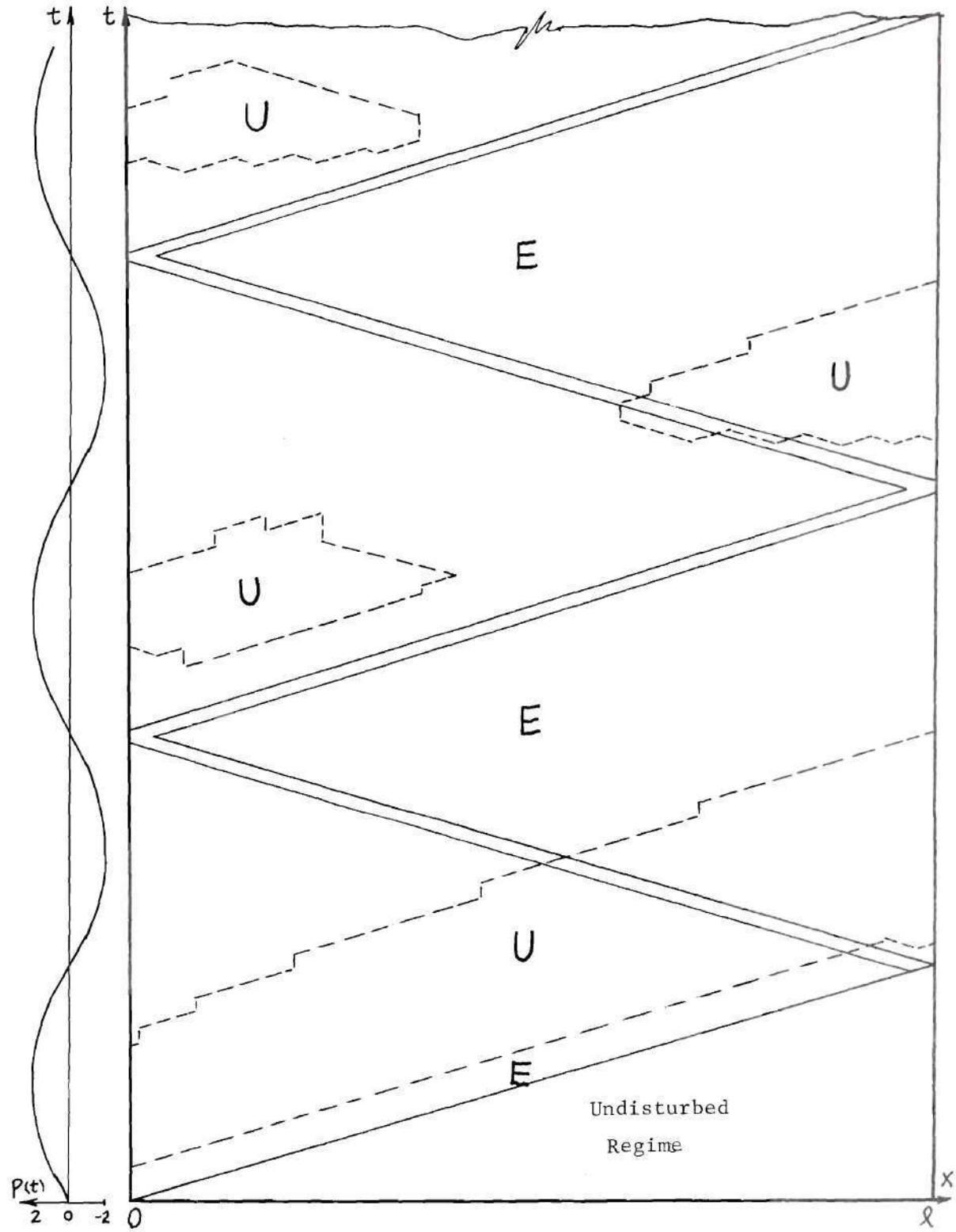

Figure 4-31. Elastic-Plastic Boundary on x-t Plane (Without the Bauschinger Effect).

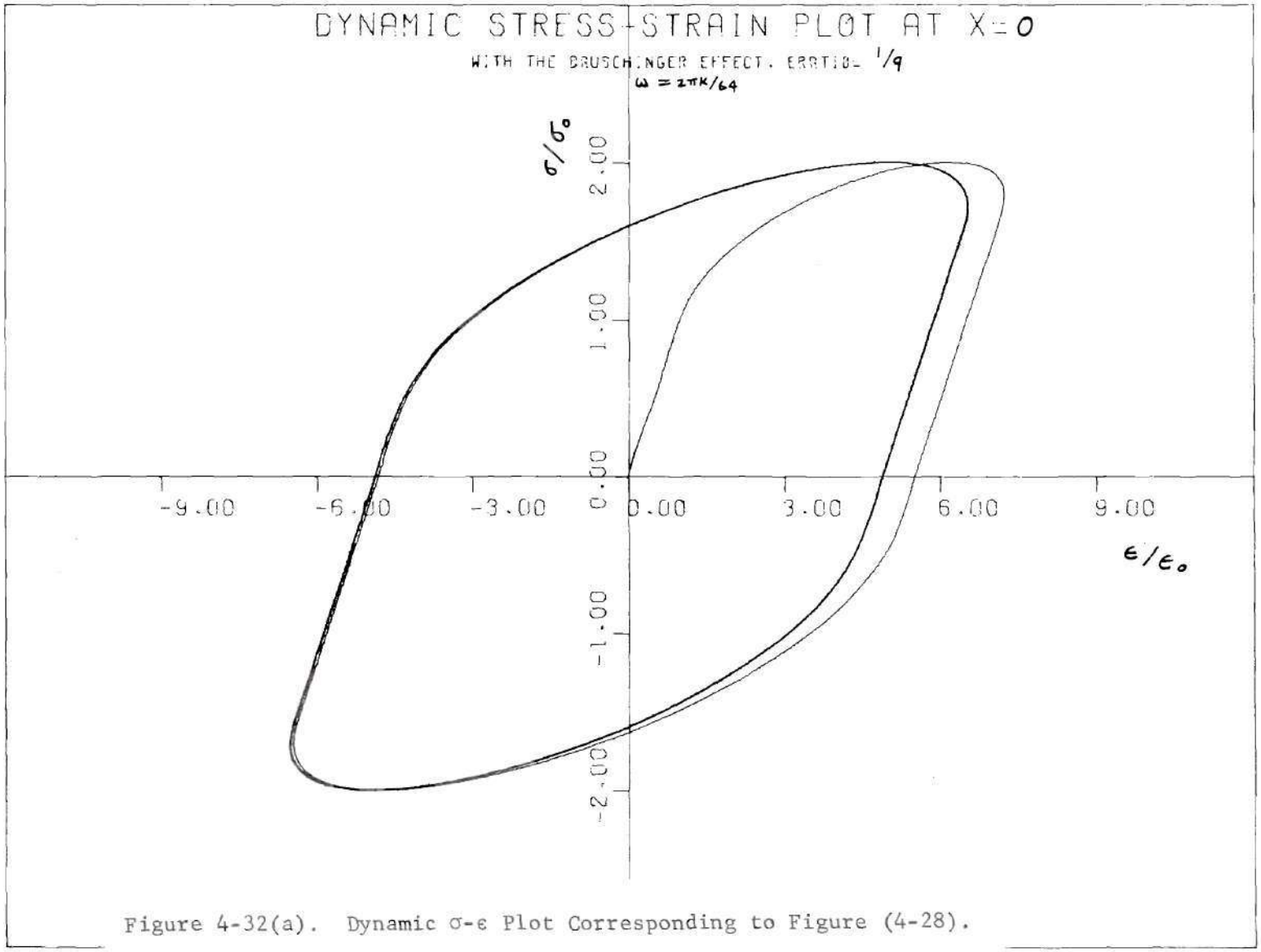

Figure 4-32(a). Dynamic σ-ε Plot Corresponding to Figure (4-28).

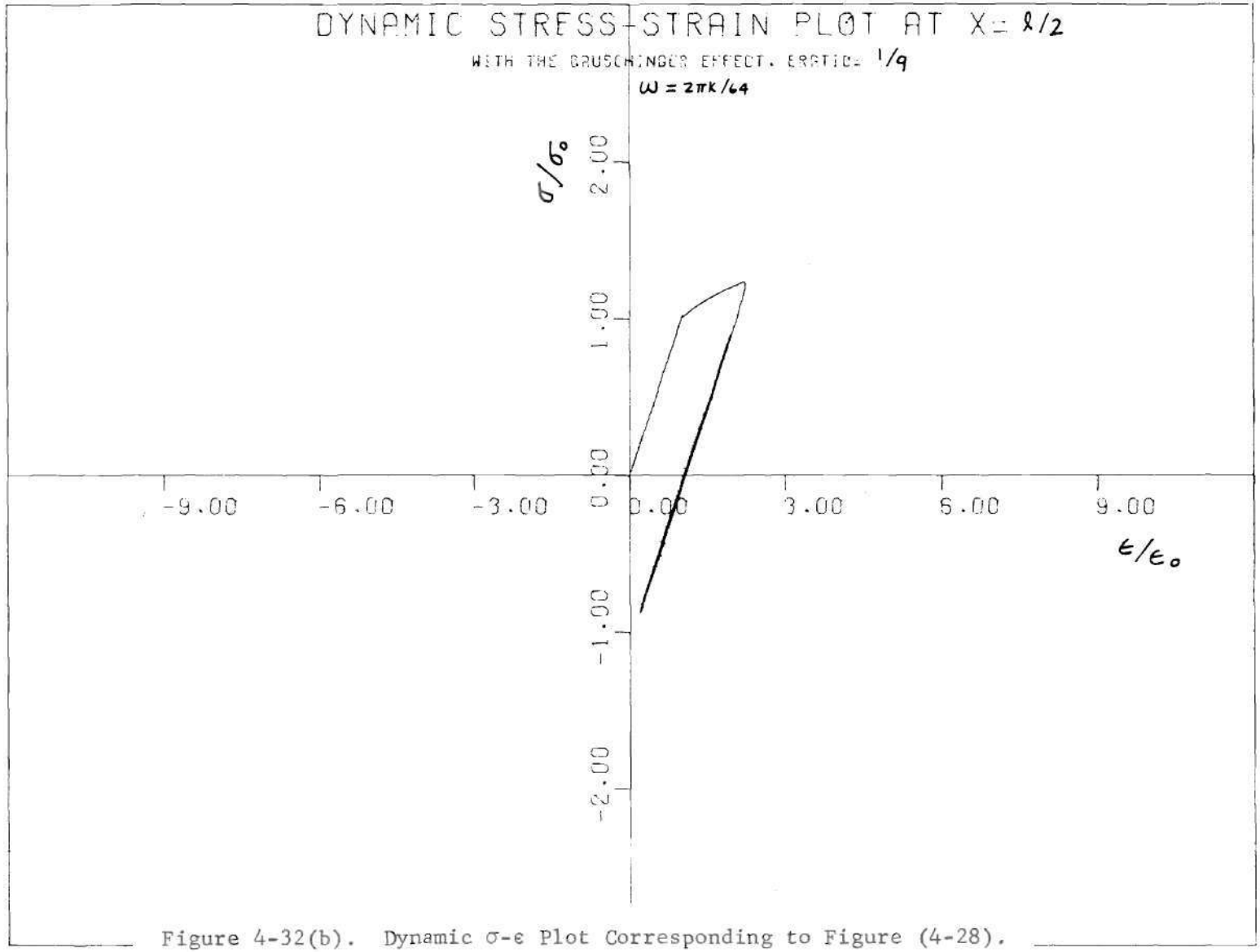

Figure 4-32(b). Dynamic σ-ε Plot Corresponding to Figure (4-28).

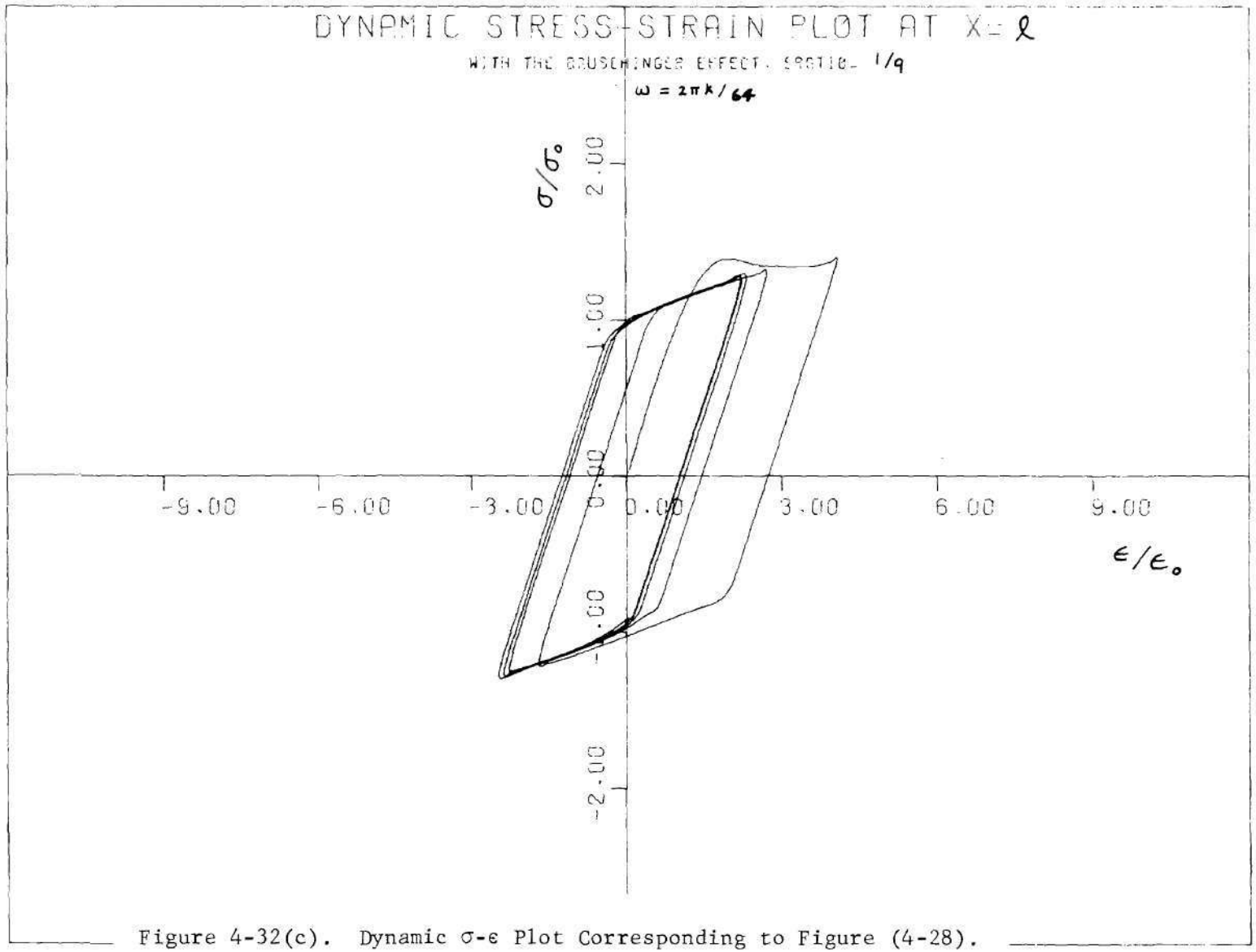

Figure 4-32(c). Dynamic σ-ε Plot Corresponding to Figure (4-28).

VI. Conservation of Energy

We desire in this section to check the numerical results of the study by considering the conservation of energy. Again, we consider a finite fixed-free elastic-plastic bar under longitudinal wave motion with a sinusoidal load at its free end. (see Figure (2-5)). In a certain time interval, from t equals zero to some later time t_1, one arrives at the following equality concerning the conservation of energy:

$$\begin{bmatrix}\text{Sum of the total work done by the applied force at the free end on the system during the time interval } 0 \le t \le t_1\end{bmatrix} = \begin{bmatrix}\text{Sum of the total kinetic energy in the system at } t = t_1\end{bmatrix} + \begin{bmatrix}\text{Sum of the total strain energy in the system at } t = t_1\end{bmatrix}$$

$$+ \begin{bmatrix}\text{Sum of the total plastic hysteresis energy in the system during the time interval, } 0 \le t \le t_1\end{bmatrix} . \qquad (4\text{-}8)$$

Due to the fact that lower yield and the Bauschinger effect are considered, plastic hysteresis energy results in the bar. The forming of the plastic hysteresis energy starts from a reloading process following unloading into the lower yield region. This energy plays an important role in dynamic plasticity as some experimental investigators (Dolan [45] and Morrow [40]) have indicated. Equation (4-8) represents conservation of energy during an arbitrary chosen time interval.

Next, let us analyze the above equation and derive a mathematical expression for the equality.

(A) External Work Done by Applied Force at the Free End of the Bar

The external work done on the system is at the free end where a sinusoidal load F(t) is applied. If a unit cross-sectional area is considered, (A = 1), and "du" is the differential of displacement at the free end, then the total work done from t = 0 to t = t_1 will be,

$$W = \int F(t)\, du$$

$$= \int_0^{t_1} F(t)\, \frac{du}{dt}\, dt$$

$$= \int_0^{t_1} F(t) \cdot v(o,t) dt$$

$$= \int_0^{t_1} \sigma(o,t) v(o,t) dt \qquad (4\text{-}9)$$

where $\sigma(o,t)$ and $v(o,t)$ represent the stress and velocity at the free end.

(B) Kinetic Energy in the System at Time t_1

The kinetic energy at a single mass point in the bar can be expressed as

$$K_m = \frac{1}{2}\, \rho_o\, v^2(x,t_1) \quad .$$

Therefore, the total kinetic energy in the system at time t_1 will be,

$$K = \int_0^{\ell} K_m A(x) dx$$

with the aid of A(x) = 1,

$$K = \frac{\rho_o}{2} \int_o^{\ell} v^2(x,t_1)dx \quad . \tag{4-10}$$

(C) Strain Energy and Hysteresis Energy in the System

No closed form analytical expression can be obtained to express the strain energy and plastic hysteresis energy for this nonlinear problem. To evaluate these two energy contributions we consider numerical results from the graph of the dynamic stress-strain. The strain energy at $t = t_1$ for a single mass point of the bar may be written mathematically as,

$$U_m = \int_o^{\epsilon_1} \sigma(\epsilon)d\epsilon \quad . \tag{4-11}$$

One also notes that the strain energy can be represented by the sweeping area between the dynamic stress-strain curve and the strain axis. Thus, the shaded are shown in Figure (4-33) represents this energy.

Therefore, the total strain energy in the system (bar) will be,

$$U = \int_o^{\ell} \int_o^{\epsilon_1} \sigma(\epsilon)d\epsilon \, dx \quad . \tag{4-12}$$

Furthermore, if the hysteresis area repeats itself, then a double-shaded region results from the plastic hysteresis energy (see Figure (4-34). One therefore finds that the double-lined shaded area of Figure (4-34) represents the amount of plastic hysteresis energy while the single-lined shaded area represents the amount of strain energy at $t = t_1$. We observe from the figure that plastic hysteresis energy will not be formed until a reloading process starts, and it will be stopped momentarily

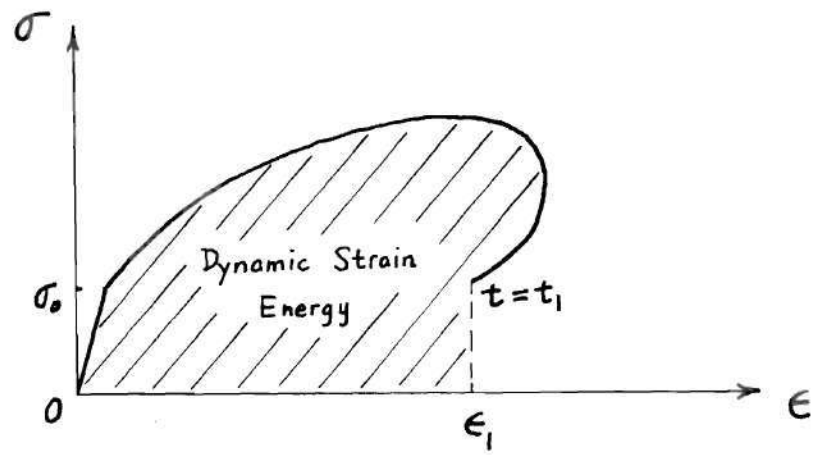

Figure 4-33. Dynamic Strain Energy on σ-ε Plot.

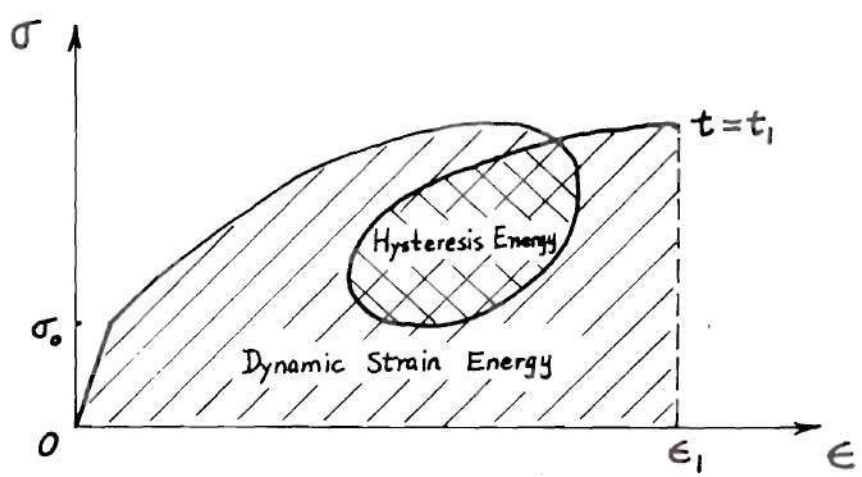

Figure 4-34. Hysteresis Energy on σ-ε Plot.

after the loop has been completed. It should be also noted that no plastic hysteresis energy exists if lower yield is not considered (refer to Figure 2-4 and 2-5). Moreover, if the trace of the dynamic stress-strain curve does not extend into the lower yield region, then hysteresis energy will not result.

One may write equation (4-8) in a mathematical form,

$$W = K + U + H \tag{4-13}$$

where

$$W = \int_o^{t_1} \sigma(o,t)v(o,t)dt$$

$$K = \frac{\rho_o}{2} \int_o^{\ell} v^2(x,t_1)dx$$

$$U = \int_o^{\ell} \int_o^{\varepsilon_1} \sigma(\varepsilon)d\varepsilon\, dx$$

and

H = sum of the total hysteresis energy in the system.

All expressions in equation (4-13) are in terms of stress, strain and particle velocity which are all available from the numerical solution.

The following dimensional analysis is required before the numerical solutions can be readily utilized. Let us rewrite the related equations again,

$$W = \int_{o}^{t_1} \sigma(o,t)v(o,t)dt$$

$$K = \frac{\rho_o}{2} \int_{o}^{\ell} v^2(x,t_1)dx$$

$$U = \int_{o}^{\ell} \int_{o}^{\epsilon_1} \sigma(\epsilon)d\epsilon dx \quad .$$

H = total area repeatedly swept by the dynamic σ-ϵ curve.

Since the unit cross-sectional area of the bar, A = 1, is considered in deriving these energy equations, then all the units of W, T, U and H must be in force/length. Now, if there exists an energy quantity W_o such that it possesses also the units of force/length, then non-dimensional energy equations can be formed by dividing all of the above equations by W_o. For this purpose, let us consider a quantity $W_o = \sigma_o v_o/k$ which possesses units of force/length, and where σ_o is the yield stress, v_o is the corresponding yield velocity ($v_o = \sigma_o/\rho_o c_o$), and k is a material constant. Therefore, equation (4-9) becomes

$$\frac{W}{W_o} = \frac{1}{\sigma_o v_o/k} \int_{o}^{t_1} \sigma(o,t)v(o,t)dt$$

or

$$\frac{W}{W_o} = \int_{o}^{kt_1} \left(\frac{\sigma(o,t)}{\sigma_o}\right)\left(\frac{v(o,t)}{v_o}\right) d(kt) \quad . \tag{4-14}$$

And equation (4-10) becomes,

$$\frac{K}{W_o} = \frac{1}{\sigma_o v_o/k} \cdot \frac{\rho_o}{2} \int_o^{\ell} v^2(x,t_1)dx$$

or

$$\frac{K}{W_o} = \frac{k\rho_o v_o \ell}{2\sigma_o} \int_o^1 \left(\frac{v(x,t_1)}{v_o}\right)^2 d\left(\frac{x}{\ell}\right) \quad .$$

Since $\sigma_o = \rho_o c_o v_o$ and $\frac{\ell}{c_o} = \frac{N}{2k}$, where N represents the nondimensional time for an elastic wave traveling a complete cycle along the bar, one arrives at

$$\frac{K}{W_o} = \frac{N}{4} \int_o^1 \left(\frac{v(x,t_1)}{v_o}\right)^2 d\left(\frac{x}{\ell}\right) \quad . \tag{4-15}$$

For the strain energy U, from Eq. (4-8) one has

$$\frac{U}{W_o} = \frac{1}{\sigma_o v_o/k} \int_o^{\ell} \int_o^{\epsilon_1} \sigma d\epsilon \, dx$$

or

$$\frac{U}{W_o} = \frac{\ell k \epsilon_o}{\sigma_o} \int_o^1 \int_o^{\epsilon_1/\epsilon_o} \left(\frac{\sigma}{\sigma_o}\right) d\left(\frac{\epsilon}{\epsilon_o}\right) d\left(\frac{x}{\ell}\right) \quad .$$

Also with the aid of $\sigma_o = E_o \epsilon_o$, $\frac{E_o}{\rho_o} = c_o^2$, $\sigma_o = \rho_o c_o v_o$ and $\frac{\ell}{c_o} = \frac{N}{2k}$ we have

$$\frac{U}{W_o} = \frac{N}{2} \int_o^1 \int_o^{\epsilon_1/\epsilon_o} \left(\frac{\sigma}{\sigma_o}\right) d\left(\frac{\epsilon}{\epsilon_o}\right) d\left(\frac{x}{\ell}\right) \tag{4-16}$$

where N is defined as in equation (4-15). Similar to the case of calculating the strain energy at a material point, one must use a graphical method to make to integration possible. For instance, in equation (4-16), in order to integrate with respect to x/ℓ, one should plot the integrand $\int_{o}^{\varepsilon_1/\varepsilon_o} \left(\frac{\sigma}{\sigma_o}\right) d\left(\frac{\varepsilon}{\varepsilon_o}\right)$ along the non-dimensional x/ℓ axis between 0 and 1. The the area under this curve should be the total strain energy in the bar.

Finally, substituting equation (4-14), (4-15), and (4-16) into equation (4-8), one has the non-dimensional energy equation,

$$\int_{o}^{kt_1} \left(\frac{\sigma(o,t)}{\sigma_o}\right)\left(\frac{v(o,t)}{v_o}\right) d(kt) = \frac{N}{4} \int_{o}^{1} \left(\frac{v(x,t_1)}{v_o}\right)^2 d\left(\frac{x}{\ell}\right)$$

$$+ \frac{N}{2} \int_{o}^{1} \int_{o}^{\varepsilon_1/\varepsilon_o} \left(\frac{\sigma(x,t)}{\sigma_o}\right) d\left(\frac{\varepsilon}{\varepsilon_o}\right) d\left(\frac{x}{\ell}\right)$$

$$+ \begin{array}{l}\text{Hysteresis energy measured} \\ \text{graphically from the plot} \\ \text{of dynamic stress-strain} \\ \text{relation.}\end{array} \qquad (4\text{-}17)$$

From the numerical results a check energy balance was calculated under the conditions of $E_1/E_o = 1/9$, $N = 66$, $kt_1 = 64$, $A = 2.0$, $B = 2.0$, $\omega = 2\pi k/32.0$ (for equation (4-17)). Results showed less than 5 per cent difference for the equality. The following table shows the numerical values of corresponding calculated energies. The error was attributed to difficulties in accurately determining areas of the hysteresis loops.

Table (4-2). Numerical Values of Energies Listed.

Work Done W	Strain Energy U	Kinetic Energy K	Hysteresis Energy H
832.70	623.72	210.28	41.81

CHAPTER V

CONCLUSIONS AND RECOMMENDATIONS

In previous chapters, this dissertation has presented the general introduction, theoretical formulation, numerical solution and discussion of results. A brief summary of this study will now be given.

As stated previously, the purpose of this thesis was to investigate a homogeneous fixed-free bar, subjected to an axially applied oscillatory stress at its free end. The applied dynamic stress is high enough that plastic strain will result. The material exhibits strain-rate sensitive behavior, which is governed by Malvern's theory. A bilinear static stress-strain curve after that of Kolsky is taken. In addition, the Bauschinger effect has been introduced and studied by considering for unloading that Prager's concept of kinematic hardening applies. Furthermore, it was postulated that rate-sensitive behavior would apply in both upper and lower yield regions.

The problem was formed under a Lagrangian description. The method of characteristics was used to solve the set of quasi-linear partial differential equations. In order to find solutions along characteristics, direct and numerical integration were employed accordingly. The resulting complete solutions, which were expressed dimensionlessly, are stress $\sigma(x,t)$, strain $\varepsilon(x,t)$, and particle velcotiy $v(x,t)$ in the $x-t$ plane. Numerical calculations were performed on a UNIVAC 1108 electronic digital computer. A CALCOMP plotter was used to plot most of the results.

The principal objective was to study the influence of the Bauschinger effect on plastic resonance. It is found in this thesis that, with lower yield effect and the Bauschinger effect, the resonant phenomenon does exist for a material that behaves plastically. The magnitude of the resonant frequency for a bar decreases as the material of the bar presents more plasticity. For a special case, if the bar is excited at or near its first fundamental frequency (elastic) then the amplification effect will decrease as the bar deviates more from its elastic behavior. This conclusion, which is a degenerate case of this study, provides good agreement with the one given by Kalaski and Wlodarczyk [33] in 1967. On the other hand, without the Bauschinger effect, the magnitude of the resonant frequency has no change for a material exhibiting a plastic property.

It was also found that lower yield and the Bauschinger effect influence the shape of the dynamic stress-strain relation, as might be expected. In the case of lower yield and the Bauschinger effect, plastic hysteresis loops are formed in the stress-strain plot. But for the case without the lower yield and the Bauschinger effect, there were no resulting plastic hysteresis loops.

The degree of strain-hardening possessed by the material had a pronounced effect, not only on the existence of plastic resonance, but also on the size and shape of the hysteresis loop. It was noted that the less plastically the material behaves, the smaller in size and the longer in shape the loop appears. When the material behaves completely elastic, the dynamic stress-strain will eventually become a line with a slope of Young's modulus.

Considering various locations of the bar, the limiting cycle of

loading for stabilizing the hysteresis loops was much less at the points near the free end than any other point along the bar. The effect of rate of dynamic loading and unloading was also studied, and it was shown that at higher frequencies of applied loading, the resulting hysteresis loops became smaller.

Also, the principle of conservation of energy was applied to this study in order to check numerical results. It was shown that the numerical results obtained satisfactorily met this criteria.

It is recommended for future study that the theory of plastic wave propagation in a finite bar here with the Bauschinger effect as given here by applied to the study of low cycle fatigue. However, most fatigue investigators have performed their experiments by controlling cyclic strain. But it will not be difficult to convert this analysis from controlling cyclic stress to cyclic strain.

APPENDIX A

FLOW-DIAGRAM FOR CALCULATING σ_N, and ϵ_N

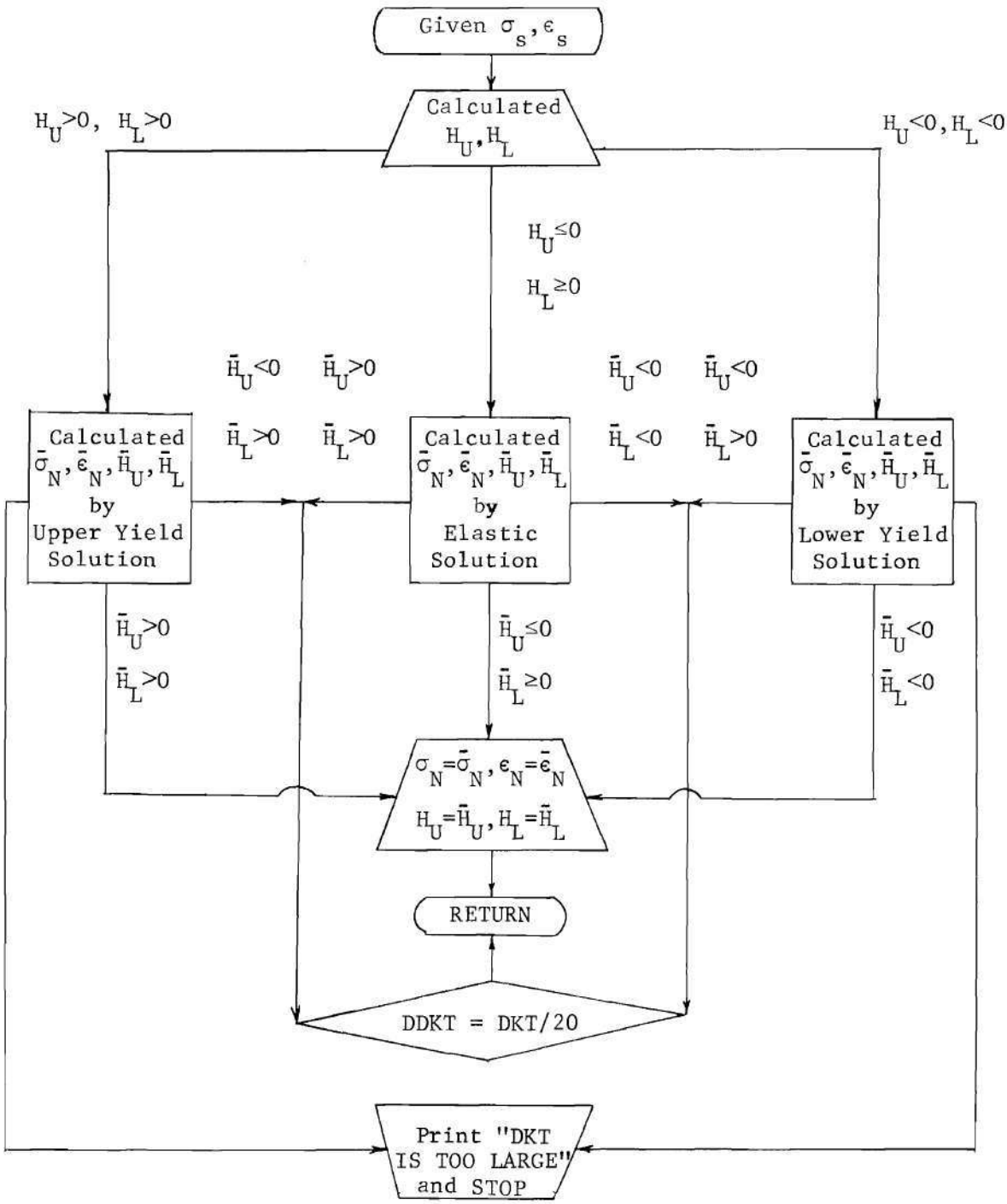

APPENDIX B

Considered here is a homogeneous elastic fixed-free bar which is axially applied oscillating load at its free end. (see Figure (B-1)). For one dimensional longitudinal vibration, the motion of the bar is governed by following differential equation (wave equation),

$$\frac{\partial^2 u(x,t)}{\partial x^2} = \frac{1}{c_o^2} \frac{\partial^2 u(x,t)}{\partial t^2} \tag{B-1}$$

where $u(x,t)$ represents the displacement of the bar under Lagrangian description and $c_o = \sqrt{\frac{E_o}{\rho_o}}$ denotes the elastic wave velocity with E_o being the Young's modulus and ρ_o being the density of the bar. The bar is initially at rest. Therefore the boundary and initial conditions can be expressed mathematically as,

Boundary Conditions:

(i) $$u(o,t) = 0$$

(ii) $$E_o A \left.\frac{\partial u(x,t)}{\partial x}\right]_{x=\ell} = P(t) \tag{B-2}$$

Initial Conditions:

(i) $$u(x,o) = 0$$

(ii) $$\left.\frac{\partial u(x,t)}{\partial t}\right]_{t=o} = 0 \quad . \tag{B-3}$$

In order to solve equation (B-1) coupled with conditions (B-2) and (B-3), the method of Fourier Sine Transform is employed. Now, if one

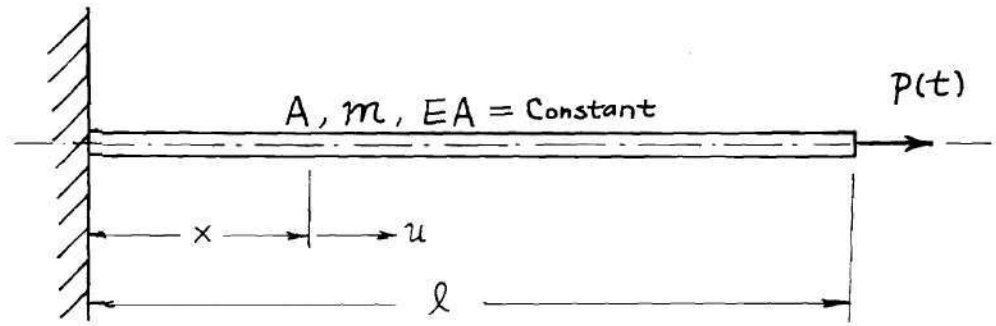

Figure (B-1)

lets the finite sine transform of u(x,t) be defined as

$$\bar{u}_s(p,t) = \int_o^{\ell} u(x,t)\sin px\, dx \ . \tag{B-4}$$

From equation (B-4) one has

$$\begin{aligned} \bar{u}_s^{(2)}(p,t) &= \int_o^{\ell} \frac{\partial^2 u(x,t)}{\partial x^2} \sin px\, dx \\ &= \left[\frac{\partial u(x,t)}{\partial x} \sin px\right]_o^{\ell} - p\left[u(x,t)\cos px\right]_o^{\ell} - p^2\bar{u}_s(p,t). \end{aligned} \tag{B-5}$$

With the aid of boundary condition (ii) of equation (B-2), equation (B-5) yields

$$\bar{u}_s^{(2)}(p,t) = \frac{P(t)}{E_o A} \sin p\ell - pu(\ell,t)\cos p\ell - p^2\bar{u}_s(p,t) \ . \tag{B-6}$$

Since $u(\ell,t)$ is an unknown function, then in order to eliminate this term, we let

$$\cos p\ell = 0 \ . \tag{B-7}$$

This is the frequency equation, which yields

$$p_n = (2n-1)\pi/2\ell \ , \qquad \text{where } n = 1,2,.... \tag{B-8}$$

and

$$\sin p_n\ell = \sin \frac{(2n-1)\pi}{2} = (-1)^{n-1} \ . \tag{B-9}$$

Next, transforming equation (B-1), one gets

$$\int_o^{\ell} \frac{\partial^2 u(x,t)}{\partial x^2} \sin px \, dx = \frac{1}{c_o^2} \int_o^{\ell} \frac{\partial^2 u(x,t)}{\partial t^2} \sin px \, dx \qquad \text{(B-10)}$$

or

$$\bar{u}_s^{(2)}(p,t) = \frac{1}{c_o^2} \frac{d^2}{dt^2} \bar{u}_s(p,t) \quad . \qquad \text{(B-11)}$$

Substituting equation (B-6) into equation (B-11) yields

$$\frac{d^2}{dt^2} \bar{u}_s(p,t) + c_o^2 p^2 \bar{u}_s(p,t) = \frac{c_o^2}{E_o A} P(t) \sin pt \quad . \qquad \text{(B-12)}$$

With the aid of equations (B-8) and (B-9) one has

$$\frac{d^2}{dt^2} \bar{u}_s(n,t) + \left[(2n-1) \frac{\pi c_o}{2\ell} \right]^2 \bar{u}_s(n,t) = (-1)^{n-1} \frac{c_o^2}{EA} P(t) \quad . \qquad \text{(B-13)}$$

The solution of this equation after combining with Initial Condition of equation (B-3) yields

$$\bar{u}_s(n,t) = \frac{2c_o \ell (-1)^{n-1}}{E_o A (2n-1)\pi} \int_o^t P(\tau) \sin(2n-1) \frac{\pi c_o}{2\ell} (t-\tau) d\tau \quad . \qquad \text{(B-14)}$$

The corresponding inversion formula is

$$\begin{aligned} u(x,t) &= \frac{2}{\ell} \sum_{n=1}^{\infty} \bar{u}_s(n,t) \sin(2n-1) \frac{\pi x}{2\ell} \\ &= \frac{2}{\ell} \sum_{n=1}^{\infty} \bar{u}_s(n,t) \sin p_n x \quad . \end{aligned} \qquad \text{(B-15)}$$

Hence, equation (B-14) becomes

$$u(x,t) = \frac{2c_o}{E_o A\ell} \sum_{n=1}^{\infty} \frac{(-1)^{n-1}}{p_n} \sin p_n x \cdot \int_o^t P(\tau)\sin p_n c_o(t-\tau)d\tau \,. \quad \text{(B-16)}$$

This is the displacement of the problem with a loading function P(t) at the free end of the bar. For $P(t) = B_o + A_o \sin \omega t$, one has

$$u(x,t) = \frac{2B_o}{E_o A\ell} \sum_{n=1}^{\infty} \frac{(-1)^{n-1}}{p_n^2} \sin p_n x \cdot [1 - \cos p_n c_o t]$$

$$+ \frac{2c_o A_o}{E_o A\ell} \sum_{n=1}^{\infty} \frac{(-1)^{n-1}}{p_n} \sin p_n x$$

$$\cdot \left[\frac{1}{\omega^2 - p_n^2 c_o^2} (\omega \sin p_n c_o t - p_n c_o \sin \omega t)\right] . \quad \text{(B-17)}$$

Hence the corresponding strain, stress and velocity along the bar are given by

$$\varepsilon(x,t) = \frac{\partial u(x,t)}{\partial x} = \frac{2B_o}{E_o A\ell} \sum_{n=1}^{\infty} \frac{(-1)^{n-1}}{p_n} \cos p_n x \cdot [1 - \cos p_n c_o t]$$

$$+ \frac{2c_o A_o}{E_o A\ell} \sum_{n=1}^{\infty} (-1)^{n-1} \cos p_n x$$

$$\cdot \left[\frac{1}{\omega^2 - p_n^2 c_o^2} (\omega - \sin p_n c_o t - p_n c_o \sin \omega t)\right] \quad \text{(B-18)}$$

$$\sigma(x,t) = E_o\varepsilon(x,t) = \frac{2B_o}{A\ell}\sum_{n=1}^{\infty}\frac{(-1)^{n-1}}{p_n}\cos p_n x\cdot[1-\cos p_n c_o t]$$

$$+\frac{2c_oA_o}{E_oA\ell}\sum_{n=1}^{\infty}(-1)^{n-1}\cos p_n x$$

$$\cdot\left[\frac{1}{\omega^2-p_n^2c_o^2}(\omega\sin p_n c_o t - p_n c_o\sin\omega t)\right] \qquad \text{(B-19)}$$

$$v(x,t) = \frac{\partial u(x,t)}{\partial t} = \frac{2c_oB_o}{E_oA\ell}\sum_{n=1}^{\infty}\frac{(-1)^{n-1}}{p_n}\sin p_n x\cdot[\sin p_n c_o t]$$

$$+\frac{2c_oA_o}{E_oA\ell}\sum_{n=1}^{\infty}\frac{(-1)^{n-1}}{p_n}\sin p_n x$$

$$\cdot\left[\frac{\omega p_n c_o}{\omega^2-p_n^2c_o^2}(\cos p_n c_o t - \cos\omega t)\right] . \qquad \text{(B-20)}$$

This completes the derivation of the general solutions of stress, strain and velocity of a homogeneous, elastic fixed-free bar. Next, we want to find the expressions for the corresponding solutions at the value of ω approaching to the bar's first fundamental frequency (at resonance). Therefore, L'Hopitals Rule can be applied and yield the following equations,

$$\lim_{\omega\to p_1c_o}\left[\frac{1}{\omega^2-p_1^2c_o^2}(\omega\sin p_1c_o t - p_1c_o\sin\omega t)\right] = -\frac{t}{2}\cos p_1c_o t \qquad \text{(B-21)}$$

$$\lim_{\omega \to p_1 c_o} \left[\frac{\omega p_1 c_o}{\omega^2 - p_1^2 c_o^2} (\cos p_1 c_o t - \cos \omega t) \right] = \frac{p_1 c_o t}{2} \sin p_1 c_o t \, . \quad \text{(B-22)}$$

With equation (B-21) and (B-22), we find the solutions at resonance are, $(\omega \to p_1 c_o)$

$$u^r(x,t) = \frac{2B_o}{E_o A \ell} \sum_{n=1}^{\infty} \frac{(-1)^{n-1}}{p_n^2} \sin p_n x \cdot [1 - \cos p_n c_o t] + \frac{2c_o A_o}{E_o A \ell}$$

$$\cdot \frac{1}{p_1} \sin p_1 x \left(- \frac{t}{2} \cos p_1 c_o t \right) + \frac{2c_o A_o}{E_o A \ell} \sum_{n=2}^{\infty} \frac{(-1)^{n-1}}{p_n} \sin p_n x$$

$$\cdot \left[\frac{1}{p_1^2 c_o^2 - p_n^2 c_o^2} (p_1 c_o \sin p_n c_o t - p_n c_o \sin p_1 c_o t) \right] \quad \text{(B-23)}$$

$$\epsilon^r(x,t) = \frac{2B_o}{E_o A \ell} \sum_{n=1}^{\infty} \frac{(-1)^{n-1}}{p_n^2} \cos p_n x \cdot [1 - \cos p_n c_o t]$$

$$+ \frac{2c_o A_o}{E_o A \ell} \cos p_1 x \left(- \frac{t}{2} \cos p_1 c_o t \right) + \frac{2c_o A_o}{E_o A \ell} \sum_{n=2}^{\infty} (-1)^{n-1} \cos p_n x$$

$$\cdot \left[\frac{1}{p_1^2 c_o^2 - p_n^2 c_o^2} (p_1 c_o \sin p_n c_o t - p_n c_o \sin p_1 c_o t) \right] \quad \text{(B-24)}$$

$$\sigma^r(x,t) = \frac{2B_o}{A \ell} \sum_{n=1}^{\infty} \frac{(-1)^{n-1}}{p_n^2} \cos p_n x \cdot [1 - \cos p_n c_o t]$$

$$+ \frac{2c_o A_o}{A\ell} \cos p_1 x\left(- \frac{t}{2} \cos p_1 c_o t\right) + \frac{2c_o A_o}{A\ell} \sum_{n=2}^{\infty} (-1)^{n-1} \cos p_n x$$

$$\cdot \left[\frac{1}{p_1^2 c_o^2 - p_n^2 c_o^2} (p_1 c_o \sin p_n c_o t - p_n c_o \sin p_1 c_o t)\right] \qquad \text{(B-25)}$$

and

$$V^r(x,t) = \frac{2c_o B_o}{E_o A\ell} \sum_{n=1}^{\infty} \frac{(-1)^{n-1}}{p_n} \sin p_n x \cdot [\sin p_n c_o t] + \frac{2c_o A_o}{E_o A\ell}$$

$$\cdot \frac{1}{p_1} \sin p_1 x \left(\frac{p_1 c_o t}{2} \sin p_1 c_o t\right) \qquad \text{(B-26)}$$

$$+ \frac{2c_o A_o}{E_o A\ell} \sum_{n=2}^{\infty} \frac{(-1)^{n-1}}{p_n} \sin p_n x\left[\frac{p_1 p_n c_o^2}{p_1^2 c_o^2 - p_n^2 c_o^2} (\cos p_n c_o t - \cos p_1 c_o t)\right]$$

BIBLIOGRAPHY

1. Kaliski, S. and Wlodarczyk, E. [1967-A], "The Problem of Resonance for Longitudinal Elastic-Plastic Waves in a Finite Bar," Proc. Vibr. Probl., Vol. 8, No. 1, pp. 47-59.

2. Donnell, L. H. [1930], "Longitudinal Wave Transmission and Impact," Trans. Amer. Soc. Mech. Engrs., Vol. 52, (Part I), paper no. APM-52-14, pp. 153-167.

3. Karman, Th. Von, [1942-A], "On the Propagation of Plastic Deformation in Solids," National Def. Res. Comm. Rep. No. A-29, (OSRD No. 365).

4. Taylor, G. I. [1942], "The Plastic Wave in a Wire Extended by an Impact Load," The Scientific Paper of G. I. Taylor, Vol. I, Mechanics of Solids (Edited by G. K. Batchelor), Cambridge University Press, pp. 467-479.

5. Rakhmatulin, Kh. A. [1945], "On Propagation of the Unloading Wave," (in Russian), Prikl. Mat. Mekh., Vol. 9, pp. 91-100.

6. White, M. P. and Griffis, L. [1947], "The Permanent Strain in a Uniform Bar Due to Longitudinal Impact," Journal of Applied Mechanics, Vol. 14, pp. A337-343.

7. White, M. P. and Griffis, L. [1948], "The Propagation of Plasticity in Uniaxial Compression," Journal of Applied Mechanics, Vol. 15, pp. 256-260.

8. Duwez, P. E. and Clark, D. S. [1947], "An Experimental Study of the Propagation of Plastic Deformation under Conditions of Longitudinal Impact," Proc. Amer. Soc. Testing Materials, Vol. 47, pp. 502-522.

9. Duwez, P. E. and Clark, D. S. [1948], "Discussion of the Forces Acting in Tension Impact Tests of Materials," Trans. A.S.M.E., Vol. 70, pp. 243-247.

10. Karman, Th. von and Duwez, P. [1950], "The Propagation of Plastic Deformation in Solids," Journal of Applied Physics, Vol. 21, pp. 987-994.

11. Lee, E. H., [1953], "A Boundary Value Proplem in the Theory of Plastic Wave Propagation," Quarterly of Applied Math., Vol. X, pp. 335-346.

12. Malvern, L. E. [1951-A], "Plastic Wave Propagation in a Bar of Material Exhibiting a Strain Rate Effect," Quarterly of Applied Math., Vol. VIII, pp. 405-411.

13. Malvern, L. E. [1951-B], "The Propagation of Longitudinal Waves of Plastic Deformation in a Bar of Material Exhibiting a Strain-Rate Effect," Journal of Applied Mechanics, Vol. 18, pp. 203-208.

14. Bell, J. F. [1951], "Propagation of Plastic Waves in Pre-Stressed Bars," Department of Mechanical Engineering, The Johns Hopkins University, Baltimore, Md., Technical Report No. 5, (Navy Contract NG-ONR-243, Task Order VIII).

15. Sternglass, E. J. and Stuart, D. A. [1953], "An Experimental Study of the Propagation of Transient Longitudinal Deformations in Elasto-Plastic Media," Journal of Applied Mechanics, Vol. 20, pp. 427-434.

16. Alter, B.E.K. and Curtis, C. W. [1956], "Effect of Strain Rate on the Propagation of a Plastic Strain Pulse along a Lead Bar," Journal of Applied Physics, Vol. 27, pp. 1109-1113.

17. Campbell, J. D. [1953], "An Investigation of the Plastic Behavior of Metal Rods Subjected to Longitudinal Impact," Journal of the Mech. and Phys. of Solids, Vol. 1, pp. 113-123.

18. Hopkins, H. G. [1961], "Dynamic Anelastic Deformations of Metals," Applied Mechanics Reviews, Vol. 14, No. 6, pp. 417-431.

19. Morland, L. W. [1959], "The Propagation of Plane Irrotational Waves Through an Elastoplastic Medium," Phil. Trans. of the Royal Society of London, Series A, Vol. 251, pp. 341-383.

20. Osiecki, J. [1962], "Propagation of Plastic Strain Waves in a Semi-infinite Bar Produced by a Periodic Load," Proc. Vibr. Probl., Vol. 3, No. 2.

21. Clifton, R. J. and Bodner, S. R. [1966], "An Analysis of Longitudinal Elastic-Plastic Pulse Propagation," Journal of Applied Mechanics, June 1966, pp. 248-255.

22. Wood, E. R. [1966], "The Effect of Lower Yield on the Propagation of Plastic Waves," Doctoral Dissertation, Yale University, New Haven.

23. Wood, E. R. and Phillips, A. [1967] "On the Theory of Plastic Wave Propagation in a Bar," J. Mech. Phys. Solids, Vol. 15.

24. Lubliner, J., [1964], "A Generalized Theory of Strain-Rate-Dependent Plastic Wave Propagation in Bars," J. Mech. Phys. Solids, Vol. 12.

25. Cristescu, N. [1965], "Loading/Unloading Criteria for Rate Sensitive Materials," Archinum Mechaniki Stosowanej, 2, 17.

26. Nowacki, W. K. [1964], "Propagation and Reflection of a Plane Stress Wave from a Deformable Support in An Elastic-Visco-Plastic Strain-Hardening Body," Proc. Vib. Probl. Vol. 5, No. 4.

27. Prager, W. [1955], "The Theory of Plasticity: A Survey of Recent Achievements," (James Clayton Lecture), Proc. Inst. of Mech. Engrs., Vol. 169, pp. 41-57.

28. Lubahn, J. D., [1955], "Bauschinger Effect in Creep and Tensile Tests on Copper," Journal of Metals, Sept. 1955, pp. 1031.

29. Ivey, H. J. [1961], "Plastic Stress-Strain Relations and Yield Surfaces for Aluminum Alloys," Journal of Mechanical Engineering Sciences, Vol. 3, pp. 15-31.

30. Phillips, A. and Sierakowski, R. L. [1965], "On the Concept of the Yield Surface," Acta Mechanica, Vol. I, No. 1, pp. 29-35.

31. Justusson, J. W. [1966], "Studies on the Yield Surface," Doctoral Dissertation, Yale University, New Haven.

32. Kaliski, S. and Wlodarczyk, E., [1967-B], "Response of a Longitudinal Shock Wave in an Elastic-Plastic Bar," Proc. Vib. Prob., Vol. 8, No. 2.

33. Kaliski, S. and Wlodarczyk, E., [1967-C], "Resonance of a Longitudinal Elastic-Visco-Plastic Wave in a Finite Bar," Proc. Vib. Prob., Vol. 8, No. 2, pp. 113-127.

34. Campbell, J. D. and Duby, J., [1956], "The Yield Behavior of Mild Steel in Dynamic Compression," Proc. Roy. Soc., A236, pp. 24-40.

35. Bauschinger, J., [1886], "Über die Veränderung der Elasticitätsgrenze und Festigkeit des Eisens," Mitt. Mech.-Tech. Lab. Kgl. Tech. Hochs, Munchen, 1886.

36. Sokolovski, V. V., [1948], "The Propagation of Elastoviscoplastic Waves in Bars," Prikl. Mat. Mech., Vol. 12, No. 3, pp. 261-280.

37. Wood, E. R. and Liu, T. H., [1969], "On the Dynamic Plastic Response of Finite Bars," AIAA Journal, Vol. 7, No. 11, Nov. 1969.

38. Kolsky, H. [1963], Stress Waves in Solids, Dover Publications, Inc., New York.

39. Hopkins, H. G. [1968], "The Method of Characteristics and its Application to the Theory of Stress Wave in Solids," Heyman, J. and Leckie, F. A., edited by, Engineering Plasticity, Cambridge University Press, 1968, pp. 277-315.

40. Morrow, J. [1965], "Cyclic Plastic Strain Energy and Fatigue of Metals," Internal Friction, Damping, and Cyclic Plasticity, Published by the American Society for Testing and Materials, Philadelphia 3, Pennsylvania 1965.

41. Neville, G. E., Jr. and Myers, C. D. [1968], "Strain Rate Effects During Reversed Loading," J. Mech. Phys. Solids, Vol. 16, pp. 187-194.

42. Lindholm, U. S. [1965], "Dynamic Deformation of Metals," Behavior of Metals Under Dynamic Loading, The American Society of Mechanical Engineers, New York, 1965.

43. Caughey, T. K. [1960], "Sinusoidal Excitation of A System with Bilinear Hysteresis," J. Appld. Mech., Dec. 1960, p. 640-643.

44. Jacobsen, L. S. and Ayre, R. S. [1958], Engineering Vibrations, McGraw-Hill Book Co., Inc., New York, 1958.

45. Dolan, T. J. [1965], "Nonlinear Response Under Cyclic Loading Conditions," Development in Mechanics, edited by Huang and Johnson, Vol. 3, Part 1, John Wiley and Sons, Inc., New York, 1965.

VITA

Thou-Han Liu was born on November 16, 1938, in Kiansu, China. He graduated from Provincial Chien-Kuo High School in 1957 and from Cheng-Kung University with the degree of Bachelor of Science in Civil Engineering in 1962. He was qualified as a Registered Professional Civil Engineer in China in 1964 by passing the examination. From 1963 to 1965, he worked as a full-time teaching assistant in Chen-Kung University.

In September, 1965, he was awarded a graduate teaching assistantship for graduate study at Duke University, Durham, North Carolina, where he completed the requirements for the Master of Science degree in Civil Engineering in September of 1967. Immediately after he graduated from Duke, he received a graduate research assistantship from the School of Engineering Science and Mechanics, Georgia Institute of Technology, for further study towards his doctoral degree. In 1970, he was granted a graduate fellowship under the National Defense Educational Act (NDEA) for graduate study in Engineering Science and Mechanics.

He is a member of the society of Sigma Xi and the American Institute of Aeronautics and Astronautics.

In 1969, he was married to the former Miss Rita Ching-Shiang Meng of Shantung, China and they have a son, David Liu.